Understanding the role of ADAM15 in osteoarthritis



Chun-Yao, Yang
Lincoln College

Supervisors: Dr Linda Troeberg and Prof. Hideaki Nagase

Kennedy Institute of Rheumatology

Nuffield Department of Orthopaedics, Rheumatology and Musculoskeletal Sciences

University of Oxford

Thesis submitted for the degree of Doctor of Philosophy (D. Phil.) in Molecular and Cellular Medicine to University of Oxford, Trinity 2018

Acknowledgements

It has been a completely unexpected journey for me to come to the UK and jumped into the world of proteins scissoring each other. This journey is much more fun, challenging and frustrating than I can ever imagine. I am certain that it is entirely impossible for an ADHD like me to survive in this world without the help from many people. First and foremost, I would like to express my most sincere gratitude to my supervisor, Dr. Linda Troeberg, who dare to take a naughty boy like me as a DPhil student. Thank you 1700 times for your scientific supervision and life wisdom. I would not have made it through without you. I would also like to thank Prof. Hideaki Nagase for his unbelievably sharp scientific instinct and wonderful mentoring. I would like to thank everyone who shared the lab with me and all the Matrix Biology people I met during my time at the Kennedy. I would like to thank the countless baseball and basketball podcasts published on iTunes which helped me to get through those painful nights when my Western blot did not care to show a faintest band and those awful days when my beloved but mischievous ADAM15 was too lazy to do anything on the cell surface. A special thank you to Sinead for accepting who I am, and for having the courage to share your life with me. Thank you all my friends in Taiwan for all your support along the way, your steady friendship is the only reason I can overcome the unpredictable British weather. Finally, to 阿貴: thank you for the lesson you taught me with your life. This degree is for you.

Abstract

Thesis title: Understanding the role of ADAM15 in osteoarthritis.

Candidate: Chun-Yao, Yang, Lincoln College

Degree: Doctor of Philosophy (D.Phil.) in Molecular and Cellular Medicine

A disintegrin and metalloproteinase 15 (ADAM15) is a member of the ADAM family of metalloproteases, which plays important roles in a wide variety of biological functions. A previous study demonstrated that *Adam15*-null mice developed accelerated age-dependent OA, suggesting that ADAM15 has protective effects in the joint. Despite this potentially important role, little is known about how ADAM15 exerts its biological functions or is regulated in joints. In this project, I demonstrated that ADAM15 expression in the joint decreases with age. This correlates with a decrease in IL-13 expression with age. I showed that IL-13 up-regulates ADAM15 *in vitro*, suggesting that reduced IL-13 expression with age may underlie the observed reduction in ADAM15 expression with age. In parallel, I showed that ADAM15 is not a highly active sheddase, as multiple mass spectrometry proteomic analyses did not identify convincing ADAM15 substrates. However, proteomic analysis of surface proteins in ADAM15-knockdown HTB-94 cells showed that ADAM15 may regulate the surface abundance of SLC26A2, an important sulfate transporter in cartilage. In summary, the reduction of ADAM15 in aged cartilage and, potentially, the consequent reduced cell surface level of SLC26A2 may elevate risk for OA in aged joints.

Table of Contents

Acknowledgements **2**

Abstract **3**

Table of Contents **4**

List of Figures **9**

List of Tables **12**

List of Abbreviations **13**

Chapter 1. Introduction **15**

1.1. Cartilage **16**

1.1.1. Anatomy of articular cartilage 16

1.1.2. Chondrocyte homeostasis and metabolism 19

1.2. Osteoarthritis **21**

1.2.1. OA epidemiology 23

1.2.2. OA aetiology and risk factors 24

1.2.2.1. Ageing 25

1.2.2.2. Obesity 30

1.2.2.3. Injuries 30

1.2.2.4. Genetic predisposition 31

1.2.3. OA pathogenesis 33

1.2.3.1. Role of chondrocytes in OA development 35

1.2.3.2. Role of subchondral bone in OA development 37

1.2.3.3. Role of synovium and synovial inflammation in OA development 38

1.2.3.4. ADAMs in OA pathogenesis 39

1.3. ADAM proteases **40**

1.3.1. ADAM topology and domain functions 40

1.3.1.1. The pro-domain 41

1.3.1.2. The metalloproteinase domain 42
1.3.1.3. The disintegrin domain 44
1.3.1.4. The cysteine-rich domain 45
1.3.1.5. The EGF-like domain 46
1.3.1.6. The cytoplasmic tail 46
1.3.2. Regulation of ADAM proteolytic activity 46
1.3.2.1. Transcriptional regulation of ADAMs 47
1.3.2.2. Alternative splicing of ADAMs 48
1.3.2.3. Post-translational modifications of ADAMs 49
1.3.2.4. Regulation of ADAM subcellular localisation 50
1.3.2.5. Endogenous regulators of ADAMs 51
1.4. ADAM15 protects murine joints against OA development 52
1.4.1. ADAM15 provides apoptotic resistance to different cells in joints 53
1.5. Functions and roles of ADAM15 in other diseases 56
1.5.1. Discovery of ADAM15 56
1.5.2. ADAM15's role as a sheddase and its proposed substrates 56
1.5.3. ADAM15 mediated cell-cell and cell-matrix adhesion 59
1.5.4. ADAM15 interacts with intracellular adaptors via its cytoplasmic tail 60
1.5.5. Phenotypes of Adam15-null mice 62
Chapter 2. Materials and Methods 65
2.1. Materials 66
2.1.1. Human tissues 66
2.1.2. Murine tissues 66
2.1.3. Cultured cells 67
2.1.4. Cell culture reagents 67
2.1.5. Molecular biology reagents 67
2.1.6. Cell biology reagents 69
2.1.7. Biochemistry reagents 71

2.1.8. Antibodies 72

2.1.9. Proteomic analysis 73

2.2. Methods 74

2.2.1. Human primary chondrocyte culture 74

2.2.2. Murine primary chondrocyte culture 74

2.2.3. Culture of human cell lines 75

2.2.4. Cell biology methods 75

2.2.4.1. Over-expression by transient transfection 75

2.2.4.2. RNA interference by transient transfection 76

2.2.4.3. Stimulation of HTB-94 cells 76

2.2.4.4. Freezing down cultured cells 77

2.2.4.5. MTS colorimetric cell proliferation assay 78

2.2.5. Molecular biology 78

2.2.5.1. Transformation by electroporation 78

2.2.5.2. RNA extraction 79

2.2.5.3. Reverse transcription 80

2.2.5.4. Real-Time PCR (qPCR) 80

2.2.6. Biochemistry methods 81

2.2.6.1. Trichloroacetic acid (TCA) precipitation 81

2.2.6.2. SDS-PAGE using the Ammediol buffer system 82

2.2.6.3. Immunoblotting 85

2.2.6.4. Immunoprecipitation of FLAG-tagged recombinant human ADAM15 87

2.2.7. Coating cover slips with gelatin for immunofluorescence staining 88

2.2.8. Immunofluorescent staining (IF) on cells and tissues 89

2.2.9. Proteomic methods 90

2.2.9.1. Sample preparation for LfQ mass spectrometry of secretome of ADAM15-over-expressing HTB-94 cells 96

2.2.9.2. Sample preparation for LfQ mass spectrometry of ADAM15-deficient HTB-94 cells 97

2.2.9.3. Sample preparation for SPECS secretome LfQ mass spectrometry analysis 98

2.2.9.4. Sample preparation for SPECS surfaceome (SurfSPECS) LfQ mass spectrometry analysis 100

2.2.9.5. Streptavidin-agarose pulldown of 'clicked' glycoproteins 102
2.2.9.6. In-gel digestion 102
2.2.9.7. Proteomic analysis using LC-MS/MS 104
2.2.9.8. Analysis of the proteomic data 105

Chapter 3. Characterising changes in ADAM15 expression with age and in OA 107

3.1. Introduction 108
3.2. ADAM15 mRNA expression in human OA and normal cartilage 110
3.3. Adam15 mRNA expression in murine joints after DMM surgery 112
3.4. Age-dependence of ADAM15 expression in human cartilage 114
3.5. Age-dependence of Adam15 expression in male murine joints 116
3.6. Expression of senescence markers Cdkn2a, Cdkn1a and Il6 in male murine joints 121
3.7. Expression of Adam15 and senescence markers in other murine tissues 124
3.8. The expression of CDKN2A and CDKN2A in human cartilage 128
3.9. CDKN1A did not regulate ADAM15 expression 130
3.10. ADAM15 expression decreased in aged human cartilage at the protein level 133
3.11. Discussion 147

Chapter 4. Identification of endogenous regulators that contribute to age-related reduction of ADAM15 in cartilage 155

4.1. Introduction 156
4.2. Induction of cellular senescence using mirin did not affect ADAM15 expression in HTB-94 cells 160
4.3. Treatment with Sirt1 modulators, resveratrol and EX-527, did not affect ADAM15 expression in HTB-94. 167
4.4. 3-MA treatment increased ADAM15 expression 168
4.5. IL-1 and RA did not regulate ADAM15 expression in HTB-94 and primary human OA chondrocytes 170

4.6. DHT and E2 treatments did not regulate ADAM15 expression in HTB-94 173

4.7. Identification of potential regulator(s) of ADAM15 expression 174

4.8. Discussion 182

Chapter 5. Identification of proteins regulated by ADAM15 192

5.1. Introduction 193

5.2 Identification of proteins regulated by ADAM15 in the secretome of ADAM15-over-expressing HTB-94 cells 198

5.3. Identification of proteins regulated by ADAM15 in the secretome of ADAM15-knockdown HTB-94 cells 211

5.4. Identification of glycoproteins regulated by ADAM15 in the SPECS secretome of ADAM15-knockdown HTB-94 cells 224

5.5. Identification of proteins regulated by ADAM15 in the secretome of Adam15-null immature murine chondrocytes 229

5.6. Identification of glycoproteins regulated by ADAM15 in the SurfSPECS of ADAM15-knockdown HTB-94 cells 232

5.7 Discussion 243

Chapter 6 Discussion 254

6.1. ADAM15 plays a minor role during development 255

6.2. Decreased ADAM15 expression with age may hamper joint protection 256

6.3. IL-13 may contribute to the age-related reduction in ADAM15 expression 257

6.4. Secretome analyses did not identify ADAM15 substrates 258

6.5. ADAM15 may protect cartilage from OA through maintaining SLC26A2 level on the cell surface 262

6.6. Concluding remarks and further direction 265

7. References 267

List of Figures

Figure 1.1 Articular cartilage can be divided into four zones according to its morphology. 19

Figure 1.2 Features of osteoarthritic knee joint. 23

Figure 1.3 Senescence-inducing pathways. 28

Figure 1.4 The schematic topography of ADAM, ADAMTS, and MMP protein structure. 41

Figure 2.1 Predicted changes caused by manipulation of ADAM15 expression using different strategies and associated proteomic analysis. 95

Figure 2.2 Illustration of the SPECS secretome and surfSPECS principle. 101

Figure 3.1 Analysed articular cartilage samples were age-matched. 111

Figure 3.2 ADAM15 showed no difference in expression between human normal and OA cartilage. 112

Figure 3.3 Adam15 expression did not change in murine joints 6 hours, 8 weeks or 12 weeks after DMM surgery. 114

Figure 3.4 ADAM15 expression in human cartilage changed with age, but was unaffected by sex. 116

Figure 3.5 Adam15 expression in the murine knee joints changed with age. 118

Figure 3.6 Age-dependent expression of Adam17, Sirt1, Runx2, and Jak2 in murine joints. 120

Figure 3.7 Expression of senescence marker Il6 increased in joints from 5.5- and 18-month old mice compared to 3-month old mice, but expression of Cdkn2a and Cdkn1a did not. 123

Figure 3.8 Adam15 but not Cdkn2a expression was significantly decreased in joint and bone from old female mice. 125

Figure 3.9 Cdkn2a and Il6, but not Adam15 expression, increased in old female murine spleen, brain and heart. 127

Figure 3.10 Neither CDKN2A nor CDKN1A exhibited age-dependent change in expression in cartilage. 129

Figure 3.11 Expression of CDKN1A was significantly decreased in human OA cartilage. 129

Figure 3.12 CDKN1A did not regulate ADAM15 expression. 131

Figure 3.13 ADAM15 repression did not affect CDKN2A and CDKN1A expression. 132

Figure 3.14 Validation of anti-ADAM15 antibody for immunofluorescence staining by over-expressing pCMV2-ADAM15-FLAG in HTB-94 cells. 135

Figure 3.15 FLAG-tagged ADAM15 was detectable in pCMV2-ADAM15-FLAG over-expressing HTB-94 cells, whilst endogenous ADAM15 was undetectable using an anti-FLAG antibody. 137

Figure 3.16 Validation of anti-ADAM15 antibody specificity by antigen blocking. 139

Figure 3.17 ADAM15 expression decreased in aged human cartilage at the protein level. 141

Figure 3.18 Immunofluorescence staining with an independent set of cartilage sections supports that ADAM15 expression decreased in aged human cartilage at the protein level. 143

Figure 3.19 ADAM15 is homogeneously distributed in porcine cartilage. 145

Figure 4.1 Mirin decreased ADAM15 expression in HTB-94 24 hours after treatment. 163

Figure 4.2 Mirin did not change ADAM15 expression in HTB-94 48 hours after treatment. 164

Figure 4.3 Mirin treatment did not affect RPLP0 expression in HTB-94. 166

Figure 4.4 Mirin treatment did not affect proliferation of HTB-94 cells. 166

Figure 4.5 Treatment with Sirt1 activity modulators did not regulate ADAM15 expression in HTB-94. 168

Figure 4.6 3-MA treatment increased ADAM15 expression. 170

Figure 4.7 IL-1α and RA did not increase ADAM15 expression at mRNA and protein levels in HTB-94 and primary human OA chondrocytes. 172

Figure 4.8 DHT and E2 treatments did not increase ADAM15 expression in HTB-94 cells. 174

Figure 4.9 Stimuli screening identified that IL-13 and GM-CSF increased ADAM15 expression in HTB-94 cells 24 hours after stimulation. 176

Figure 4.10 qPCR and immunoblotting validated that IL-13 increased ADAM15 expression at both the mRNA and protein levels. 179

Figure 4.11 Il13 expression decreased with age in murine joints. 181

Figure 5.1 Anti-ADAM15 antibodies used for this study were validated using recombinant ADAM15 proteins and immunoprecipitated ADAM15-FLAG. 201

Figure 5.2 Over-expression of ADAM15 in HTB-94 was optimised and did not cause increased cell death. 202

Figure 5.3 Optimisation of ADAM15 over-expression protocol for LfQ mass spectrometry analysis of the secretome. 204

Figure 5.4 Identification of proteins regulated by ADAM15 in the secretome of ADAM15-over-expressing cells. 207

Figure 5.5 Immunoblotting validation showed that CTGF abundance decreased in CM of ADAM15-over-expressing HTB-94. 210

Figure 5.6 Identification of proteins regulated by ADAM15 in the secretome of ADAM15-knockdown cells 214

Figure 5.7 AXL expression decreased at the mRNA and protein levels upon ADAM15 knockdown. 216

Figure 5.8 The off-target effects of siADAM15 on gene expression were mainly due to siADAM15_2218

Figure 5.9 ADAM15 expression was significantly decreased at both mRNA and protein levels in HTB-94 cells treated with siADAM15_1 36, 48 and 72 hours after transfection. 221

Figure 5.10 Effects of ADAM15 knockdown on solubilised and transmembrane AXL expression were time dependent. 223

Figure 5.11 Identification of proteins regulated by ADAM15 in the SPECS secretome of ADAM15-knockdown cells. 228

Figure 5.12 Identification of proteins regulated by ADAM15 in the secretome of Adam15-null immature murine costal chondrocytes 232

Figure 5.13 Identification of glycoproteins regulated by ADAM15 in the SurfSPECS of ADAM15-repressing HTB-94 cells.....235

Figure 5.14 ADAM15 knockdown did not affect mRNA expression of PDCD1LG2, SLC26A2 and VASORIN. 238

Figure 5.15 ADAM15 knockdown may decrease surface levels of SLC26A2. 242

List of Tables

Table 2.1 Suppliers of cell culture reagents.....67

Table 2.2 Details of TaqMan Gene Expression Assay primers 69

Table 2.3: Suppliers of transfection reagents utilised 70

Table 2.4: Details of Silencer Select siRNA used 70

Table 2.5: Suppliers of SDS-PAGE and immunoblotting reagents 71

Table 2.6: Details of antibodies and detection reagents used.....72

Table 2.7: Suppliers of proteomic materials and reagents 73

Table 2.8: Concentrations used for each stimulus.....77

Table 2.9: Composition of buffers in Ammediol SDS-PAGE buffer system 82

Table 2.10: Composition of SDS-PAGE with various polyacrylamide concentrations.....85

Table 2.11 Components of RIPA buffer (10 X) 88

Table 2.12 LC gradient used for LC-MS/MS separation of tryptic peptides. 105

Table 3.1 Changes in gene expression in old (17-18 months) relative to young (3 months) tissues (↓, reduced; ↑, increased; —, no change; N/A, not analysed).....146

Table 4.1 Changes in ADAM15 expression in diseases. 160

Table 4.2 Proposed regulators of ADAM15 expression 160

List of Abbreviations

ADAM A disintegrin and metalloproteinase domain-containing protein

ADAMTS A disintegrin and metalloproteinase with thrombospondin motifs

AP Alkaline phosphatase

APS Ammonium persulfate

BACE1 B-secretase beta-site amyloid precursor protein

BMP Bone morphogenetic protein

BSA Bovine serum albumin

CD Cluster of differentiation

CDK Cyclin-dependent kinase

CTGF Connective tissue growth factor

DMEM Dulbecco's modified Eagle's medium

DMOADs Disease-modifying osteoarthritis drugs

DMSO Dimethyl sulfoxide

DNA Deoxyribonucleic acid

ECM Extracellular matrix

EDTA Ethylenediaminetetraacetic acid

EGF Epidermal growth factor

GAG Glycosaminoglycans

GWAS Genome-wide association studies

HA Hyaluronic acid

HCl Hydrogen chloride

HRP Horseradish peroxidase

IGF-1 Insulin-like growth factor 1

IL Interleukin

LPS lipopolysaccharide

MMP Matrix metalloproteases

mRNA Messenger RNA

OA Osteoarthritis

PAGE polyacrylamide gel electrophoresis

PBS Phosphate buffered saline

PCM Pericellular matrix

PCR Polymerase chain reaction

PDGF Platelet derived growth factor

qPCR Real-Time PCR

RA retinoic acid

RNA Ribonucleic acid

SDS Sodium dodecyl sulfate

sE-cad Soluble E-cadherin

siRNA Small interfering RNA

SNP Single nucleotide polymorphism

SPECS Secretome protein enrichment with click sugars

TACE Tumor necrosis factor converting enzyme

TCA trichloroacetic acid

TEMED N,N,N′,N'-tetramethylethane-1,2-diamine

TNF Tumor necrosis factor

TGF Transforming growth factor

Tris Trisaminomethane

VEGF vascular endothelial growth factor

vWF von Willebrand factor

Chapter 1. Introduction

1.1. Cartilage

Cartilage is a ECM-rich connective tissue. Depending on the relative abundance of proteoglycan and collagen in the ECM, cartilage can be categorised into four different types: elastic, fibro-, fibroelastic and hyaline (Bhosale et al., 2008). In synovial joints, the interface between two opposing bones is covered by a specialised hyaline cartilage called articular cartilage (Bhosale et al., 2008), that is important in providing compressive strength, tensile resistance and lubrication (Boschetti et al., 2008). Due to its important role in joint function, the following introduction will focus on articular cartilage.

1.1.1. Anatomy of articular cartilage

Articular cartilage is an avascular, aneural and alymphatic tissue containing a single cell type, the chondrocyte. The tissue has low cellularity, with chondrocytes accounting for around 5% of the wet weight of articular cartilage, and less than 10% of its volume (Ulrich-Vinther et al., 2003). Despite their low density, chondrocytes are responsible for producing all of the cartilage ECM components, including collagens and proteoglycans. In addition to chondrocytes, the main components of cartilage are water, collagen and proteoglycans (Bhosale et al., 2008). Type II collagen is the main collagen found in articular cartilage (90-95% of the total collagen) and it forms the structural framework of the cartilage ECM, conferring tensile resistance (Bhosale et al., 2008; Boschetti et al., 2008). It is a fibrillar collagen, and forms triple helices under physiological conditions. In healthy articular cartilage, it has a very slow turnover rate and is cross-linked to itself, other minor collagens and proteoglycans (Ulrich-Vinther et al., 2003), furthering increasing tensile strength.

Aggrecan is the most abundant proteoglycan found in articular cartilage, and it is composed of a core protein substituted with many chondroitin sulfate (approximately 100) and keratan sulfate (around 60) glycosaminoglycans (GAG), as well as various O- and N-linked oligosaccharides (Kiani et al., 2002). The N-terminus of the aggrecan core protein is folded into a global domain, and binds via link protein to hyaluronic acid, a negatively charged, unbranched, long polysaccharide (Kiani et al., 2002; Ulrich-Vinther et al., 2003). Each hyaluronic acid molecule interacts with a large number of aggrecan molecules, forming an interconnected network within articular cartilage. The negatively charged sulfate groups in the GAG chains and the negative charge of hyaluronic acid enable articular cartilage ECM to retain high levels of cations, thus creating a high osmotic pressure and enabling the matrix to retain a large volume of water, providing compressive strength to articular cartilage (Bhosale et al., 2008; Ulrich-Vinther et al., 2003).

Water is the principal component of articular cartilage, accounting for approximately 75% of its wet weight (Ulrich-Vinther et al., 2003). As mentioned above, water retained in articular cartilage is responsible for providing high hydrostatic pressure, which counteracts compressive forces (Boschetti et al., 2008; Ulrich-Vinther et al., 2003). Water and other lubricants such as lubricin found at the interface of the two opposing articular cartilage surfaces are also important to provide lubrication on these gliding surfaces (Bhosale et al., 2008; Jay et al., 2014; Ulrich-Vinther et al., 2003).

Morphologically, articular cartilage can be divided into four different zones (from surface to bottom, Figure 1.1): the superficial zone, transitional zone, deep zone and calcified cartilage zone (Bhosale et al., 2008). The composition and architecture of the

ECM in each zone is slightly different, as are the chondrocyte morphology and functions (Bhosale et al., 2008). The superficial zone is one to three chondrocytes deep, and the cells have a flat morphology and are arranged parallel to the surface (Mollenhauer, 2008). These chondrocytes are specialised to express lubricin, which covers the surface of the superficial zone and provides lubrication to the gliding surface of articular cartilage (Schumacher et al., 1994). The superficial zone contains a relatively high collagen to proteoglycan ratio, with the collagen fibrils arranged horizontal to the surface (Ulrich-Vinther et al., 2003). The collagen fibrils are relatively thick and long in this zone (Schumacher et al., 1994). In the transitional zone, chondrocytes are rounded and arranged in an oblique, random pattern (Ulrich-Vinther et al., 2003). They express higher levels of proteoglycans and collagens (Bhosale et al., 2008). In the deep zone, chondrocytes are spherical and arranged vertically (perpendicular to the surface) in a columnar manner (Ulrich-Vinther et al., 2003). The deep zone has the highest concentration of proteoglycans and thus contains the largest amount of water (Ulrich-Vinther et al., 2003). Chondrocyte density is highest in the superficial zone and gradually decreases towards the bottom (Ulrich-Vinther et al., 2003). Finally, at the bottom of cartilage is the calcified cartilage zone. This zone is separated from the deep zone by the tidemark (Havelka et al., 1984). Chondrocytes in the calcified cartilage zone are higher in density, metabolically less active and display a hypertrophic phenotype. They are specialised to synthesise higher amounts of type X collagen, which provides an essential shock-absorbing ability to articular cartilage and protects the less resilient subchondral bone (Bhosale et al., 2008). Together, these four zones form the 2 to 5 mm thick articular cartilage covering subchondral bones in humans (Ulrich-Vinther et al., 2003).

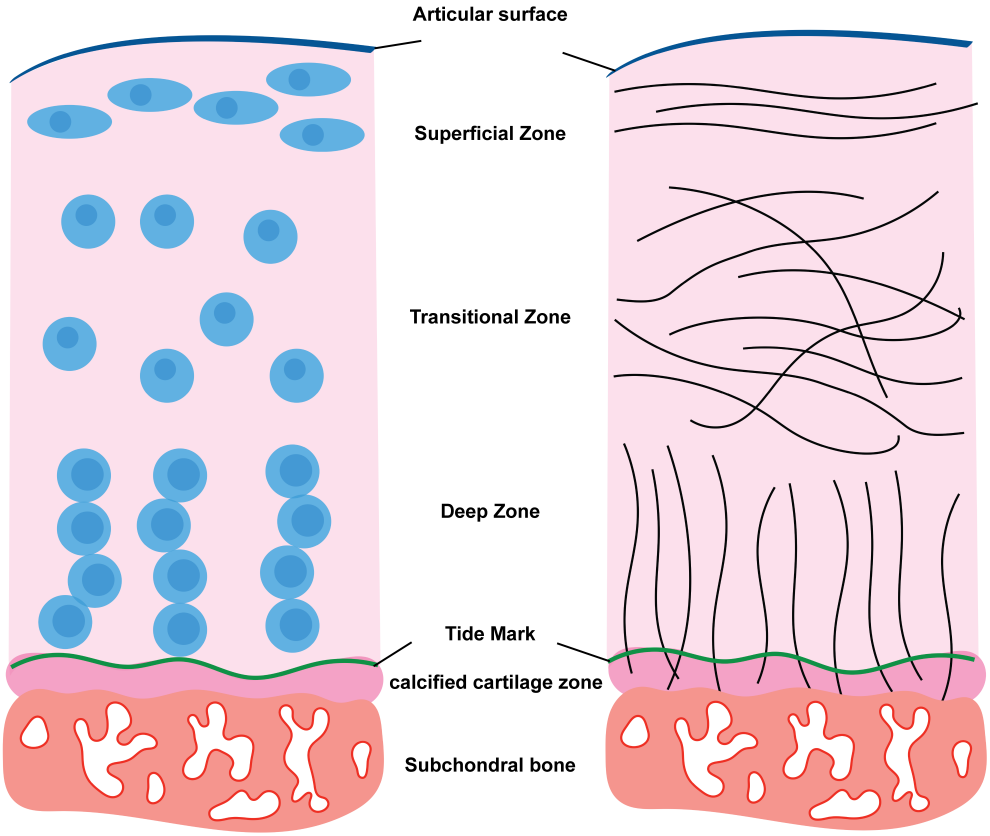

Figure 1.1 Articular cartilage can be divided into four zones according to its morphology.
Articular cartilage can be divided into 4 zones: the superficial, transitional, deep and calcified cartilage zones. The panel on the left-hand side shows the morphology of chondrocytes residing in each zone. The superficial zone chondrocytes are flat, the transitional zone chondrocytes are spherical, whilst those in the deep zone are rounded and arranged in a columnar manner. The calcified cartilage zone chondrocytes have a hypertrophic phenotype. The panel on the right-hand side illustrates the collagen fibre organisation in each zone. Collagen fibres are horizontally aligned in the superficial zone, irregularly arranged in the transitional zone and perpendicularly aligned in the deep and calcified cartilage zones.

1.1.2. Chondrocyte homeostasis and metabolism

Chondrocytes balance their anabolic and catabolic activities to maintain the articular cartilage ECM in healthy joints. Under homeostatic states, chondrocytes maintain the cartilage ECM through synthesising ECM components (e.g. type II collagen and aggrecan) and secreting ECM-degrading enzymes which remodel the ECM [e.g. matrix metalloprotease (MMP)-13, a disintegrin and metalloproteinase with thrombospondin motifs (ADAMTS)-4 and -5)] (Lin et al., 2006; Mollenhauer, 2008). Although articular cartilage is avascular and hypoxic, chondrocytes are highly responsive to the

surrounding environment. Without blood vessels, chondrocytes acquire nutrients and oxygen through diffusion from the synovial fluid and generate energy mainly through anaerobic metabolic pathways (i.e. glycolysis) (Ulrich-Vinther et al., 2003). Chondrocytes are also in constant contact with various growth factors, cytokines, chemokines and hormones which are present in the interstitial fluid and diffuse from other tissues such as the synovium (Ulrich-Vinther et al., 2003). The interactions between these factors are critical in sustaining chondrocyte homeostasis and thus, cartilage health. Various growth factor pathways are known to contribute to cartilage homeostasis, e. g. TGF-β (Shen et al., 2014; Wang et al., 2016), Wnt (Monteagudo et al., 2017; Usami et al., 2016), and IGF-1 (Schmidt et al., 2006; Zhang et al., 2017). Interestingly, studies have suggested that the effects of these pathways on cartilage may depend on cell type and context in which these pathways are activated or inhibited. For example, the TGF-β-Smad3 has been shown to have protective and catabolic effects, with mice lacking *Smad3* (both whole body knockout and cartilage-specific knockout) developing accelerated OA (Chen et al., 2012; Yang et al., 2001), but inhibition of TGF-β signalling in subchondral bone mesenchymal stem cells protecting mice from OA (Zhen et al., 2013).

In addition to signalling pathways activated by growth factors, mechanical stress is also critical in regulating chondrocyte homeostasis via mechanical force-activated signalling pathways. Cartilage is under intermittent mechanical stress in joints, and this is critical for exchanging nutrients and cellular waste within the articular cartilage ECM. When force is applied, the ECM is compressed and water flows out from the ECM, removing waste. When the force is reduced, water flows back into the tissue and brings nutrients into the ECM, nourishing chondrocytes (Ulrich-Vinther et al., 2003).

Mechanical force has also been shown to affect biosynthesis of ECM components by chondrocytes (Kim et al., 1994; Liu et al., 2016). Therefore, mechanical loading is an indispensable factor regulating chondrocyte behaviour. The cross-talk between these pathways and their cumulative effects are central to chondrocyte homeostasis and cartilage health, and are areas of active investigation. More effort in this area is crucial to unravel the mechanisms regulating cartilage health and OA development, and to uncover novel targets for developing disease-modifying OA drugs (DMOADs).

1.2. Osteoarthritis

Osteoarthritis (OA) is the most prevalent degenerative joint disease (Chen et al., 2017), and it causes tremendous global economic burden, as healthcare costs for OA are estimated to account for 1.0-2.5% of the gross domestic product in Australia, Canada, France, the UK, and the USA (March et al., 1997). It also causes immense societal burden since patients with OA suffer from severe, chronic joint pain, joint stiffness, and movement disability. Due to the unavailability of DMOADs, current therapies for OA generally involve symptomatic relief using analgesia, rather than resolving the pathogenesis and reversing disease progression (Zhang et al., 2016). Furthermore, joint replacement is generally required to alleviate pain and improve movement in advanced disease, but artificial joints are limited in terms of function and durability (Goodman et al., 2009), impairing patients' quality of life.

OA is a disease affecting the whole joint. The main defining features of OA include cartilage degradation, subchondral bone thickening, synovitis, osteophyte formation, ligament and meniscus degeneration (in the case of knee OA), and joint capsule hypertrophy (Chen et al., 2017). These features are illustrated in Figure 1.2. Previously,

these changes were thought to be the result of inevitable "wear and tear" of the ageing joints, but now research has unravelled that these structural changes are the result of cumulative abnormalities in several signalling pathways, leading to degradation of the ECM in cartilage (Berenbaum, 2013; Bland, 1983; Chanalaris et al., 2017; Koonce et al., 2013). Although our understanding of OA pathogenesis has deepened tremendously and has thus uncovered more opportunities to develop novel therapies to treat OA, DMOADs are still currently lacking, leaving a huge unmet medical need. Additional research is required to improve our understanding of OA pathogenesis and to accelerate development of DMOADs. In the following sections, I summarise our current understanding of OA and highlight outstanding knowledge gaps which require further investigation.

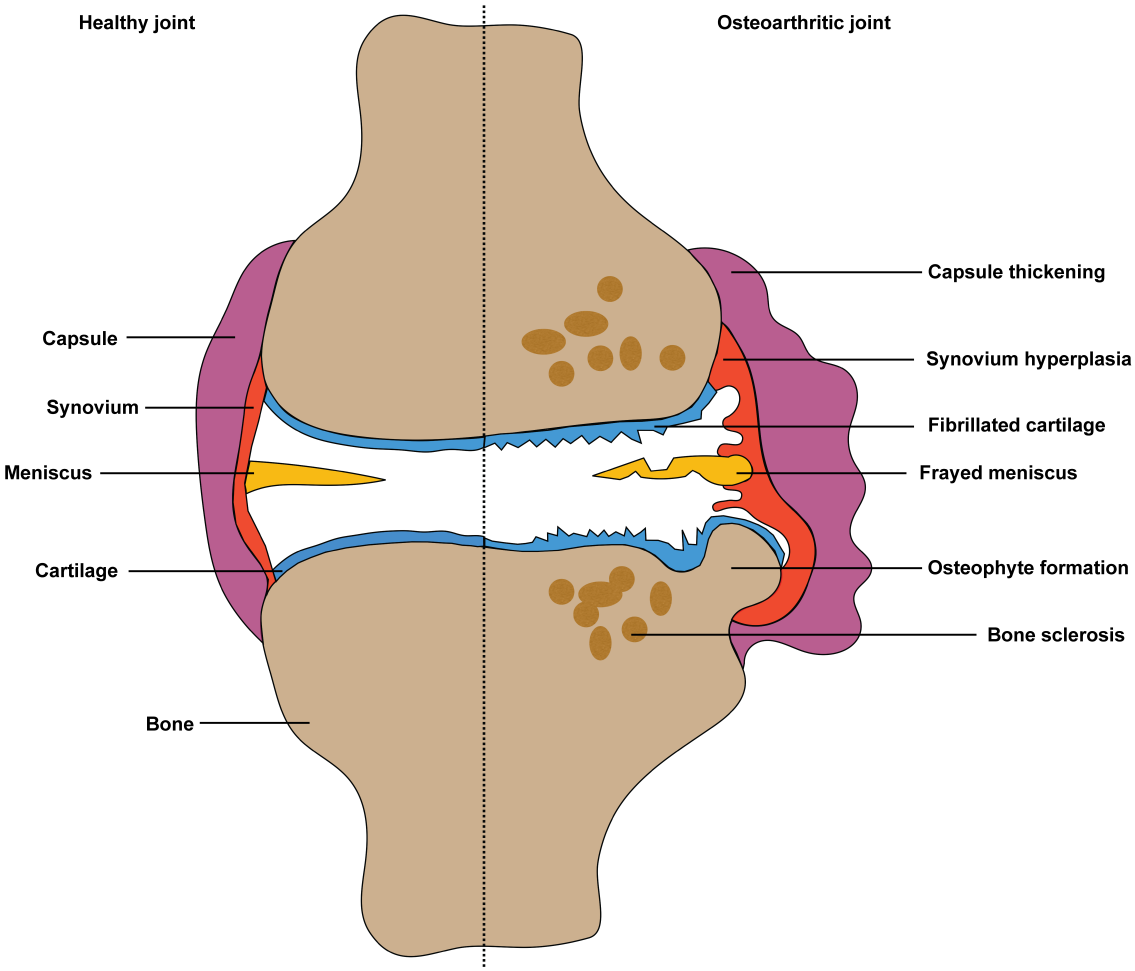

Figure 1.2 Features of osteoarthritic knee joint.
Key characteristics of knee joint OA include capsule thickening, synovitis and accompanying synovial hyperplasia, frayed meniscus, bone sclerosis, fibrillated damaged cartilage, and osteophyte formation. This causes pain and imparts movement for affected individuals.

1.2.1. OA epidemiology

OA can affect every diarthrodial joint in the body (Martel-Pelletier et al., 2016), although there are noticeable differences in prevalence and incidence of OA in different joints. For example, hand OA is reported to affect around 60% of North Americans and Europeans older than 65 years of age, while only 33% and 5% of the same population suffer from knee and hip OA, respectively (Felson et al., 1987; van

Saase et al., 1989). Importantly, the high prevalence and incidence of OA are not limited to Caucasians, with the disease affecting every ethnic group around the globe. However, considerable geographical and ethnic variations in its general prevalence and joint-specific incidence occur, as evidenced by hand OA being more frequent in white American than in Native and African American groups (Johnson et al., 2014). Similarly, hip OA is less prevalent in South-East Asian than in other ethnic groups (Martel-Pelletier et al., 2016).

Another prominent feature of OA epidemiology is that its prevalence and incidence are low in young adults, but increase dramatically with age regardless of which joint is considered, making it a disease that primarily affects the elderly (Martel-Pelletier et al., 2016). This is particularly relevant to today's society since population ageing is a global phenomenon, and the already astronomical OA healthcare costs are projected to increase substantially in the near future. Helmick et al. (2008) estimated that 25% of adults in the USA will suffer from OA by 2020, making OA one of the most challenging diseases for our healthcare system.

Finally, significant gender differences in OA prevalence and incidence are also evident in populations older than 50 years of age, with women being more susceptible to the disease (Martel-Pelletier et al., 2016). Variations in gender difference can be found in different joints, with hand and knee OA having the greatest gender disparity (Martel-Pelletier et al., 2016).

1.2.2. OA aetiology and risk factors

OA is a complex disease with compound aetiology. Similar to other complex diseases,

its development is the cumulative result of interactions between several environmental and genetic factors. Several risk factors are known to be associated with OA susceptibility, but it is not fully understood how the interplay between these risk factors leads to OA. OA risk factors can be categorised into those that increased OA susceptibility at the individual level (e. g. age, sex, and genetics), and those which affect the susceptibility of each joint in the same person (e. g. joint-specific injuries, repeated use of joints and joint anatomy and hence the mechanical loading). In the next sections, I will summarise our current understanding of some of the most relevant OA risk factors.

1.2.2.1. Ageing

Ageing is by far the most prominent risk factor for OA (Johnson et al., 2014). Except for post-traumatic OA, which is prevalent in younger people after a joint injury, OA is most commonly found in people older than 50 years old, with several studies indicating that its incidence peaks between the ages of 55 and 70 years (Losina et al., 2013; Martel-Pelletier et al., 2016; Prieto-Alhambra et al., 2014). This high incident rate and the unavailability of DMOADs result in high prevalence of OA in the elderly, with several studies conducted in multiple countries suggesting that the majority of people older than 65 years of age can be shown to have radiographic OA in one or more joints (Andrianakos et al., 2006; Dillon et al., 2006; Felson et al., 1987; Jordan et al., 2007; van Saase et al., 1989).

The molecular mechanisms by which ageing contribute to OA pathogenesis remain an active area of investigation. Research has suggested that multiple age-related changes at the tissue and cellular levels are collectively responsible for the increased OA risk in

the elderly. For example, Greene et al. (2015) suggested that ageing-related reductions in muscle mass and expansion of adipose tissues change mechanical loading of joints, which in turn leads to elevated levels of pro-inflammatory cytokines and adipokines being produced in the aged body, resulting in a chronic, low-grade inflammation (called inflammageing), that may drive the activation of catabolic processes in chondrocytes and consequently, result in ECM degradation via nuclear factor-κB (NF-κB)-dependent signalling pathways (Fernandes et al., 2002; Kapoor et al., 2011; Martel-Pelletier et al., 1999).

One of the most prominent adipose-associated, ageing-related pro-inflammatory cytokines is IL-6, and Livshits et al. (2009) identified that elevated serum IL-6 level is a strong predictor of human knee OA, suggesting that increased IL-6 levels caused by inflammageing may contribute to the association between ageing and OA. Notably, de Hooge et al. (2005) reported that male mice lacking *Il6* developed more severe spontaneous OA upon ageing, indicating that the role of IL-6 in OA pathogenesis may be complicated and more studies are needed to fully elucidate its role in OA development. Indeed, some studies suggested that IL-6 signalling mediated by membrane-bound IL-6 receptor (classical IL-6 signalling), and by soluble IL-6 receptor (IL-6 trans-signalling) may serve different, cell type-dependent functions, and soluble IL-6 receptor may be beneficial to OA (Akeson et al., 2017). A double-blinded, randomised, placebo-controlled Phase III clinical trial evaluating the effects of tocilizumab, a IL-6 receptor antagonistic monoclonal antibody, to treat hand OA is currently underway (the TIDOA study, ClinicalTrials.gov Identifier: NCT02477059). This trial is expected to be completed in 2019, and may further shed light on the role of IL-6 in OA.

Another pronounced ageing-related change in tissues is the accumulation of senescent cells (Campisi, 2013; Lopez-Otin et al., 2013). Senescent cells are arrested from the cell cycle and prevent neoplastic transformation. Various cellular insults, such as telomere shortening, DNA damage, and proto-oncogene activation, result in intracellular signalling that increases expression of the cell cycle inhibitors p16 and p21 in a p53-independent or -dependent manner, respectively (Hernandez-Segura et al., 2018). p16 and p21 are cyclin-dependent kinase (CDK) inhibitors. p16 binds to the CDK4/6 complex, preventing it from binding to cyclin D and halting cell cycle progression from G1 to S phase. During the G1 phase, cyclin D starts to be synthesised and to form complexes with CDK4 or CDK6. The cyclin D-CDK4/6 complex is the major driver of the G1-S transition, acting by directly phosphorylating the retinoblastoma protein (Rb) (Hernandez-Segura et al., 2018). Similarly, p21 binds to CDK2, preventing it from binding to cyclin E (van Deursen, 2014). The cyclin E-CDK2 complex also contributes to G1-S transition by regulating Rb phosphorylation, and may play additional roles in the S phase (Gladden et al., 2003). In its unphosphorylated state, Rb physically associates with E2F factors and impedes its transactivation domain. Once phosphorylated, pRb dissociates from E2F, allowing E2F molecules to transactivate each other, and become activated transcription factors. These transcription factors then drive the expression of a plethora of S phase-promoting genes, facilitating the G1-S transition (Otto et al., 2017). In summary, the expression of p16 and p21 is able to disrupt the formation of cyclin D–CDK4/6 and cyclin E-CDK2, which leads to the constant association of Rb and E2Fs, causing cell cycle arrest at the G1 phase. These senescence-inducing pathways are summarised in Figure 1.3. In aged joints, accumulation of p16- or p21-expressing senescent cells may lead to decreased repair capacity (Chen et al., 2017), making joints more susceptible to degeneration.

Additionally, ageing is associated with reduced autophagy, increased oxidative stress and mitochondrial dysfunction, all of which promote cell death. Together, the decreased repair capacity and increased cell death undermine tissue repair and regeneration in joints after injury and may accelerate OA pathogenesis.

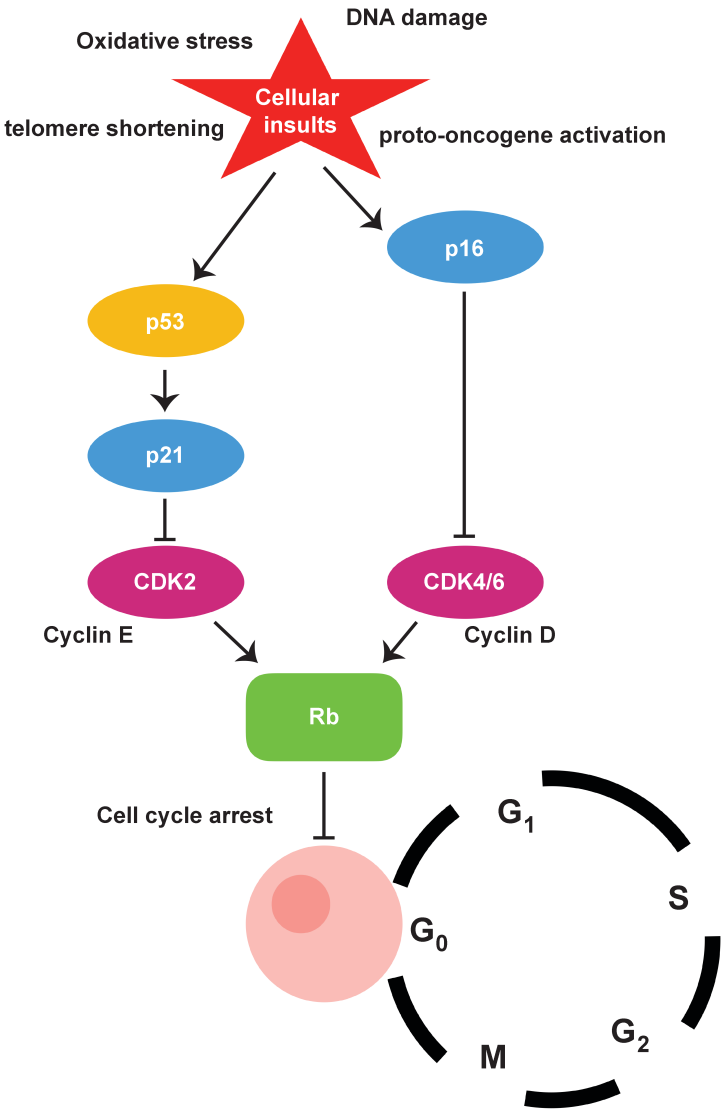

Figure 1.3 Senescence-inducing pathways.
Formation of cyclin D–CDK4/6 or cyclin E-CDK2 complexes promotes G1-S transition during cell cycle progression by phosphorylating Rb, releasing E2Fs from pRb. Released E2Fs molecules transactivate each other and drive the expression of multiple genes which are essential for cell cycle progression.Various cellular insults activate cellular senescence through the p53-p21-CDK2 axis, or the p16-CDK4/6 axis. These two pathways converge on Rb, and inhibit its phosphorylation, thereby inducing cell cycle arrest, making cells senescent.

Another characteristic of senescent cells that may contribute to OA development is the senescence-associated secretory phenotype (SASP) characterised by elevated expression of pro-inflammatory cytokines (e.g. IL-1, IL-6 and IL-8), and proteases that remodel the ECM (e.g. MMP-1, -3, -10, -12, -13, -14). Since many SASPs factors are pro-inflammatory cytokines, accumulation of senescent cells is associated with enhanced inflammageing which, as described previously can contribute to OA pathogenesis. Degradation of articular cartilage ECM components, especially aggrecan and type II collagen, is central to OA pathogenesis (reviewed by Troeberg et al., 2012). One of the SASP proteases, MMP-13, is the primary collagenase responsible for degrading type II collagen in cartilage, with Little et al. (2009) showing that *Mmp13*$^{-/-}$ mice are protected from surgically-induced OA. In parallel, SASP cytokines, such as IL-1 and IL-6, are known to dramatically induce MMP-13 expression. Therefore, senescent cells exhibiting SASP are able to maintain high levels of MMP-13 expression and to induce cartilage ECM destruction. Taken together, SASP not only contributes to OA via inflammageing, but more importantly, it shifts tissue homeostasis towards catabolic processes which degrade the cartilage ECM.

Finally, age-related increased formation of advanced glycation end-products (AGEs) by spontaneous non-enzymatic glycation of proteins and deposition of calcium pyrophosphate and basic calcium phosphate crystals up-regulate matrix-degrading enzymes and also changes the biomechanical properties of cartilage ECM, making it stiffer and more susceptible to fibrillations, which are considered to be the precursors of OA (Lotz et al., 2012). Similar changes in ECM properties are found in other joint tissues, such as ligaments (Hasegawa et al., 2012) and meniscus (Pauli et al., 2011), and may alter mechanical loading of joints.

1.2.2.2. Obesity

Obesity is a well-established risk factor for OA. Overweight individuals not only have a higher risk of developing OA (Martel-Pelletier et al., 2016), but also develop OA earlier and have more severe, less manageable symptoms (Chen et al., 2017). Traditionally, this association is considered to be due to increased weight bearing, and hence altered mechanical loading, in joints. However, obesity also increases OA susceptibility in non-weight-bearing joints. For example, a systemic review by Yusuf et al. found that people with body mass index (BMI): >25 kg m^{-2} have a risk ratio of 1.9 for hand OA (Yusuf et al., 2010), suggesting that factors other than altered mechanical loading are involved. One of these factors is thought to be increased secretion of adipokines by adipose, which trigger inflammageing (Conde et al., 2011; Das, 2001; Fain, 2010) and promote cartilage breakdown.

1.2.2.3. Injuries

Injury increases risk of post-traumatic OA and mainly affects a younger group than the majority of OA patients. Roos et al. (2005) reviewed the relevant literature and concluded that 51% of women with anterior cruciate ligament (ACL) injuries developed OA 12 years later, whilst 41% of men with the same injury developed OA after 14 years. In addition to ligament injuries like ACL, other common injuries associated with OA development are cartilage tears and joint dislocation (Chen et al., 2017). The two main pathological mechanisms are thought to be reduced joint stability after injury with concomitant changes in mechanical loading of the injured joint, and the increased inflammation associated with the injury (Chen et al., 2017). Elevated inflammation results in similar processes as described for inflammageing, and may

lead to cartilage damage and accelerated OA development.

1.2.2.4. Genetic predisposition

Although twin studies (Spector et al., 1996) and linkage analyses (Loughlin et al., 2000) have long suggested that OA has a hereditary component, recent improvements in genomics technologies (e.g. genome-wide association studies, or GWAS) have propelled identification of a large number of OA-associated genes. Taking advantage of improved pathway analysis software, alleles or SNPs identified by GWAS can now be categorised into several pathways. Although these associations require further validation, such studies have shed light on the broader picture of OA pathogenesis, and suggested a role for signalling pathways involving the TGF-β and bone morphogenetic protein (BMP) proteins (Chen et al., 2017). Both are critical in regulating development of cartilage and bone, the two most important tissues in the joint. For example, *SMAD3* (rs12901499) in the TGF-β pathway and *GDF5* (rs143383) in the BMP pathway are the two most commonly identified genes associated with OA in their respective pathway (Valdes et al., 2011), and both have been implicated in OA pathogenesis by *in vitro* and *in vivo* studies (Parrish et al., 2017; Pregizer et al., 2018; Ratnayake et al., 2014; van de Laar et al., 2011; Yang et al., 2001).

In addition to genes involved in joint development, other OA-associated genes have been mapped to pathways related to apoptosis [*ANP32A* (Valdes et al., 2009)], Wnt signalling [*SFRP3* (Loughlin et al., 2004)], and mitochondrial damage [mtDNA haplogroup T (Soto-Hermida et al., 2014) and haplogroup J (Rego et al., 2010; Rego-Perez et al., 2008)]. Several pro-inflammatory genes have also been associated with OA (e.g. *IL1*, *IL6* and *IL10*), with *IL1RN*, a gene encoding the interleukin-1 receptor

antagonist, having the strongest association reported by Valdes et al. (2011) in their review. However, most of these associations were not reproducible in large scale meta-analyses. Other immune genes, such as *MHC*-related genes, have also been reported to be associated with OA in various GWAS studies (Nakajima et al., 2010), but large scale confirmatory studies are necessary.

Two genes involved in thyroid metabolism, *DIO2* and *DIO3*, which encode a type II and III iodothyronine deiodinase, have been found to associate with OA in different European cohorts or using meta-analyses (Meulenbelt et al., 2011; Meulenbelt et al., 2008). It has been suggested that thyroid hormone may affect chondrocyte proliferation via BMP-dependent pathways (Robson et al., 2000; Williams, 2013), but it is not known how these two genes affect OA.

The final group of genes associated with OA are genes encoding ECM components, such as *COL2A1*, which was identified in a case-control study in the Mexican Mestizo population (Galvez-Rosas et al., 2010) and *COL10A1*, which was identified using hip OA patient-derived bone marrow mesenchymal stem cells (Lamas et al., 2010). Since both genes were identified using small sample sizes, large-scale meta-analyses are necessary to examine the reproducibility of these findings.

Notably, even though genetic susceptibility to OA is estimated to range from 40% to 65% depending on the joint site (Tsezou, 2014), most of these identified SNPs or gene mutations are considered to have only small to moderate effects on OA susceptibility (Martel-Pelletier et al., 2016). This points to the possibility that OA development may be the cumulative result of many small changes in cellular functions and tissue

homeostasis over several decades, and the small effect size of individual genes may hinder their identification by GWAS. Moreover, these small effects may not be easily captured by genetic manipulation or surgical OA induction in model organisms, since changes induced by these methods may be more rapid and pronounced.

1.2.3. OA pathogenesis

Although OA is now commonly regarded as a whole-joint disease (Loeser et al., 2012), articular cartilage degradation is still considered as the most prominent feature of its pathogenesis (Troeberg et al., 2012). This degradation is driven by breakdown of two major cartilage ECM components type II collagen and aggrecan. Degradation of aggrecan is driven by proteolytic enzymes termed aggrecanases and researchers have identified several different aggrecanases, all of which belong to the family named a disintegrin and metalloproteinase with thrombospondin motifs (ADAMTS-1, -4, -5, -8, -9, -15, -16 and -18) (Abbaszade et al., 1999; Collins-Racie et al., 2004; Gendron et al., 2007; Kuno et al., 2000; Little et al., 2002; Sandy, 2006; Sandy et al., 2001; Somerville et al., 2003; Tortorella et al., 1999; Zeng et al., 2006). Amongst them, ADAMTS-4 and -5 exhibit greatest aggrecan-cleaving activity *in vitro* (Gendron et al., 2007), leading researchers to suspect these two enzymes to be the main aggrecanases *in vivo*. Subsequently, two knockout mouse studies performed by Stanton et al. (2005) and Glasson et al. (2005) showed that ADAMTS-5 is the major aggrecanase in a surgical destabilisation of the medial meniscus (DMM) model of OA and an inflammatory arthritis model, as mice-lacking ADAMTS-5 were protected from aggrecan cleavage and cartilage degradation in both models, and exhibited decelerated OA progression. Conversely, an ADAMTS-4 deletion experiment performed by Glasson et al. (2004) concluded that ADAMTS-4 has a limited role in the murine joint. However, *in vitro*

studies using bovine, porcine and human cartilage, synovium, and chondrocytes showed that ADAMTS-4 is more responsive to various pro-inflammatory stimuli including IL-1 and TNF, suggesting that ADAMTS-4 may have a more active role in the joints of these species (Bondeson et al., 2008; Verma et al., 2011). Therefore, which enzyme is more important for OA development in human cartilage remains debatable.

In addition to aggrecan degradation, subsequent breakdown of type II collagen is also thought to be central to OA pathogenesis. Neuhold et al. (2001) showed that inducible over-expression of human MMP-13 in cartilage caused cartilage breakdown, resulting from increased type II collagen degradation. Moreover, two *Mmp13* knockout mouse studies showed that *Mmp13* deficiency significantly decelerated the progression of surgically-induced cartilage breakdown and OA progression and reduced type II collagen cleavage (Little et al., 2009; Wang et al., 2013). Interestingly, the knockout mouse study performed by Little et al. (2009) and a study conducted by Pratta (2003) demonstrated that aggrecan degradation precedes type II collagen breakdown, implying that aggrecan protects type II collagen from MMP-13 cleavage.

Although the main enzymes responsible for cartilage breakdown have been characterised, mechanisms regulating their expression and activity in OA remain an active area of investigation. Pro-inflammatory cytokines (e.g. IL-1, IL-6, and TNF) or mediators (e.g. prostaglandin E2, nitric oxide, and complements), and ECM-derived breakdown products (e.g. fibronectin fragments and hyaluronic acid) have all been suggested to modulate protease activity in the joint (Martel-Pelletier et al., 2016). These changes are summarised in the following sections, with a particular emphasis on the role of chondrocytes in OA pathogenesis.

1.2.3.1. Role of chondrocytes in OA development

Chondrocytes are the only cell type found in cartilage and they are responsible for maintaining cartilage homeostasis. Several models have been proposed regarding how changes in chondrocyte homeostasis initiate OA pathogenesis. One of these models is the PCM-initiated OA development model. Under physiological conditions, chondrocytes reside within a pericellular matrix (PCM) composed of type VI collagen and other PCM proteins such as fibronectin 1 and perlecan (Guilak et al., 2018; Wilusz et al., 2014). Since chondrocytes are enclosed in the PCM (a chondrocyte and its PCM are called a "chondron"), the PCM mediates the interactions between chondrocytes and their surrounding environment, acting as a transducer of various molecular and osmotic signals (Guilak et al., 2018). Additionally, the PCM is sensitive to mechanical loading, potentially through mechanical sensors such as connexin 43 (Cx43) (McGlashan et al., 2006; Ruhlen et al., 2014) and ion channels such as transient receptor potential vanilloid 4 (TRPV4), which is expressed on the primary cilia of chondrocytes (Phan et al., 2009). These mechanical sensors can trigger various signalling pathways which play critical roles in cartilage homeostasis (Guilak et al., 2018; Wilusz et al., 2014). Moderate mechanical loading is critical for maintaining cartilage health, as both under- and over-loading increase OA risk (Leong et al., 2014; Sun, 2010). Moderate loading has been reported to inhibit the NF-κB pathway, which activates expression of several proteases (Goldring et al., 2009; Kapoor et al., 2011; Leong et al., 2014; Rigoglou et al., 2013; Yasuda, 2011), and induces anti-inflammatory responses (Chowdhury et al., 2006; Ferretti et al., 2006; Leong et al., 2011; Ramachandran et al., 2011). The PCM model proposes that changes in the PCM cause altered mechanical sensing, which in turn, contributes to OA pathogenesis.

Another model of OA pathogenesis recognises the importance of an environmental

factor, hypoxia, in maintaining cartilage homeostasis. In healthy cartilage, chondrocytes reside in a low oxygen tension environment, which induces the expression of hypoxia-inducible factor (HIF) 1α and 2α. HIF1α is crucial for protecting cartilage, potentially through inhibiting Wnt/β-catenin signalling, hence preventing expression of MMP-13 (Bouaziz et al., 2016; Thoms et al., 2013), whilst HIF2α induces anabolic responses in cartilage by directly binding to the regulatory site of *SOX9* (Thoms et al., 2013), the master regulator of chondrogenesis (Bell et al., 1997; Bi et al., 1999; Hino et al., 2014; Ng et al., 1997). Late stage OA chondrocytes express elevated levels of hypertrophic markers (e. g. type X collagen) (Alvarez et al., 2000; Kirsch et al., 1992; Nurminskaya et al., 1996), as well as angiogenic factors (e. g. VEGF), which change chondrocyte phenotypes and lead to cartilage vascularisation, innervation and calcification, contributing to joint degeneration and pain (Chen et al., 2017; Hunter et al., 2006; Martel-Pelletier et al., 2016).

Finally, a developmental model has also been proposed which links chondrocyte developmental processes to OA. OA articular chondrocytes have been shown to recapitulate pathways occurring in developing growth plate hypertrophic chondrocytes. For example, in early OA, elevated overall GAG synthesis and an increased chondroitin-6-sulfate to chondroitin-4-sulfate ratio have been documented, resembling fetal cartilage (Bayliss et al., 1999; Roughley et al., 1980; Sandy et al., 1987). Similarly, expression of type X collagen, a marker of hypertrophic chondrocytes, is also found in OA chondrocytes (Hoyland et al., 1991; von der Mark et al., 1992). Many other molecular characteristics associated with chondrocyte hypertrophy, including SOX9 down-regulation, MMP-13 up-regulation, increased apoptosis, and angiogenesis, are also found in OA chondrocytes (Pitsillides et al., 2011), and some of

these molecular features have been shown to contribute to OA pathogenesis. One prime example is MMP-13, which is critical in degrading type II collagen, and thus in cartilage breakdown. Whether re-activation of these developmental pathways is a consequence or cause of OA pathogenesis remains to be determined, but it is likely that more investigation into this question may uncover novel drug targets that could be used to develop DMOADs.

1.2.3.2. Role of subchondral bone in OA development

Like cartilage, subchondral bone shows gradual changes with OA progression. At early stages of OA development, subchondral bone exhibits increased vascularisation and reduced bone density, caused by increased bone remodelling. The underpinning mechanism of elevated bone remodelling remains unclear, but pro-inflammatory cytokines (e.g. IL-1 and IL-6), growth factors associated with OA (e. g. TGFβ and IGFs) and catabolism-promoting molecules which are up-regulated in OA (e. g. prostaglandin E2) are all known promoters of bone remodelling (Burr et al., 2012; Mansell et al., 2007; Massicotte et al., 2002). Additionally, the RANKL/RANK-NF-κB pathway may also contribute to bone remodelling (Boyce et al., 2015). As mentioned in Section 1.2.3., cartilage breakdown generates a positive feedback loop producing more pro-inflammatory cytokines and pro-catabolic molecules, which exacerbates cartilage ECM destruction. Since these factors also contribute to bone remodelling, crosstalk between cartilage and subchondral bone may enhance bone remodelling (Burr et al., 2012; Goldring, 2009).

In late stage OA, subchondral bone sclerosis becomes apparent, characterised by reduced bone turnover, thickening of calcified cartilage and thinning of trabeculae

(Karsdal et al., 2008). Subchondral sclerosis is known to dramatically change the mechanical properties of subchondral bone, by reducing mineralisation and increasing bone volume (Grynpas et al., 1991). Decreased mineralisation has been linked to increased production of TGFβ and dysregulated Wnt signalling in osteoblasts (Chan et al., 2011). Elevated TGFβ production promotes formation of osteophytes, which contribute to joint space narrowing seen in radiographic OA (van der Kraan et al., 2007). Notably, although subchondral sclerosis is a prominent feature of OA, research suggests that increased subchondral bone density alone does not lead to OA (Burr et al., 2012), and the relationship between subchondral sclerosis, cartilage breakdown, and synovial inflammation in OA pathogenesis remains to be defined.

1.2.3.3. Role of synovium and synovial inflammation in OA development

The synovium is composed of the synovial membrane and synovial fluid, and is critical in providing lubricant factors for the articular surface (Scanzello et al., 2012). It is well-characterised that synovitis, featuring lymphocyte infiltration and synovial hyperplasia, is a common feature of OA (Scanzello et al., 2012). Studies have established that synovitis correlates with structural damage to the joint and OA progression, however, the roles of inflammation in OA development remain controversial (Goldring et al., 2011). As mentioned in Section 1.2.3., pro-inflammatory cytokines resulting from cartilage breakdown trigger up-regulation of ECM-degrading proteases, leading to further cartilage damage. Additionally, damage-associated molecular patterns (DAMPs) , which are potentially derived from apoptotic chondrocytes, and Toll-like receptors (TLRs), integrins or receptor for advanced glycation end-products (RAGE), have also been shown to sustain chronic inflammation and production of catabolic molecules (Houard et al., 2013; Liu-Bryan et

al., 2015; Loeser et al., 2012; Scanzello et al., 2012).

Interestingly, Wang et al. (2011) suggested that components of the classical complement pathway also play a role in OA pathogenesis. By conducting proteomic and transcriptomic analyses of synovial fluids and membranes, they identified that activation of the membrane attack complex (MAC) in the classical complement pathway was higher in OA joints than in healthy controls. They validated these results using *C5*, *C6*, and *CD59a*-deficient mice (all three are MAC components) and illustrated that *C5*-deficient mice were protected against meniscectomy-induced OA. Mechanistically, MAC activation may contribute OA pathogenesis through up-regulation of ECM-degrading proteases (e. g. MMP-13, ADAMTS4 and ADAMTS5) and pro-inflammatory cytokines (e. g. CCL2, CSF1, and CCL5) (Wang et al., 2011). Since *C5* whole body knockout mice were used in their study, effects of *C5*-deficiency on different joint tissues could not be differentiated. Further research using tissue-specific knockout mice will be necessary to fully dissect the relative contribution of cartilage, synovium and subchondral bone in complement-mediated OA pathogenesis.

1.2.3.4. ADAMs in OA pathogenesis

Multiple ADAMs have been suggested to contribute to OA development. For example, expression of ADAM8, 9, 10, 12, 15, 22, 23, 28, 33 have all been reported to increase in OA cartilage (Yang et al., 2017). However, most of these studies were observational and focused on expression at the mRNA level. These studies did not take into account that activities of ADAMs are often regulated post-translationally and by their subcellular localisation. Detailed review of these findings and the current knowledge gap regarding ADAMs' roles in OA pathogenesis are beyond the scope of this

introduction, but are reviewed by my colleagues and I in a recently published literature review (Yang et al., 2017). In the following sections, I will first focus on summarising our understanding of ADAM proteases, and highlight the roles of ADAM15 in OA pathogenesis.

1.3. ADAM proteases

The A Disintegrin and Metalloproteinase (ADAM, or adamalysin) family are conserved type-I transmembrane multi-domain metalloproteinases belonging to the metzincin superfamily of metalloproteases, and they are highly homologous to other metzincins such as ADAMTSs and MMPs (Giebeler et al., 2016; Yang et al., 2017). ADAMs have been shown to be critical in fine-tuning cell adhesion, migration, proteolysis and signalling, thereby regulating various physiological processes such as inflammation, wound healing and fertilisation. Dysfunctional or aberrant ADAM activities contribute to the development of a variety of diseases ranging from osteoarthritis, Alzheimer's disease, cancers, to cardiovascular diseases (Edwards et al., 2008; Seals et al., 2003).

1.3.1. ADAM topology and domain functions

All ADAMs share a similar domain structure and contain a pro-domain, a metalloproteinase domain, a disintegrin domain, a cysteine-rich domain (because of these three conserved domains, ADAMs are historically known as MDC proteins, or metalloproteinase/disintegrin/cysteine-rich proteins), and an EGF-like domain, a transmembrane domain, and a cytoplasmic tail (Giebeler et al., 2016). The ADAM domain structure is illustrated in Figure 1.4.

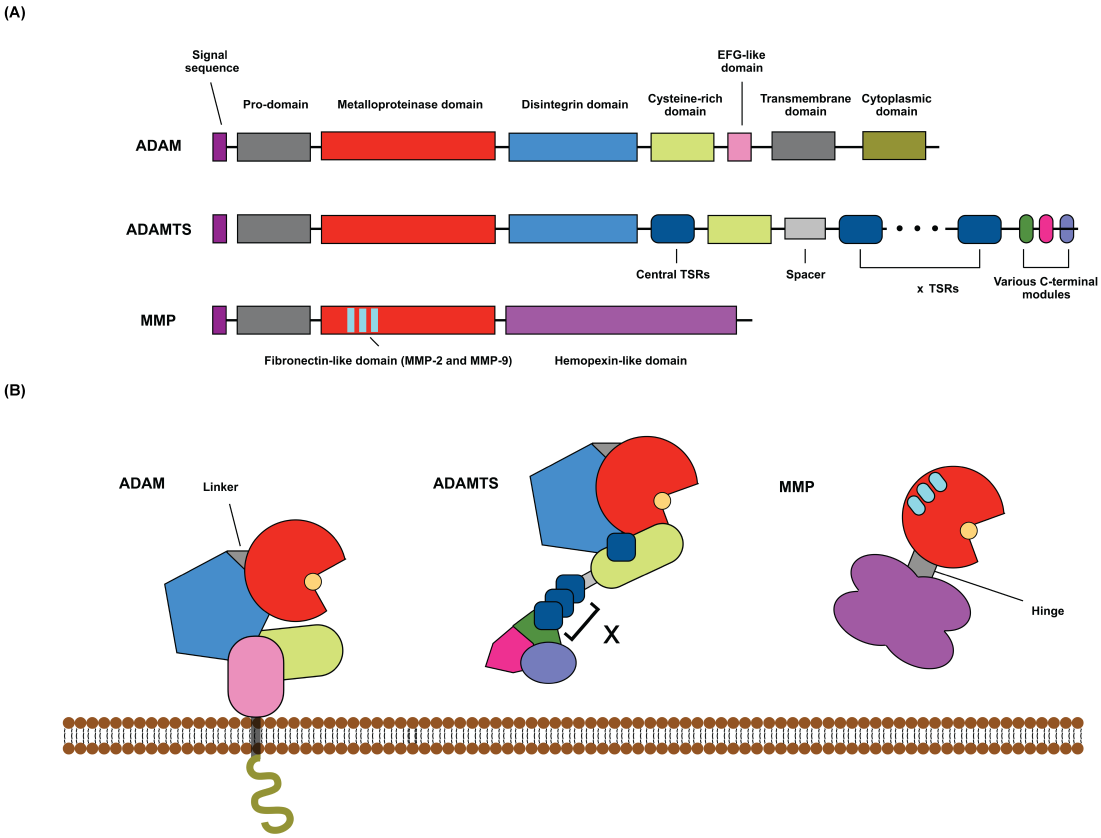

Figure 1.4 The schematic topography of ADAM, ADAMTS, and MMP protein structure.
ADAMs are highly conserved metalloproteinases sharing similar domain topography. Starting from the N-terminal is a signal peptide, a pro-domain, a metalloproteinase, disintegrin-like, cysteine-rich, epidermal growth factor (EGF)-like, transmembrane and cytoplasmic tail domains.
(A) Representative schematic modular structure, from N-terminus to C-terminus, of ADAMs, ADAMTSs and MMPs.
(B) Diagrammatic topology of the same three metzincins. Orange circle in **(B)** represents zinc ion in the catalytic domain of these metzincins. This zinc ion is essential for the proteolytic activity of the enzymes and binds to their conserved HEXGHXXGXXHD motif (found in most metalloproteinases) to achieve cleavage of target peptide bonds in substrate proteins.

1.3.1.1. The pro-domain

Like many other proteases, ADAMs are synthesised intracellularly as inactive zymogens, in which the pro-domain at the N-terminus keeps the metalloproteinase domain inactive through a "cysteine switch" mechanism commonly found in metalloproteinases, where a cysteine residue in the pro-domain binds to the zinc ion which is required for catalysing proteolysis (Van Wart et al., 1990).

After their synthesis, ADAMs enter the secretory pathway and are activated by furin-mediated removal of their pro-domain in the Golgi apparatus. Most ADAM zymogens contain a conserved furin or other proprotein convertase (PCs) cleavage site (e.g. Rx(R/K)R) at the boundary between the pro-domain and the metalloproteinase domain (Seals et al., 2003; Wong et al., 2015). Several *in vitro* and *in vivo* studies support that furin and other PCs are critical in ADAM zymogen activation. For example, Anders et al. (2001) showed that furin and PC over-expression increased levels of processed ADAM10, whilst inhibition of these convertases blocked ADAM10 processing. Additionally, mutation of the Rx(R/K)R PC cleavage site impeded ADAM10 (Anders et al., 2001), ADAM12 (Loechel et al., 1998), and ADAM19 (Kang et al., 2002) maturation. Finally, furin has been shown to cleave ADAM15 *in vitro* and Lum et al. (1998) showed in pulse-chase experiments that the pro-domain of mouse ADAM15 was removed by furin in a late Golgi compartment, providing a first evidence that ADAM15 maturation happens intracellularly. Additionally, important non-inhibitory functions of the pro-domains have also been uncovered. Studies performed on ADAM9 and ADAM17 suggest that the pro-domain may act as a chaperone and that it is important for correct folding and to prevent degradation of ADAMs (Milla et al., 1999; Roghani et al., 1999). Furthermore, studies performed on ADAM10 and 17 indicate that the pro-domain may also have a role in regulating intracellular trafficking of ADAMs (Anders et al., 2001; Gonzales et al., 2004). Therefore, the pro-domain is crucial in regulating maturation of ADAMs through multiple mechanisms.

1.3.1.2. The metalloproteinase domain

Although all ADAMs have a conserved metalloproteinase domain, not all of them are

proteolytically active. To date, 34 ADAMs have been identified across all species and 20 of them are present in the human genome (Yang et al., 2017). 8 of these human ADAMs are considered to be proteolytically inactive. Although their biological functions have not been fully elucidated, they are generally considered to play roles in regulating cell adhesion and migration (Duffy et al., 2011). The other 12 ADAMs (ADAM8, ADAM9, ADAM10, ADAM12, ADAM15, ADAM17, ADAM19, ADAM20, ADAM21, ADAM28, ADAM30 and ADAM33) share a conserved HEXGHXXGXXHD zinc-binding motif and a downstream 'Met turn' in the metalloproteinase domain, and are therefore predicted to be proteolytically active and capable of cleaving protein substrates in a zinc ion-dependent manner (Edwards et al., 2008). These catalytically active ADAMs are generally considered as sheddases, i. e. they cleave their trans-membrane substrates at a juxta-membrane position, releasing the ectodomain from the cell surface (Duffy et al., 2011; Edwards et al., 2008; Yang et al., 2017).

Most studies regarding ADAMs' roles as sheddases have been performed on ADAM10 and 17. Both enzymes show broad substrate selectivity and display basal level, constitutive catalytic activities which can be elevated by various stimuli and intracellular signalling (Le Gall et al., 2010; Maretzky et al., 2015; Matthews et al., 2017). Substrates of ADAM10 include Notch (Pan et al., 1997), N-cadherin (Reiss et al., 2005), E-cadherin (Maretzky et al., 2005), VE-cadherin (Schulz et al., 2008), ephrin A5 (Janes et al., 2005), and amyloid precursor protein (APP) (Slack et al., 2001) to name a few. Due to its ability to shed Notch receptors, ADAM10 is considered to play critical roles in embryonic development, as Notch signalling is required for embryogenesis (Artavanis-Tsakonas et al., 1999; Lewis, 1998; Schweisguth, 2004). Indeed, *Adam10*-deficiency was found to be embryonic lethal (Hartmann et al., 2002).

Various ADAM17 substrates have also been reported, including pro-TNFα (Black et al., 1997), TNF receptors (Peschon et al., 1998; Reddy et al., 2000), pro-EGFs (Sahin et al., 2004), IL-1 receptors (Reddy et al., 2000), L-selectin (Peschon et al., 1998), VCAM-1 (Garton et al., 2003), IL6 receptor (Chalaris et al., 2007), and pro-amphiregulin (Gschwind et al., 2003). Given the central roles of EGFs in embryogenesis (Wang et al., 2006a), the ability of ADAM17 to regulate EGF signalling through pro-EGF shedding (especially HB-EGF) suggests it also plays a crucial role in embryo development, and mice lacking *Adam17* are perinatally lethal (Peschon et al., 1998). Additionally, *Adam17* deletion in mice completely abolishes TNF release in response to pro-inflammatory stimuli (Black et al., 1997), indicating its irreplaceable role in TNF shedding, and it is also named TNFα-converting enzyme (TACE) based on this finding. Interestingly, ADAM10 and 17 also have the largest metalloproteinase domains of the proteolytically active ADAMs, which may partially explain their broad substrate specificity.

Substrates of the other ADAMs are less well characterised and have been mainly identified from *in vitro* analysis of candidate substrates using non-systematic methods [substrates of ADAMs were reviewed elsewhere (Duffy et al., 2011; Edwards et al., 2008)]. Few agnostic substrate discovery studies have been carried out for these ADAMs. Therefore, the biologically relevant substrates and roles of these ADAMs are less well understood. Whether these ADAMs act as active sheddases, active proteases which performs non-sheddase functions, or have other non-catalytic roles remains to be further defined.

1.3.1.3. The disintegrin domain

The ADAM disintegrin domain is homologous to the disintegrin domains of the snake

venom haemorrhagic metalloproteinases (SVMPs). The snake venom disintegrins are known for their ability to bind to human integrins via their RGD motif and to disrupt platelet aggregation (Calvete et al., 2005). Similarly, the ADAM disintegrin domain is considered to play important roles in mediating protein-protein interactions, particularly via binding to integrins (Duffy et al., 2011; Edwards et al., 2008; Giebeler et al., 2016; Yang et al., 2017). However, with the exception of ADAM15 which has a conserved RGD motif in its disintegrin domain, human ADAMs do not have the RGD motif and interact with integrins mainly via aspartic acid-containing xCD sequences (Giebeler et al., 2016). Since integrins are important regulators of cell adhesion, migration and outside-in signalling (Stupack, 2007), ADAMs have been suggested to regulate these cellular processes via their disintegrin domain.

1.3.1.4. The cysteine-rich domain

The cysteine-rich domain contains a significant number of cysteine residues (more than 10) (Heinlein et al., 1994), and its function is poorly understood. Studies have proposed that it regulates the binding specificity of the disintegrin domain. For example, Gaultier et al. (2002) demonstrated that binding of the ADAM13 disintegrin domain to fibronectin is dependent on the cysteine-rich domain, whilst Thodeti et al. (2003) suggests that the cysteine-rich domain in ADAM12 supports the binding of its disintegrin domain to syndecan-4. In one of the few studies looking at the role of the cysteine-rich domain *in vivo*, Smith et al. (2002) showed in domain-swapping experiments that the cysteine-rich domain of ADAM13 regulates its substrate specificity *in vivo*.

1.3.1.5. The EGF-like domain

The EGF-like domain contains 6 highly conserved cysteine residues with characteristic spacing (Lu et al., 2010). The functional importance of the EGF-like domain is even less well understood than that of the cysteine-rich domain. Since this domain is absent in ADAM10 and ADAM17, and these two sheddases are highly active, it is unlikely that the EGF-like domain is essential for the catalytic activity of ADAMs (Edwards et al., 2008), and its functional importance remains to be elucidated.

1.3.1.6. The cytoplasmic tail

ADAMs, unlike ADAMTSs and MMPs which are both secreted proteases, are transmembrane proteases and have intracellular tails, which are the most variable domains in terms of length and sequence. Many human ADAM cytoplasmic domains contain proline-rich Src homology (SH)-2 and/or SH3-binding sites, indicating that they are able to trigger intracellular signalling (Seals et al., 2003). Some of them also contain potential serine-threonine and/or tyrosine phosphorylation sites, making them plausible adaptors for conveying communication between the cell and its surroundings (Seals et al., 2003). The biological significance of these signalling events is an active area of research.

1.3.2. Regulation of ADAM proteolytic activity

As with all genes, expression of ADAM genes can be regulated at the transcriptional, post-transcriptional and post-translational levels. Since ADAMs regulate numerous homeostatic cellular processes such as inflammation, cell fate determination and cell migration, ADAM proteolytic activities need to be tightly regulated to maintain health.

Dysregulated ADAM activities can lead to various diseases, as evident from *Adam* knockout mouse studies. The most severe phenotype is found in *Adam10*, *17* and *22*-deficient mice, which are embryonic, perinatal and postnatal lethal, respectively (Hartmann et al., 2002; Peschon et al., 1998; Sagane et al., 2005), demonstrating the important roles of these genes in developmental processes. Some *Adam* deficiencies lead to more subtle abnormalities, such as impaired spatial learning and reduced pain perception in *Adam11*-deficient mice (Takahashi et al., 2006a; Takahashi et al., 2006b), while *Adam3* deficiency leads to male infertility in mice, indicating its indispensable role in fertilisation (Cho et al., 1998). Finally, *Adam8*, *9*, and *33* deficiencies cause no apparent pathology, suggesting that redundancy may exist for these proteases. Phenotypes of these *Adam* knock out mice are reviewed by Edwards et al. (2008).

Regulation of ADAM proteolytic activities is achieved by transporting ADAMs and their substrates into or out of membrane micro-domains, regulating surface levels of ADAMs through membrane trafficking (e. g. entering the secretory pathways and endocytosis), and by binding to endogenous inhibitors, such as Tissue inhibitors of metalloproteinases (TIMPs). In the following sections, I summarise our current understanding of these regulatory mechanisms. Notably, a huge part of our current understanding of ADAM regulation has been gained from extensive investigation of ADAM10 and 17, and extrapolation of these findings needs to be done with caution.

1.3.2.1. Transcriptional regulation of ADAMs

Expression of *ADAMs* has been found to change in various diseases, including cancer, rheumatoid arthritis, atherosclerosis and inflammatory lung diseases (Baren et al., 2012; Dreymueller et al., 2015; Isozaki et al., 2013; Kappelhoff et al., 2017; Oksala et al.,

2009; Scarisbrick, 2008; van der Vorst et al., 2012; Yang et al., 2017), suggesting that changes in their catalytic activity and/or protein-protein interactions may contribute to pathogenesis of these diseases. Several stimuli have been suggested to affect *ADAM* expression. For example, retinoic acid, sirtuin-1, and X-box binding protein (XBP)-1 are all reported to up-regulate *ADAM10* expression at the mRNA level (Nikolaev et al., 2009; Theendakara et al., 2013; Tippmann et al., 2009), whilst melatonin is able to activate transcription of both *ADAM10* and *ADAM17* (Shukla et al., 2015).

1.3.2.2. Alternative splicing of ADAMs

Multiple ADAMs can be alternatively spliced, often in the cytoplasmic tail [e. g. ADAM15 (Kleino et al., 2007; Kleino et al., 2009; Zhong et al., 2008), ADAM22 (Sagane et al., 1998), ADAM29 and 30 (Cerretti et al., 1999)]. Such splicing affects membrane anchoring and also signal transduction capability, as has been shown for ADAM15, where alternative splicing results in differential binding affinity for SH3, with the splicing isoforms associated with cancer progression (Kleino et al., 2007; Kleino et al., 2009; Zhong et al., 2008). However, in most ADAMs, the functional consequences of cytoplasmic tail alternative splicing remain unclear.

In contrast, alternative splicing of ADAM9 (Hotoda et al., 2002), ADAM10 (Yavari et al., 1998), ADAM12 (Gilpin et al., 1998; Shi et al., 2000), and ADAM28 (Roberts et al., 1999) results in expression of secreted forms of the proteases. Some of these secreted forms have been shown to retain catalytic activity. For example, alternative spliced, secreted ADAM12 cleaves insulin-like growth factor-binding protein (IGFBP)-3 and -5. Both IGFBPs have been associated with OA, thus implicating ADAM12 in OA pathogenesis (Clemmons et al., 2002; Wei et al., 2015).

Alternative splicing can also affect where ADAMs are expressed in the body. For example, secreted ADAM28 is highly expressed in the spleen, while membrane-anchored ADAM28 is preferentially found in lymph nodes (Roberts et al., 1999). Adding to the complexity, species differences exist in alternatively splicing (e. g. ADAM28 has 3 isoforms in mouse but only 2 in humans). Research using patient samples or humanised mice may be necessary to fully elucidate the biological significance of alternatively spliced ADAM isoforms.

1.3.2.3. Post-translational modifications of ADAMs

The most evident post-translational modification of ADAMs is pro-domain removal, which is a common mechanism regulating ADAM proteolytic activity. Other post-translational modifications, though less thoroughly investigated, have also been identified. For example, ADAM10 (Escrevente et al., 2008) and 17 (Peiretti et al., 2003) have been reported to exist in N-glycosylated forms. Although the functional consequences of such post-translational modifications are unclear, these modifications may affect ADAM functions. For example, Escrevente et al. (2008) reported that, dependent on its location, N-glycosylation can affect degradation of ADAM10 and its subcellular localisation, while serine and threonine phosphorylation of the ADAM17 cytoplasmic domain affects its proteolytic activity and may be responsible for phorbol ester (PMA)- and EGF-induced ADAM17 activation (Diaz-Rodriguez et al., 2002; Fan et al., 2003). The specific effects of phosphorylation at each potential serine and threonine phosphorylation site, and which residue is phosphorylated in response to individual ADAM17 activators, remains an area of fierce debate, since contradictory data have been reported (Gooz, 2010).

1.3.2.4. Regulation of ADAM subcellular localisation

As mentioned in Section 1.3.1.1., the maturation of ADAMs happens intracellularly in the Golgi apparatus. ADAMs, regardless of their function as sheddases or as binding partners of other membrane proteins such as integrins, need to be transported to the plasma membrane to exert their functions. Trafficking of these enzymes thus offers a way to regulate their activities. For example, Lorenzen et al. (2016) reported that without stimulation, only a fraction of active ADAM17 is found on the plasma membrane, since active ADAM17 is constantly internalised through clathrin-mediated endocytosis, resulting in the majority of the enzyme been localised intracellularly. Upon PMA stimulation, active ADAM17 is rapidly re-localised to the surface, greatly enhancing its accessibility to substrates and hence proteolytic activity. This elevated ADAM17 activity is quickly resolved, in part through re-internalisation and degradation of the enzyme (Lorenzen et al., 2016). Moreover, some ADAMs, such as ADAM17 (Tellier et al., 2006) and 19 (Wakatsuki et al., 2004), are sequestered in cholesterol-rich lipid rafts, hence their activities are regulated by accessibility of their ligands. Tellier et al. (2008; 2006) further supported this hypothesis by showing that disruption of lipid rafts increases the shedding of ADAM17 substrates without increasing the activity of ADAM17. This observation raises the possibility that the selectivity of ADAM ectodomain shedding may be determined by which ligands enter the lipid raft. This led Hartmann et al. (2013) to propose that the selectivity of some ADAMs may, at least in part, be rooted in their ligands rather than being an intrinsic feature of the ADAMs themselves.

Finally, as mentioned in Section 1.3.2.2., some ADAMs exist in both secreted and membrane-anchored forms. The secreted ADAMs may cleave their substrates in the

extracellular space, as demonstrated by soluble ADAM12, which cleaves IGFBP-3 (Shi et al., 2000). Additionally, Lee et al. (2012) reported that ADAM15 was found in exosomes secreted by macrophages, and that such exosomes showed anti-tumour activity, through an undetermined mechanism. These studies suggest that release of ADAMs from cells may be another way to regulate the location of their activities.

1.3.2.5. Endogenous regulators of ADAMs

The proteolytic activities of ADAMs can be regulated by endogenous inhibitors, particularly TIMPs. To date, four mammalian TIMPs, TIMP-1 to TIMP-4, have been identified (Murphy, 2011). TIMPs have an N-terminal domain which fits tightly (Ki ≈ 1 nM) into the catalytic domain of metalloproteinases, thereby hindering access of substrates to the catalytic domain, whereas their C-terminal is important for interacting with their binding partners (Brew et al., 2010). Although originally discovered as endogenous inhibitors of MMPs, TIMPs also inhibit other metalloproteinases. For examples, TIMP-1 inhibits ADAM10 (Amour et al., 2000), TIMP-2 inhibits ADAM12 (Jacobsen et al., 2008), and TIMP-4 inhibits both ADAM17 (Lee et al., 2005) and ADAM28 (Mochizuki et al., 2004). TIMP-3 has by far the broadest inhibitory profile, and inhibits the proteolytic activities of ADAM10, ADAM12, ADAM17, ADAM19 and ADAM33 (Murphy, 2011). It is also the only TIMP that can inhibit both ADAMs and ADAMTSs, with TIMP-3 shown to inhibit ADAMTS-1 (Rodriguez-Manzaneque et al., 2002), ADAMTS-4 (Kashiwagi et al., 2001), ADAMTS-5 (Kashiwagi et al., 2001), and weakly, ADAMTS-2 (Wang et al., 2006b). Interestingly, TIMP-1 (Moss et al., 2016), TIMP-2 (Kuefer et al., 2006) and TIMP-3 (Maretzky et al., 2009b) have been suggested to inhibit ADAM15, but detailed biochemical characteristics of these interactions have not been characterised.

1.4. ADAM15 protects murine joints against OA development

Adam15 expression is high in cartilage (Horiuchi et al., 2003), and Bohm et al. (1999; 2005) investigated the function of this enzyme in the joint. They firstly showed that *ADAM15* expression was higher in OA cartilage compared to in healthy control by *in situ* hybridisation (Bohm et al., 1999) [notably, more recent, microarray-based studies found no difference in *ADAM15* expression between OA and normal cartilage (Yang et al., 2017)]. Bohm et al. (2005) then examined knee joints from 3-month old, 6-month old and 12-14-month old *Adam15*-null mice and their age-matched littermates by histology. Synovial hyperplasia was identified in >50% of the 3-month old and all the 6-month old *Adam15*-null mice, but the overall OA histologic score (using a 10-parameter scoring system) was only marginally elevated and did not reach statistical significance. OA features became more apparent in the 12-14-month old *Adam15*-null mice, with chondrocyte clustering and fibrillation and fissuring of cartilage noted. Additionally, loss of proteoglycans was detected by toluidine blue staining. Complete loss of cartilage was observed in some lesions. OA features beyond cartilage were also documented, including degeneration of the meniscus, cellular metaplasia of ligaments and osteophyte formation. Importantly, accelerated OA development was observed in *Adam15*-null mice on a different genetic background, suggesting that this phenomenon was not background-specific. OA score was significantly elevated in 12-14-month old *Adam15*-null mice compared to their wild-type littermates, indicating that mice without *Adam15* developed accelerated, spontaneous OA upon ageing. ADAM15 is thus the only ADAM that has been reported to protect against OA development.

The increase in OA score was more evident in male mice lacking *Adam15* than in

females (Bohm et al., 2005), but female mice lacking *Adam15* also showed a trend towards elevation in OA score. This is consistent with previous murine OA studies which found that male mice have a higher incidence of OA than females (Silberberg et al., 1963a, b; Sokoloff, 1956), and develop more severe OA in both the collagenase-induced and surgical destabilisation of the medial meniscus (DMM) models of OA (Glasson et al., 2005; Glasson et al., 2004; van Osch et al., 1993).

1.4.1. ADAM15 provides apoptotic resistance to different cells in joints

To explore the molecular mechanism of ADAM15's protective effect in mouse joints, Bohm et al. (2005) over-expressed ADAM15 in the T/C28a4 chondrocyte cell line and observed enhanced binding to type II and VI collagens. The enhanced binding to type II collagen was RGD-dependent, as addition of a high concentration of RGD peptide (300 μM), but not GRADSP control peptides impeded this interaction. Bohm et al. further showed that adhesion of ADAM15 to type II collagen was potentially through integrins, as α1, α2, and β1 integrin-blocking antibodies abolished the interactions. In the same study, Bohm et al. also showed that *ADAM15*-over-expressing chondrocytes were more resistant to apoptosis under prolonged serum starvation, which led them to suggest that the strengthened ADAM15-matrix interactions promote anti-apoptotic effects in chondrocytes.

In a subsequent study, Bohm et al. (2010) showed that *ADAM15*-over-expressing chondrocytes displayed significantly reduced activation of caspase 3 upon serum starvation or intermittent matrix withdrawal compared to mock-transfected control cells. Additionally, they identified that cytotoxic stress induced by camptothecin (which inhibits topoisomerases and induces apoptosis) triggered higher up-regulation

of X-linked inhibitor of apoptosis (XIAP) in *ADAM15*-over-expressing cells than in control cells. XIAP inhibits the cleavage of caspase 3, thus preventing its activation and promoting cell survival. Therefore, ADAM15-mediated XIAP up-regulation may explain the anti-apoptotic effects observed in ADAM15-over-expressing cells upon serum starvation. Indeed, the decreased caspase 3 cleavage found in *ADAM15*-over-expressing chondrocytes was reversed by transfection with siRNA against *XIAP*, supporting the conclusion that ADAM15-mediated anti-apoptotic effects are XIAP-dependent. Importantly, *ADAM15* or *XIAP* knockdown in OA chondrocytes also increased caspase 3 activity upon camptothecin treatment, suggesting that ADAM15 may exert protective effects even when OA has developed. Together, these findings suggest that ADAM15 provides anti-apoptotic resistance to chondrocytes under various cellular stresses, and may partially explain how ADAM15 protects joints against OA.

Fried et al. (2012) showed that ADAM15's ability to provide resistance to camptothecin-induced apoptosis depended on its cytoplasmic domain, as T/C28a4 chondrocytes over-expressing a truncated ADAM15 lacking the cytoplasmic domain lost the ability to suppress caspase 3 activation. Interestingly, enhanced Focal Adhesion Kinase (FAK) phosphorylation at Tyr-397, Tyr-576, and Tyr-861 sites was observed in wild-type ADAM15 over-expressing T/C28a4 chondrocytes, but not those expressing truncated ADAM15. A direct interaction between ADAM15 and FAK has been shown using various approaches, including immunoprecipitation and mammalian two-hybrid. Furthermore, their study suggested that interaction between ADAM15 and Src was indirectly mediated through FAK, as FAK inhibition abolished ADAM15-induced caspase 3 inhibition. They also showed that phosphorylation of

FAK and Src was increased in OA chondrocytes upon camptothecin treatment.

Bohm et al. (2009) showed that interactions between ADAM15 and type II collagen depended on the pro-domain of the enzyme, as deletion of this region abolished interaction. Lum et al. (1998) demonstrated that both pro- and mature ADAM15 are present on the cell surface and in the intracellular space, supporting the possibility of pro-domain-dependent interactions on the cell surface. Interaction between the pro-domain and type II collagen was shown to trigger tyrosine phosphorylation of various proteins, dependent on the ADAM15 cytoplasmic domain. The role of FAK in these phosphorylation events was not demonstrated, and the relationship between pro-domain- and RGD-triggered phosphorylation was also not elucidated. Since pro-domain deletion may affect ADAM15 folding, it will be important to determine whether the disrupted ADAM15-type II collagen interactions was a result of ADAM15 misfolding. In summary, these studies demonstrating that ADAM15 promotes cell survival upon various cellular stresses, including serum starvation and genotoxicity. This increased survival depends on the ability of ADAM15 cytoplasm domain to convey intracellular signalling.

ADAM15 also has functions in tissues other than cartilage. Bohm et al. (2013) reported that ADAM15 has FAK-dependent anti-apoptotic effects in synovial fibroblasts, similar to that reported in chondrocytes. Activation of phosphatidylinositol 3-kinase (PI3K) and NF-κB were also observed. Moreover, Marzia et al. (2011b) reported that *Adam15*-null mice showed increased bone volume and thickness, with elevated osteoblast proliferation and activity, as shown by enhanced alkaline phosphatase (AP) staining and increased nodule deposition and mineralisation. In *Adam15*-null osteoblasts,

increased nuclear β-catenin and up-regulation of β-catenin downstream targets such as cyclin D1 and c-Jun, were observed. This suggests that ADAM15 protects joints against OA development by regulating homeostasis in multiple joint tissues, mainly through enhancing resistance to apoptosis in various joint cell types.

1.5. Functions and roles of ADAM15 in other diseases

In addition to its role in OA, ADAM15 has been shown to contribute to pathogenesis of other diseases through roles other than resistance to apoptosis. Findings from these studies may pinpoint important direction for investigating the mechanisms by which ADAM15 protects against OA. In the following sections, I summarise our current understanding of ADAM15.

1.5.1. Discovery of ADAM15

ADAM15 was first cloned and characterised in 1996 by Kratzschmar et al. (1996) as a disintegrin metalloproteinase with an RGD sequence in its disintegrin domain. Originally named metargidin (metalloprotease-RGD-disintegrin), it was the only member in the human ADAM protease family (previously known as MDCs, or metalloprotease, disintegrin and cysteine-rich) that contained an RGD sequence in its disintegrin domain. Mature ADAM15 has a predicted molecular weight of 85 kDa, with 5 potential N-glycosylation sites giving rise to a glycosylated form of the enzyme on the cell surface (Kratzschmar et al., 1996).

1.5.2. ADAM15's role as a sheddase and its proposed substrates

The metalloprotease domain of ADAM15 contains a conserved HEXXHXLGXXHD

zinc-binding motif, indicating that ADAM15 is an active metalloprotease. Various ADAM15 substrates have been proposed. For example, two independent studies reported that ADAM15 cleaved gelatin using a zymography (Martin et al., 2002; Moss et al., 2016). However, in both studies, only modest cleavage was observed. Martin et al. further showed that affinity-purified ADAM15 was able to cleave type IV collagen *in vitro*, and proposed that this enhanced glomerular mesangial cell migration (Martin et al., 2002). However, cleavage was demonstrated using a high ADAM15/type IV collagen ratio (1.111 μg/10 μg) and an extended incubation time (96 hours), indicating weak activity and questionable biological relevance.

ADAM15 has also been implicated in cancer pathogenesis. For example, ADAM15 is associated with metastatic bladder cancer and an aggressive subset of prostate cancer cells in humans (Burdelski et al., 2017; Hiles et al., 2016). Mechanistically, ADAM15 shedding of various membrane substrates has been proposed to contribute to cancer progression. For example, Schafer et al. (2004) reported that ADAM15 cleaved pro-amphiregulin, an autocrine growth factor belonging to the EGF family, while Hart et al. (2005) reported that ADAM15 cleaved proHB-EGF in MDA-MB231 cells. This suggests ADAM15 may provide survival signals to cancer cells.

Additionally, Najy et al. (2008a) showed that suppression of ADAM15 expression reduced levels of soluble N-cadherin in the CM of PC-3 prostate cancer cells, and that recombinant ADAM15 cleaved N-cadherin *in vitro*, suggesting that ADAM15 promoted prostate cancer cell metastasis through cleaving N-cadherin and hence disrupting cell-cell adhesion and promoting cancer cell migration. However, ADAM15 and N-cadherin were incubated at a 1:1 (v/v) ratio for 6 hours to detect proteolytic

activity, suggesting limited catalytic activity. Interestingly, in the same study, Najy et al. (2008a) reported that ADAM15 did not show activity against gelatin by zymography. Subsequently, Najy et al. (2008b) reported that over-expression of ADAM15 in MCF-7 breast cancer cells increased levels of E-cadherin (sE-cad) in the CM, while ADAM15 knockdown had the opposite effect. sE-cad was shown to mediate dimerisation of HER2 and HER3 in an ErbB receptor-dependent manner. Notably, these proposed ADAM15 substrates identified using cancer cell lines seem to be highly cell type-dependent, thus their relevance in cartilage remains unclear.

Other proposed ADAM15 substrates have mainly been identified using *in vitro* screening systems. For example, CD23 was identified in a peptide library screening experiment. However, validation of CD23 hydrolysis was limited to flow cytometry (Fourie et al., 2003). Similarly, FGFR2iiib was identified as an ADAM15 substrate using alkaline phosphatase (AP)-tagging of candidate substrates in cell-based assays (Maretzky et al., 2014), but the effect size was relatively small compared to inactive (E305A) ADAM15, and the biological relevance of this finding requires further validation. Finally, Dong et al. (2015) reported that ADAM15 enhanced MMP-9-mediated gelatin degradation by activating pro-MMP-9 (2015). They also reported that ADAM15-over-expression increased *MMP9* expression at the mRNA level in the A549 lung carcinoma cell line, and concluded that ADM15 indirectly promoted MMP-9-mediated lung cancer invasion through these two mechanisms. However, this was not confirmed *in vivo*.

In summary, although multiple *in vitro* studies have suggested substrates for ADAM15, these have limited validation and unclear biological relevance. No

systematic exploration of ADAM15 substrates has been undertaken. Such an unbiased study is required to better understand how ADAM15-mediated shedding may contribute to its protective effects against OA.

1.5.3. ADAM15 mediated cell-cell and cell-matrix adhesion

As mentioned in Section 1.5.1., ADAM15 is the only human ADAM which contains a conserved RGD motif in its disintegrin domain (Kratzschmar et al., 1996). This RGD sequence is followed by an additional cysteine residue that is only found in other non-RGD-containing disintegrins, but not in RGD-containing disintegrins (Kratzschmar et al., 1996), implying that the ADAM15 RDG sequence may be a result of a back mutation of the non-RGD sequence found in other human ADAMs. Notably, murine ADAM15 does not have the RDG sequence, further supporting the back mutation hypothesis.

The RGD motif is known to interact with integrins (D'Souza et al., 1991; Ruoslahti, 1996), and ADAM15 has been shown to interact with integrins $\alpha 5\beta 1$ and $\alpha v\beta 3$ via this sequence (Nath et al., 1999; Zhang et al., 1998). ADAM15 has thus long been proposed to regulate integrin-mediated biological processes. Al-Fakhri et al. (Al-Fakhri et al., 2003) showed that up-regulation of $\alpha 5\beta 1$ and $\alpha v\beta 3$ elevated ADAM15 expression in human arterial and venous vascular smooth muscle cells, suggesting that integrin up-regulation may enhance ADAM15-integrin interactions, forming a positive feedback loop. RGD-independent interactions with $\alpha 9\beta 1$ have also been reported (Eto et al., 2000), which may be particular relevant for murine ADAM15, which lacks the RGD sequence and thus cannot interact with integrins through this motif (Eto et al., 2000).

ADAM15 has been shown to regulate cell-cell and cell-matrix adhesion. For example, ADAM15 over-expression increased cell-cell adhesion in NIH3T3 fibroblasts (Herren et al., 2001), but disrupted interaction between $\alpha v\beta 3$ and vitronectin in OV-MZ-6, a human ovarian cancer cell line, likely through competition (Beck et al., 2005). ADAM15 can also regulate cell migration indirectly, with over-expression of ADAM15 in ECV304 endothelial-like cells enhancing adhesion to platelets under physiological high shear stress conditions, potentially through interacting with $\alpha IIb\beta 3$ (Jeon et al., 2007; Langer et al., 2005). In addition, treatment of platelets with recombinant ADAM15 induced expression of CD154 (Langer et al., 2005), the ligand of CD40 (CD40L) whose expression triggers chemokine secretion and expression of adhesion molecules in endothelial cells (Henn et al., 1998; Massberg et al., 2002; May et al., 2002). Since platelet adhesion is known to induce pro-inflammatory cytokine production and recruitment of inflammatory cells, through enhancing platelet adhesion and up-regulation of CD154, ADAM15 is thought to be able to indirectly regulate inflammatory cell migration, and may play an important role in thrombus formation and atherosclerosis pathogenesis (Henn et al., 1998; Massberg et al., 2002; May et al., 2002).

1.5.4. ADAM15 interacts with intracellular adaptors via its cytoplasmic tail

In addition to the aforementioned functions mediated by its ectodomain, the cytoplasmic domain of ADAM15, which contains SH2 and SH3 binding sequences, may also contribute to its regulation of cell migration, as signalling induced by the cytoplasmic domain has been shown to affect endothelial permeability and neutrophil migration (Sun et al., 2010). Indeed, Poghosyan et al. (2002) reported that ADAM15 interacted with multiple Src family protein-tyrosine kinases (PTKs), including Hck and

Lck, *in vivo* and *in vitro* in multiple haematopoietic cell lines. ADAM15 was shown to be tyrosine-phosphorylated *in vivo*, potentially by Hck and Lck, and this may initiate intracellular signalling. Similarly, Howard et al. (1999) showed that two SH3-containing proteins, endophilin I and SH3PX1, interacted with the cytoplasmic domain of ADAM15 in COS-7 cells. Interestingly, they showed that these two SH3-containing proteins preferentially interacted with pro-ADAM15, and hypothesised that these interactions may affect the intracellular processing, trafficking, or subcellular localisation of ADAM15 (Howard et al., 1999). Since pro-ADAM15 is also found on the cell surface (Lum et al., 1998), signal transduction may be preferentially mediated by the pro-form of ADAM15.

Importantly, alternatively splicing of the ADAM15 cytoplasmic domain is thought to affect its ability to trigger intracellular signalling or to activate different signalling pathways through interaction with different adaptor molecules. For example, Shimizu et al. (2003) reported that murine ADAM15 splice variants showed different capabilities for interaction with Lck and Hck. Zhong et al. (2008) reported that alternatively spliced ADAM15 cytoplasmic domain variants displayed distinct, or even opposite functions in human mammary carcinoma cells, as two of the 3 variants studied were associated with poor disease prognosis, while the other was associated with better relapse-free survival (variant C). Interestingly, the three variants had different effects on cell adhesion, migration and invasion, and displayed different interaction with intracellular signalling adaptors including Nck and the Src and Brk tyrosine kinases (Zhong et al., 2008). Furthermore, Maretzky et al. (2009a) demonstrated that ADAM15 splice variants displayed different shedding capability, with the most malignant variant showing strongest shedding of FGFR2iiib in cell-

based assays. This indicated that the cytoplasmic domain of ADAM15 and its interactions with intracellular signalling adaptor molecules may regulate the proteolytic activity of the enzyme. Since the native substrates of ADAM15 in breast cancer cells remain to be fully defined, the biological relevance of this finding needs to be further dissected using *in vivo* disease model systems.

1.5.5. Phenotypes of *Adam15*-null mice

The biological functions of ADAM15 has been explored in several different cell types *in vitro* and its involvement in various cancers is well-documented (Beck et al., 2005; Dong et al., 2015; Hiles et al., 2016; Najy et al., 2008a, b). Given its well-established roles in regulating cell migration and adhesion, it is not surprising that ADAM15 is also associated with various inflammatory diseases including atherosclerosis (Bultmann et al., 2011; Sun et al., 2012), lung inflammation (Dreymueller et al., 2015; Sun et al., 2013), rheumatoid arthritis (Bohm et al., 2001; Gao et al., 2015) and inflammatory bowel disease (Mosnier et al., 2006).

Detailed phenotypic characterisation of the *Adam15*-null mice generated by Horiuchi et al. (2003) showed them to be indistinguishable from age- and gender-matched littermates up to 2 years after birth. Since *Adam15* expression is high in blood vessels, its effect on vasculature was further assessed using a retinopathy of prematurity (ROP) model, where 7-day-old mice are placed in a high oxygen chamber for 5 days, and then returned to normoxia. The sudden lowering of oxygen concentration triggers angiogenesis, causing pathological neovascularisation in the retina. In *Adam15*-null mice, neovascularisation was significantly inhibited (Horiuchi et al., 2003). Since *Adam15*-null mice had normal physiological angiogenesis during development, this

suggests that ADAM15 is required for pathological angiogenesis. Horiuchi et al. (2003) also showed that subcutaneous injection of B16F0 mouse melanoma cells gave rise to larger tumours in wild-type than in *Adam15*-null mice, which they suggest supports a role for ADAM15 in pathological neovascularisation.

The overall phenotype of *Adam15*-null mice is thus limited, and challenge is required to reveal its function. This suggests that ADAM15's physiological role easily may be overlooked. A more comprehensive study may thus be necessary to identify potential mechanisms underpinning its protective role in joints. As summarised above, investigation of ADAM15's functions has mainly been conducted using hypothesis-based approaches and has not been characterised systematically. Moreover, its potential role as a sheddase has not been evaluated in OA. Given that ADAM15 is proteolytically active and its sheddase activity has been demonstrated to be critical in other diseases (mainly in cancer) (Charrier-Hisamuddin et al., 2008; Najy et al., 2008a, b), it is possible that shedding of membrane proteins by ADAM15 also contributes to its protective effects in the joint. Importantly, most studies so far suggest that ADAM15 primarily exerts its functions on the cell surface, therefore, agnostic, proteomic approaches focusing on detecting changes on the cell surface may greatly facilitate our understanding of ADAM15's biological activity and the underpinning mechanisms of its protective effects against OA in joints. Therefore, to uncover the mechanisms underpinning ADAM15's role in protecting joints, I planned to investigate how ADAM15 is regulated in cartilage and to identify which membrane proteins it regulates. In Chapter 3, I describe analysis of ADAM15 regulation with ageing. In Chapter 4, I identified that IL-13, a chondroprotective cytokine (Cleaver et al., 2001), up-regulated expression of ADAM15. Finally, in Chapter 5, I detail comprehensive

proteomic studies performed to analyse membrane proteins regulated by ADAM15.

Chapter 2. Materials and Methods

2.1. Materials

2.1.1. Human tissues

Human osteoarthritic cartilage was obtained from the Oxford Musculoskeletal Biobank (OMB) and collected with informed donor consent in compliance with national and institutional ethical requirements, the United Kingdom Human Tissue Act, and the Declaration of Helsinki (HTA Licence 12217 and Oxford REC C 09/H0606/11). Donors either underwent unicompartmental knee arthroplasty (UKA) or total knee arthroplasty (TKA) for OA. Human normal cartilage for RNA analysis was purchased from Articular Engineering, in compliance with the legal and ethical requirements of the country of collection (USA), and ethical approval for using this tissue in the current project was granted by the Medical Sciences Inter-divisional Research Ethics Committee of the University of Oxford. Normal cartilage is defined as that derived from patients without a diagnosis of osteoarthritis at the time of collection. Harvested tissues were immersed in liquid nitrogen until frozen, then stored at -80 °C. RNA from cartilage of four young donors (9-16 years old) was kindly provided by Dr. Chris Murphy and Dr. Christine Seidl [Kennedy Institute Of Rheumatology (KIR), University of Oxford].

2.1.2. Murine tissues

Murine tissues were acquired from C57BL/6 mice at various ages with or without surgical destabilisation of the medial meniscus (DMM). Mice were purchased from Charles River Laboratories, and kept in the animal care core facilities of KIR under appropriate conditions (in ventilated cages, at 21 °C ambient temperature, and under 12-hour-light/12-hour-dark cycles). Harvested tissues were stored at -80 °C.

2.1.3. Cultured cells

HTB-94 human chondrosarcoma cell line and HEK-293 human embryonic kidney epithelial cell line were purchased from American Type Culture Collection (ATCC). Human primary OA chondrocytes were isolated from cartilage acquired from OMB.

2.1.4. Cell culture reagents

Materials used for cell culture were purchased from various suppliers as listed in Table 2.1.

Table 2.1 Suppliers of cell culture reagents

Reagents	Supplier	Catalogue No.
Dulbecco's modified Eagle's medium (DMEM) with L-glutamine	Lonza	BE12-604F
Penicillin-Streptomycin (P/S)	Lonza	DE17-602E
Ethylenediaminetetraacetic acid (EDTA)	Lonza	BE17-161E
Fetal bovine serum (FCS)	Gibco	10500064
Opti-MEM I Reduced Serum Medium	Gibco	31985062
Opti-MEM I Reduced Serum Medium, no phenol red	Gibco	11058021
Phosphate buffered saline (PBS), pH 7.4	Gibco	10010023
	Sigma	D8537
Dimethyl sulfoxide (DMSO)	Santa Cruz Biotechnology	CAS 67-68-5
Collagenase type 2 (Clostridium histolyticum)	Worthington	LS004177

2.1.5. Molecular biology reagents

The full-length human ADAM15 sequence (from the signal peptide and pro-domain to

the intracellular domain, transcript variant 1, NM_207191.1, National Center for Biotechnology Information) with a C-terminal FLAG tag in a pCMV2 vector was purchased from Stratech Scientific Ltd.

DNA extraction was performed using QIAGEN Plasmid Plus Maxi Kits (QIAGEN, Cat. 12963), RNA extraction was conducted using RNeasy Mini Kits (QIAGEN, Cat. 74104), reverse-transcription was performed using High-Capacity cDNA Reverse Transcription Kits (Thermo Fisher Scientific, Cat. 4368814) and quantitative PCR (qPCR) was performed using TaqMan Fast Universal PCR Master Mix (Thermo Fisher Scientific, Cat. 4352042) with various TaqMan Gene Expression Assays primers (Thermo Fisher Scientific). Primer details are listed in Table 2.2.

Table 2.2 Details of TaqMan Gene Expression Assay primers

Primer name	Species	Catalogue No.
ADAM15	Human	Hs00187052_m1
CDKN1A	Human	Hs00355782_m1
CDKN2A	Human	Hs00923894_m1
IL6	Human	Hs00174131_m1
JAK1	Human	Hs01026983_m1
JAK2	Human	Hs01078136_m1
JAK3	Human	Hs00354555_m1
RPLP0	Human	Hs99999902_m1
TYK2	Human	Hs01105953_m1
Adam15	Mouse	Mm00477328_m1
Adam17	Mouse	Mm00456428_m1
Cdkn1a	Mouse	Mm04205640_g1
Cdkn2a	Mouse	Mm00494449_m1
Il13	Mouse	Mm00434204_m1
Il6	Mouse	Mm00446190_m1
Jak2	Mouse	Mm01208489_m1
Rplp0	Mouse	Mm00725448_s1
Runx2	Mouse	Mm00501584_m1
Sirt1	Mouse	Mm01168521_m1

2.1.6. Cell biology reagents

Transfection materials used for over-expression and RNA interference (RNAi) were purchased from suppliers listed in Table 2.3. Small interfering RNAs (siRNA) used for RNAi were purchased from Thermo Fisher Scientific (Table 2.4). Interleukin (IL)-1α (Cat. 200-01A), IL-4 (Cat. 200-04), IL-13 (Cat. 200-13), granulocyte macrophage colony-stimulating factor (GM-CSF, Cat. 300-03) and M-CSF (Cat. 300-25) were purchased from PeproTech. Tumour necrosis factor (TNF), IL-6 and IL-10 were kindly provided by Dr. Wen-Yi Tseng (KIR). Dihydrotestosterone (DHT, Cat. D-073), β-estradiol (E2, Cat. E8875) and retinoic acid (RA, Cat. R2625), phorbol 12-myristate 13-acetate (PMA,

Cat. P8139) were acquired from Sigma-Aldrich. Lipopolysaccharides (LPS, ultrapure LPS from *E. coli* 0111:B4, TLR4 agonist, Cat. tlrl-3pelps) was purchased from InvivoGen. Interferon-ϒ, fibroblast growth factor (FGF)-2, FGF18, connective tissue growth factor (CTGF) and activin were kindly provided by Dr. Anastasios Chanalaris (KIR). Transforming growth factor (TGF)-β1 was kindly provided by Dr. Yoshifumi Itoh (KIR).

Table 2.3: Suppliers of transfection reagents utilised

Reagents	Supplier	Catalogue No.
*Trans*IT-2020 transfection reagent	Mirus Bio	MIR 5400
Lipofectamine 2000 transfection Reagent	Invitrogen	11668019
jetPRIME transfection Reagent	Polyplus	114-15

Table 2.4: Details of Silencer Select siRNA used

	Thermo Fisher Scientific
Reagents	**Catalogue No.**
Silencer Select Negative Control No. 1 siRNA	4390844
siADAM15	s16681
	s16682
siCDKN1A	s416

2.1.7. Biochemistry reagents

SDS-PAGE and immunoblotting reagents were purchased from various suppliers (Table 2.5). Recombinant human ADAM15 ectodomain was acquired from Abcam (amino acid sequence 1-772, Cat. ab131862) and Sino Biological (amino acid sequence1-696, Cat. 10517-H08H-10). FLAG-tagged human recombinant ADAM15 was expressed in HEK-293 or HTB-94 cell lines and immunoprecipitated using anti-FLAG M2 affinity gel (Sigma-Aldrich, Cat. A2220).

Table 2.5: Suppliers of SDS-PAGE and immunoblotting reagents

Reagents	Supplier	Catalogue No.
30 % (w/v) acrylamide/bis-acrylamide	Severn Biotech	20-2100-10
2-amino-2-methyl-1,3-propanediol N,N,N′,N′-tetramethylethylenediamine (TEMED)	Sigma-Aldrich	T9281
Ammonium persulfate (APS)	Sigma-Aldrich	215589
Trichloroacetic acid (TCA)	Sigma-Aldrich	T0699
Trans-Blot Turbo Transfer System	Bio-Rad Laboratories	170-4155
Clarity Western ECL Blotting Substrates	Bio-Rad Laboratories	1705060
ECL Western Blotting Detection Reagent	Amersham/GE	RPN2106
Western Blue Stabilised Substrate for Alkaline Phosphatase	Promega	S3841
NuPAGE 4-12% Bis-Tris Protein Gels	Thermo Fisher Scientific	NP0322BOX
PageRuler Plus Prestained Protein Ladder, 10 to 250 kDa	Thermo Fisher Scientific	26619

2.1.8. Antibodies

Primary and secondary antibodies used for immunohistochemistry (IHC), immunofluorescence (IF) and immunoblotting are listed in Table 2.6.

Table 2.6: Details of antibodies and detection reagents used

Primary antibodies

Antibody name	Species	Supplier	Catalogue No.
Anti-ADAM15 antibody_EPR [EPR5619]	Human	Abcam	ab124698
Anti-ADAM15_HTA	Human	Atlas Antibodies / Cambridge Bioscience	HPA011633
Anti-Actin	Human	Abcam	ab3280
High Sensitivity Streptavidin-HRP, Pre-Diluted	n.a.	Pierce / Thermo Fisher Scientific	21134
Monoclonal ANTI-FLAG M2 antibody	Mouse	Sigma-Aldrich	F3165

Secondary antibodies

Antibody name	Species	Supplier	Catalogue No.
Anti-Mouse IgG (H+L), AP Conjugate	Goat	Promega	S3721
Anti-Rabbit IgG (Fc), AP Conjugate	Goat	Promega	S3731
ECL Rabbit IgG, HRP-linked $F(ab')_2$ fragment	Donkey	Amersham / GE	NA9340
Polyclonal Rabbit Anti-Mouse Immunoglobulins / HRP	Rabbit	Dako	P0260
Goat Anti-Rabbit IgG H&L (HRP)	Goat	Abcam	ab6721

2.1.9. Proteomic analysis

Proteomic reagents were obtained from various suppliers with details listed in Table 2.7.

Table 2.7: Suppliers of proteomic materials and reagents

Reagents	Supplier	Catalogue No.
N-azidoacetylmannosamine tetraacylated (ManNAz)	Thermo Fisher Scientific	88904
High Capacity Streptavidin Agarose	Pierce/Thermo Fisher Scientific	20357
Sodium dodecyl sulfate (SDS)	Thermo Fisher Scientific	BP-166
Sulfo-Dibenzylcyclooctyne (DBCO)-Biotin Conjugate	Jena Bioscience	CLK-A116-10
Poly-Prep Columns	Bio-Rad Laboratories	731-1550
Tris, Hydrochloride, ULTROL Grade	Merck Group	648313
Sodium Chloride (NaCl)	Merck Group	567440
EDTA	Merck Group	34103
Water (LC-MS Grade)	Merck Group	1153331000
Ultra-15 Centrifugal Filter Unit with Ultracel-30 membrane	Amicon/Merck Group	UFC903024
Ultra-0.5 Centrifugal Filter Unit with Ultracel-30 membrane	Amicon/Merck Group	UFC503024
Triton X-100	Sigma-Aldrich	X-100

2.2. Methods

2.2.1. Human primary chondrocyte culture

Human primary OA chondrocytes were isolated by finely chopping surgically-removed knee cartilage, and incubating the cartilage pieces at 37 °C with 20 mg/ml collagenase type II (Worthington Biochemical) in 20 ml DMEM with 10% FBS and 1% P/S (complete DMEM) overnight with shaking at 180 r.p.m. The supernatants were filtered through 0.48 μm cell strainers (Corning/Sigma-Aldrich) and cells pelleted by centrifugation (10 minutes, 530 x g) and washed twice using serum-free DMEM. Cells were seeded at an appropriate density in complete DMEM and incubated at 37 °C under 5% (v/v) CO_2 without disruption for at least 5 days (passage 0, P0). Experiments were performed using chondrocytes within the first three passages (P3) after isolation.

2.2.2. Murine primary chondrocyte culture

Murine immature costal chondrocytes were isolated according to Gosset et al. (2008). Briefly, 5 to 6 day old mice were euthanised and rib cages removed and washed in DMEM. All soft tissues were removed from the ribs, the rib cages washed once with PBS, and incubated in 15 ml complete DMEM with 3 mg/ml collagenase type II (Worthington) at 37 °C in an incubator under 5% CO_2 for 45 min. Digested material was passed through a 25 ml pipette to disrupt the tissue, and placed in a new Petri dish with 15 ml complete DMEM and 0.5 mg/ml collagenase type II (Worthington) at 37 °C in an incubator under 5% CO_2 overnight. Digested tissues and supernatants were sequentially passed through 25 ml, 10 ml, 5 ml, and 1 ml pipettes to disperse cell aggregates. The resultant cell suspensions were filtered through a sterile 48 μm

Corning cell strainer (Sigma-Aldrich), centrifuged (10 minutes, 400 x g, 20 °C), and washed once in PBS. Cells were re-suspended, counted and seeded at an appropriate density.

2.2.3. Culture of human cell lines

HEK-293 and HTB-94 cells were cultured in 15 ml complete DMEM in a 10 cm^2 cell culture plate in an incubator maintained at 37 °C under 5% (v/v) CO_2. Cells were grown to confluence (2-3 days) before passage. For passaging, culture media were removed and cells washed with 5 ml PBS, followed by addition of 1 ml trypsin-EDTA to cover the plate. The plate was then maintained at 37 °C in the incubator for approximately 2 minutes. Once cells started detaching from the plate, 9 ml complete DMEM was added and cells washed off the plate by pipetting repeatedly. The resultant cell suspension was collected and pelleted by centrifugation (5 minutes, 510 x g), the supernatant discarded and the cell pellet resuspended in 20 ml complete DMEM. Cells were plated at an appropriate density for maintaining or for subsequent experiments.

2.2.4. Cell biology methods

2.2.4.1. Over-expression by transient transfection

Over-expression of recombinant proteins was achieved by transiently transfecting an expression vector into either HTB-94 or HEK-293 cells using *Trans*IT-2020 reagent according to the manufacturer's guide (Mirus Bio). Cells were seeded ($5x10^5$ cells per well in 2 ml complete DMEM) in a 6-well plate the day before transfection. Expression vector DNA (1 µg) was added to 250 µl of Opti-MEM, mixed thoroughly, and 7.5 µl

*Trans*IT 2020 reagent added. The mixture was incubated for 15-30 minutes at room temperature. Cells were washed with 2 ml PBS and placed in 1.75 ml Opti-MEM. The transfection mixture was added to the cells and incubated for 48-72 hours.

2.2.4.2. RNA interference by transient transfection

RNAi was performed by transiently transfecting siRNA (10-30 nM) into HTB-94 cells using jetPRIME reagent according to the manufacturer's guide (Polyplus). Cells were seeded ($1x10^5$ cells per well in 2 ml complete DMEM) in a 6-well plate the day before transfection. On the next day, an appropriate amount of siRNA or non-targeting negative control siRNA was added to 200 µl jetPRIME buffer and mixed thoroughly. jetPRIME transfection reagent (4 µl) was added to the siRNA-buffer mixture, mixed thoroughly and incubated for 10 minutes at room temperature. Cells were washed with 2 ml PBS, and placed in 1.8 ml serum-free DMEM, Opti-MEM or complete DMEM. The transfection mixture was added to cells and incubated for 24, 48 or 72 hours.

2.2.4.3. Stimulation of HTB-94 cells

HTB-94 cells were seeded ($1x10^5$ per well in a 12-well plate, or $4x10^5$ per well in a 6-well plate, in complete DMEM. Cells were changed to serum-free DMEM the day before stimulation or for at least 16 hours. On the day of stimulation, cells were washed with PBS, media changed to 1 (12-well plate) or 2 ml (6-well plate) fresh serum-free DMEM with the indicated concentrations of stimuli for the indicated time period. Reagents were diluted using serum-free DMEM. Instead stated otherwise, concentrations used for each stimulus are listed in Table 2.8.

Table 2.8: Concentrations used for each stimulus

Stimulus	Final concentration
Activin	50 ng/ml
CTGF	100 ng/ml
Dexamethasone	1 μM
DHT	0.1 μM
DMSO	0.1%
E2	0.1 μM
FGF18	100 ng/ml
FGF2	100 ng/ml
GM-CSF	50 ng/ml
hTGF-β	10 pg/ml
	100 pg/ml
	1 ng/ml
	10 ng/ml
IFN-ϒ	100 ng/ml
IL-1	100 ng/ml
IL-10	10 ng/ml
IL-13	20 ng/ml
IL-4	20 ng/ml
IL-6	20 ng/ml
LPS	100 ng/ml
M-CSF	100 ng/ml
OP-1/BPM-7	100 ng/ml
PMA	100 nM
RA	1 μM
TNF	100 ng/ml

2.2.4.4. Freezing down cultured cells

Cells were grown to confluence and trypsinised according to Section 2.2.3. After cells were washed and pelleted, they were re-suspended in 10 % (v/v) cell-culture grade

DMSO in FBS at a density of $4x10^6$ cells/ml, and aliquoted at 1 ml per 1.2 ml Cryovial (Thermo Fisher Scientific, Cat. T310-1A) and frozen at -80 °C in a Mr. Frost Freezing Container (Thermo Fisher Scientific, Cat. 5100-0001) overnight before being moved to a liquid nitrogen tank for long-term storage.

2.2.4.5. MTS colorimetric cell proliferation assay

MTS colorimetric cell proliferation assay was performed using the CellTiter 96 AQueous One Solution Cell Proliferation Assay (Promega, Cat. G3582), according to the manufacturer's guide. 10000 cells were seeded in 100 µl full DMEM per well in a 96-well plate the day before treatment. Gene manipulation (over-expression or RNAi) was generally performed using transient transfection for 36-48 hours. When gene manipulation was not needed, higher cell numbers (20000 to 40000 cells per well) were used. Each condition was performed in triplicate.

MTS reagent was left to thaw completely at room temperature, then 20 µl of MTS reagent was mixed with 100 µl full DMEM per reaction. Conditioned media were removed from cells and 120 µl MTS-DMEM mixture added per well. Absorbance (490 nm) was measured at 0 minutes and 90 minutes. Average absorbance of blank controls at 0 minutes were deduced from absorbance at 90 minutes. Optimal cell number and incubation time were determined experimentally.

2.2.5. Molecular biology

2.2.5.1. Transformation by electroporation

Electro-competent *Escherichia coli* (*E. coli*) DH5α cells (laboratory stock) were used for

electroporation. An appropriate amount of plasmid DNA was determined experimentally and electroporated into *E. coli* DH5α using a BTX Electrocell Manipulator 630 (Holliston) with settings of 2250 V, 200 Ω, and 25 μF. Cells were incubated in 800 μl Luria-Bertani (LB) broth (Thermo Fisher Scientific, Cat. 12780052) at 37 °C, 200 r.p.m. to recover for 1 hour after electroporation. An appropriate volume of cell suspension was then plated on LB agar (Thermo Fisher Scientific, Cat. 22700025) with kanamycin (100 μg/ml, Sigma-Aldrich, Cat. 60615) overnight. Kanamycin-resistant colonies were selected and cultured in LB broth supplemented with 100 μg/ml kanamycin overnight (37 °C, 200 rpm) and DNA was extracted using a QIAGEN Plasmid Plus Maxi Kit according to the manufacturer's guide.

2.2.5.2. RNA extraction

Total RNA was extracted from cultured cells using a RNeasy Mini Kit according to the manufacturer's guide. Cells were lysed in RLT buffer (350 μl) supplement with β-mercaptoethanol (β-ME, 1μl per 1 ml RLT), collected in an eppendorf and centrifuged (3 minutes, 17000 x g) to pellet cell debris. The supernatant was placed in a new eppendorf and mixed with an equal volume of 70% ethanol (EtOH). The resultant mixture was applied to an RNeasy mini spin column, and centrifuged for 15 seconds at ≥8000 x g. The RNeasy mini spin column was then washed with 350 ml of RW1 buffer. RNase-free DNase (QIAGEN, Cat. 79254) was mixed with RDD buffer (10 μl DNase with 70 μl RDD per sample), applied to the column (80 μl), and incubated at room temperature for 10 minutes. The column was washed with 350 ml RW1 buffer, followed by washing with RPE buffer twice. The column was dried by centrifugation (2 minutes, 17000 x g) and RNA eluted using an appropriate volume of nuclease-free water. The concentration of the purified RNA was determined using a Nanodrop 1000

(Thermo Fisher Scientific).

For murine tissue RNA extraction, tissue was either placed in 1 ml TRIZOL and fine-chopped using sharp surgical scissors (for most soft tissues such as liver, spleen, heart and brain), or macerated using a hammer after freezing in liquid nitrogen and then placed in 1 ml TRIZOL (for joint and bone). For RNA extraction from human cartilage, pieces of cartilage were frozen in liquid nitrogen, ground using a metal mortar and pestle and placed in 1 ml TRIZOL. The resultant mixture was vortexed at room temperature for 10 minutes and centrifuged (3 minutes, 3000 x g) to pellet tissue debris. The supernatant was placed in a new eppendorf and mixed with 100 µl 1-bromo-3-chloropropane (BCP) by vortexing for 10 minutes at room temperature and centrifuged (20 minutes, 4°C, 17000 x g). The clear, transparent supernatant was placed in a new eppendorf. When the upper supernatant was not clear, 500 ml TRIZOL was added with 50 µl BCP, and the vortex and centrifugation steps were repeated until the upper supernatant cleared. The supernatant was mixed with an equal volume of EtOH, and RNA extraction followed as described above.

2.2.5.3. Reverse transcription

RNA (300-600 ng) was reversely transcribed to cDNA using the High-Capacity cDNA Reverse Transcription Kit (Thermo Fisher Scientific, Cat. 4368814) according to the manufacturer's guide.

2.2.5.4. Real-Time PCR (qPCR)

qPCR was performed using TaqMan Fast Universal PCR Master Mix (Thermo Fisher Scientific, Cat. 4352042) according to the manufacturer's guide. Master Mix (6 µl per

reaction) was mixed with nuclease-free water (0.4 µl per reaction) and a specific primer for the gene of interest (0.6 µl per reaction, Table 2.2). The resultant qPCR reagent mixture (7 µl) was aliquoted into 0.1 ml tubes (QIAGEN, Cat. 981103). cDNA was diluted 5-fold using nuclease-free water and the diluted cDNA (5 µl per reaction) added to the qPCR tubes containing the reagent mixture. qPCR was performed using a Rotor-Gene 6000 Real Time PCR machine (Corbett Research). Data were analysed using Excel and Numbers software, ΔCt was calculated by subtracting the Ct value of the gene of interest from the Ct value of the housekeeping gene for that sample, and fold change (FC) was calculated using the formula $FC = 2^{-(\Delta\Delta Ct)}$

2.2.6. Biochemistry methods

2.2.6.1. Trichloroacetic acid (TCA) precipitation

Proteins in a dilute solution can be concentrated by lowering the pH, disrupting the electrostatic interactions between charged residues, resulting in denaturation of their three-dimensional structure. Denatured proteins have reduced solubility, and consequently precipitate out of the solution. By re-suspending the precipitated proteins in a smaller volume, concentration can be effectively achieved. TCA is a common acidic reagent used for protein precipitation and concentration. To perform TCA precipitation, 5 % (v/v) TCA was added to the protein solution and the tubes repeatedly inverted to thoroughly mix the solution, before incubation at 4 °C overnight. The solution was centrifuged (10,000 x g, 10 min at 4 ºC) and the resulting pellet resuspended in an appropriate volume of 2X SDS-PAGE sample buffer (Table 2.9).

Table 2.9: Composition of buffers in Ammediol SDS-PAGE buffer system

Buffer	Composition
Ammediol upper gel buffer	84 mM Ammediol
	62 mM HCl
	0.02 % NaN_3
Ammediol lower gel buffer	110 mM Ammediol
	47 mM HCl
	0.02 % NaN_3
Ammediol upper running buffer	10 mM ammediol
	10 mM glycine
	0.01 % SDS
Ammediol lower running buffer	10 mM ammediol
	10 mM glycine
	0.01 % SDS
Sucrose solution	50 % (w/v) sucrose
	50 % (v/v) dH_2O
Ammonium persulfate (APS) solution	10 % (w/v) ammonium persulfate
	90 % (v/v) dH_2O
SDS sample buffer (2x)	2 % SDS
	5.0 ml Ammediol Upper gel buffer
	0.1 % (w/v) bromophenol blue
	50 % (w/v) glycerol
	+/- 1 % (v/v) β-mercaptoethanol
	0.01 % (w/v) sodium azide

2.2.6.2. SDS-PAGE using the Ammediol buffer system

Sodium dodecyl sulfate-polyacrylamide gel electrophoresis (SDS-PAGE) is a commonly used method to separate proteins according to molecular weight. SDS is a highly negatively charged detergent whose hydrophobic tail binds quantitatively (proportional to the length of the amino acid sequence) to proteins. These hydrophobic

interactions disrupt the three-dimensional structure of proteins and denature them to linear polypeptide chains. Additionally, since each SDS molecule contributes two negative charges to the protein it binds, binding of many SDS molecules overwhelms the charge of the protein, making the charge of each protein proportional to its molecular weight. Therefore, when current is applied, proteins will migrate to the positive electrode (anode) at a speed proportional to their molecular weight.

Polyacrylamide gels form cross-linked, mesh-like matrices. When negatively charged linear polypeptides move toward the anode, pores formed in this mesh-like structure apply resistance to the polypeptides. This resistance is positively correlated with the polypeptide size, thus the smaller the proteins, the faster they move toward the anode. By this mean, proteins with different molecular weights can be resolved on a single polyacrylamide gel. Various polyacrylamide concentrations can be used to achieve the best resolution for proteins with different molecular weights. This is because the pore size of a polyacrylamide gel is determined partially by the total amount of monomeric acrylamide. As the total amount of monomeric acrylamide increases, the pore size decreases, and the smaller pores give better resolution of smaller polypeptides, whilst larger pores result in better resolution of larger polypeptides. Hence, better resolution is achieved by using a higher percentage gel for small proteins, and vice versa.

Various buffer systems are used for SDS-PAGE. In this project, the ammediol buffer system was chosen for its high resolution (Bury, 1981). Buffers used in the ammediol system are detailed in Table 2.9, and the composition of SDS-PAGE gels with various polyacrylamide concentrations is listed in Table 2.10.

SDS-PAGE gels were cast using Hoefer Gel Casters (Hoefer Gel Casters, Cat. SE215). The lower running gel was cast by mixing lower gel solution thoroughly using the recipe detailed in Table 2.10 (with TEMED and APS added last), and pouring the solution into the gel caster with sufficient space being left for the upper gel. An appropriate volume of water-saturated butanol was added to cover the top of the lower gel to provide a smooth interface between the upper and lower gels and to facilitate polymerisation by excluding oxygen. The lower gel was allowed to set either at room temperature for >2 hours, or at 37°C for >30 minutes. Water-saturated butanol was discarded and the upper gel solution was mixed thoroughly using the recipe in Table 2.10 (again with TEMED and APS added last) and poured on top of the lower gel. A well-comb was then quickly inserted to the upper gel to create loading wells. The upper gel was allowed to set at room temperature for >1 hour, and stored at 4°C.

To perform SDS-PAGE, gels were secured in the running tank, the lower running buffer (anode buffer) added to the lower chamber, and the upper running buffer added to the upper (cathode) chamber. Samples were mixed with an equal volume of SDS sample buffer (2x), and loaded into the wells. alongside a pre-stained molecular weight marker (5 μl). A current (150-170 V) was applied for 90 minutes, or until the bromophenol blue in the SDS sample buffer reached the bottom of the gel.

Table 2.10: Composition of SDS-PAGE with various polyacrylamide concentrations

Reagents	Volume of reagent			
Total volume: ~4 ml	6 % gel	7.5 % gel	10 % gel	12 % gel
Acrylamide:bis acrylamide solution	0.8 ml	1.0 ml	1.32 ml	1.61 ml
Lower gel buffer	1.0 ml	1.0 ml	1.0 ml	1.0 ml
50 % sucrose	0.86 ml	0.86 ml	0.86 ml	0.86 ml
H_20	1.34 ml	1.14 ml	0.82 ml	0.53 ml
Ammonium persulfate	14 µl	14 µl	14 µl	14 µl
TEMED	1.5 µl	1.5 µl	1.5 µl	1.5 µl

2.2.6.3. Immunoblotting

Immunoblotting is an antibody-based technique commonly used for target protein detection. A single protein can be detected specifically by using a specific antibody and by its molecular weight, calculated in relation to markers on SDS-PAGE. Samples were separated using SDS-PAGE, and then transferred to a methanol-activated PVDF or nitrocellulose membrane using the Trans-Blot Turbo Transfer System according to the manufacturer's guide (Bio-Rad Laboratories). The membrane was placed in PBS with 5 % milk (blocking buffer) for >1 hour at room temperature. Membranes were then incubated with 5 ml blocking buffer containing a primary antibody recognising the protein of interest at an experimentally-determined optimal concentration (normally 1 in 200 to 1 in 1000). The membrane was incubated with primary antibody at 4°C overnight with agitation. Unbound antibodies were washed off by immersing the membrane in 0.1 % TWEEN20 (Sigma-Aldrich, Cat. P9416) in PBS (wash buffer) for 10 minutes, three times. After the last wash, the membrane was immersed in blocking buffer containing a species-specific secondary antibody which recognises the

conserved epitopes of the primary antibody, at an experimentally-determined optimal concentration (1 in 1000 to 1 in 5000) and incubated for >4 hours. Unbound antibodies were washed off (3 x 10 minutes with wash buffer) and the membrane rinsed with deionised water before development.

The secondary antibodies used in this project were conjugated with either alkaline phosphatase (AP) or horseradish peroxidase (HRP), allowing signal to be detected using enzymatic reaction-based colorimetric or chemiluminescent assays, respectively. For the AP-colorimetric assay, a coloured product precipitated onto the membrane, whilst for the HRP-chemiluminescent assay, the chemiluminescent signal was captured by photographic film. Both detection systems result in signal enhancement and protein signal visualisation, with HRP-based chemiluminescent assays being more sensitive.

The AP-colorimetric assay was chosen when expression of the protein of interest was abundant, with 5 ml Western Blue Stabilised Substrate for Alkaline Phosphatase (Promega, Cat. S3841) applied to the membrane and incubated until bands were clearly visible by eye. The enzymatic reaction was stopped using AP stop buffer (20 mM Tris-HCl pH 7.5 and 10 mM EDTA, 15 minutes).

For less abundant proteins, the HRP-chemiluminescent assay was used, with either Amersham ECL Western Blotting Detection Reagent or Clarity Western ECL Blotting Substrate (for low abundance proteins or low tier antibodies) applied onto the membrane according to the manufacturer's guide and chemiluminescence detected in a darkroom using high-sensitivity film.

Developed membranes or films were scanned using a Canon CanoScan LiDE 210 flatbed high-resolution scanner at a resolution of 600 dpi.

2.2.6.4. Immunoprecipitation of FLAG-tagged recombinant human ADAM15

M-pCMV2-human ADAM15-FLAG was over-expressed in HEK-293 or HTB-94 cells according to Section 2.2.4.1. 48 hours after transfection, conditioned media were removed and cells were washed with 10 ml PBS containing 14 μM cysteine peptidase inhibitor L-trans-epoxysuccinyl-leucylamido (4-guanidino) butane (E-64) and 2 mM serine protease inhibitor 4-(2-aminoethyl)benzenesulfonyl fluoride hydrochloride (AEBSF). Cells were lysed in 1 ml RIPA buffer (Table 2.11) containing 14 μM E-64 and 2 mM AEBSF. Cell lysates were collected in a 1.5 ml eppendorf tube and incubated on ice for 1 hour. Cell lysates were sonicated for 5 minutes, centrifuged (4 °C, 10 minutes, 17000 x g), and supernatants transferred to a new 1.5 ml eppendorf tube. 50 μl of the supernatant was used to analyse over-expression of ADAM15 by immunoblotting. 200 μl per sample of anti-FLAG M2 affinity gel (Sigma-Aldrich, Cat. A2220) was centrifuged (4 °C, 10 minutes, 900 x g) and the supernatant discarded. The anti-FLAG M2 affinity beads were washed twice with 1 ml TBS containing 14 μM E-64 and 2 mM AEBSF (4 °C, 10 minutes, 900 x g) and re-suspended in 1 ml RIPA buffer containing 14 μM E-64 and 2 mM AEBSF. 200 μl of bead suspension was added to cell lysates on ice, and incubated at 4 °C on a rotator overnight. Beads were collected by centrifugation (4 °C, 10 minutes, 900 x g). The supernatant was stored for immunoblotting to examine the efficiency of immunoprecipitation. Beads were washed three times with 1 ml RIPA buffer containing 14 μM E-64 and 2 mM AEBSF, then three times with 1ml TBS containing 14 μM E-64 and 2 mM AEBSF. Beads were collected by centrifugation (4 °C, 10 minutes, 1500 x g) and the supernatant discarded. Beads were re-suspended in 3X

FLAG Peptide (2% in 100 µl TBS), mixed thoroughly, and incubated at 4 °C on a rotor for 10 minutes to elute recombinant ADAM15-FLAG protein. Beads were centrifuged (4 °C, 10 minutes, 900 x g) and the supernatant collected and stored at -80 °C. The remaining beads were boiled in 15 µl SDS sample buffer (2x) for 10 minutes and the sample buffer collected. Additionally, 15 µl of the supernatant was immunoblotted to confirm elution efficiency.

Table 2.11 Components of RIPA buffer (10 X)

Reagents	Concentration
NaCl	4 M
NaN_3	2 % (v/v)
Tris-HCl, pH 8.0	2 M
Triton X-100	20 % (v/v)
Deoxycholic acid	10 % (v/v)
SDS	10 % (v/v)
in ddH_2O	

2.2.7. Coating cover slips with gelatin for immunofluorescence staining

To perform immunocytostaining, cells were seeded on gelation-coated coverslips. A drop (~150 µl) of 0.1% gelatin in H_2O was applied onto parafilm and the coverslip put on top of the gelatin drop (20 minutes, room temperature). The coverslip was moved onto a drop of 1% glutaraldehyde in H_2O with the gelatin-coated side facing downward and incubated for 15 minutes at room temperature to crosslink gelatin. Free aldehyde groups were blocked using 1 M ammonium chloride in H_2O (15 minutes, room temperature). Coated coverslips were immersed in 70% ethanol overnight and washed three times with serum-free DMEM before cells were seeded.

2.2.8. Immunofluorescent staining (IF) on cells and tissues

Cartilage slides embedded in Optimal cutting temperature compound (OCT, Thermo Fisher Scientific, Cat. LAMB/OCT) were taken from the laboratory stock prepared by Dr. Linda Troeberg (KIR) or were sectioned by Dr. Anastasios Chanalaris and myself, and kept at -80 °C for at least 24 hours before use. Sections were air dried (1 h, room temperature) before fixation in 200 µl Neutral Buffered Formalin (NBF, 5 min, room temperature) and ice-cold acetone (10 minutes , -20 °C). Tissue was circled using a hydrophobic pen to create a boundary for maintaining aqueous solutions. To ensure that tissue was fully covered by staining solutions, 250 µl of each solution was used in the following steps. Tissue was digested in 0.1 U chondroitinase ABC (Sigma-Aldrich, Cat. C3667) in 1 x glycosaminoglycan (GAG) buffer (100 mM sodium acetate, 50 mM Tris-HCl pH 8.0, 50 mM EDTA) for 30 minutes (37 °C). Sections were blocked (1 h, room temperature) in IHC blocking buffer (1% goat serum, 5% BSA in PBS). When cell permeabilisation was required, 0.1 % Triton X-100 in PBS was added to the sections (15 minutes, room temperature). Sections were washed 3 times using PBS. Experimentally determined concentrations of primary antibodies (approximately 1 in 50 to 1 in 250) were added to the IHC blocking buffer and applied onto the sections. Sections were incubated with primary antibodies (overnight, 4 °C) and washed three times using PBS. Sections were then incubated with experimentally determined concentrations of secondary antibodies (generally 1 in 500) in IHC blocking buffer (1 hour, room temperature). Sections were washed three times in PBS, and 4',6-diamidino-2-phenylindole, dihydrochloride (DAPI, Sigma-Aldrich, Cat. D9542) in IHC blocking buffer (1:200 dilution) applied to the section (1 hour, room temperature). DAPI binds to AT-rich regions of DNA and thus allows visualisation of cell nuclei by fluorescent microscopy when excited at 405 nm. Unbound DAPI was washed off 3 times using

PBS. Sections were mounted using ProLong Diamond Antifade Mountant (Thermo Fisher Scientific, Cat. P36961) and molecules of interest visualised using a fluorescent microscope.

To perform IF on cells, 10,000 cells were seeded per gelatin-coated (Section 2.2.7) coverslip. Gene expression was generally manipulated using transient transfection for 36-48 hours before IF staining. If transient transfection was not needed, higher cell densities were used (20,000 - 30,000 cells per coverslip). Cells were fixed in 300 μl 3% paraformaldehyde in PBS (10 minutes, room temperature) and washed three times with PBS. Cells were blocked in IHC blocking buffer (1 hour, room temperature) and the IF protocol described above followed. When actin staining was required, phalloidin (1:100 dilution) was added together with DAPI. Phalloidin is a toxin from the mushroom *Amanita phalloides* which binds to and inhibits depolymerisation of actin. Fluorochrome-conjugated phalloidin thus allows actin visualisation.

2.2.9. Proteomic methods

Traditionally, biological investigation of protein function has been based on hypothesis-driven approaches, where careful observation is coupled with logical experimental design to unravel the function of proteins of interest. These biological experiments are generally designed such that only one intervention is introduced at a time and the potential changes (i.e. the readout of the experiment) induced by the intervention are scrupulously characterised. One caveat of this approach is that the readout is based on previous knowledge, so when knowledge of the protein of interest is lacking, it is extremely difficult to investigate its function, and so scientific

breakthroughs are mainly driven by serendipity. An example of this limitation is identification of metalloproteinase substrates. Some metalloproteinases (e.g. MMP-3, ADAM10 and ADAM17) have broad substrate specificity which makes their substrate identification easier, whilst others have fewer substrates or can only cleave their substrates under specific conditions. For example, the only identified substrate of ADAMTS13 is the blood clot-inducing protein von Willebrand factor (vWf), and ADAMTS13 can only cleave vWf under conditions of shear stress, which promotes proteolysis by altering the conformation of the enzyme and its substrate. It is extremely difficult to identify the substrates of such highly selective enzymes using conventional, hypothesis-driven methods. Moreover, due to limitations in time and resources, researchers are generally limited to the number of readouts they can realistically measure for a particular intervention in a controlled experiment. Therefore, it is almost impossible to capture how the "whole picture" is affected by introducing a particular intervention using conventional methods.

Mass spectrometry-based proteomic analysis has circumvented these difficulties and made it possible to investigate changes in the whole proteome induced by a particular intervention. Moreover, the advent of label-free quantitative (LfQ) proteomic technology has made hypothesis-free, systematic investigation of protein function possible without using radioactive substances which are both hazardous to human health and can introduce potential labelling bias. For example, by comparing the proteomes in conditioned media from wild-type- and *Adam10*-deficient mouse neurons using a specialised LfQ technique, Kuhn et al. (2016) not only identified several novel, less abundant substrates of ADAM10, but were also able to determine the relative contribution of ADAM10 to shedding particular substrates, e.g. shedding

of neurexins 2 and 3 was reduced by less than 50% reduction in *Adam10*-deficient neurons, suggesting that ADAM10 only plays a minor role in their shedding.

Since its invention, several specialised proteomic analyses have been developed to identify novel protease substrates, cytoplasmic protein-protein interactions, changes in ECM components, and protein phosphorylation. I used one such specialised proteomic analysis, called 'secretome protein identification with click sugars (SPECS)', extensively in my study. To perform SPECS, cells were cultured with tetraacetyl-N-azidoacetyl-mannosamine (ManNAz), a sugar that is metabolically converted to N-azidoacetyl-sialic acid and incorporated into N- and O-linked glycans at the terminal positions (Sletten et al., 2011). When ManNAz is added to cell culture, it is incorporated only into newly synthesised glycoproteins. N-azidoacetyl-sialic acid-containing glycoproteins can then be covalently linked to membrane impermeable sulfo-dibenzylcyclooctyne-biotin conjugates (sulfo-DBCO-biotin conjugate) via copper-free click chemistry-mediated biotinylation (Jewett et al., 2010) and the resultant glycoprotein-biotin conjugates pulled down using streptavidin-agarose. This method enriches newly-synthesised glycoproteins, whose abundance is generally low and which are easily masked by more abundant proteins in mass spectrometry, which can only detect proteins within 4 orders of magnitude range in abundance (Anderson et al., 2002). Given that 66% of secreted proteins and 87% of type I and type II transmembrane proteins are glycoproteins, SPECS is suitable to investigate changes in plasma membrane proteome (the surfaceome) and changes in proteins shed or secreted into the conditioned media (the secretome) (Kuhn et al., 2016; Kuhn et al., 2012). This method is thus suited to studying the function of ADAMs, as they mainly

regulate the abundance of membrane proteins.

For proteomic analysis to be successful, it is critical to optimise the sample preparation procedure. Various methods have been developed for different proteomic analyses (e.g. secretome, interactome, degradome, etc.), but mass spectrometry sample preparation for shot-gun proteomics generally involves 8 steps: protein solubilisation, enrichment, elution, reduction, alkylation, digestion, cleanup, and buffer exchange. Generally, cells will be lysed using an experimentally optimised detergent-containing lysis buffer to denature and solubilise proteins. Solubilise proteins will then be enriched to suit the purpose of the experiment, often on an affinity resin. For example, SPECS is well-suited to enrich glycoproteins, and there are other methods to enrich phosphoproteins, nuclear proteins, exosomal proteins, etc. The enriched proteins are eluted from the affinity resin either before or after they are digested using one or more proteases. For protease digestion to be effective, enriched proteins need to remain denatured and disulfide bonds reduced and alkylated to prevent reformation of disulfide bonds. Protein fragmentation is essential for shot-gun proteomics, since this type of mass spectrometry analysis involves ionisation of the sample, and proteins are generally too large to be ionised, whilst peptide fragments are ionised more easily. Protease digestion is generally conducted using one or more proteases with a defined cleavage site (e.g. trypsin or Lys-C), so that digestion of the proteome can be simulated by a computer and mass spectra obtained compared with all peptide sequences predicted to be generated by this protease to determine protein identity. After digestion, peptides are dialysed and de-salted (cleanup), before exchange to a buffer compatible with the subsequent LC-MS/MS analysis.

In this study, LfQ mass spectrometry analysis with and without SPECS was used to

detect changes in the surfaceome and/or secretomes of HTB-94 cells treated with siRNA against ADAM15 and non-targeting control siRNA, transiently transfected with ADAM15 or control expression vector. The predicted results of these manipulation are summarised in Figure 2.1. Each of these analyses required different sample preparation methods, as detailed in the following sections.

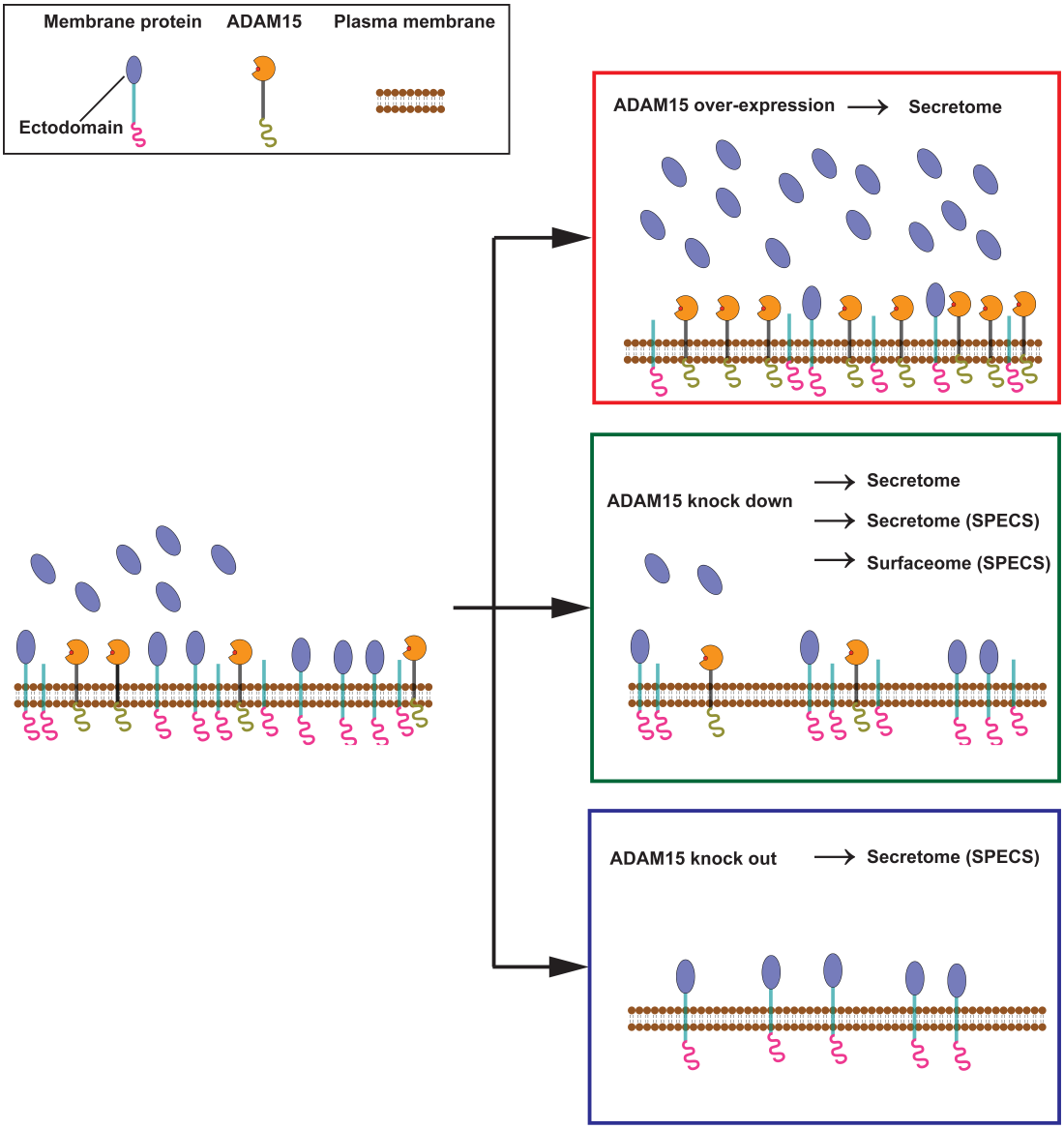

Figure 2.1 Predicted changes caused by manipulation of ADAM15 expression using different strategies and associated proteomic analysis.
ADAM15 expression was manipulated in HTB-94 cells or murine costal chondrocytes. When *ADAM15* is over-expressed in HTB-94 cells, more ADAM15 is predicted to be expressed and transported to the cell surface, resulting in increased proteolytic cleavage of the ectodomain of its substrates (shedding). These shed substrates are released to the CM and quantitatively detected using LfQ secretome analysis by comparing the relative abundance of detected proteins in the secretomes of mock-transfected and ADAM15-over-expressing HTB-94. On the contrary, decreased shedding is predicted to occur when HTB-94 cells are transfected with si*ADAM15*, and proteins with decreased abundance in the CM of *ADAM15*-deficient HTB-94 compared to non-targeting control are predicted to be ADAM15 substrates. Similar results are expected in *Adam15*-null chondrocytes. In addition to conventional analysis, I used SPECS to enrich glycoproteins in the secretome and surfaceome. SPECS only labels newly synthesised glycoproteins, so it may be more sensitive to subtle changes in protein abundance, especially for proteins which are turned over more slowly. In this project, SPECS was used to compared secretomes and surfaceomes of HTB-94 treated with si*ADAM15* and non-targeting control.

2.2.9.1. Sample preparation for LfQ mass spectrometry of secretome of *ADAM15*-over-expressing HTB-94 cells

HTB-94 cells were seeded (5.5×10^6 cells in 10 ml full DMEM per 10 cm^2 dish) the night before transfection. Cells were washed twice with 10 ml ice-cold PBS and once with 15 ml of ice-cold PBS immediately before transfection. Media were then changed to 10 ml Opti-MEM. Transient transfection was performed using TransIT 2020 transfection reagent (Section 2.2.4.1), with the amount of reagents used scaled up according to the manufacturer's guide (i.e. 15 μg plasmid DNA was added to 0.5 ml of Opti-MEM, mixed thoroughly, then 45 μl TransIT 2020 reagent added). 3 replicates of CM from ADAM15-over-expressing HTB-94 and 3 replicates of CM from mock transfected controls were analysed.

Cells were changed to fresh Opti-MEM (15 ml) 48 hours after transfection and left for another 24 hours for proteins to accumulate in the CM. CM were then collected in a 50 ml tube, and centrifuged (5 minutes, 510 x g) to pellet cell debris. The resultant supernatants were collected, filtered through a 0.2 μm Corning syringe filters and concentrated 75-fold (15 ml to 200 μl) on 10 kDa MWCO Microcon centrifugal filters (Millipore), followed by a smaller capacity 5 kDa MWCO Vivaspin 500 (GE Healthcare) spin filter. Concentrated CM were frozen at -80 °C, and shipped on dry ice to the German Center for Neurodegenerative Diseases (DZNE), Technical University Munich (TUM), Munich.

The following mass spectrometry sample preparation steps were performed by our collaborators, Dr. Simone Dario Scilabra and Dr. Stephan Müller, at DZNE. Protein

concentration was determined using the Bio-Rad protein assay according to the manufacturer's guide. 25 μg of protein per sample was subjected to proteolytic digestion with trypsin using the filter-assisted sample preparation (FASP) method (Wisniewski et al., 2009). Digested peptide fragments were de-salted and purified by stop-and-go extraction (STAGE) with C18 tips (Rappsilber et al., 2003). The resultant peptides were dried by vacuum centrifugation and dissolved in 40 μL 0.1% formic acid and analysed by LC-MS/MS.

2.2.9.2. Sample preparation for LfQ mass spectrometry of *ADAM15*-deficient HTB-94 cells

HTB-94 cells (1×10^5 cells in 2 ml full DMEM per well in a 6-well plate) were plated the night before transfection, and washed twice with 2 ml ice-cold PBS and once with 3 ml of ice-cold PBS immediately before transfection. Media were changed to 1.8 ml serum-free DMEM and transient transfection was performed using jetPRIME transfection reagent according to the manufacturer's guide. A suitable volume of jetPRIME Buffer (200 μl per well) was aliquoted into an Eppendorf tube and mixed thoroughly with 10 nM of si*ADAM15* or the same concentration of the non-targeting control siRNA by vortexing. 4 μl of jetPRIME reagent was added to the jetPRIME Buffer-siRNA mixture and mixed thoroughly by vortexing. The transfection mixture was incubated (room temperature, 10 minutes) and added to wells. Cells were cultured at 37 °C for 24 hours, changed to fresh serum-free DMEM and left for another 48 hours for proteins to accumulate in the CM. CM were then collected in a 15 ml tube, and centrifuged (5 minutes, 510 x g) to pellet cell debris. Conditioned media (CM) from all 6 wells in a 6 well plate were pooled together (12 ml total) and treated as one

sample. 6 replicates of siADAM15 and 6 replicates of non-targeting control were analysed.

Supernatants (12 ml) were collected, filtered through a 0.2 μm Corning syringe filter and concentrated 50-fold (10 ml to 200 μl) on 10 kDa MWCO Microcon centrifugal filters (Millipore), followed by a smaller capacity 5 kDa MWCO Vivaspin 500 (GE Healthcare) spin filter and frozen at -80 °C. Samples were shipped on dry ice to the German Center for Neurodegenerative Diseases (DZNE), Technical University Munich (TUM), Munich, and mass spectrometry analysis performed (Section 2.2.9.1).

A similar secretome analysis was also performed on wild-type and *Adam15*-null immature murine costal chondrocytes. Murine costal chondrocytes were isolated from 6-day old C57Bl/6 mice using a method published by Gosset et al. (2008). Isolated chondrocytes were allowed to attach to a tissue culture flask for 6 days in full DMEM, washed twice using 10 ml PBS and once with 15 ml PBS before changing to 15 ml Opti-MEM for an additional 48 hours. CM were then frozen and shipped on dry ice to the German Center for Neurodegenerative Diseases (DZNE), Technical University Munich (TUM), Munich and further processed by myself and our collaborators, Dr. Simone Dario Scilabra and Dr. Stephan Müller.

2.2.9.3. Sample preparation for SPECS secretome LfQ mass spectrometry analysis

HTB-94 cells were plated (1×10^5 cells in 2 ml full DMEM per well in a 6-well plate) the night before transfection and washed twice with 2 ml ice-cold PBS immediately

before transfection. Media were changed to 1.8 ml full DMEM, and transient transfection performed using jetPRIME transfection reagent (Section 2.2.9.1). Cells were cultured at 37 °C for 12 hours before addition of 50 μM ManNAz sugar to the culture for another 24 hours. CM in all 6 wells in a 6 well plate were pooled together and treated as one sample. 3 replicates of si*ADAM15* and 3 replicates of non-targeting control were analysed.

CM were filtered through a 0.2 μm Corning syringe filter, and incubated with concavalin A-conjugated magnetic beads (2 hours, 4 °C). Magnetic beads were collected using a magnet and the supernatant discarded. The beads were washed 3 times using MS wash buffer (50 mM Tris-HCL, pH 7.5, 150 mM NaCl, 2 mM EDTA, 1% Triton), and proteins eluted using concanavalin A elution buffer (500 mM methyl-alpha-D-mannopyranoside, 10 mM EDTA, 20 mM Tris-HCl, pH 7.5). Eluted proteins were incubated with magnetic DBCO beads in the dark (16 hours, 4 °C). Magnetic DBCO beads were collected using a magnet and the supernatant discarded. DBCO beads were washed three times in MS SDS buffer (100mM Tris-HCl, pH 8.5, 1% SDS, 250 mM NaCl), three times in MS urea buffer (8 M urea in 100 mM Tris-HCl, pH 8.5), and three times in 20% acetonitrile with 0.1% sodium deoxycholate. Protein denaturation, disulfide bond reduction and cysteine alkylation were performed using the mass spectrometry procedure detailed in Section 2.2.9.6. Proteins bound to the DBCO beads were digested with LysC for 3 hours, followed by digestion with trypsin for 16 hours. The resultant peptide fragments were reconstituted in 8% formic acid (FA), and de-salted using the STAGE procedure (Section 2.2.9.1) before LC-MS/MS analysis.

2.2.9.4. Sample preparation for SPECS surfaceome (SurfSPECS) LfQ mass spectrometry analysis

ADAM15 knockdown and ManNAz sugar addition were performed according to Section 2.2.9.3. Cell lysates in all 6 wells in a 6 well plate were pooled together and treated as one sample. 3 replicates of *siADAM15* and 3 replicates of non-targeting control were analysed.

Cells were washed twice with 2 ml ice cold PBS (pH 7.4), and changed to 2 ml PBS. 1 μl sulfo-DBCO-biotin conjugate (from 50 mM stock) was added to the culture and incubated for 2 hours at 4 °C in the dark. Cells were washed twice with 10 ml ice cold PBS to remove excess sulfo-DBCO-biotin conjugate, then lysed in 2 ml MS lysis buffer (50 mM Tris, pH 7.5, 150 mM NaCl, 2 mM EDTA, 1% Triton-X-100). Cells were scraped and cell lysates collected in a 15 ml tube before incubation on ice for 15 minutes. Cell lysates were then centrifuged (5 minutes, 4000 × g, 4 °C) and the resultant supernatants filtered through a 0.2 μm Corning syringe filter and collected in a 15 ml tube. Biotinylated proteins were pulled down using the streptavidin pulldown procedure described in Section 2.2.9.5. Summary of the SPECS procedure is illustrated in Figure 2.2.

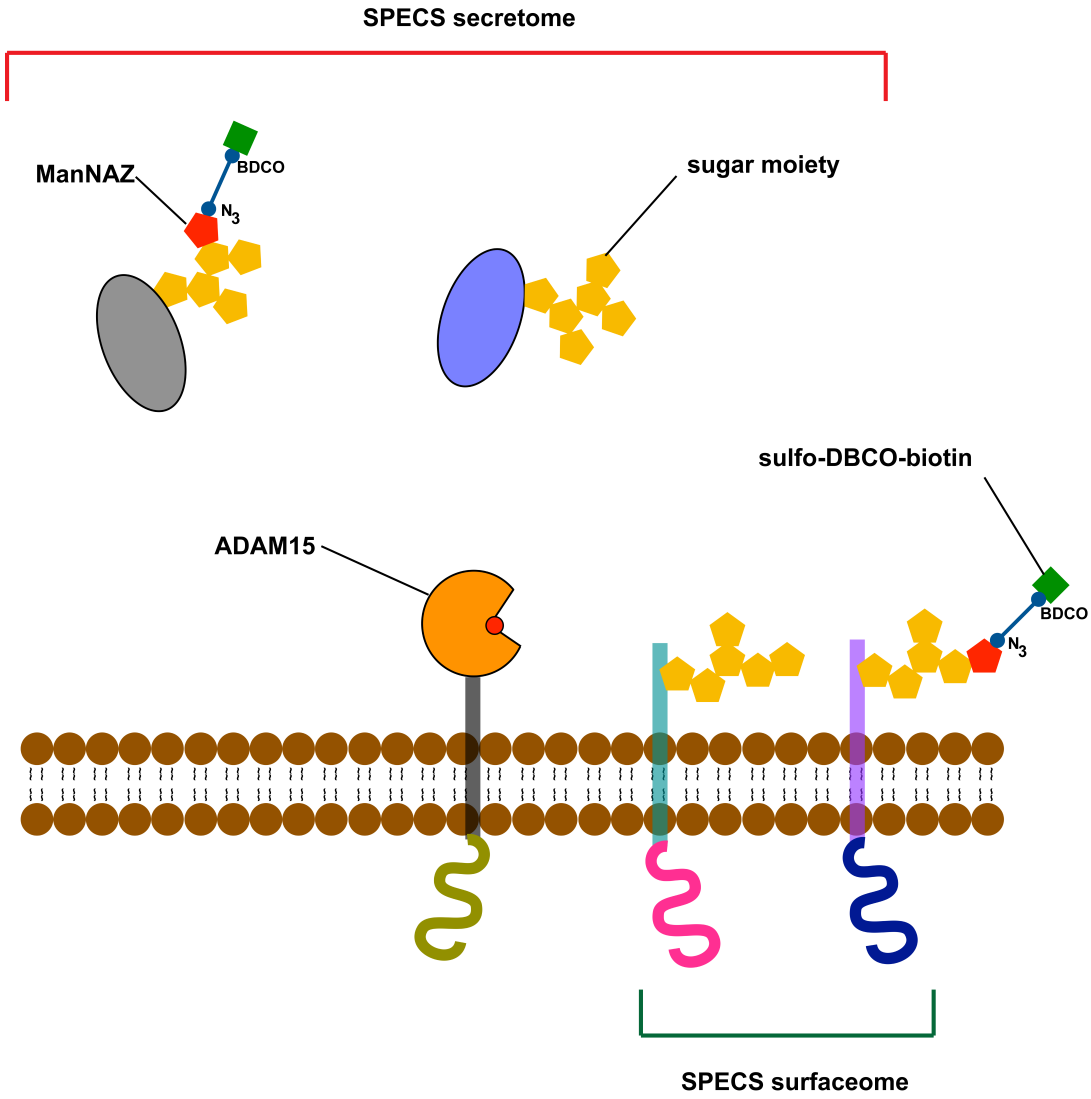

Figure 2.2 Illustration of the SPECS secretome and surfSPECS principle.
To label newly synthesised glycoproteins whose abundance was affected by changes in ADAM15 expression, ManNAz sugar was added to the culture medium after ADAM15 expression was manipulated. ManNAz is permeable to the plasma membrane and is incorporated into the sugar moiety of glycoproteins during their synthesis. Glycoproteins containing ManNAz are 'clicked' using sulfo-DBCO-biotin. The DBCO moiety forms a covalent bond with the N3 group in the ManNAz, thus the ManNAz-containing glycoproteins are linked to the sulfo-DBCO-biotin and can be pulled down using streptavidin-agarose. Since the sulfo-DBCO-biotin is membrane impermeable, sulfo-DBCO-biotin will only 'click' glycoproteins on the plasma membrane and in the extracellular space. The SPECS method is ideal to enrich glycoproteins, especially those that are turned over more slowly. Therefore, SPECS can more accurately reflects the changes induced by changes in ADAM15 expression and help us to identify glycoproteins regulated by ADAM15. Another advantage of SPECS is that labelled proteins are pulled down and non-specifically bound proteins washed off using stringent conditions. This helps to remove abundant proteins in the culture medium which can mask the rare proteins in mass spectrometry analysis. With the SPECS method, it is possible to perform both SPECS secretome and surfSPECS on the same cells treated with siADAM15 or non-targeting siRNA, capturing a more complete picture of changes induced by ADAM15 knockdown.

2.2.9.5. Streptavidin-agarose pulldown of 'clicked' glycoproteins

To perform streptavidin-agarose pulldown, 300 µl of Pierce high capacity streptavidin-agarose (Thermo Fisher) was loaded to a Poly-Prep chromatography column (Bio-Rad Laboratories) and washed once with 10 ml PBS by gravity. 'Clicked' CM or cell lysates were loaded onto the column, the flow-through collected and re-loaded onto the column. Streptavidin-agarose was washed twice with 10 ml MS wash buffer to remove non-specifically bound material. Streptavidin-agarose beads were re-suspended in 500 µl MS wash buffer and transferred to new Eppendorf tubes. Another 500 µl MS wash buffer was added to the column to gather remaining beads which were pooled with the first wash in the same Eppendorf tube. Beads were centrifuged (1 minute, 7000 × g, room temperature) and the resultant supernatant collected and stored at -20 °C. Beads were dried by aspiration using a fine bore pipette tip to prevent beads being sucked up and stored at -20 °C until they were shipped to Munich on dry ice. Peptides were eluted using MS elution buffer (8M urea, 2% SDS, 10% glycerol, 5% mercaptoethanol, 0.002% bromphenol-blue, 62.5 mM TrisHCl, pH 6.8) with 3 mM biotin, and boiled (95 °C, 5 minutes). Eluates were collected in an Eppendorf tube using a fine-bore pipette tip, and electrophoresed on a 10% acrylamide SDS-PAGE gel. The gel was stained using Coomassie brillant blue (30-60 minutes), and de-stained overnight with 10% acetic acid. Qualitatively equal gel slices were then excised from the gel and proteins in the gel slices digested with trypsin using the in-gel digestion protocol described in Section 2.2.9.6.

2.2.9.6. In-gel digestion

In-gel digestion was performed according to the method published by Shevchenko et al. (Shevchenko et al., 2006). Protein lanes from the de-stained acrylamide gel were

sliced out vertically and divided into 8 equal horizontal pieces above the BSA band (the thickest band at around 64 kDa on the gel) and 6 equal horizontal pieces below the BSA band. Great care was taken to prevent any contamination, especially from polyethylene glycol which impairs the mass spectrometry detection of fragmented peptides. Pieces were further sliced into 1 mm^3 cubes and collected in a 96-well plate. 150 µl of HPLC grade acetonitrile (ANC) was added to the wells and incubated (room temperature, 10 minutes) with gentle rotation. Gels were de-hydrated using vacuum centrifugation. The ANC-vacuum centrifugation step was repeated until gels were completely dry and appeared white. It generally took three rounds of vacuum centrifugation for complete de-hydration. To break disulfide bonds, 10 mM dithiothreitol (DTT) solution in 100 mM ammonium bicarbonate (ABC) was prepared immediately before use, and 50 µl of the DTT solution added to each well (55 °C, 30 minutes). Gels were cooled to room temperature and another 150 µl ANC was added to the wells, followed by vacuum centrifugation for 10 minutes. To prevent re-formation of disulfide bonds between cysteine residues, 55 mM iodoacetamide (IAA) solution was prepared immediately before use in 100 mM ABC and the solution added to wells to cover the gel pieces, and incubated for 20 minutes in the dark to alkylate cysteine residues. Gels were then de-hydrated using 150 µl ANC. Meanwhile, MS trypsin buffer was freshly prepared (10 mM ABC in 10% ACN) and trypsin powder was reconstituted at 3 ng/µl in MS trypsin buffer. 50 µl of reconstituted trypsin was added to cover each gel piece completely, and trypsin incubation performed on ice for 30 minutes. If the trypsin solution was absorbed completely by the gel, more MS trypsin buffer was added and gels left on ice for another 90 minutes. ABC was then added to cover the gel pieces completely, the 96-well plate covered with its lid, and placed into a 37 °C incubator overnight. On the following day, 5% formic acid (FA) and

ACN were mixed (1:2 volume:volume ratio) immediately before use and 100 µl of the mixture added to wells before incubation at room temperature with gentle shaking for 15 minutes to extract fragmented peptides. The resultant supernatant was collected in an Eppendorf tube, and the extraction step repeated (generally 3 times) until gel pieces were completely de-hydrated. Peptides in the supernatant were de-hydrated using vacuum centrifugation and reconstituted in 33 µl 0.1% FA.

2.2.9.7. Proteomic analysis using LC-MS/MS

To perform liquid chromatography tandem mass spectrometry (LC-MS/MS), approximately 1 µg of peptides from each sample were loaded onto the nanoLC system (EASY-nLC 1000, Proxeon) using an in-house packed C18 column (50 cm x 75 µm ID, ReproSil-Pur 120 C18-AQ, 1.9 µm, Dr. Maisch GmbH, Germany) with a binary gradient (Table 2.12) of water and acetonitrile containing 0.1% FA at a column temperature of 50 °C. The nanoLC system was coupled with a Q-Exactive mass spectrometer (Thermo Fisher Scientific, USA) via an nanospray ex ion source system (Proxeon) online. Mass spectra were acquired at a resolution of 70,000 and the top 10 peptide ions exceeding an intensity of 2.5×10^4 were chosen for collision-induced dissociation to sequence peptides via fragmentation. The resultant fragment ion spectra were acquired at a resolution of 17,500. A dynamic exclusion of 120 seconds was used for peptide fragmentation.

Table 2.12 LC gradient used for LC-MS/MS separation of tryptic peptides.

Time [min]	Duration [min]	Flow [nL/min]	Acetonitrile [%]
0	-	50	2
5	5	250	5
185	180	250	25
230	45	250	35
250	20	250	60
255	5	250	95
270	15	250	95

2.2.9.8. Analysis of the proteomic data

Data generated by LC-MS/MS was analysed using Maxquant 1.5.2.8. (Max-Planck Institute Munich, Germany). Proteomic data generated were compared against a reviewed canonical FASTA database of *Homo sapiens* from UniProt. Trypsin or trypsin plus LysC were pre-defined as the protease(s) used for digestion. Two missed cleavages were allowed when performing database searches. A pilot search was used to re-calibrate the peptide masses within a window of 20 ppm, then a main search was conducted using peptide and peptide fragment mass tolerances of 4.5 and 20 ppm, respectively. Carbamidomethylation of cysteine was set as a static modification, whilst acetylation of the protein N-terminus and oxidation of methionine were set as variable modifications. False discovery rates (FDR) of both peptides and proteins were adjusted to less than 5% using a decoy proteomic data base using the same criteria as the real canonical FASTA database. Label-free quantification (LfQ) for protein abundance was only performed when at least two ratio counts of unique peptides were detected in each experimental conditions (e.g. non-targeting vs. knockdown, or mock transfection vs. over-expression). Additionally, only unique peptides were used for LfQ. The LfQ values were transformed to $\log_2$-based values and a two-sided heteroscedastic

student's t-test was used to perform statistical analysis of significance. A p-value less than 5%, corrected with the FDR, was set as the significance threshold.

Chapter 3. Characterising changes in ADAM15 expression with age and in OA

3.1. Introduction

Adam15 is widely expressed in a variety of murine tissues, with high expression found in endothelial cells, endocardium, hypertrophic chondrocytes in developing bone, and some areas of the brain (Horiuchi et al., 2003). Human *ADAM15* is known to be expressed in kidney mesangial cells (Martin et al., 2002), smooth muscle cells (Al-Fakhri et al., 2003), colon and small intestine (Charrier et al., 2005), and at a low level in synovium (Bohm et al., 2001). Additionally, *ADAM15* expression can be detected in articular cartilage using RT-PCR and Northern blotting (McKie et al., 1997). Altered ADAM15 expression has been linked to several important physiological and pathological processes, such as inflammation (Charrier-Hisamuddin et al., 2008), neovascularisation (Horiuchi et al., 2003) and tumour metastasis (Najy et al., 2008a, b), which indicates the enzyme is likely to have important roles in tissue homeostasis.

Interestingly, ADAM15 has been found to play an important role in cartilage, as *Adam15*-deficient mice developed accelerated OA upon ageing (Bohm et al., 2005). Several studies have attempted to compare the mRNA expression of human and murine *ADAM15* in normal and OA articular cartilage, with contradictory results. I reviewed the available literature and found that most studies (12 out of 13) concluded that *ADAM15* expression was not significantly different in normal and OA cartilage (Yang et al., 2017). One study found that *ADAM15* expression was up-regulated in OA chondrocytes using *in situ* hybridisation (Bohm et al., 1999), whilst all other studies reviewed examined expression using DNA microarrays. ADAM15 expression at protein level in normal and OA cartilage has not been characterised in human or murine tissues.

Although cartilage is composed of a single cell type (the chondrocyte), phenotypic differences in chondrocytes can be observed in different zones of articular cartilage, especially in humans and larger mammals (Sophia Fox et al., 2009). For example, superficial zone chondrocytes are flatter, whilst chondrocytes in the middle zone and deeper zone are rounder and larger. In terms of density and arrangement, the superficial zone tends to have a higher chondrocyte density, whilst middle zone chondrocytes are more dispersed. Both superficial and middle zone chondrocytes are more randomly arranged, whilst deeper zone chondrocytes are often arranged in columns.

Chondrocytes in different zones are known to express different molecules, or differential expression of individual molecules. For example, lubricin is mainly expressed in superficial zone chondrocytes (Jay et al., 2014). Additionally, the composition, arrangement and orientation of ECM components varies in different zones, e.g. the superficial zone has a higher concentration of collagen and lower concentration of proteoglycans, and the collagen fibrils are thinner. In contrast, the deeper zone has a higher concentration of proteoglycans, and the thickest collagen fibrils (Bhosale et al., 2008). Altered expression or distribution of these molecules may lead to loss of cartilage homeostasis and disease pathogenesis (Troeberg et al., 2012).

Even though *ADAM15* mRNA has been detected in human articular cartilage, its distribution in cartilage has not been characterised, and potential changes in this distribution in OA have not been studied. Such analyses may further understanding of ADAM15's role in maintaining cartilage homeostasis. Therefore, in this study, I aimed to characterise ADAM15 expression both at the mRNA and protein level, and to

compare its distribution in normal and osteoarthritic cartilage.

3.2. *ADAM15* mRNA expression in human OA and normal cartilage

I set out to compare *ADAM15* expression in human normal and OA cartilage. I confirmed that there was no statistically significant difference in the ages of normal and OA donors. Figure 3.1 (A) shows the difference in mean ages of OA and normal samples relative to the mean age of all samples examined, Figure 3.1 (B) shows the difference in mean ages of male and female samples relative to the mean age of all samples, whilst Figure 3.1 (C) shows the difference in mean ages of OA male, OA female, normal male and normal female samples relative to the mean age of all samples used. Overall, OA samples were from slightly older donors than normal samples (OA average age: 64.50, normal average age: 58.67, difference: 5.83), with OA male samples having the highest average age (65.67) and normal female samples having the lowest (57.33). Average difference between sexes was low (1.62).

I isolated OA chondrocytes using the method detailed in Section 2.2.1. RNA was extracted from isolated OA chondrocytes growing in monolayer according to the method described in Section 2.2.5.2. Normal chondrocyte RNA was kindly provided by Dr. Linda Troeberg, KIR. I also extracted RNA directly from cartilage as described in Section 2.2.5.2. RNA obtained using both methods was reverse transcribed to cDNA, and the relative *ADAM15* expression relative to a housekeeping gene *RPLP0* quantified using qPCR.

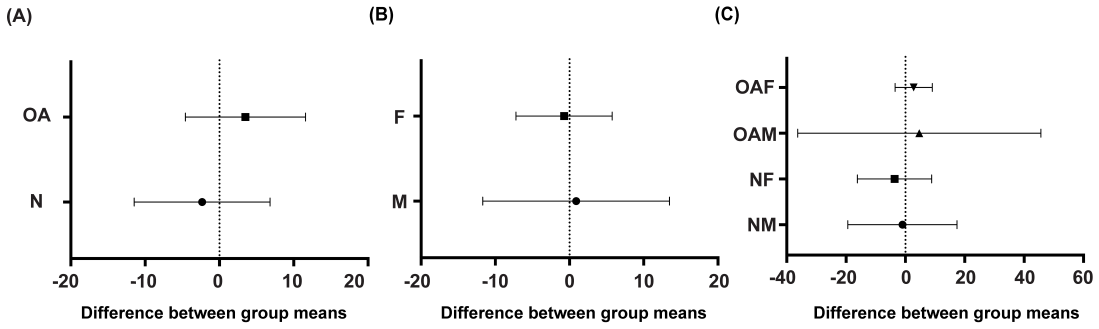

Figure 3.1 Analysed articular cartilage samples were age-matched.
(A) Mean age for all samples (OA + normal, n = 20) was calculated and subtracted from the mean age of OA (n = 8) and normal (n = 12) groups, respectively (ΔMean [all - OA]: 3.5, 95% CI: [-4.581, 11.58], ΔMean [all - normal]: -2.333, 95% CI: [-11.47, 6.803], difference between ΔMean [all - OA] and ΔMean [all - normal]: 5.83). Difference in ΔMeans was not statistically significant (p = 0.3297).
(B) Mean age for all samples was calculated and subtracted from the mean age of female (n = 9) and male (n = 11) groups (ΔMean [all - female]: -0.7273, 95% CI: [-7.207, 5.752], ΔMean [all - male]: 0.8889, 95% CI: [-11.71, 13.49], difference between ΔMean [all - male] and ΔMean [all - female]: 1.62). Difference in ΔMeans was not statistically significant (p = 0.7865)
(C) Mean age for all samples was calculated and subtracted from the mean age of OA females (n = 5), OA males (n = 3), normal females (n = 6) and normal males (n = 6) (ΔMean [all - OA female]: 2.8, 95% CI: [-3.495, 9.095], ΔMean [all - OA male]: 4.667, 95% CI: [-36.33, 45.66], ΔMean [all - normal females]: -3.667, 95% CI: [-16.2, 8.868], ΔMean [all - normal males]: -1, 95% CI: [-19.42, 17.42]. Difference between ΔMean [all - OA females] and ΔMean [all - OA males]: 1.87, difference between ΔMean [all - OA females] and ΔMean [all - normal females]: 6.47, difference between ΔMean [all - OA females] and ΔMean [all - normal males]: 3.8, difference between ΔMean [all - OA males] and ΔMean [all - normal females]: 8.34, difference between ΔMean [all - OA males] and ΔMean [all - normal males]: 5.67, difference between ΔMean [all - normal females] and ΔMean [all - normal males]: 2.67). Differences in ΔMeans were not statistically significant (p = 0.7886).
Data are depicted as mean plus 95% CI. OA: osteoarthritis, N: normal, F: female, M: male. The statistical significance of comparison in (A) and (B) were analysed with Student's t test (two-tailed), and the comparison in (C) was analysed using one-way ANOVA.

Figure 3.2 shows that *ADAM15* expression was significantly decreased in OA monolayer chondrocytes compared with normal monolayer chondrocytes (Figure 3.1 (A), p = 0.0129, 95 % CI: [-0.6904 , -0.09374]). However, when RNA was directly extracted from cartilage, no difference in *ADAM15* expression was found between normal and OA cartilage (p = 0.7883, 95 % CI: [-1.263, 1.64]). This is consistent with my review of the literature (Yang et al., 2017).

The decrease in *ADAM15* expression in monolayer OA chondrocyte culture indicates that monolayer chondrocyte culture may introduce artificial changes to *ADAM15* expression and may not be ideal to model the phenotype and behaviour of

chondrocytes residing in their native environment. To better capture changes in gene expression of chondrocytes residing in their native environment, in the following experiments, RNA was directly extracted from cartilage or whole joints whenever possible.

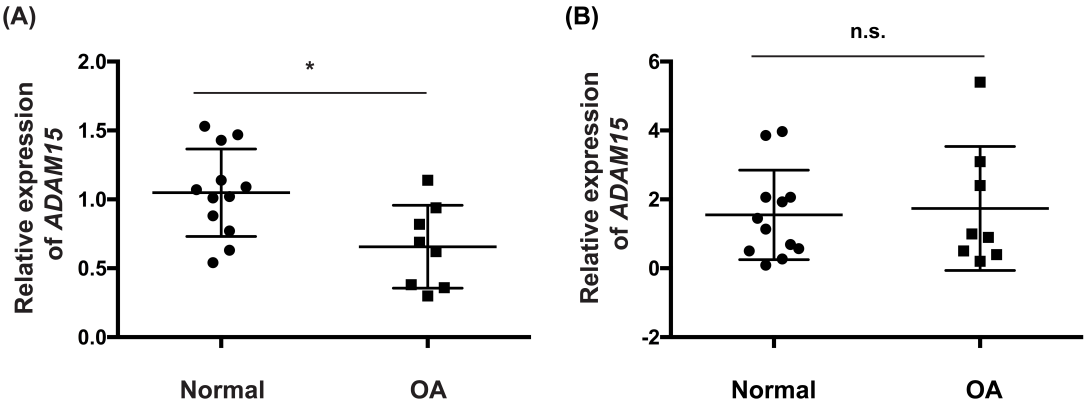

Figure 3.2 *ADAM15* showed no difference in expression between human normal and OA cartilage.
RNA extracted from normal and OA monolayer chondrocytes or normal and OA cartilage was reverse transcribed and quantified using qPCR. Expression of *ADAM15* was normalised to the housekeeping gene *RPLP0* and calculated using the ΔΔCt method (Section 2.2.5.4). Relative expression of *ADAM15* was normalised to the average of *ADAM15* expression in normal samples.
(A) *ADAM15* expression was significantly decreased ($p = 0.0129$, 95 % CI: [-0.6904 , -0.09374]) in OA monolayer chondrocytes ($n = 8$) compared to normal monolayer chondrocytes ($n = 12$).
(B) *ADAM15* expression showed no change between normal ($n = 12$) and OA ($n = 8$) cartilage ($p = 0.7883$, 95 % CI: [-1.263, 1.64]).
Data are shown as mean ± SD, *, $p \leq 0.05$, n.s., not significant. The statistical significance of comparison between normal and OA was analysed with Student's t test (two-tailed).

3.3. *Adam15* mRNA expression in murine joints after DMM surgery

The human cartilage used in Section 3.2.1. was obtained from patients who underwent either UKA or TKA knee replacement surgery (Section 2.1.1.) for end stage disease. Although these data suggests that *ADAM15* was not differentially regulated in normal and OA human cartilage, it is possible that *ADAM15* expression is regulated differently early in disease. To circumvent this limitation, I analysed samples from the

mouse DMM model of OA, which allowed me to follow changes in *Adam15* expression at all stages of disease progression.

I analysed samples from an existing project in the Troeberg group to look at changes in gene expression after DMM surgery. DMM was performed on C57BL/6 mice by Dr. Jadwiga Zarebska (KIR) and mouse joints were harvested by Dr. Anastasios Chanalaris (KIR) at 6 hours, 8 weeks and 12 weeks after DMM surgery. The three time points chosen here represent the acute phase after surgery, early OA and late OA. RNA from the 6-hour time point was extracted and analysed by Dr. Anastasios Chanalaris using a microfluidic card TaqMan gene expression assay (Thermo Fisher Scientific). I extracted RNA from mouse joints 8- and 12-weeks after surgery, reverse transcribed them to cDNA and quantified *Adam15* expression using qPCR.

Figure 3.3 shows that *Adam15* expression did not change between sham and DMM-operated joints at all time points analysed (6 hours after DMM : $p = 0.4944$, 95 % CI: [-0.2273, 0.1152]; 8 weeks after DMM: $p = 0.1713$; 12 weeks after DMM: $p = 0.0694$).

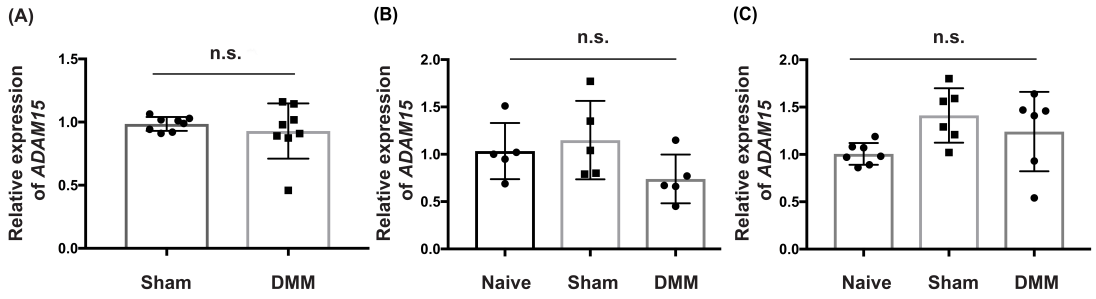

Figure 3.3 *Adam15* expression did not change in murine joints 6 hours, 8 weeks or 12 weeks after DMM surgery.
RNA extracted from murine joints 6 hours, 8 weeks and 12 weeks after DMM surgery was reverse transcribed and quantified using qPCR. Expression of *Adam15* was normalised to the housekeeping gene *Rplp0* and calculated using the ΔΔCt method (Section 2.2.5.4).
(A) *Adam15* expression was not significant altered (p = 0.4944, 95 % CI: [-0.2273, 0.1152]) in sham (n = 8) and DMM (n = 8) joints 6 hours after surgery. Relative expression of *Adam15* was normalised to the average *Adam15* expression in sham samples. Data were generated by Dr. Anastasios Chanalaris.
(B) *Adam15* expression was not significantly changed (p = 0.1713) in murine joints across all three groups (n = 5 per group) 8 weeks after DMM surgery.
(C) *Adam15* expression showed no significant change (p = 0.0694) in murine joints across all three groups (n = 6 per group) 12 weeks after DMM surgery.
Data are shown as mean ± SD, n.s., not significant. In (B) and (C), relative expression of *Adam15* was normalised to the average *Adam15* expression of naive samples. The statistical significance of comparison between sham and DMM treated groups (6 hours) was analysed with Student's t test (two-tailed), whilst the statistical significance of comparison between naive, sham and DMM groups at 8 and 12 weeks was analysed with one-way ANOVA.

3.4. Age-dependence of *ADAM15* expression in human cartilage

To examine whether expression of ADAM15 was regulated with age, a known risk factor for OA, I extracted RNA from normal and OA cartilage, reverse transcribed it to generate cDNA, and quantified *ADAM15* expression relative to the housekeeping gene *RPLP0* using qPCR. RNA from cartilage of four donors aged between 9-16 years old was kindly provided by Dr. Chris Murphy and Dr. Christine Seidl (KIR).

Relative *ADAM15* expression was normalised to the average *ADAM15* expression in normal cartilage samples. I then depicted relative *ADAM15* expression of each sample against age. Since the results in Section 3.2.1. indicate that *ADAM15* expression did not differ between normal and OA cartilage, data from normal (•) and OA (×) cartilage were analysed together. Indeed, as shown in Figure 3.4 (A), data from normal and OA

samples did not cluster into two groups.

ADAM15 expression displayed an inverse parabola relationship with age. Cartilage from young donors (9-16 years old) had low *ADAM15* expression, and expression then increased with age to a maximum in donors aged approximately 45-55 years old. Expression then decreased gradually after approximately 55 years of age. Notably, though sex is known to influence susceptibility to OA (Srikanth et al., 2005), *ADAM15* expression was not different in male and female donors ($p = 0.2187$, 95 % CI: [-2.204, 0.5396]), as shown in Figure 3.4 (B).

This data set contains relatively few samples from donors between 20 to 45 years of age, due to the limited availability of cartilage samples from this age group. As mentioned above, the prevalence of OA is much higher in the elderly, hence most of our OA samples came from relatively old patients who underwent TKA or UKA. Due to this limitation, this data set is not suitable for performing correlation analysis or nonlinear regression. Moreover, this limitation also makes the data unsuitable for linear regression analysis on Ct values of the housekeeping gene *RPLP0*, so I was unable to evaluate whether *RPLP0* is a suitable control across different ages.

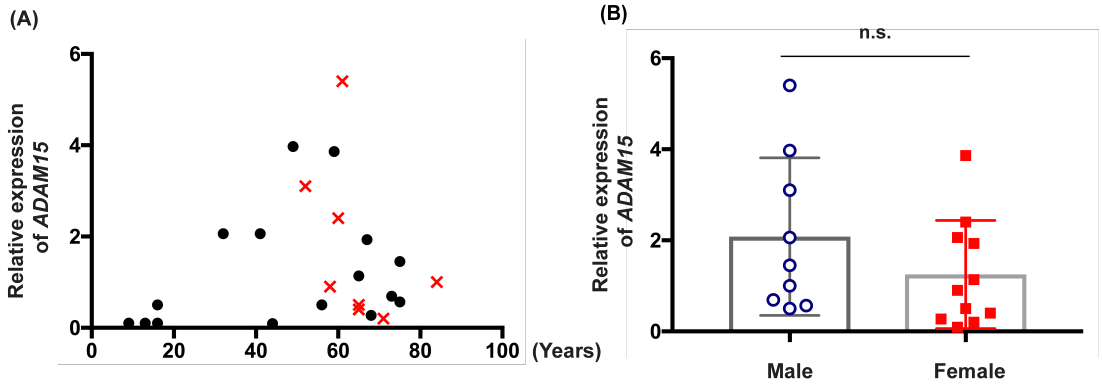

Figure 3.4 *ADAM15* expression in human cartilage changed with age, but was unaffected by sex.
RNA was extracted from normal and OA cartilage from donors of different ages, reverse transcribed and quantified using qPCR. *ADAM15* expression was normalised to the housekeeping gene *RPLP0* and relative expression calculated using the ΔΔCt method (Section 2.2.5.4). Relative expression of *ADAM15* was normalised to the average *ADAM15* expression of normal samples.
(A) *ADAM15* expression displayed an inverse U relationship with age. *ADAM15* expression was low in young donors of 9-16 years of age, high in adulthood, and decreased steadily after approximately 55 years of age. Black dots (•, n = 16) represent from normal samples, and red crosses (×, n = 8) represent OA samples.
(B) Data were separated by sex irrespective of age. Relative expression of *ADAM15* was normalised to the average *ADAM15* expression in female donors. No difference in *ADAM15* expression was found between male (•, n =9) and female (▪, n =11) donors (p = 0.2187, 95 % CI: [-2.204, 0.5396]). Samples younger than 20 years of age were excluded from the analysis due to lack of information regarding their genders. Data in **(B)** are shown as mean ± SD, n.s., not significant. The statistical significance of comparison between male and female was analysed with Student's t test (two-tailed).

3.5. Age-dependence of *Adam15* expression in male murine joints

To circumvent the constraints of human sample availability, I performed age-controlled experiments using murine joints. Joints from male mice of different ages (0.2 months, 3 months, 4.5 months, 5.5 months, and 18 months of age) were harvested by Maarten Swart, Dr. Linda Troeberg, and myself. I extracted RNA from the joints, made cDNA by reverse transcription and quantified *Adam15* expression using qPCR. *Adam15* expression was normalised to the housekeeping gene *Rplp0* and relative expression of *Adam15* was normalised to the average *Adam15* expression of the 18 month-old group. Figure 3.5 shows that *Adam15* expression in the joints of old mice (18 months old) was significantly decreased by >97% compared to the 3-month, 4.5-month and 5.5-month old groups when post hoc multiple comparisons were performed and corrected using

Tukey's test (3-month old vs. 18-month old: adjusted $p < 0.0001$, mean difference: 34.86, 95 % CI: [19.38, 50.35]; 4.5-month old vs. 18-month old: adjusted $p < 0.0001$, mean difference: 44.83, 95 % CI: [25.18, 64.48]; 5.5-month old vs. 18-month old: adjusted $p < 0.0001$, mean difference: 38.33, 95 % CI: [19.72, to 56.94], percentage of decrease was calculated using the following formula: {1 - [1 ÷ (mean difference)] } %).

Similarly, *Adam15* expression in young murine joints (0.2 months old) was significantly decreased (> 95%) compared to 3-month, 4.5-month and 5.5-month old mice (0.2-month old vs. 3-month old: adjusted $p = 0.0086$, mean difference: -21.22, 95 % CI: [-38.23, -4.213]; 0.2-month old vs. 4.5-month old: adjusted $p = 0.0012$, mean difference: -31.19, 95 % CI: [-52.06, -10.32]; 0.2-month old vs. 5.5-month old: adjusted $p < 0.0090$, mean difference: -24.69, 95 % CI: [-44.58, -4.79], percentage of decrease was calculated using the following formula: { 1 - [1 ÷ (-mean difference)] } %). However, no difference was found between the 0.2-month old and 18-month old age groups (adjusted $p = 0.2383$, mean difference: 13.64, 95 % CI: [-4.97, 32.25]).

The age-dependent, inverse parabola pattern of ADAM15 expression observed in human cartilage was thus also observed in murine joints.

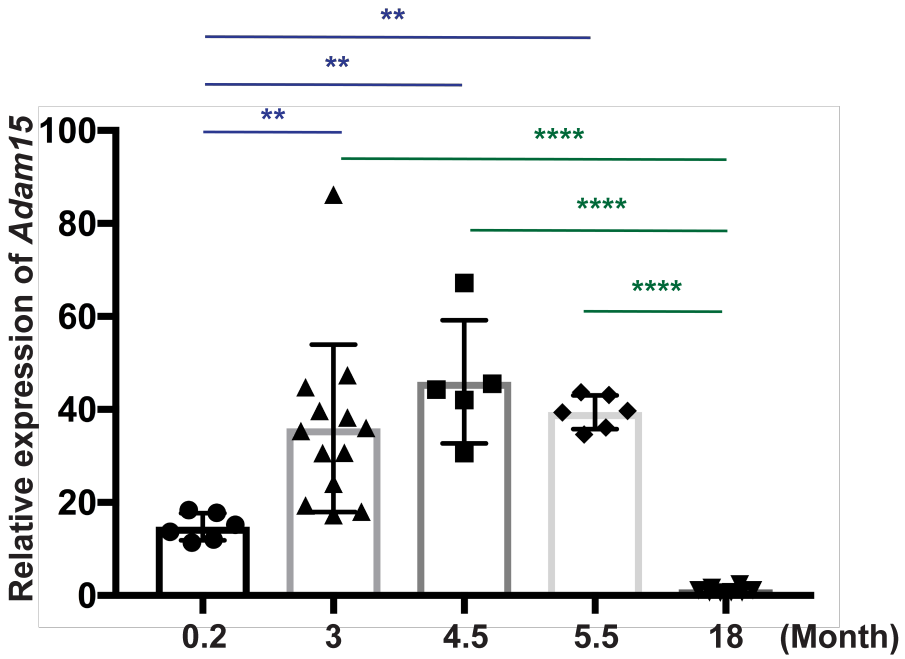

Figure 3.5 *Adam15* expression in the murine knee joints changed with age.
RNA extracted from joints from 0.2-month (n = 6), 3-month (n = 13), 4.5-month (n = 5), 5.5-month (n = 6) and 18-month (n = 8) old male mice was reverse transcribed and quantified using qPCR. Expression of *Adam15* was normalised to the housekeeping gene *Rplp0* and relative expression calculated using the ΔΔCt method (Section 2.2.5.4). Relative expression of *Adam15* in each age group was normalised to the average *Adam15* expression of 18-month old mice. *Adam15* expression in the joints of 18-month old mice was significantly decreased compared to 3-month old mice (adjusted $p < 0.0001$, mean difference: 34.86, 95 % CI: [19.38, 50.35]), 4.5-month old mice (adjusted $p < 0.0001$, mean difference: 44.83, 95 % CI: [25.18, 64.48]), and 5.5-month old mice (adjusted $p < 0.0001$, mean difference: 38.33, 95 % CI: [19.72, to 56.94]). Likewise, *Adam15* expression was significantly lower in the joints of 0.2-month old mice than in 3-month old mice (adjusted $p = 0.0086$, mean difference: -21.22, 95 % CI: [-38.23, -4.213]), 4.5-month old mice ($p = 0.0012$, mean difference: -31.19, 95 % CI: [-52.06, -10.32]), and 5.5-month old mice (adjusted $p < 0.0090$, mean difference: -24.69, 95 % CI: [-44.58, -4.79]). No statistically significant difference was found between 0.2-month old mice and 18-month old mice, nor between the 3-, 4.5- and 5.5-month old groups. Data are shown as mean ± SD, ****, $p \leq 0.0001$, ** $p \leq 0.01$. The statistical significance of comparison between age groups was analysed with one-way ANOVA, with post hoc multiple comparisons corrected using Tukey's test.

To investigate whether this age-dependent expression was specific to *Adam15*, common among *Adam* metalloproteinases, or reflected a general down-regulation of genes in murine joints with ageing, the expression of *Adam17* and three other chosen genes (i.e. *Sirt1*, *Runx2*, and *Jak2*) was quantified in the same samples. These three genes were chosen because of primer availability and, in the case of *Sirt1* and *Runx2*, for their relevance in bone and cartilage ageing. Figure 3.6 (A) shows that *Adam17* displayed a similar inverse parabola pattern of expression as *Adam15*, with its

expression highest in 4.5-month old joints, and significantly lower in joints from 0.2-month old, 5.5-month old and 18-month old mice (0.2-month old vs. 4.5-month old: adjusted p = 0.0074, mean difference: -0.795, 95 % CI: [-1.424, -0.1664]; 4.5 month old vs. 5.5 month old: adjusted p = 0.0496, mean difference: 0.5925, 95 % CI: [0.0006824, 1.184]; 4.5 month old vs. 18 months old: adjusted p = 0.0012, mean difference: 0.8863, 95 % CI: [0.2944, 1.478]). However, less than 2-fold change in expression was observed, while up to 46-fold change in *Adam15* expression was observed.

Figure 3.6 (B-D) shows mRNA expression of *Sirt1*, *Runx2*, and *Jak2* relative to age. mRNA expression of the NAD-dependent deacetylase *Sirt1* increased by approximately 3-fold in 0.2-month old joints relative to 4.5-month old joints (adjusted p = 0.0012, mean difference: -2.19, 95 % CI: [-3.635, -0.7459]), but its expression was not significantly changed with age. Expression of *Runx2*, the gene encoding the master transcription factor regulating osteoblast differentiation and skeleton formation (Komori et al., 1997; Otto et al., 1997), decreased with age, with expression approximately halved in 5.5-month and 18-month old joints compared to 3-month old and 4.5-month old joints (3-month old vs. 5.5-month old: adjusted p = 0.0022, mean difference: 0.6396, 95 % CI: [0.1951, 1.084]; 3-month old vs. 18-month old: adjusted p < 0.0001, mean difference: 0.8596, 95 % CI: [0.4151, 1.304]; 4.5-month old vs. 5.5-month old: adjusted p = 0.0107, mean difference: 0.5743, 95 % CI: [0.105, 1.043]; 4.5-month old vs. 18-month old: adjusted p = 0.0003, mean difference: 0.7943, 95 % CI: [0.325, 1.263]). *Jak2* expression was low in 0.2-month old joints, and increased significantly with age (0.2-month old vs. 3-month old: adjusted p = 0.0004, mean difference: -1.41, 95 % CI: [-2.26, -0.5598]; vs. 4.5-month old: adjusted p < 0.0001, mean difference: -1.851, 95 % CI: [-2.742, -0.959]; vs. 5.5-month old: adjusted p = 0.0016, mean difference: -1.178, 95 %

CI: [-1.973, -0.3826]; vs. 18-month old: adjusted p = 0.0002, mean difference: -1.415, 95 % CI: [-2.235, -0.596]) and remained relatively constant in adulthood (3-, 4.5-, and 5.5-month old), and in old age (18-month old). None of these genes showed a similar age-dependent, inverse parabola pattern of expression as was observed for *Adam15*, suggesting that changes in *Adam15* expression were not a general age-related phenomenon. These expression data are summarised in Table 3.1 at the end of this chapter.

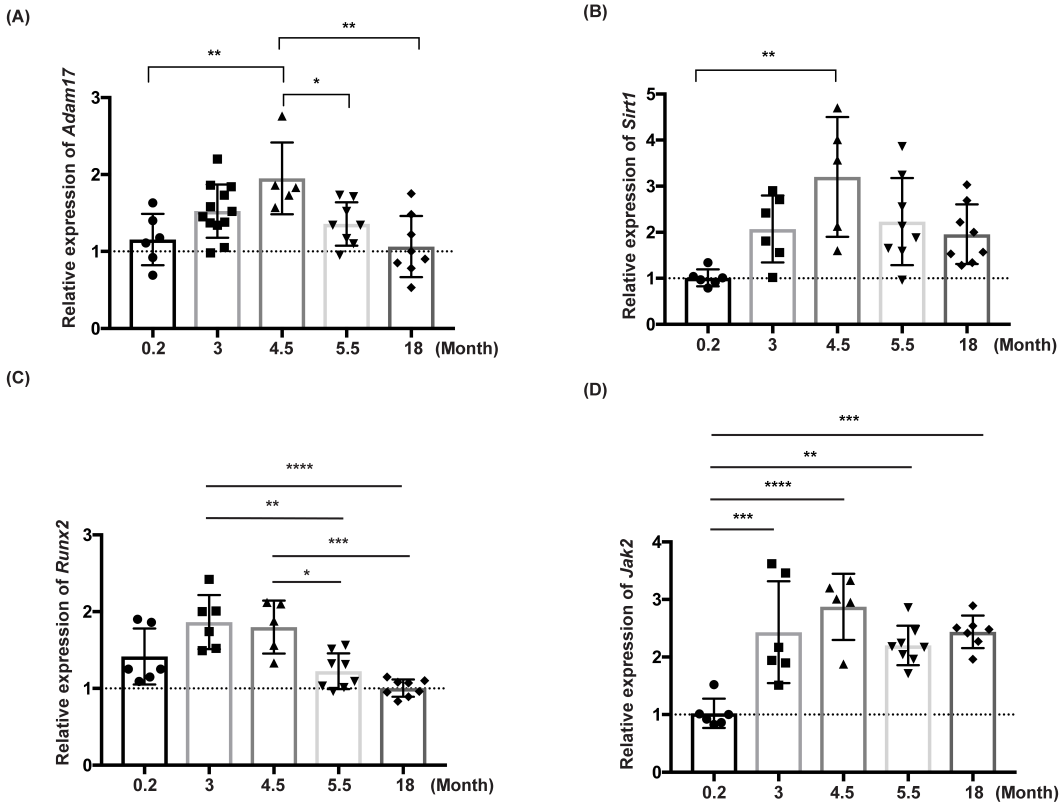

Figure 3.6 Age-dependent expression of *Adam17*, *Sirt1*, *Runx2*, and *Jak2* in murine joints.
RNA extracted from joints of 0.2-month (n = 6), 3-month (n = 6), 4.5-month (n = 5), 5.5-month (n = 8) and 18-month (n = 8) old male mice was reverse transcribed and quantified using qPCR. Expression of the genes of interest was normalised to the housekeeping gene *Rplp0* and relative expression calculated using the ΔΔCt method (Section 2.2.5.4).
(A) Expression of *Sirt1* was significantly up-regulated in 4.5-month old murine joints compared to 6-day old joints (adjusted p = 0.0012, mean difference: -2.19, 95 % CI: [-3.635, -0.7459]).
(B) Expression of *Runx2* was significantly down-regulated in 5.5-month and 18-month old murine joints compared to the 3-month old group (3-month old vs. 5.5-month old: adjusted p = 0.0022, mean difference: 0.6396, 95 % CI: [0.1951, 1.084]; 3-month old vs. 18-month old: adjusted p < 0.0001, mean difference: 0.8596, 95 % CI: [0.4151, 1.304]). Likewise, *Runx2* expression was significantly down-regulated in 5.5-month and 18-month old murine joints compared to the 4.5-month old group (4.5-month old vs. 5.5-month old: adjusted p = 0.0107, mean difference: 0.5743, 95 % CI: [0.105, 1.043]; 4.5-month old vs. 18-month old: adjusted p = 0.0003, mean difference: 0.7943, 95 % CI: [0.325, 1.263]).

(C) Expression of *Jak2* was significantly down-regulated in 0.2-month old murine joints compared to all other age groups examined (0.2-month old vs. 3-month old: adjusted p = 0.0004, mean difference: -1.41, 95 % CI: [-2.26, -0.5598]; vs. 4.5-month old: adjusted p < 0.0001, mean difference: -1.851, 95 % CI: [-2.742, -0.959]; vs. 5.5-month old: adjusted p = 0.0016, mean difference: -1.178, 95 % CI: [-1.973, -0.3826]; vs. 18-month old: adjusted p = 0.0002, mean difference: -1.415, 95 % CI: [-2.235, -0.596]).
The statistical significance of comparison between age groups was analysed with one-way ANOVA, with post hoc multiple comparisons corrected using Tukey's test.

3.6. Expression of senescence markers *Cdkn2a*, *Cdkn1a* and *Il6* in male murine joints

In addition to their chronological age, I sought to investigate whether the joint samples from old mice exhibited biological signs of ageing. Cellular senescence is a protective process which arrests the proliferation of damaged cells and prevents them from neoplastic transformation. Many forms of age-related cellular damage, such as shortened telomeres, DNA damage, oncogenic mutation of proto-oncogenes, etc., are able to induce cellular senescence (Campisi et al., 2007) and senescence is recognised as one of the hallmarks of biological ageing (Lopez-Otin et al., 2013). Evidence suggests that these cellular insults convey both p53-dependent and -independent signals, that converge on either p16 or p21 (encoded by *CDKN2A* and *CDKN1A*, respectively). When expressed, these two cell cycle-regulating genes maintain the retinoblastoma protein (Rb) in its unphosphorylated state, impeding cell cycle transition. Rb is encoded by the tumour suppressor *RB* gene and functions as the major G1 phase cell cycle checkpoint inhibitor (Giacinti et al., 2006). Thus, the activation of p16 or p21 induces cell cycle arrests through preventing Rb phosphorylation (Munoz-Espin et al., 2014). Studies have also identified up-regulation of p16 and p21 as markers of cellular senescence (Munoz-Espin et al., 2014).

To examine whether mouse joints exhibited increased senescent in old age, I examined

expression of *Cdkn2a* and *Cdkn1a* in these samples, and found [Figure 3.7 (A), (B)] that expression of neither gene was significantly changed with age (*Cdkn2a*: adjusted p value = 0.2941; *Cdkn1a*: adjusted p value = 0.1101).

Another feature of senescent cells is that they frequently exhibit a distinct senescence-associated secretory phenotype (SASP), characterised by increased expression and secretion of pro-inflammatory cytokines and ECM remodelling proteases (Coppe et al., 2010). IL-6 has been reported to be the most prominent marker of SASP (Coppe et al., 2010), so I quantified the expression of *Il6* in the previously analysed murine joint samples. Figure 3.7 (C) shows that expression of *Il6* was low in 0.2-month old murine joints, and increased with age, with joints from 5.5-month old mice (adjusted p value = 0.0002, 95 % CI: [-5.026, -1.377]) and 18-month old mice (adjusted p value = 0.0013, 95 % CI: [-4.578, -0.9282]) showing significantly higher *Il6* expression. Up-regulation of *Il6* expression was also observed in joints from 3- and 4.5-month old mice compared to 0.2-month old mice, though in both cases this did not reach statistical significance (0.2-month old vs. 3-month old: adjusted p value = 0.5596, 95 % CI: [-2.967, 0.9341]; 0.2-month old vs. 4.5-month old: adjusted p value = 0.0804, 95 % CI: [-3.938, 0.1543]). Additionally, *Il6* expression in joints from 5.5-month old mice was significantly higher than from 3-month old mice (adjusted p value = 0.0130, 95 % CI: [-4.01, -0.3603]). However, in joints from old mice (18-month old), *Il6* expression was not significantly higher than that from 3-, 4.5-, 5.5-month old mice when Turkey's post hoc comparisons were performed (3-month old vs. 18-month old: adjusted p value = 0.0681, 95 % CI: [-3.561, 0.08849]; 4.5-month old vs. 18-month old: adjusted p value = 0.6918, 95 % CI: [-2.787, 1.065]; 5.5-month old vs. 18-month old: adjusted p value = 0.9360, 95 % CI: [-1.241, 2.138]).

In summary, I found that expression of the SASP cytokine *Il6* increased in joints from 5.5-month old murine mice compared to 3-month old mice, but not in 18-month old mice, although the p value is relatively close to the pre-determined cut-off of 0.05 (0.0681). Independent replicate experiments with increased sample size is needed to evaluate whether *Il6* expression indeed only increases in joints of 5.5-month old but not 18-month old mice. Additionally, expression of senescence markers *Cdkn2a* and *Cdkn1a* did not change with ageing. From these data, I was not able to conclude whether joints from 18-month old mice were more senescent than those from younger animals.

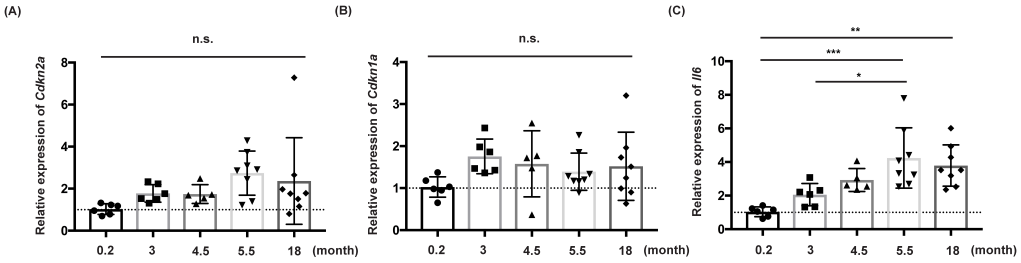

Figure 3.7 Expression of senescence marker *Il6* increased in joints from 5.5- and 18-month old mice compared to 3-month old mice, but expression of *Cdkn2a* and *Cdkn1a* did not.

RNA extracted from joints of 0.2-month (n = 6), 3-month (n = 6), 4.5-month (n = 5), 5.5-month (n = 8) and 18-month (n = 8) old male mice was reverse transcribed and quantified using qPCR. Expression of the genes of interest were normalised to the housekeeping gene *Rplp0* and calculated using the ΔΔCt method detailed in Section 2.2.5.4.

(A) The expression of *Cdkn2a* did not change between all age groups tested (p = 0.1101).

(B) The expression of *Cdkn1a* did not change between all age groups tested (p = 0.2941).

(C) The expression of *Il6* in joints from 5.5-month (adjusted p value = 0.0002, 95 % CI: [-5.026, -1.377]) and 18-month old mice (adjusted p value = 0.0013, 95 % CI: [-4.578, -0.9282]) was significantly higher than from 0.2-month old mice, and *Il6* expression in joints from 3-month old mice was significantly lower than in from 5.5-month old mice (adjusted p value = 0.0130, 95 % CI: [-4.01, -0.3603]). However, *Il6* expression in joints from -, 4.5- and 5.5-month old mice was not significantly different 18-month old mice (3-month old vs. 18-month old: adjusted p value = 0.0681, 95 % CI: [-3.561, 0.08849]; 4.5-month old vs. 18-month old: adjusted p value = 0.6918, 95 % CI: [-2.787, 1.065]; 5.5-month old vs. 18-month old: adjusted p value = 0.9360, 95 % CI: [-1.241, 2.138]).

Data are shown as mean ± SD, ***, p ≤ 0.001, ** p ≤ 0.01, *, p ≤ 0.05, n.s., not significant. The statistical significance of comparison between age groups was analysed with one-way ANOVA, with post hoc multiple comparisons corrected using Tukey's test.

3.7. Expression of *Adam15* and senescence markers in other murine tissues

To investigate whether the observed age-dependent pattern of *Adam15* expression is cartilage-specific or is a common phenomenon amongst mouse tissues, I collected spleen, brain (including cerebellum and cerebrum), heart and bone (tibia-fibula) from young (3-month old) and old (17-month old) mice and extracted RNA from these tissues, reverse transcribed the resultant RNA to cDNA and quantified the expression of *Adam15* using qPCR. Female mice available in the group were utilised for this study. I first examined *Adam15* expression in the joint to validate my previous finding (Figure 3.5) from joints of male mice. Figure 3.8 (A) confirms that, similar to what I observed in joints of male mice, the expression of *Adam15* in the joints of female mice was significantly reduced in old (17-month old) compared to the young (3-month old) animals ($p = 0.0175$, 95% CI: [-1.986, -0.2543]), although the difference was smaller than that in males (approximately 50% decrease in the female joints versus more than 97% decrease in the males). Likewise, Figure 3.8 (C) shows that the expression of *Adam15* in the bones from the old females was also significantly decreased compared to the young females ($p = 0.0006$, 95% CI: [-2.303, -0.9374]), indicating that the observed reduction of *Adam15* in the old joints may mainly reflect changes in bone.

As observed in males (Figure 3.7), the expression of *Cdkn2a* in old female joints and bones did not show any significant change compared to the young animals, as shown in Figure 3.8 (B) and (D).

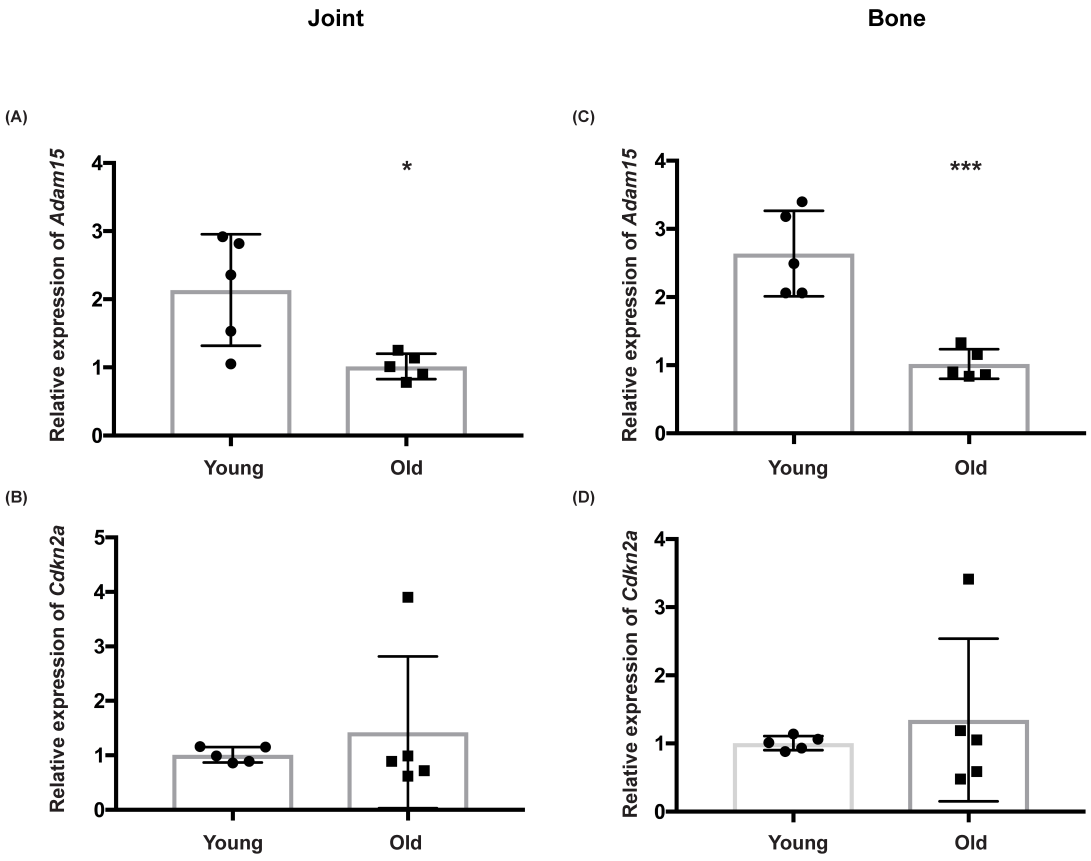

Figure 3.8 *Adam15* but not *Cdkn2a* expression was significantly decreased in joint and bone from old female mice.

RNA extracted from joints and bone (tibia-fibula) of 3-month (n = 5) and 17-month (n = 5) old female mice was reverse transcribed and quantified using qPCR. Expression of the genes of interest was normalised to the housekeeping gene *Rplp0* and relative expression calculated using the ΔΔCt method detailed in Section 2.2.5.4.

(A) The expression of *Adam15* decreased significantly in the joints from old female mice (p = 0.0175, 95% CI: [-1.986, -0.2543]).

(B) The expression of *Cdkn2a* did not change in joints from old female mice compared to young (p = 0.5267, 95% CI: [-1.028, 1.856]).

(C) The expression of *Adam15* decreased significantly in the old female murine bone (p = 0.0006, 95% CI: [-2.303, -0.9374]).

(D) The expression of *Cdkn2a* did not change in bones from old female mice compared to young (p = 0.5432, 95% CI: [-0.895, 1.575]).

Data are shown as mean ± SD, young, 3-month old; old, 17-month old, ***, $p \leq 0.001$, *, $p \leq 0.05$. The statistical significance of comparison between young and old tissues was analysed with Student's t test (two-tailed).

Figure 3.9 shows that *Adam15* expression was not different in brain and heart samples from young and old female mice (brain: p = 0.9397, 95% CI: [-0.1714, 0.1834]; heart: p = 0.8019, 95% CI: [-0.221, 0.277). The expression of *Adam15* was decreased in spleens from old female mice, where *Adam15* is highly expressed. However, this did not reach

statistical significance (p = 0.1264, 95% CI: [-8.556, 1.28]). On the contrary, expression of the senescence marker *Cdkn2a* (spleen: p = 0.0362, 95% CI: [0.6385, 14.85]; brain: p = 0.0006, 95% CI: [0.8667, 2.153]; heart: p = 0.0019, 95% CI: [1.167, 3.569]) and SASP factor *Il6* (spleen: p = 0.0075, 95% CI: [0.3688, 1.739]; brain: p = 0.0336, 95% CI: [0.06749, 1.293]; heart: p = 0.0036, 95% CI: [0.6363, 2.3]) was significantly up-regulated with age in all three tissues. This suggests that the age-dependent change in *Adam15* expression in the joint is not a general phenomenon, and that p16-induced, *Il6*-associated senescence was higher in spleen, brain and heart of aged female mice, but not in bone and joint. These data also indicate that *Cdkn2a* may not be a suitable marker for tracking cellular senescence in naturally aged murine bone and joint.

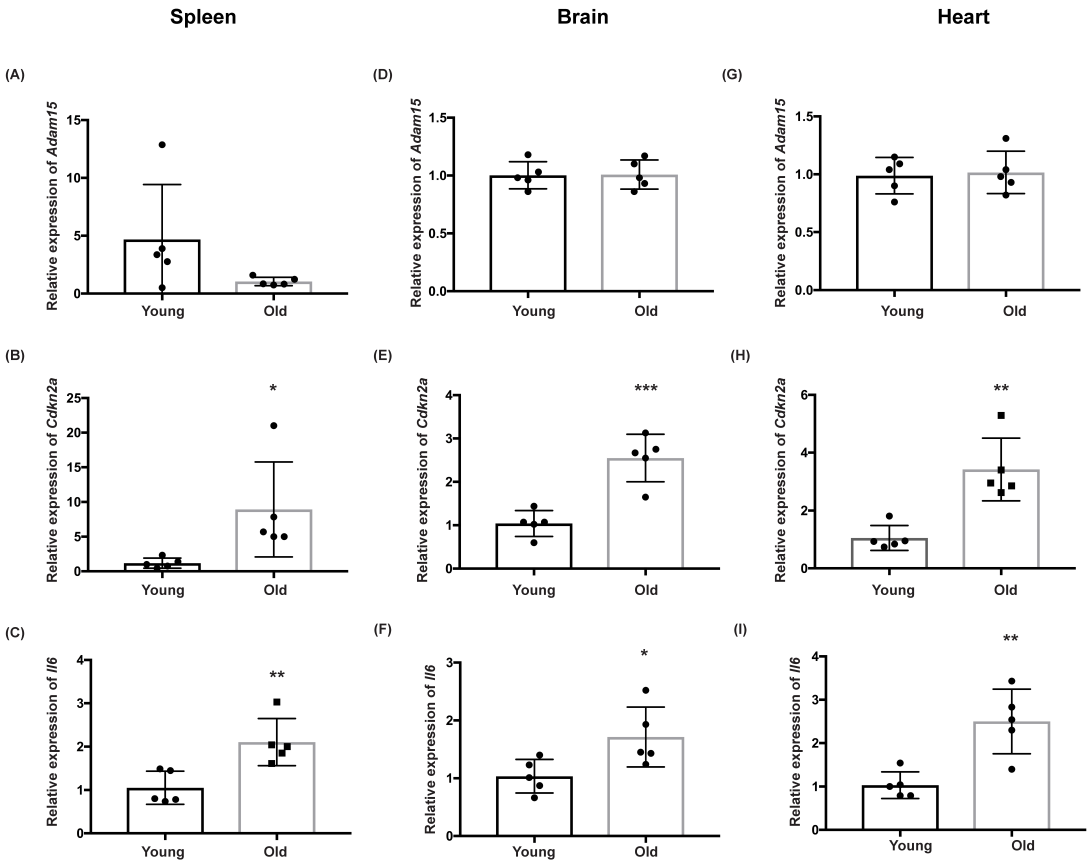

Figure 3.9 *Cdkn2a* and *Il6*, but not *Adam15* expression, increased in old female murine spleen, brain and heart.

RNA extracted from spleens, brains and hearts of 3-month (n = 5) and 17-month (n = 5) old female mice was reverse transcribed and quantified using qPCR. Expression of the genes of interest were normalised to the housekeeping gene *Rplp0* and relative expression calculated using the ΔΔCt method (Section 2.2.5.4).

(A) Decrease of *Adam15* expression in spleens from old female mice did not reach statistical significance (p = 0.1264, 95% CI: [-8.556, 1.28]).

(B) The expression of *Cdkn2a* increased significantly in spleens from old female mice (p = 0.0362, 95% CI: [0.6385, 14.85]).

(C) The expression of *Il6* increased significantly in spleens from old female mice (p = 0.0075, 95% CI: [0.3688, 1.739]).

(D) The expression of *Adam15* was not different in brains from young and old female mice (p = 0.9397, 95% CI: [-0.1714, 0.1834]).

(E) The expression of *Cdkn2a* increased significantly in brains from old female mice (p = 0.0006, 95% CI: [0.8667, 2.153]).

(F) The expression of *Il6* increased significantly in brains from old female mice (p = 0.0336, 95% CI: [0.06749, 1.293]).

(G) The expression of *Adam15* was not different in hearts from young and old female mice (p = 0.8019, 95% CI: [-0.221, 0.277]).

(H) The expression of *Cdkn2a* increased significantly in hearts from old female mice (p = 0.0019, 95% CI: [1.167, 3.569]).

(I) The expression of *Il6* increased significantly in hearts from old female mice (p = 0.0036, 95% CI: [0.6363, 2.3]).

Data are shown as mean ± SD, young, 3-month old; old, 17-month old, ***, $p \leq 0.001$, ** $p \leq 0.01$, *, $p \leq 0.05$. The statistical significance of comparison between young and old tissues was analysed with Student's t test (two-tailed).

3.8. The expression of *CDKN2A* and *CDKN2A* in human cartilage

As shown in Sections 3.6. and 3.7., unlike in spleen, heart and brain, the expression of the senescence marker *Cdkn2a* was not increased in joints from the old male and female mice. Complementing this finding, I also found that *Cdkn2a* expression in bone did not change with age. The joint samples analysed are mainly composed of bone, so changes in expression of *Cdkn2a* in old cartilage may not be captured in this analysis.

To explore this possibility, I took advantage of our human cartilage RNA samples and quantified expression of *CDKN2A* and *CDKN1A*. Figure 3.10 (A) and (B) show that, similar to murine joint and bone, neither *CDKN2A* nor *CDKN1A* exhibited an age-dependent change in expression. However, I found that *CDKN1A* expression clustered into two groups, with OA samples having lower expression [Figure 3.10 (B)]. I analysed the relative expression of *CDKN2A* and *CDKN1A* in human normal and OA cartilage and, as shown in Figure 3.11 (B), found that *CDKN1A* expression was indeed significantly lower in OA cartilage ($p = 0.0005$, 95% CI: [-1.707, -0.5852]). Figure 3.11 (A) shows that *CDKN2A* was not similarly regulated.

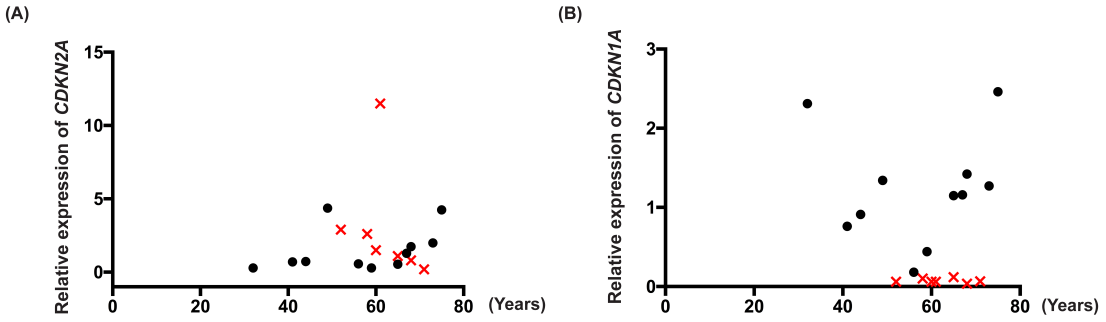

Figure 3.10 Neither *CDKN2A* nor *CDKN1A* exhibited age-dependent change in expression in cartilage.
RNA was extracted from normal (•) and OA (×) cartilage, reverse transcribed and quantified using qPCR. *CDKN2A* and *CDKN1A* expression was normalised using the housekeeping gene *RPLP0* and relative expression calculated using the ΔΔCt method (Section 2.2.5.4). Relative expression of *CDKN2A* and *CDKN1A* was normalised to their average expression in normal samples.
(A) Expression of *CDKN2A* showed no age-dependent pattern in human cartilage, and no clustering between normal and OA samples was observed.
(B) Expression of *CDKN1A* showed no age-dependent patten in human cartilage, but normal and OA samples were found to cluster into two groups, with OA samples showing lower *CDKN1A* expression.

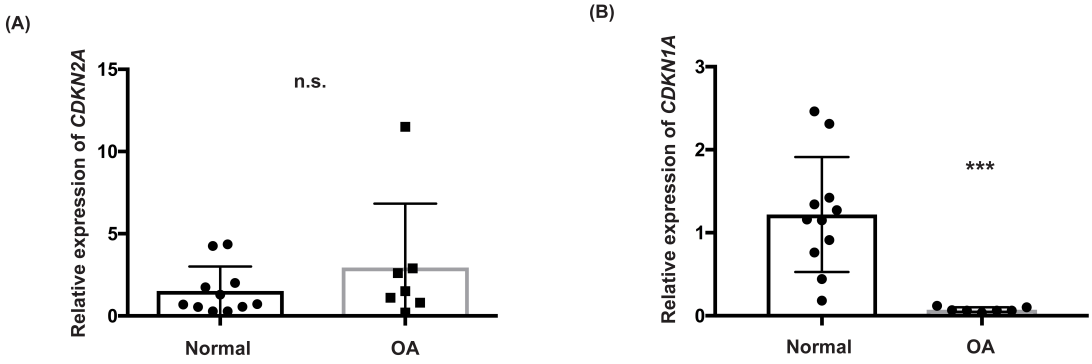

Figure 3.11 Expression of *CDKN1A* was significantly decreased in human OA cartilage.
RNA was extracted from normal (n = 11) and OA (n = 7) cartilage, reverse transcribed and quantified using qPCR. *CDKN2A* and *CDKN1A* expression was normalised using the housekeeping gene *RPLP0* and relative expression calculated using the ΔΔCt method detailed in Section 2.2.5.4. Relative expression of *CDKN2A* and *CDKN1A* was normalised to their average expression in normal samples.
(A) Expression of *CDKN2A* was not significantly different in human normal and OA cartilage ($p = 0.2846$, 95% CI: [-1.302, 4.147]).
(B) Expression of *CDKN1A* was significantly reduced in human OA cartilage ($p = 0.0005$, 95% CI: [-1.707, -0.5852]).
Data are shown as mean ± SD, ***, $p \leq 0.001$, n.s., not significant. The statistical significance of comparison between normal and OA was analysed with Student's t test (two-tailed).

3.9. *CDKN1A* did not regulate *ADAM15* expression

Although the expression of *CDKN1A* was down-regulated in human OA cartilage, *ADAM15* expression showed no change between normal and OA cartilage [Figure 3.2 (B)]. Furthermore, unlike *ADAM15*, *CDKN1A* expression did not change with age. Taken together, these data suggest that it is unlikely that *CDKN1A* is responsible for the age-dependent changes in *ADAM15* expression. To prove that there was no correlation between *ADAM15* and *CDKN1A* expression, I repressed *CDKN1A* expression using RNAi. As shown in Figure 3.12 (A-B), expression of *CDKN1A* was successfully knockdown in HTB-94 cells 48 hours after transfection with 10, 20 or 40 nM si*CDKN1A* siRNA (10 nM: $p = 0.0005$, 95% CI: [-0.9921, -0.5685]; 20 nM: $p < 0.0001$, 95% CI: [-0.8905, -0.6467]; 40 nM: $p = 0.0001$, 95% CI: [-1.021, -0.6983]). However, *ADAM15* expression remained unchanged (10 nM: $p = 0.1224$, 95% CI: [-0.4542, 0.07896]; 20 nM: $p = 0.0845$, 95% CI: [-0.1008, 1.035]; 40 nM: $p = 0.1864$, 95% CI: [-0.5866, 0.1589]), suggesting that *ADAM15* expression was not regulated by *CDKN1A*.

In parallel, I examined whether suppression of *ADAM15* had any effect on *CDKN1A* and *CDKN2A* expression. Figure 3.13 shows that neither *CDKN2A* nor *CDKN1A* expression was affected by suppression of *ADAM15* 36, 48 and 72 hours after si*ADAM15* transfection (*CDKN2A*: 36 hours: $p = 0.2412$, 95% CI: [-0.4731, 1.401]; 48 hours: $p = 0.5431$, 95% CI: [-0.4158, 0.2553]; 72 hours: $p = 0.1619$, 95% CI: [-0.8274, 3.491]; *CDKN1A*: (36 hours: $p = 0.1074$, 95% CI: [-0.06548, 0.4481]; 48 hours: $p = 0.1179$, 95% CI: [-0.07326, 0.4417]; 72 hours: $p = 0.2012$, 95% CI: [-0.1819, 0.627]).

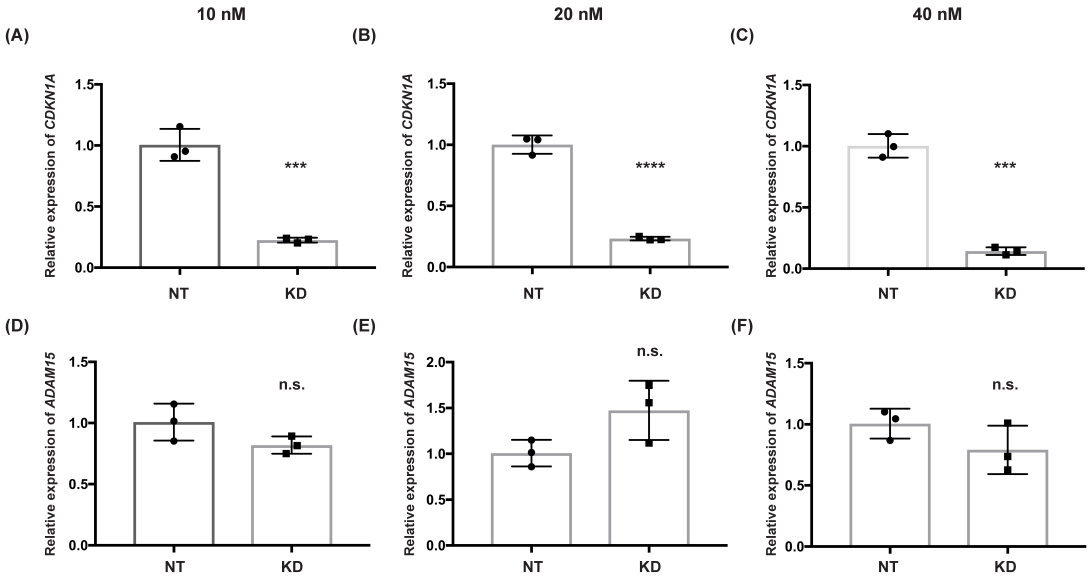

Figure 3.12 *CDKN1A* did not regulate *ADAM15* expression.
RNA interference of *CDKN1A* was performed by transiently transfecting the indicated concentration of si*CDKN1A* small interfering RNA into HTB-94 cells for 48 hours. RNA was extracted, reverse transcribed, and gene expression quantified using qPCR. *CDKN1A* and *ADAM15* expression were normalised using the housekeeping gene *RPLP0* and relative expression calculated using the ΔΔCt method (Section 2.2.5.4). Relative expression of *CDKN1A* and *ADAM15* was normalised to average expression of each gene in the non-targeting control.
(A) *CDKN1A* expression was significantly reduced 48 hours after transfection with 10 nM si*CDKN1A* ($p = 0.0005$, 95% CI: [-0.9921, -0.5685]).
(B) *CDKN1A* expression was significantly reduced 48 hours after transfection with 20 nM si*CDKN1A* ($p < 0.0001$, 95% CI: [-0.8905, -0.6467]).
(C) *CDKN1A* expression was significantly reduced 48 hours after transfection with 40 nM si*CDKN1A* ($p = 0.0001$, 95% CI: [-1.021, -0.6983]).
(D-F) The expression of *ADAM15* did not change 48 hours after transfection with 10, 20 or 40 nM si*CDKN1A* (10 nM: $p = 0.1224$, 95% CI: [-0.4542, 0.07896]; 20 nM: $p = 0.0845$, 95% CI: [-0.1008, 1.035]; 40 nM: $p = 0.1864$, 95% CI: [-0.5866, 0.1589]).
Data are shown as mean ± SD, NT, non-targeting control, KD, *CDKN1A* knockdown, ****, $p \leq 0.0001$, ***, $p \leq 0.001$, n.s., not significant. The statistical significance of comparison between NT and KD was analysed with Student's t test (two-tailed).

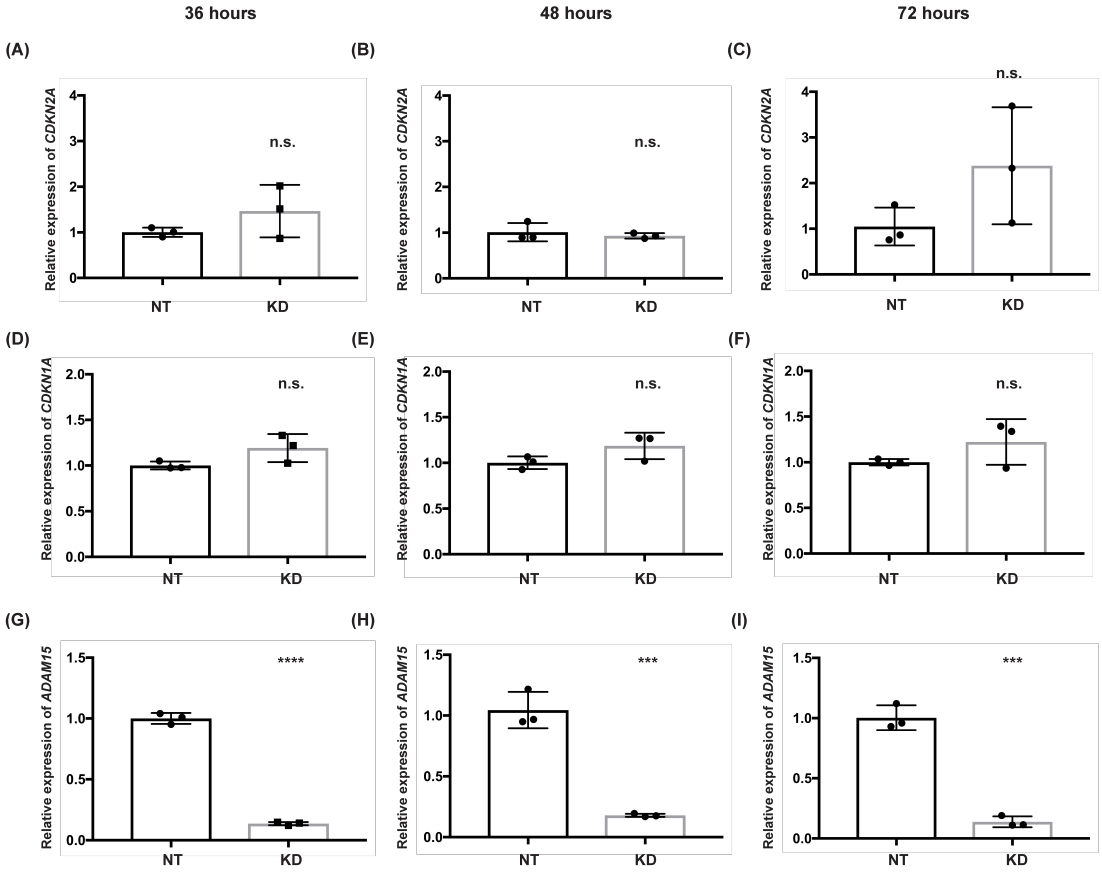

Figure 3.13 *ADAM15* repression did not affect *CDKN2A* and *CDKN1A* expression.
RNAi of *ADAM15* was performed by transiently transfecting 20 nM of si*ADAM15* small interfering RNA into HTB-94 cells for the indicated time. RNA was extracted, reverse transcribed, and gene expression quantified using qPCR. *CDKN2A* and *CDKN1A* expression were normalised using the housekeeping gene *RPLP0* and relative expression calculated using the ΔΔCt method (Section 2.2.5.4). Relative expression of *CDKN2A* and *CDKN1A* were normalised to average expression of each gene in the non-targeting control.
(A-C) *CDKN2A* expression was not affected by *ADAM15* suppression 36, 48 and 72 hours after RNA interference (36 hours: $p = 0.2412$, 95% CI: [-0.4731, 1.401]; 48 hours: $p = 0.5431$, 95% CI: [-0.4158, 0.2553]; 72 hours: $p = 0.1619$, 95% CI: [-0.8274, 3.491]).
(D-E) *CDKN1A* expression was not affected by *ADAM15* suppression 36, 48 and 72 hours after RNA interference (36 hours: $p = 0.1074$, 95% CI: [-0.06548, 0.4481]; 48 hours: $p = 0.1179$, 95% CI: [-0.07326, 0.4417]; 72 hours: $p = 0.2012$, 95% CI: [-0.1819, 0.627]).
(G-I) *ADAM15* expression was significantly decreased 36, 48 and 72 hours after RNA interference (36 hours: $p < 0.0001$, 95% CI: [-0.9394, -0.7886]; 48 hours: $p = 0.0006$, 95% CI: [-1.106, -0.6247]; 72 hours: $p = 0.0002$, 95% CI: [-1.045, -0.6845]).
Data are shown as mean ± SD, NT, non-targeting control, KD, *ADAM15* knockdown, ****, $p \leq 0.0001$, ***, $p \leq 0.001$, n.s., not significant. The statistical significance of comparison between NT and KD was analysed with Student's t test (two-tailed).

3.10. ADAM15 expression decreased in aged human cartilage at the protein level

Previous experiments in this chapter indicate that *ADAM15* expression decreased with aged in human cartilage and murine joints at the mRNA level. In this section, I explored whether the observed reduction at the mRNA level was reflected by changes at the protein level. I started by validating an anti-ADAM15 antibody (The Human Protein Atlas Antibody, Cambridge Bioscience, Cat. HPA011633) for immunofluorescent (IF) staining of HTB-94 cells. Cover slips were coated with gelatin (as per Section 2.2.7) and placed in a 12-well plate, and cells (10,000 per cover slip) seeded the day before transfection. To test whether the anti-ADAM15 antibody (anti-ADAM15_HTA) recognises ADAM15 when performing immunocytostaining, transient transfection of ADAM15 (pCMV2-ADAM15-FLAG) for 48 hours was performed as described in Section 2.2.4.1, followed by IF staining as described in Section 2.2.8. Phalloidin was used to visualise the actin cytoskeleton, whilst DAPI was used to visualise nuclei. Figure 3.14 shows that expression of endogenous ADAM15 was detectable in mock-transfected HTB-94 using the anti-ADAM15_HTA antibody, with increased staining observed in ADAM15-over-expressing cells. Merged images indicate that most endogenous ADAM15 was localised in the perinuclear region, potentially in the secretory pathway. In order to compare the relative expression of ADAM15, the exposure time of individual channels was kept constant for mock transfected and ADAM15 over-expressing HTB-94. Since the ADAM15 signal was extremely strong in ADAM15-over-expressing cells, a relatively short exposure time was used and this explains the low intensity of endogenous ADAM15 signal in mock-transfected cells. When over-expressed, ADAM15 showed a similar perinuclear localisation as the endogenous ADAM15.

To further confirm the subcellular localisation of endogenous ADAM15 and demonstrate that the observed perinuclear localisation of ADAM15 was not a transfection artefact, IF was performed on untreated HTB-94 using the anti-ADAM15_HTA antibody, phalloidin and DAPI. Cells were visualised at a higher magnification (60X vs. 100X) and a longer exposure time. Figure 3.14 (B) shows that endogenous ADAM15 was indeed localised in the perinuclear region.

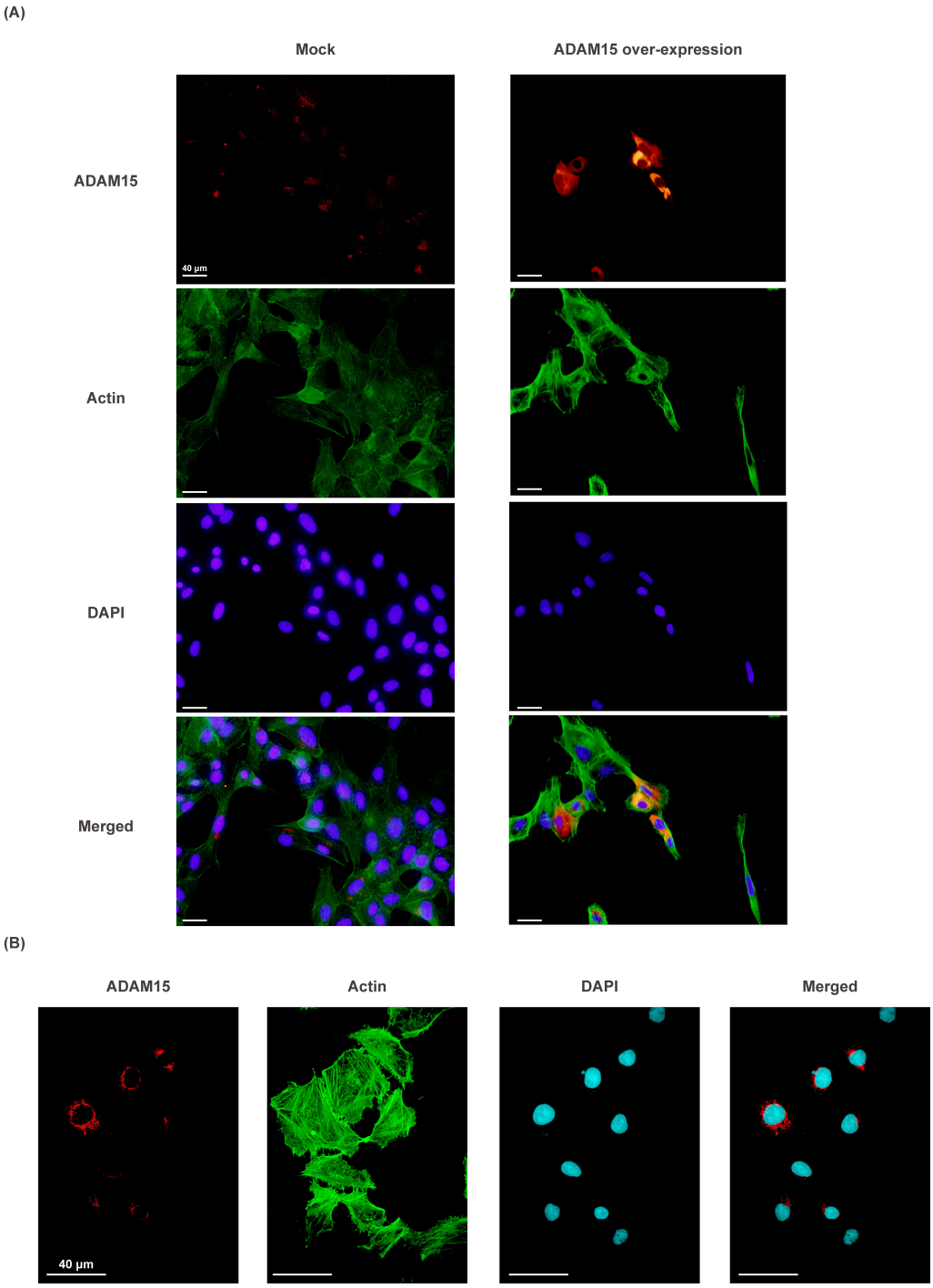

Figure 3.14 Validation of anti-ADAM15 antibody for immunofluorescence staining by over-expressing pCMV2-ADAM15-FLAG in HTB-94 cells.

Cover slips were coated with gelatin (Section 2.2.7) and seeded with HTB-94 cells (10,000 per cover slip) in a 12-well plate. Cells were transfected with an ADAM15 over-expression vector (Section 2.2.4.1) for 48 hours and immunofluorescence staining performed as described in Section 2.2.8. For comparison, the exposure times of individual channels in **(A)** were kept the same for mock transfected and ADAM15 over-expressing cells. In **(B)**, higher exposure times were used to visualise the subcellular localisation of untreated HTB-94. Actin was visualised using phalloidin staining, whilst nucleui was visualised with DAPI. Cells were visualised with a 60X lens in **(A)** and a 100X lens in **(B)**.

(A) ADAM15 expression was detectable but relatively weak in mock transfected HTB-94 cells compared to cells transfected with pCMV2-ADAM15-FLAG using the anti-ADAM15_HTA antibody.

(B) ADAM15 was observed in the perinuclear region upon higher magnification (100X).

Red, ADAM15 (anti-rabbit Alexa Fluor 568); Green, actin (phalloidin-Alexa Fluor 488); Blue, DAPI (UV

405 nm).

Since the recombinant ADAM15 was FLAG-tagged, IF was performed with an anti-FLAG antibody (Sigma-Aldrich, Cat. F3165) for comparison. Figure 3.15 shows that in the ADAM15-over-expressing cells, FLAG staining was intense, whilst in mock-transfected cells, staining was undetectable.

Taken together, these data suggest that the anti-ADAM15_HTA antibody I used was able to detect ADAM15 by immunocytostaining, as the ADAM15 signal increased dramatically in ADAM15 over-expressing cells.

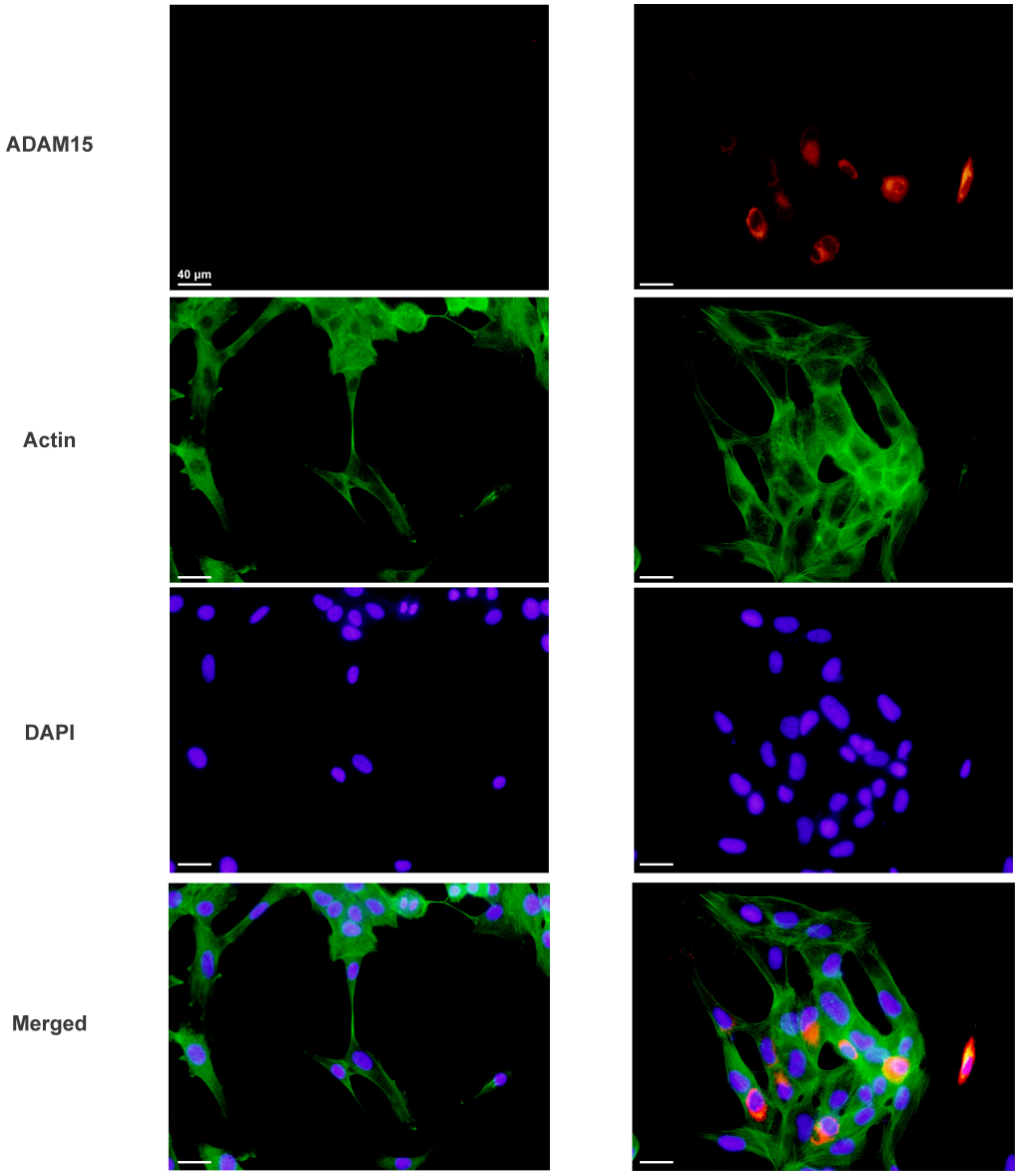

Figure 3.15 FLAG-tagged ADAM15 was detectable in pCMV2-ADAM15-FLAG over-expressing HTB-94 cells, whilst endogenous ADAM15 was undetectable using an anti-FLAG antibody.
To perform ADAM15 over-expression, cover slips were coated using method described in Section 2.2.7. HTB-94 cells were seeded on to the cover slips at a density of 10,000 cells per cover slips in a 12-well plate. Over-expression was performed using method described in Section 2.2.4.1. for 48 hours and immunofluorescence staining was conducted using the method described in Section 2.2.8. For comparison, the exposure times of individual channel in were kept the same for mock transfected and ADAM15 over-expressing cells. Cells were visualised with a 60X lens. Red, ADAM15 (anti-rabbit Alexa Fluor 568); Green, actin (phalloidin-Alexa Fluor 488); Blue, DAPI (UV 405 nm).

Although the over-expression experiments demonstrate that the anti-ADAM15_HTA antibody I used was able to detect ADAM15, the specificity of this antibody remained to be determined. It is possible that in the mock transfected control, the signal I

detected was due to non-specific binding of the primary antibody. The specificity issue is particularly problematic when performing IF staining on cartilage, as non-specific binding is generally more prominent when IF is performed on tissue sections. To test the specificity of the anti-ADAM15_HTA antibody, an antigen blocking experiment was conducted. A 10-fold molar excess of recombinant ADAM15 (Abcam, Cat. ab131862) was pre-incubated with the anti-ADAM15_HTA antibody. To perform IF, ~0.5 μg anti-ADAM15_HTA antibody in 100 μl IHC blocking buffer was used. Taking the molecular weight of an antibody as ~150 kDa, this equates to a molarity of ~33.3 nM. To achieve a 10-fold molar excess (333 nM) in a 100 μl solution, ~3.663 μg recombinant ADAM15 (110 kDa) was required. The concentration of recombinant ADAM15 I used was 0.05 μg/μl, hence 73.26 μl recombinant ADAM15 and 5 μl anti-ADAM15_HTA antibody (0.1 μg/μl) were added to 21.74 μl PBS, pre-incubated at room temperature for 30 minutes to allow immune complex formation, then centrifuged (15 min, 17000 x g) to pellet the immune complexes. The supernatant was collected and the same concentration of antigen neutralised anti-ADAM15_HTA antibody and un-neutralised anti-ADAM15_HTA antibody were applied to human cartilage cryosections, followed by IF staining as described in Section 2.2.8. Anti-perlecan antibody and DAPI were also added to visualise the pericellular matrix and nucleus, respectively. Figure 3.16 shows that, while ADAM15 signal was detectable when un-neutralised anti-ADAM15_HTA antibody was used as the primary antibody, no ADAM15 signal was detected after antigen neutralisation. Perlecan and DAPI staining was unaffected. The exposure times of individual channels were kept constant to allow accurate comparison. This experiment indicates that the anti-ADAM15_HTA antibody used was specific for ADAM15. Taken together, the over-expression and the antigen blocking experiments successfully validated the anti-ADAM15_HTA antibody

I used was suitable for performing IF on cartilage cryosections.

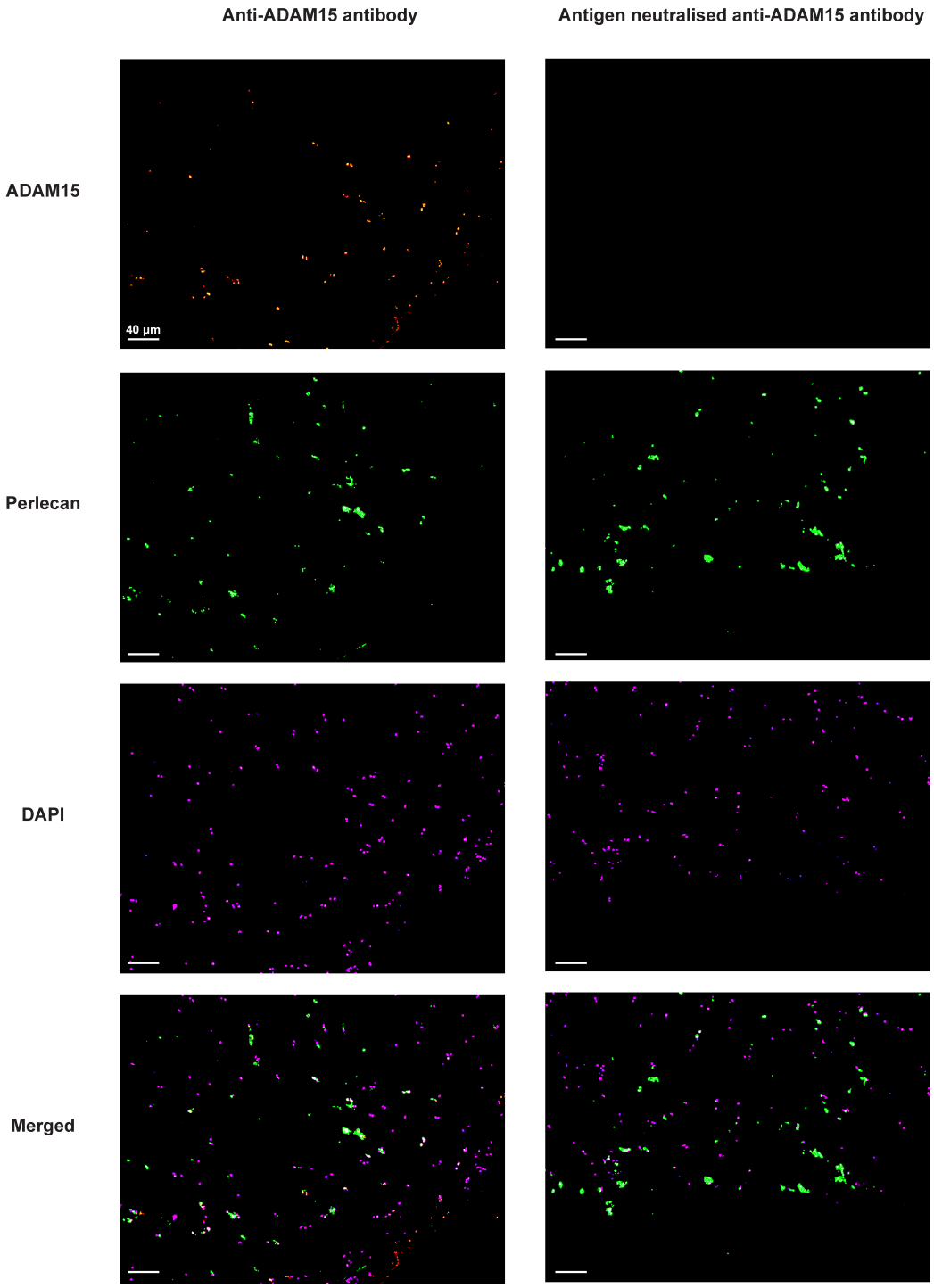

Figure 3.16 Validation of anti-ADAM15 antibody specificity by antigen blocking.
Immunofluorescent staining was performed on human cartilage cryosections as detailed in Section 2.2.8. Antigen blocking was performed according to the manufacturer's guide. In brief, a 10-fold molar excess of recombinant ADAM15 (Abcam, Cat. ab131862) was pre-incubated with the anti-ADAM15 antibody in PBS at room temperature for 30 minutes. The antigen-antibody mixture was centrifuged (15 min, 17000 x g). The supernatant was collected and the same concentration of antigen neutralised anti-ADAM15 antibody

and un-neutralised anti-ADAM15 antibody were applied to tissue sections. For comparison, the exposure times of individual channels were kept constant. Tissues were visualised with a 40X lens. ADAM15 expression was undetectable by the antigen-neutralised anti-ADAM15_HTA antibody, but staining was detachable when the anti-ADAM15_HTA antibody without antigen blocking was incubated.
Red, ADAM15 (anti-rabbit Alexa Fluor 568); Green, perlecan (anti-rat Alexa Fluor 488); Blue, DAPI (UV 405 nm).

Next, I performed IF on cartilage cryosections from human donors of different ages to investigate whether ADAM15 expression decreased in cartilage from older donors at the protein level. Reduced ADAM15 signal was observed in cartilage from 58- and 83-year old donors with OA compared to a 49-year old donor without OA (Figure 3.17). No obvious differences in cell number or perlecan expression were noticed. When the ADAM15 channel and the DAPI channel were merged, it is apparent that the number of ADAM15-expressing cells were also decreased.

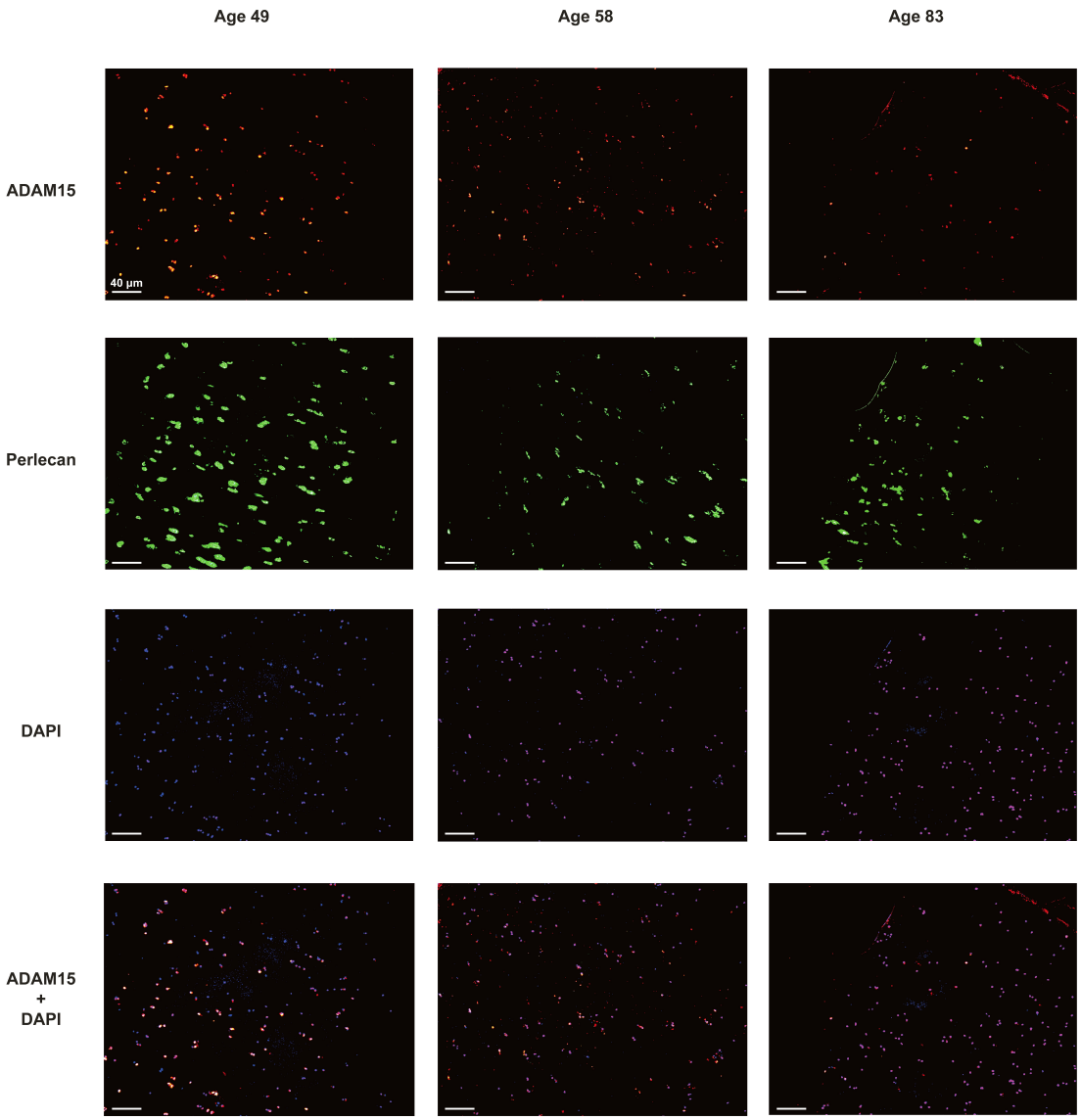

Figure 3.17 ADAM15 expression decreased in aged human cartilage at the protein level.
Immunofluorescent staining was performed on human cartilage crysections as detailed in Section 2.2.8. Representative images from cartilage section of a 49-year old donor (without OA), a 58-year old OA patient and a 83-year old OA patient are shown. For comparison, the exposure times of individual channels were kept the same for all sections. Tissues were visualised with a 20X lens. Perlecan expression did not show apparent change between adult and aged cartilages. DAPI was used to visualised nuclei. Total cell number per field view was estimated from DAPI staining. Relative expression of ADAM15 and number of cells expressing ADAM15 were estimated by superimposing the ADAM15 channel on the DAPI channel. ADAM15 expression was strongest in the younger, 49-year old adult. Older, OA cartilage showed less strong staining, with fewer cells expressing detectable ADAM15. Red, ADAM15 (anti-rabbit Alexa Fluor 568); Green, perlecan (anti-rat Alexa Fluor 488); Blue, DAPI (UV 405 nm).

As mentioned in the previous paragraph, older donors in Figure 3.17 (age 58 and 83) had OA, whilst the youngest cartilage was from a donor without OA. Even though data in Figure 3.2 (B) and Figure 3.4 (A) suggest that *ADAM15* expression was not

differentially regulated between OA and normal human cartilage at the mRNA level, it is possible that the observed reduction of ADAM15 protein expression in Figure 3.17 was due to the disease status of the donors, rather than their different ages. To explore this possibility, I performed confirmatory IF staining using three different cartilage samples from a 47-year old normal donor, a 54-year old OA donor and a 90-year old normal donor. As shown in Figure 3.18, a similar trend was observed, with ADAM15 expression decreased in cartilage from the older donor, with fewer ADAM15-expressing chondrocytes evident. No apparent difference in perlecan expression and cell number were observed. This experiment supported the conclusion that ADAM15 expression was decreased at the protein level in an independent set of samples. Due to the limited availability of cartilage from young and middle age donors, I was not able to collect enough samples to conduct a statistical comparison of the signal intensities of ADAM15 and number of ADAM15-expressing chondrocytes.

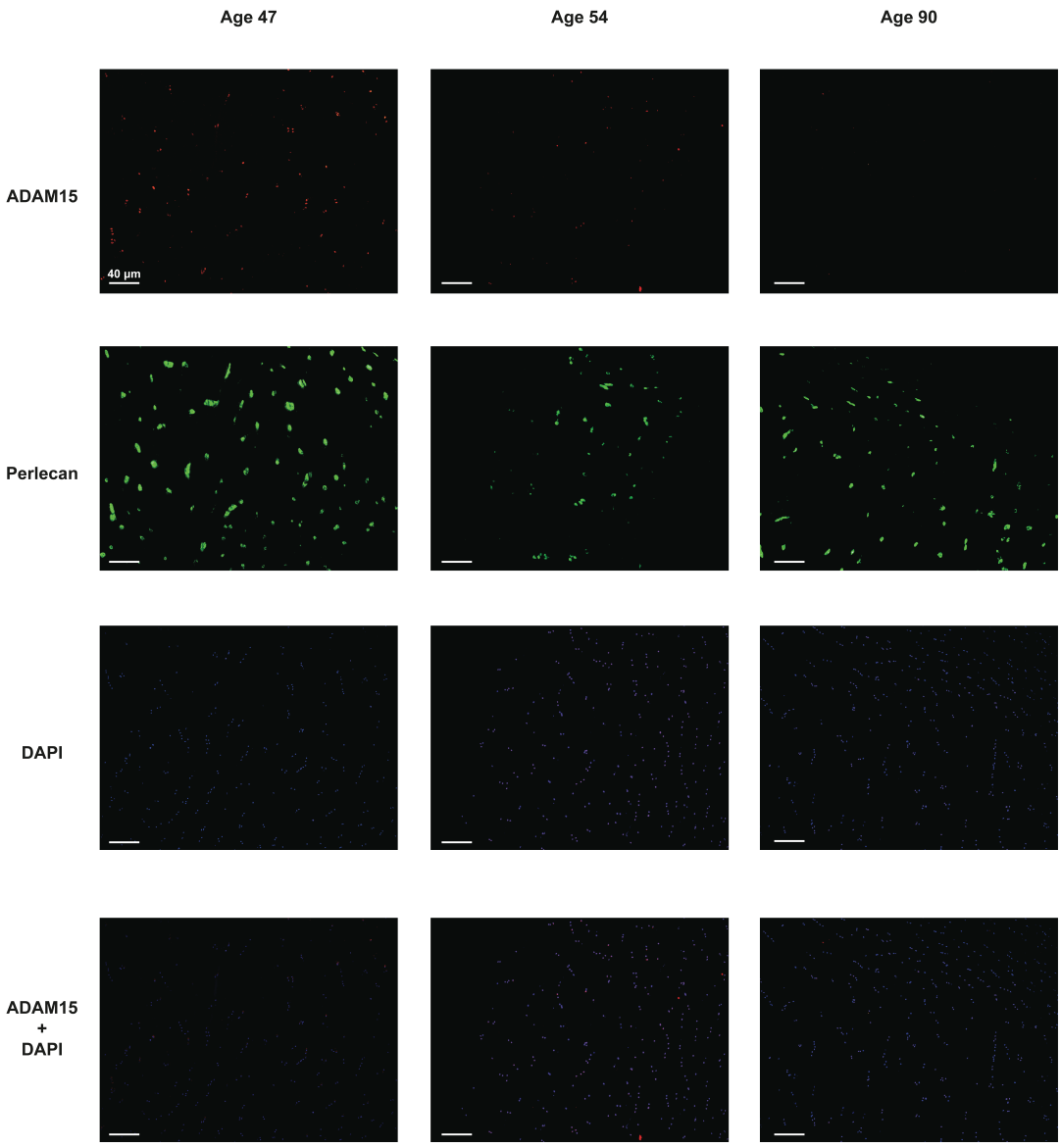

Figure 3.18 Immunofluorescence staining with an independent set of cartilage sections supports that ADAM15 expression decreased in aged human cartilage at the protein level.
Immunofluorescence staining was performed on an independent set of human cartilage crysections as detailed in Section 2.2.8. Representative images from cartilage sections of a 47-year old normal donor, a 54-year old OA patient and a 90-year old normal donor are shown. For comparison, the exposure times of individual channels were kept the same for all sections. Perlecan expression did not show apparent change between adult and aged cartilage. DAPI was used to visualised nuclei. Total cell number per field view was estimated from DAPI staining. Relative expression of ADAM15 and number of cells expressing ADAM15 were estimated by superimposing the ADAM15 channel on the DAPI channel. ADAM15 expression was strongest in the youngest, 47-year old adult. Older normal and OA cartilage showed less strong staining, with fewer cells expressing detectable ADAM15. Red, ADAM15 (anti-rabbit Alexa Fluor 568); Green, perlecan (anti-rat Alexa Fluor 488); Blue, DAPI (UV 405 nm).

Finally, the tissue distribution of ADAM15 in cartilage was explored. Since the human cartilage cryosections I used did not span the full depth of cartilage, porcine cartilage

cryosections were used to investigate the tissue distribution of ADAM15 in cartilage. Figure 3.19 shows that ADAM15 expression was detectable throughout the porcine cartilage sections, with no obvious heterogeneity observed. The expression of perlecan and location of nuclei indicate that the tissue and cell morphology were largely conserved. Perlecan staining also indicates the cartilage orientation, as chondrocytes on the cartilage surface (the superficial zone) were flatter and had less intense perlecan staining. Merged images in Figure 3.19 suggest that ADAM15 expression was largely intracellular and the most porcine chondrocytes expressed ADAM15. In summary, ADAM15 was uniformly expressed in porcine cartilage, with no obvious difference in its expression observed between superficial, middle and deeper zones.

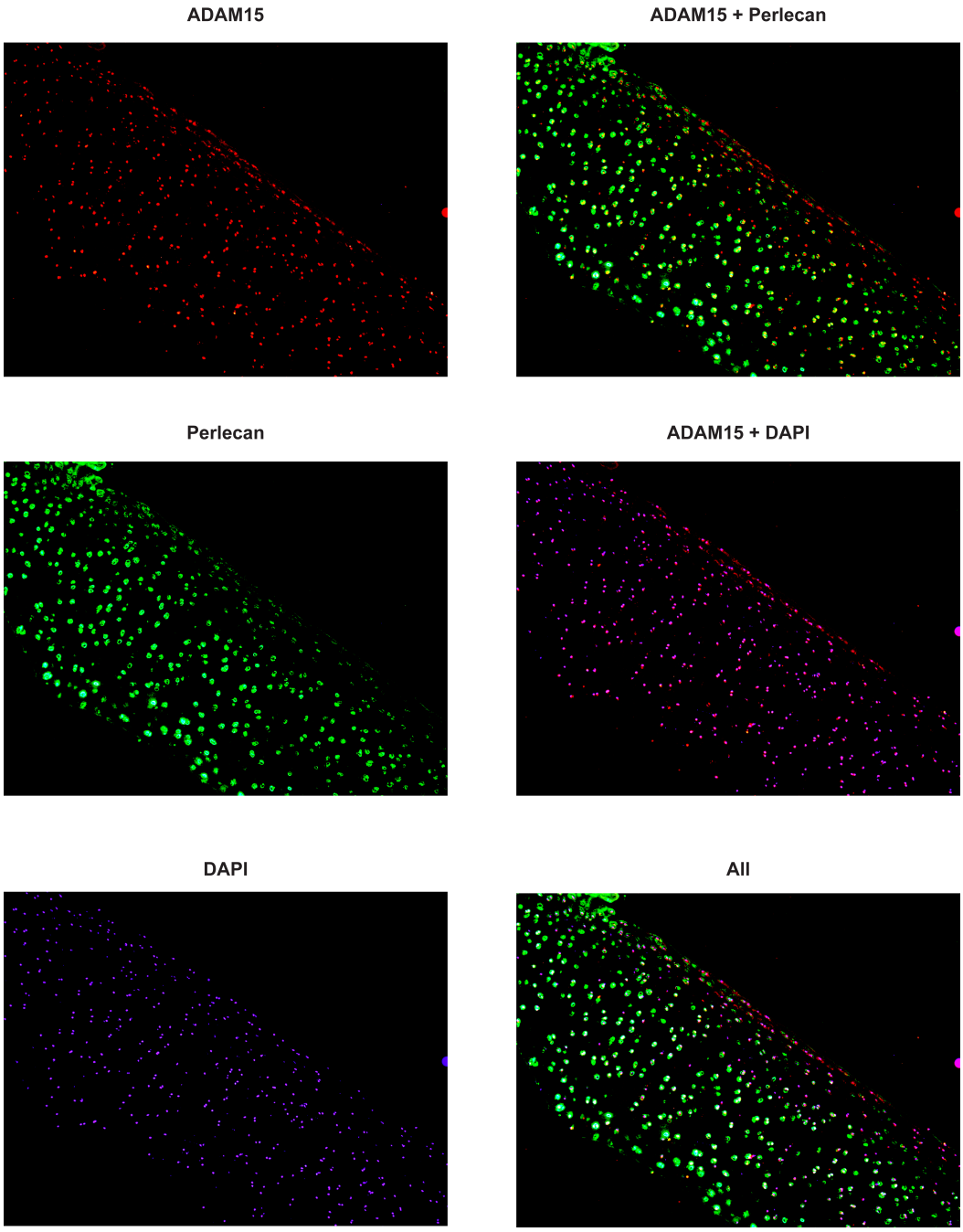

Figure 3.19 ADAM15 is homogeneously distributed in porcine cartilage.
Immunofluorescence staining was performed on porcine cartilage crysections as detailed in Section 2.2.8. Representative images from 4 porcine cartilage sections are shown. To investigate the tissue distribution of ADAM15 in cartilage, an image which includes the superficial zone and deep zone was selected. ADAM15 expression was detectable throughout the whole cartilage and was evenly distributed across different zone. Perlecan staining was less intense in the superficial zone. Perlecan staining also revealed that chondrocytes in different zones have different morphology, i.e., superficial zone chondrocytes are small and flat, whilst chondrocytes in the deep zone are larger and more rounded. DAPI was used to visualised nuclei. From the nuclear staining, columnar arrangements were observed in some middle zone chondrocytes. Red, ADAM15 (anti-rabbit Alexa Fluor 568); Green, perlecan (anti-rat Alexa Fluor 488); Blue, DAPI (UV 405 nm).

Table 3.1 Changes in gene expression in old (17-18 months) relative to young (3 months) tissues (↓, reduced; ↑, increased; -, no change; N/A, not analysed)

Gene name		Mouse					Human	Sheep
		Joint	Bone	Brain	Spleen	Heart	Cartilage	Cartilage
ADAM15	mRNA	↓	↓	—	—	—	↓	N/A
	Protein			N/A	N/A	N/A	↓	
CDKN2A	mRNA	—	—	↑	↑	↑	—	N/A
CDKN1A	mRNA	—	N/A	N/A	N/A	N/A	—	N/A
IL6	mRNA	—/↑*	N/A	↑	↑	↑	↑	N/A
SIRT1	mRNA	—	N/A	N/A	N/A	N/A	N/A	N/A
RUNX2	mRNA	↓	N/A	N/A	N/A	N/A	N/A	N/A
JAK2	mRNA	—	N/A	N/A	N/A	N/A	N/A	N/A
ADAM17	mRNA	—/↓¥	N/A	N/A	N/A	N/A	N/A	N/A

* Il6 expression was significantly higher in 5-month old joints compared to 3-month old joints. Il6 expression in 18-month old joints was not significantly reduced compared to 3-month old joints ($p = 0.0681$).

¥ Adam17 expression was significantly decreased in 18-month old joints compared to 4.5-month old joints. Adam17 expression was not significantly reduced in 18-month old joints compared to 3.5-month old joints ($p = 0.0595$).

3.11. Discussion

The metalloproteinase ADAM15 is considered to be protective against OA, as *Adam15*-deficient mice develop spontaneous, accelerated knee OA upon ageing (Bohm et al., 2005). In this chapter, I investigated *ADAM15* expression first at the mRNA level in human cartilage and murine joints, then studied its expression at the protein level in human cartilage, with the aim of understanding whether changes in ADAM15 expression contribute to OA development.

I began by comparing *ADAM15* expression in gender- and age-matched normal and OA cartilage directly, and in isolated normal and OA chondrocytes cultured as a monolayer. I found that *ADAM15* expression showed no difference between normal and OA cartilage, but was significantly decreased in OA chondrocytes compared to normal chondrocytes. It is known that culturing chondrocytes as a monolayer results in chondrocyte de-differentiation, loss of phenotype, and changes in gene expression (Lefebvre et al., 1990; Ryu et al., 2002), causing them to behave differently from chondrocytes residing in their physiological environment. Indeed, previous studies in our Institute (KIR) have shown that isolated chondrocytes cultured as a monolayer have different gene expression profiles and responses to stimuli than cartilage explants. Culturing chondrocyte as a monolayer may thus introduce artefacts, and I considered that the result obtained from direct analysis of cartilage was more reliable.

In the microarray studies I reviewed (Yang et al., 2017) and in the current study (Section 3.2), *ADAM15* expression was quantified in OA samples at a single time point, mostly in end-stage OA cartilage acquired from patients undergoing UKA or TKA. Though informative, this approach is not able to analyse changes in *ADAM15*

expression through the course of OA pathogenesis. To investigate whether *ADAM15* expression changes between early and late OA, I took advantage of an on-going project in our laboratory and extracted RNA from joints of mice after DMM surgery. No difference in *Adam15* expression was found 6 hours, 8 weeks and 12 weeks after DMM surgery, suggesting that *Adam15* expression remained unchanged during the course of OA development. Together with published data, these results indicate that *ADAM15* expression is not differentially regulated in normal and OA cartilage.

I next investigated whether factors that increase risk of OA may affect *ADAM15* expression. I firstly examined whether gender has any effect on *ADAM15* expression, as gender has been identified as a major risk factor of OA, with higher OA prevalence in females (Price et al., 2009). However, no difference in *ADAM15* cartilage expression was found between males and females. Ageing is a prominent risk factor for OA (Loeser et al., 2016), with epidemiological studies reporting that OA incidence and prevalence increase with age (Johnson et al., 2014; Prieto-Alhambra et al., 2014). Although the detailed molecular mechanism by which ageing contributes to OA pathogenesis is not fully understood, mounting evidence suggests that age-related changes in gene expression contribute to OA pathogenesis (Loeser et al., 2016). Therefore, it is possible that *ADAM15* expression may change with age and I hypothesised that reduced *ADAM15* expression with age may contribute to increased OA risk with age. To explore the relationship between *ADAM15* expression and age, I plotted the relative expression of *ADAM15* against age and, surprisingly, an inverse parabola relationship was found between *ADAM15* expression and age, with low *ADAM15* expression cartilage from young and old donors, and peak expression of *ADAM15* in cartilage from donors 45-55 years of age. The relative expression of

ADAM15 was normalised to the housekeeping gene *RPLP0*, as a previous study in our group using TaqMan gene expression assays on microfluidic cards with multiple housekeeping genes showed that *RPLP0* is steadily expressed in cartilage from juvenile to aged donors (Dr. Anastasios Chanalaris, KIR, personal communication). The low expression of *ADAM15* in young, musculoskeletally immature cartilage suggests that ADAM15 is not required or plays only a limited role in cartilage and bone development, which is consistent with the finding that *Adam15*-deficient mice were viable without obvious musculoskeletal defects (Horiuchi et al., 2003). How *ADAM15* expression is regulated in young cartilage and how its expression increases after entering adulthood are unclear, and due to the limited availability of young cartilage samples, I did not further investigate the underpinning mechanism of this observation in the present project. Rather, I focused my study in how ageing reduced *ADAM15* expression in cartilage.

The fact that *ADAM15* expression decreased in aged cartilage supports my hypothesis that decreased *ADAM15* expression causes loss of protection in cartilage, and increases the risk of OA development. However, due to the limited sample availability, I was not able to gather a sufficient sample size to perform meaningful statistical analyses such as regression analysis. To strengthen the exploratory findings in human cartilage, I extracted RNA from knee joints of male mice of varying ages (0.2, 3, 4.5, 5.5 and 18 months old). Consistent with my findings in human cartilage, expression of murine *Adam15* displayed a similar inverse parabola relationship with age. Expression of four randomly chosen genes (namely, *Adam17*, *Sirt1*, *Runx2*, and *Jak2*) was also examined in these samples. Amongst the four genes, only *Adam17* displayed a relatively similar relationship with age, although the change of *Adam17* expression was much smaller

than observed for *Adam15*, suggesting that the age-dependent change in *Adam15* expression is particular to this gene, and is unlikely to be an artefact created during RNA extraction from cartilage of different ages.

Strikingly, *Adam15* expression in joints from 18-month old mice was ~95% lower than that from younger animals. A careful histological examination conducted by Dr. Chanalaris suggests that some, but not all, of these 18-month old mice had early unilateral OA, indicating that the dramatic reduction of *Adam15* in the joints of these mice was not sufficient to induce OA. Therefore, loss of ADAM15 in old age is more likely to cause subtle changes which predispose an individual to development of OA, rather than to induce OA directly. This is supported by my finding that ADAM15 expression does not correlate with clinical OA, and by several microarray studies that similarly show no decrease in *ADAM15* expression in OA (Yang et al., 2017).

To explore whether the chronologically old joints I used in this study also displayed characteristics of biological ageing, expression of cellular senescence markers *Cdkn2a*, *Cdkn1a* and *Il6* was examined. Surprisingly, although numerous reports suggest that p16 and p21 are master regulators of cellular senescence, I found that neither gene showed increased expression in aged murine joints. Moreover, even though a statistically significant increase of *Il6* expression was found in the 5.5-month old joints, the 18-month old joints did not showed higher *Il6* expression.

To validate my findings in human cartilage and male murine joints, I set up an independent experiment using RNA extracted from knee joints of young and old female mice and examined whether the same relationship between *Adam15* and ageing

could be established. I found that *Adam15* expression was similarly decreased in cartilage from old females, but among the other tissues examined (tibial bone, spleen, brain and heart), only bone displayed a similar reduction in *Adam15* expression with age. Since the murine joint samples I used to establish pattern of *Adam15* expression with age were mainly composed of bone, it is possible that the joint phenomenon I observed mainly represents changes in bone. Notably, the study showing that *Adam15*-deficient mice exhibit increased spontaneous OA was a whole body, constitutive knock out of *Adam15* (Bohm et al., 2005), so the observed protective effect of *Adam15* may not have come solely from its effects on cartilage, and my results suggest a major contribution from bone cannot be excluded. Micro-dissection of murine cartilage or cartilage-specific knock out of *Adam15* in mice will be required to provide a more definite answer on whether murine cartilage indeed displays similar age-dependent *Adam15* expression as joint and bone, and whether the protective effects of ADAM15 come from bone, cartilage or both.

Another interesting finding is that expression of cellular senescence markers *Cdkn2a* and *Il6* was increased in murine spleen, brain and heart, but joint and bone showed no increased *Cdkn2a* expression. This may suggest that murine bone and joint are less senescent that these other tissues, or that cellular senescence in the bone and joint is driven by pathways other than p16. Since I only examined the expression of senescence-related genes at the mRNA level, it is also possible that p16, p21 or SASP were up-regulated post-transcriptionally. Future studies (e. g. examining the activity of β-galactosidase) are required to resolve whether murine bone and cartilage are indeed less senescent upon ageing.

Several studies have reported the involvement of p16-induced cellular senescence in OA pathogenesis (Dai et al., 2006; Philipot et al., 2014; Zhou et al., 2004). Jeon et al. (2017) suggested that murine joints were more senescent after surgically-induced, post-traumatic OA, and local clearance of p16-expressing cells in murine joints attenuated the severity of post-traumatic OA in these mice. Whether this finding can be extrapolated to spontaneous, non-post-traumatic OA is debatable, but it strongly implied a causal relationship between p16-induced cellular senescence and OA development in the authors' model. Zhou et al. (2004) directly investigated whether p16 expression is up-regulated in spontaneous OA and showed that p16 expression was higher in OA cartilage at both the mRNA and protein levels. However, a relatively small sample size was used to examine protein expression of p16 (n = 6 for OA, age-matched normal and fetal cartilage) and mRNA expression of *CDKN2A* (n = 3 for OA, age-matched normal and fetal cartilage), and mRNA expression was examined using a less quantitative method (traditional reverse transcription rather than real time PCR). My data in Figure 3.11 thus represent a slightly larger scale experiment (normal, n = 11; OA, n = 7) using a more advanced, quantitative technique at least at the mRNA level. Other projects in our group looking at the expression of senescence markers at the mRNA level in other cell types also found that their up-regulation with age was highly variable (unpublished data). Therefore, more experiments with sufficient power are needed to determine whether the expression of senescence markers is indeed up-regulated at the mRNA and/or protein level in OA.

Since the previous studies mentioned above were performed using age-matched normal and OA mice, they can only address the question of whether p16 expression increases in OA cartilage, rather than explore whether ageing leads to more p16-

induced senescence in cartilage. My preliminary finding that p16 expression is not increased in aged murine bone and joint thus represents a novel observation that directly addresses the relationship between p16 expression and ageing in murine bone and joint. Furthermore, similar to these results in mice, I saw that *CDKN2A* and *CDKN1A* expression did not increase in aged human cartilage, suggesting that my murine findings can be translated to human joints with high confidence. Notably, in human, *CDKN2A* and *CDKN1A* expression was examined in cartilage directly, and even though my finding in murine joints may mostly reflect changes in bone, this suggests that murine cartilage may behave similarly.

Another surprising finding is that I found expression of *CDKN1A* was significantly decreased in human OA cartilage. This excludes the possibility that p21 is a major regulator of cellular senescence in cartilage. Whether p21 reduction plays any role in OA pathogenesis remain to be determined in the future, but data in Figure 3.12 suggest that *CDKN1A* expression did not regulate *ADAM15* expression, thus even if it does play a role in OA pathogenesis, it is not acting in an ADAM15-dependent manner.

In summary, my experiments in these chapter established an age-dependent reduction in *ADAM15* expression in cartilage, which is consistent with its postulated chondroprotective role. Based on these data, I next investigated the expression of ADAM15 at the protein level in aged cartilage. Data obtained using IF suggests that ADAM15 expression also displayed an age-dependent reduction at the protein level. However, apparent caveats exist for the IF experiments. In each cartilage section, considerable variability in ADAM15 expression was observed across cartilage and

inter-experiment variations were observed. In addition, the IF experiments were conducted using too small a sample size for meaningful statistical analyses of significance. Therefore, even though the ADAM15 protein expression data is consistent with the *ADAM15* mRNA data, the results need to be interpreted with caution and are more suitably viewed as exploratory studies.

Taken together, my data in this chapter established that ADAM15 expression is decreased with age in joints. This reduction in ADAM15 is not a general phenomenon since it was not observed for other genes examined, and is unlikely to be driven by the master senescence regulators p16 and p21.

Chapter 4. Identification of endogenous regulators that contribute to age-related reduction of ADAM15 in cartilage

4.1. Introduction

Aberrant expression of ADAM15 has been associated with multiple pathological conditions. For example, increased ADAM15 expression has been linked to faster progression of human prostate and breast adenocarcinomas (Burdelski et al., 2017), potentially by enhancing cell invasion and migration, thus contributing to cancer metastasis. Mechanistically, this increased metastatic activity may be the consequence of ADAM15 cleaving N- and E-cadherins, which was demonstrated by Najy et al. in prostate (Najy et al., 2008b) and breast (Najy et al., 2008a) cancer cell lines. On the contrary, reduced ADAM15 expression in humans was found to be associated with metastatic melanoma but not primary melanoma (Ungerer et al., 2010), suggesting that ADAM15 may suppress neoplastic transformation of melanocytes. These results imply that ADAM15 has tissue-specific functions, and whether ADAM15 contributes to cancer pathogenesis or inhibits cancer progression may be context-dependent.

In addition to carcinogenesis and metastasis, abnormal expression of ADAM15 is also known to lead to abnormalities in other tissues. *Adam15* deficiency in mice has been linked to increased bone mass (Marzia et al., 2011a), impaired non-developmental neovascularisation in the retina (Horiuchi et al., 2003), and accelerated development of spontaneous knee OA (Bohm et al., 2005), whilst ADAM15 over-expression has been associated with atherosclerosis (Ricci et al., 2015). These studies highlight that maintaining an adequate level of ADAM15 expression is important to sustain homeostasis. Therefore, understanding how ADAM15 is regulated in cells may lead to discovery of potential treatments for diseases such as OA and cancers.

Mechanisms by which ADAM15 expression is regulated post-translationally (e.g. via

endocytosis and proteasome-mediated degradation) remain elusive, but there is increasing evidence of how the enzyme is regulated at the transcriptional and post-transcriptional levels. Most of our knowledge regarding ADAM15 regulation come from studies done on endothelial and cancer cells, where ADAM15 is highly expressed and known to have important functions. For example, the male hormone DHT has been found to increase *ADAM15* expression at the mRNA level in androgen receptor over-expressing MCF-7. In the knee, where ADAM15 has been shown to have a protective role (Bohm et al., 2005), very little is known about regulation of ADAM15 under physiological or pathological conditions, and its endogenous regulators and regulatory pathways have also not been elucidated. Flannery et al. (1999) showed that, in articular chondrocytes cultured as a monolayer, *ADAM15* expression was up-regulated by IL-1β and retinoic acid (RA), and, to my knowledge, this represents the only study focused on identifying regulators of ADAM15 in chondrocytes. There is no evidence that these two molecules regulate the age-related change in ADAM15 expression described in Chapter 3.

Post-transcriptionally, evidence suggests that *ADAM15* mRNA is subject to alternative splicing and each alternatively spliced variant differs in its relative expression in different healthy tissues (Kleino et al., 2007), and also in its ability to interact with intracellular adaptor proteins, and thus to convey intracellular signalling (Kleino et al., 2009; Yasui et al., 2004). Ortiz et al. (2004) found that there was a non-random bias towards expression of certain variants in various breast cancer cell lines. Some of these variants were negatively associated with clinical prognosis, and their influence on cell morphology, adhesion, migration and invasion ability of cancer cells were different (Maretzky et al., 2009a; Zhong et al., 2008). However, not all ADAM15 variants are

tumourigenic, as one ADAM15 variant was associated with better prognosis, though the mechanism underpinning this improved prognosis is unclear (Zhong et al., 2008).

In addition to alternative splicing, *ADAM15* expression is also subject to microRNA regulation. Chatterjee et al. (2014) showed that miR-147b inhibited the expression of *ADAM15* by targeting the 3' UTR of its mRNA in human endothelial cells and so attenuated LPS-induced endothelial barrier dysfunction. Additionally, ADAM15 expression is elevated in human arterial and venous vascular smooth muscle cells by platelet-derived growth factor (PDGF), which itself was up-regulated in macrophages in atherosclerotic lesions (Ricci et al., 2015). Although this finding may partially explain the over-expression of ADAM15 found in human atherosclerotic arteries, this PDGF-induced increase in ADAM15 expression was likely to be secondary to the up-regulation of αvβ3 and α5β1 integrins, which preceded elevation of ADAM15 expression (Al-Fakhri et al., 2003).

In breast cancer cells, ADAM15 expression is reportedly elevated by miR-24 in an EGFR-dependent manner. miR-24 has been shown to repress two phosphatases, i.e. tyrosine-protein phosphatase non-receptor type 9 (PTPN9) and receptor-type tyrosine-protein phosphatase F (PTPRF), by targeting them directly. Both PTPN9 and PTPRF decrease EGFR activation, thus their inhibition augments EGFR signalling (Du et al., 2013). However, how amplified EGFR signalling affects ADAM15 expression mechanistically requires further investigation.

As mentioned earlier, only limited studies have examined ADAM15 regulation, and it is unclear whether any of the identified ADAM15 regulators contribute to the age-

related reduction of ADAM15 expression in human cartilage. Therefore, in this chapter, I examined potential regulators of ADAM15 which may be responsible for the age-related change of its expression, using a chondrosarcoma cell line HTB-94 and primary human OA chondrocytes. Although HTB-94 cells are an immortalised cell line which does not age normally and may have aberrant senescence regulation, they were a useful initial model system because they display less biological heterogeneity than primary chondrocytes and do not need to be controlled for age. Healthy chondrocytes were not available in our Institute (KIR) and there are limitations associated with use of primary OA chondrocytes. Firstly, primary chondrocytes cultured as a monolayer have a different gene expression profile than chondrocytes residing in their native tissue environment (unpublished data), and my data indicate that normal and OA chondrocytes differ from each other in their regulation of ADAM15 expression in monolayer culture (Figure 3.2). Secondly, primary OA chondrocytes display more biological heterogeneity than cell lines, and variation in ADAM15 expression with donor age is likely to complicate interpretation of results, especially since ADAM15 expression is low in cartilage from older donors (Chapter 3). We thus considered HTB-94 to be a suitable model system for initial screening of factors regulating ADAM15 expression, to generate a short list for further evaluation using primary chondrocytes. All experiments in this Chapter were performed using HTB-94, unless stated otherwise.

I began by modulating the activities of ageing-related cellular processes, including cellular senescence, and then studied the effect of some published regulators of ADAM15 identified by other researchers in primary chondrocytes or in other cell lines. Finally, I screened various other stimuli to identify possible novel regulators of

ADAM15 expression.

Table 4.1 Changes in ADAM15 expression in diseases.

Diseases	ADAM15 expression	Effects
Prostate cancer	⬆	Faster progression
Breast cancer	⬆	Faster progression
Melanoma	⬇	Increased metastasis
Bone abnormality	Deficiency	Increased bone mass
Retinopathy	Deficiency	Impaired novascularisation
Knee osteoarthritis	Deficiency	Accelerated progression

Table 4.2 Proposed regulators of ADAM15 expression

Regulators	ADAM15 expression	Cell types
DHT	⬆ (> 2 X)	AR-over-expressing MCF-7
IL-1β	⬆ (~2.5 X)	Primary human OA chondrocyte
Retinoic acid	⬆ (~2.5 X)	Primary human OA chondrocyte
miR-147b	⬇ (> 0.5 X)	HUVECs and HLMECs
PDGF/αvβ3/α5β1 integrin	⬆ (19 X)	Human smooth muscle cells
miR-24	⬆ (indirect, n.a.)	Human mammary carcinomas, MT-1

HUVECs: Human umbilical vein endothelial cells; HLMECs: Human lung microvascular endothelial cells

4.2. Induction of cellular senescence using mirin did not affect *ADAM15* expression in HTB-94 cells

Since senescent cells accumulate in aged tissues (Lopez-Otin et al., 2013), and *ADAM15* expression was found to be decreased in aged human cartilage (Figure 3.4) and murine joints (Figure 3.5), it is plausible that genes regulating senescence

induction may be involved in the reduction of *ADAM15* expression in aged cartilage. However, Figure 3.7 and 3.10 show that *CDKN2A* and *CDKN1A* expression did not change with age in human cartilage and murine joints. Moreover, even though *CDKN1A* expression decreased significantly in human OA cartilage compared to normal (Figure 3.10 and 3.11), I found that siRNA against the senescence marker *CDKN1A* did not affect the expression of *ADAM15* in HTB-94 cells (Figure 3.12) . This suggests that the observed reduction in *ADAM15* mRNA expression in human cartilage and murine joints is not due to *CDKN2A*- and *CDKN1A*-induced senescence.

To further investigate whether senescence affects *ADAM15* expression, I induced cellular senescence in HTB-94 cells using mirin, a small molecule inhibitor of the DNA double strand break-sensing MRN complex. Inhibition of this complex by mirin abolishes homology-dependent and non-homologous end joining DNA repair, thus disrupting the G2/M checkpoint of the cell cycle (Dupre et al., 2008; Rass et al., 2009). Moreover, Li et al. (2016a) have shown that mirin induces ageing-related phenotypes, including SASP and up-regulation of *CDKN1A* and *CDKN2A* in infiltrating T cells. Taken together, these results suggest that disruption of the DNA damage sensor machinery by mirin leads to accumulation of DNA damage and induction of cellular senescence.

To test the effect of mirin on *ADAM15* expression, HTB-94 cells were treated with 50 μM mirin for 24 or 48 hours. Cells were treated with mirin in full DMEM (no serum starvation) to allow cell division and mirin-dependent accumulation of DNA damage upon replication. Figure 4.1 (A) shows that mirin reduced *ADAM15* expression in HTB-94 by approximately 40% compared to the DMSO-treated control 24 hours after

treatment (p value = 0.0298, 95 % CI: [-0.6994, -0.06061]). However, as shown in Figure 4.1 (B-D), expression of the senescence markers *CDKN2A* and *CDKN1A* was not up-regulated in response to mirin treatment, nor was expression of the SASP cytokine *Il6* (*CDKN2A*: p value = 0.0668, 95 % CI: [-1.344, 0.07071]; *CDKN1A*: p value = 0.0942, 95 % CI: [-0.03697, 0.3103]; *Il6*: p value = 0.7564, 95 % CI: [-1.104, 1.404]). Furthermore, Figure 4.2 (A) shows the effect of mirin on *ADAM15* expression was not observed 48 hours after treatment (p value = 0.6595, 95 % CI: [-1.437, 1.017]), and all senescence markers remained unchanged (*CDKN2A*: p value = 0.6355, 95 % CI: [-0.7662, 1.113]; *CDKN1A*: p value = 0.6945, 95 % CI: [-1.313, 0.9661]; *Il6*: p value = 0.0965, 95 % CI: [-0.06514, 0.5251]). A similar level of *ADAM15* inhibition at 24 hours but not 48 hours was observed in an independent replicate experiment (data not shown), indicating that the reduction of *ADAM15* expression at the 24-hour time point was unlikely to be due to chance.

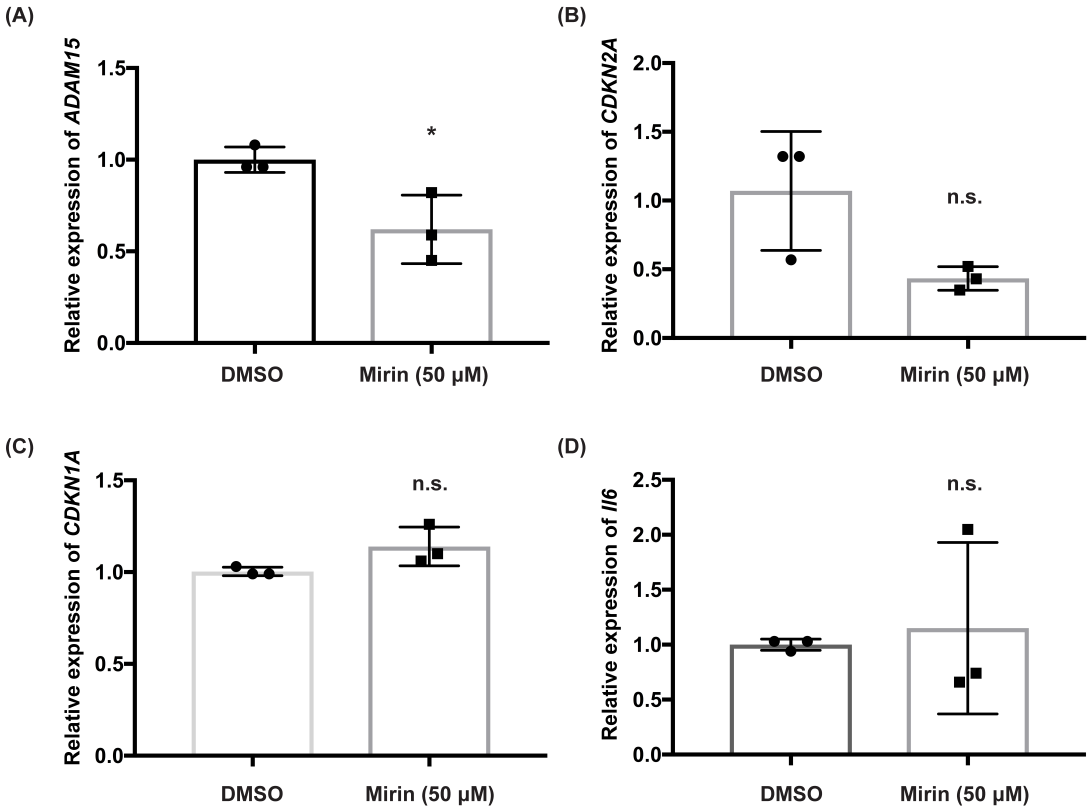

Figure 4.1 Mirin decreased *ADAM15* expression in HTB-94 24 hours after treatment.
HTB-94 cells were treated with 50 μM mirin for 24 hours. Mirin was dissolved in DMSO, so DMSO was added to the cells as a control. RNA was extracted 24 hours after treatment from controls and stimulated cells, reverse transcribed and quantified using qPCR. *ADAM15*, *CDKN2A*, *CDKN1A* and *Il6* expression was normalised using the housekeeping gene *RPLP0* and calculated using the ΔΔCt method detailed in Section 2.2.5.4.
(A) *ADAM15* expression was decreased by mirin 24 hours, but not 48 hours, after treatment (p value = 0.0298, 95 % CI: [-0.6994, -0.06061]). Relative expression of *ADAM15* was normalised to the average *ADAM15* expression of the untreated control. Figure shows representative data from two independent experiments (n = 3 each).
(B) *CDKN2A* expression did not significantly differ between DMSO- and mirin-treated cells 24 hours after treatment (n = 3, p value = 0.0668, 95 % CI: [-1.344, 0.07071]). Relative expression of *CDKN2A* was normalised to the average *CDKN2A* expression of the untreated control.
(C) Expression of *CDKN1A* did not differ between DMSO- and mirin-treated cells 24 hours after treatment (n = 3, p value = 0.0942, 95 % CI: [-0.03697, 0.3103]). Relative expression of *CDKN1A* was normalised to the average *CDKN1A* expression of the untreated control.
(D) Expression of *Il6* did not differ between DMSO- and mirin-treated cells 24 hours after treatment (n = 3, p value = 0.7564, 95 % CI: [-1.104, 1.404]). Relative expression of *Il6* was normalised to the average *Il6* expression of the untreated control.
Data are shown as mean ± SD, n.s., not significant, *, $p \leq 0.05$. The statistical significance of comparisons were analysed with Student's t test (two-tailed).

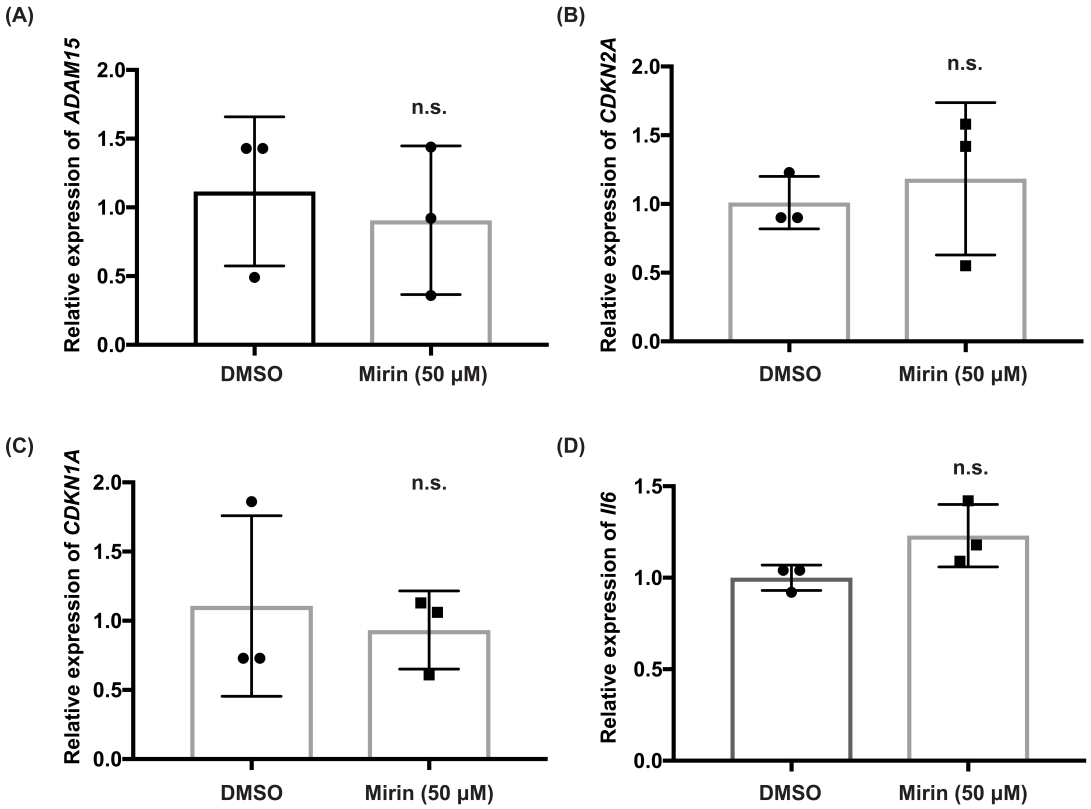

Figure 4.2 Mirin did not change *ADAM15* expression in HTB-94 48 hours after treatment.
HTB-94 cells were treated with 50 µM mirin for 48 hours. Mirin was dissolved in DMSO, so DMSO was added to the cells as a control. RNA was extracted 48 hours after treatment from controls and stimulated cells, reverse transcribed and quantified using qPCR. *ADAM15*, *CDKN2A*, *CDKN1A* and *Il6* expression was normalised using the housekeeping gene *RPLP0* and calculated using the ΔΔCt method detailed in Section 2.2.5.4.
(A) *ADAM15* expression did not differ between DMSO- and mirin-treated cells 48 hours after treatment (p value = 0.6595, 95 % CI: [-1.437, 1.017]). Relative expression of *ADAM15* was normalised to the average *ADAM15* expression of the untreated control. Figure shows representative data from two independent experiments (n = 3 each).
(B) *CDKN2A* expression did not differ between DMSO- and mirin-treated cells 48 hours after treatment (n = 3, p value = 0.6355, 95 % CI: [-0.7662, 1.113]). Relative expression of *CDKN2A* was normalised to the average *CDKN2A* expression of the untreated control.
(C) Expression of *CDKN1A* did not differ between DMSO-and mirin-treated cells 48 hours after treatment (n = 3, p value = 0.6945, 95 % CI: [-1.313, 0.9661]). Relative expression of *CDKN1A* was normalised to the average *CDKN1A* expression of the untreated control.
(D) Expression of *Il6* did not differ between DMSO- and mirin-treated cells 48 hours after treatment (n = 3, p value = 0.0965, 95 % CI: [-0.06514, 0.5251]). Relative expression of *Il6* was normalised to the average *Il6* expression of the untreated control.
Data are shown as mean ± SD, n.s., not significant. The statistical significance of comparisons were analysed with Student's t test (two-tailed).

To examine whether the observed decrease in *ADAM15* expression at the 24-hour time point was due to a change in expression of the housekeeping gene *RPLP0*, I normalised relative expression of *RPLP0* of mirin-treated cells to DMSO-treated cells. Figure 4.3 shows that *RPLP0* expression did not differ between DMSO- and mirin-

treated cells at both time points (24-hour: p value = 0.3970, 95 % CI: [-0.2381, 0.4847]; 48-hour: p value = 0.5198, 95 % CI: [-0.8068, 0.4801]). Additionally, since mirin was used with an attempt to induce cell cycle arrest, I also examined whether mirin treatment had any effect on cell proliferation using an MTS colorimetric assay (Promega). The MTS assay assesses cell metabolic activity, and is often used as a preliminary assay to evaluate cell viability. However, if the stimuli used influence cell metabolism without affecting cell viability, the results of the MTS assay can be misleading, and thus need to be interpreted with caution. Figure 4.4 shows that mirin treatment for 24 and 48 hours had no effect on cell proliferation compared to the DMSO-treated control (DMSO 24 hr vs. Mirin 24 hr: adjusted p value = 0.9213, DMSO 48 hr vs. Mirin 48 hr: adjusted p value = 0.9773, DMSO 24 hr vs. DMSO 48 hr: adjusted p value = 0.3429, Mirin 24 hr vs. Mirin 48 hr: adjusted p value = 0.2502). Importantly, data in Figure 4.4 suggested that cell numbers were higher in the mirin-treated groups 48 hours after treatment compared to the 24-hour time point, suggesting that mirin did not stop cells from growing. Taken together, these data suggest that the observed effect of mirin on *ADAM15* expression at 24-hour time point was not an experimental artefact. However, since senescence markers examined did not increase after mirin treatment, and no difference in cell proliferation was observed, indicating that mirin did not induce cell cycle arrest and cellular senescence in HTB-94. Our observation that mirin decreased *ADAM15* expression at 24-hour time point was thus unlikely to be due to cellular senescence.

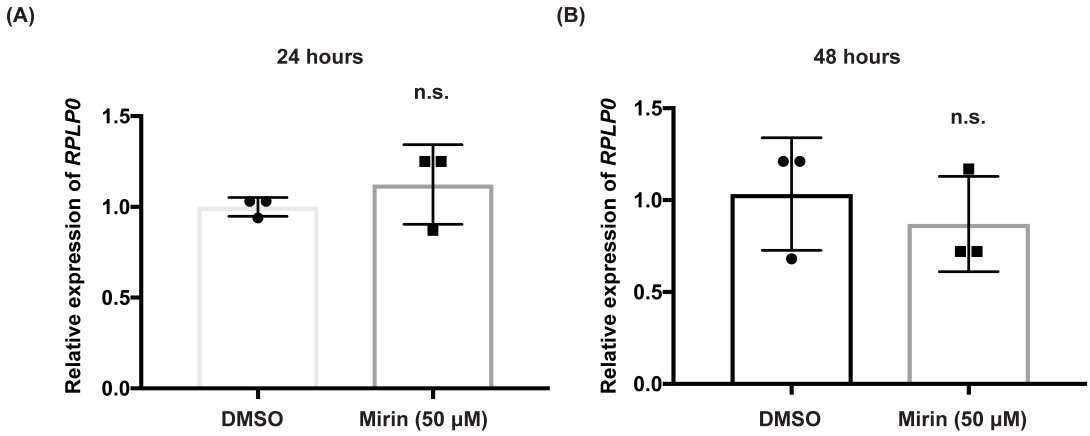

Figure 4.3 Mirin treatment did not affect *RPLP0* expression in HTB-94.
HTB-94 cells were treated with 50 µM mirin for 24 or 48 hours. Mirin was dissolved in DMSO, so DMSO was added to the cells as a control. RNA was extracted at each time point from controls and stimulated cells, reverse transcribed and quantified using qPCR. Expression of *RPLP0* was normalised to the average Ct value of the DMSO control, and relative expression was calculated using the ΔΔCt method detailed in Section 2.2.5.4.
(A) *RPLP0* expression did not differ between DMSO and mirin treated cells 24 hours after treatment (p value = 0.3970, 95 % CI: [-0.2381, 0.4847]). Relative expression of *RPLP0* was normalised to the average *RPLP0* expression of the untreated control. Figure represents a representative data from two independent experiments (n = 3 each).
(B) *RPLP0* expression did not differ between DMSO and mirin treated cells 48 hours after treatment (p value = 0.5198, 95 % CI: [-0.8068, 0.4801]). Relative expression of *RPLP0* was normalised to the average *RPLP0* expression of the untreated control. Figure represents a representative data from two independent experiments (n = 3 each).
Data are shown as mean ± SD, n.s., not significant. The statistical significance of comparisons were analysed with Student's t test (two-tailed).

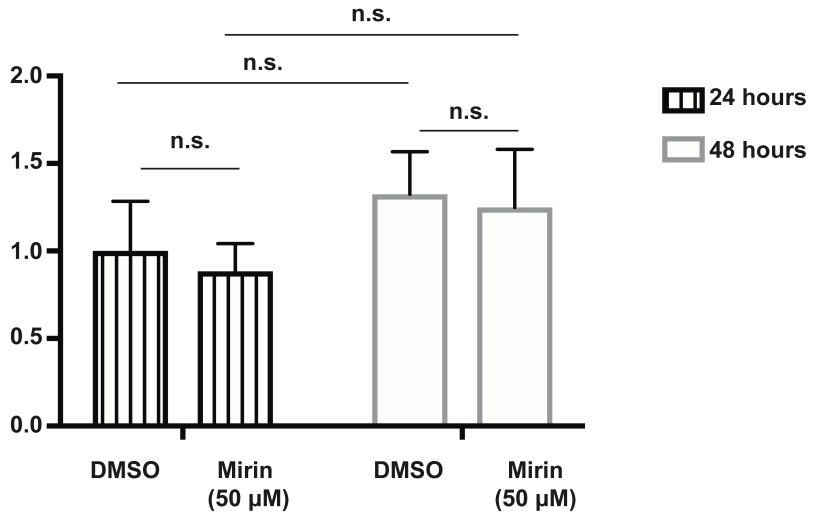

Figure 4.4 Mirin treatment did not affect proliferation of HTB-94 cells.
To test the effect of mirin on HTB-94 cells, 10,000 cells per well were seeded in a 96-well plate with 100 µl DMEM the day before mirin treatment. Cells were treated with 50 µM mirin for 24 or 48 hours (each time point in an individual 96-well plate). MTS assay was performed and data analysed according to Section 2.2.4.5., data were normalised to the average value of the DMSO group at 24 hours time. No difference was found between DMSO-treated and Mirin-treated groups at each time point, suggesting that mirin treatment did not affect cell proliferation. Data are shown as mean ± SD, n.s., not significant. The statistical significance of comparison between DMSO and mirin groups was analysed with one-way ANOVA, with post hoc multiple comparisons corrected using Tukey's test.

4.3. Treatment with Sirt1 modulators, resveratrol and EX-527, did not affect *ADAM15* expression in HTB-94.

In addition to *CDKN2A*, *CDKN1A* and *IL6*, the expression of many other genes changes with ageing. One primary example of an ageing-related gene is *SIRT1*, which encodes an NAD-dependent histone deacetylase. Studies have established that *SIRT1* expression decreases in many tissues with age and weakens mitochondrial biogenesis, increases cellular senescence and contributes to other ageing-related phenotypes (Yuan et al., 2016). Conversely, *Sirt1*-overexpressing mice showed delayed ageing and expanded life span (Satoh et al., 2013). The anti-ageing effects of SIRT1 are mainly attributed to its ability to catalyse deacetylation of histones, which regulates expression of various transcription factors (Yuan et al., 2016). Thus, SIRT1 modulation is expected to have effects on age-related phenotypes.

Given its role in ageing, I examined the effect of SIRT1 activators and inhibitors on *ADAM15* expression in HTB-94. I treated cells with resveratrol, a polyphenol found in various plants that has been found to activate SIRT1 by binding directly to the protein and inducing a conformational change. Figure 4.5 (A) shows that *ADAM15* expression did not change in HTB-94 treated with resveratrol at concentrations of 10, 50 and 100 μM for 24 hours after 24-hour serum starvation (p value = 0.2661). In parallel, I treated HTB-94 cells with EX-527, a small molecule inhibitor of SIRT1, after HTB-94 were serum starved for 24 hours. As shown in Figure 4.5 (B), cells treated with 1 and 10 μM EX-527 (IC_{50} = 38 nM according to the supplier's guide) for 24 hours did not affect *ADAM15* expression (p value = 0.0909). Furthermore, in Figure 3.6 (B), I showed that *Sirt1* expression did not change in the old murine joints. Taken together, these data support the conclusion that treatment with reagents which can modulate SIRT1

activity did not alter the age-dependent change of *ADAM15* expression in human cartilage. Notably, since the effects of resveratrol and EX-527 on SIRT1 activity were not confirmed, these experiments cannot fully exclude the involvement of SIRT1 in regulating *ADAM15* expression.

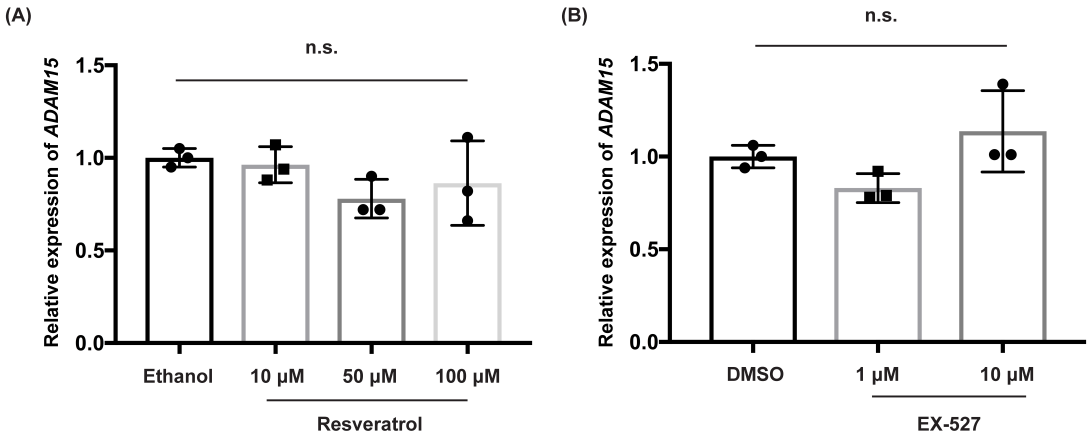

Figure 4.5 Treatment with Sirt1 activity modulators did not regulate *ADAM15* expression in HTB-94.
To analyse the effect of Sirt1 modulators on *ADAM15* expression at the mRNA level in HTB-94, cells were serum starved for 24 hours, then treated with resveratrol (a known Sirt1 activator) or EX-527 (a Sirt1 inhibitor) at the indicated concentrations for 24 hours. Resveratrol was dissolved in ethanol, whilst EX-527 was dissolved in DMSO, so ethanol or DMSO were added to cells as controls, respectively. RNA was extracted, reverse transcribed and quantified using qPCR. *ADAM15* expression was normalised using the housekeeping gene *RPLP0* and calculated using the ΔΔCt method detailed in Section 2.2.5.4. In each case, relative expression of *ADAM15* was normalised to the average expression of the unstimulated control.
(A) The Sirt1 activator resveratrol did not affect *ADAM15* expression at any of the concentrations tested (n = 3 for each concentration, p value = 0.2661).
(B) The Sirt1 inhibitor EX-527 did not affect *ADAM15* expression at both concentrations tested (n = 3 for each concentration, p value = 0.0909).
Data are shown as mean ± SD, n.s., not significant. The statistical significance of comparison between treatment groups were analysed with one-way ANOVA, with post hoc multiple comparisons corrected using Dunnett test.

4.4. 3-MA treatment increased *ADAM15* expression

Another hallmark cellular process of ageing is reduction in autophagy. Three different forms of autophagy have been identified in mammals- macroautophagy, microautophagy, and chaperone-mediated autophagy (CMA) (Martinez-Lopez et al., 2015). Extensive studies have shown that macroautophagy decreases with age, and

emerging evidence has suggested that CMA also reduces during ageing (Martinez-Lopez et al., 2015). Meanwhile, *in vivo* studies have found that induction of autophagy using rapamycin extends lifespan in several organisms (Bjedov et al., 2010; Rubinsztein et al., 2011). Therefore, it is possible that autophagy regulates *ADAM15* expression and ageing-related reduction in autophagy underlies the age-related reduction of *ADAM15* expression in human cartilage.

To test this hypothesis, I treated HTB-94 cells with 3-methyladenine (3-MA), a small molecule inhibitor of Phosphatidylinositol 3-kinases (PI3K). PI3K is critical for the formation of autophagosomes, thus its inhibition abolishes macroautophagy (Martinez-Lopez et al., 2015). To perform the experiment, HTB-94 cells were serum starved for 24 hours, and cells were treated with 5 μM 3-MA (concentration chosen according to the manufacturer's guide). Figure 4.6 shows that 3-MA treatment slightly increased *ADAM15* expression by approximately 27% (n = 3, mean difference: 0.2687 ± 0.05607, p value = 0.0087, 95 % CI: [0.113, 0.4243]). Although this increase in *ADAM15* expression was statistically significant, the absolute difference between the ethanol-treated control and the 3-MA treated cells was only 27%, thus the biological significance of this increase may be relatively small. Additionally, 3-MA also has other effects on cells, such as enhancing LPS-induced NF-κB activation and pro-inflammatory cytokine expression via a GSK3β-dependent mechanism (Lin et al., 2012). Therefore, the up-regulation of *ADAM15* found in 3-MA-treated HTB-94 may reflect the autophagy-independent changes induced by 3-MA. Finally, this result contradicts my hypothesis that reduced autophagy in aged cartilage decreases *ADAM15* expression. Consequently, autophagy is unlikely to be the main regulator of change in *ADAM15* expression with age.

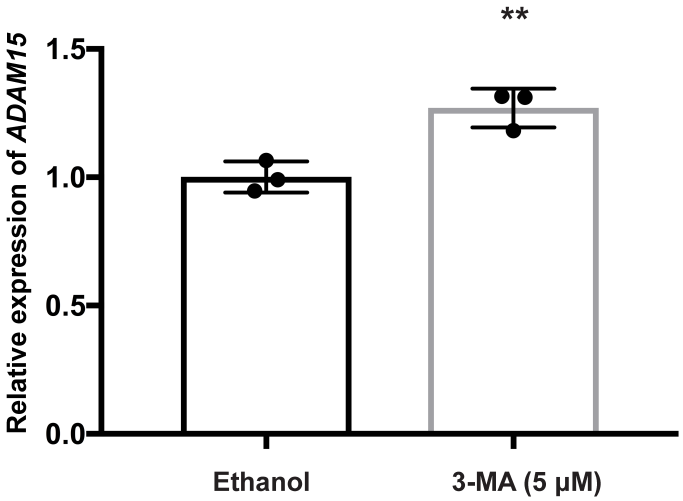

Figure 4.6 3-MA treatment increased *ADAM15* expression.
To analyse the effect of autophagy on *ADAM15* expression at the mRNA level in HTB-94, cells were serum starved for 24 hours, then treated with 3-MA (5 μM), a small molecule inhibitor of autophagy for 24 hours. 3-MA was dissolved in ethanol, so ethanol was added to cells as a control. RNA was extracted, reverse transcribed and quantified using qPCR. *ADAM15* expression was normalised using the housekeeping gene *RPLP0* and calculated using the ΔΔCt method detailed in Section 2.2.5.4. Relative expression of *ADAM15* was normalised to the average expression of the unstimulated control. Figure 4.6 shows that 3-MA increased *ADAM15* expression 24 hours after treatment (n = 3, mean difference: 0.2687 ± 0.05607, p value = 0.0087, 95 % CI: [0.113, 0.4243]). Data are shown as mean ± SD, **, $p \leq 0.01$. The statistical significance of comparisons were analysed with Student's t test (two-tailed).

4.5. IL-1 and RA did not regulate ADAM15 expression in HTB-94 and primary human OA chondrocytes

Some studies have identified regulators of ADAM15 in chondrocytes or other cell types. These regulators may be responsible for the age-related decrease of ADAM15 expression in cartilage. Thus, I examined whether these published stimuli have any effect on *ADAM15* expression in HTB-94 and primary human OA chondrocytes. Since the effect of IL-1β and RA on ADAM15 expression has previously been reported, these experiments were performed as confirmatory studies rather than stimuli screening, and positive controls were included in the experiments.

Flannery et al. (1999) found that IL-1β (10 ng/ml) and RA (1 μM) up-regulated *ADAM15* expression in OA chondrocytes cultured as a monolayer by approximately 2.5-fold. Since HTB-94 cells may be less responsive to IL-1 than chondrocytes (Gebauer et al., 2005), I stimulated HTB-94 with different concentrations of IL-1α for 24 hours to identify the optimal concentration for HTB-94 stimulation. Studies have suggested that the biological roles of IL-1α and IL-1β are largely similar (Weber et al., 2010), thus human recombinant IL-1α, instead of IL-1β, was used in my experiments due to availability. After stimulation, HTB-94 were lysed and RNA was extracted, reverse transcribed to cDNA, and the expression of *MMP-13*, a IL-1-responsive gene, was quantified according to the method described in Section 2.2.5.2 to 2.2.5.4. As shown in Figure 4.7 (A), although increase in *MMP-13* expression can be detected at a concentration as low as 10 ng/ml, 100 ng/ml IL-1α showed a higher effect. Therefore, all the following experiments were performed using 100 ng/ml human recombinant IL-1α. Figure 4.7 (B) shows that neither IL-1α nor RA increased *ADAM15* expression in HTB-94 (IL-1α: p value = 0.2891, 95 % CI: [-1.727, 0.5267]; RA: p value = 0.2624, 95 % CI: [-1.757, 0.4967]). Due to this unexpected result, I also stimulated primary human OA chondrocytes cultured as a monolayer from relatively young OA patients with IL-1α or RA for 24 hours [Figure 4.7 (C), age 59 and 67, respectively, which I expected to still express appreciable levels of ADAM15] and, unlike the results published by Flannery et al. (1999), I found that neither molecule increased *ADAM15* expression (IL-1α: p value = 0.9924, 95 % CI: [-0.3621, 0.3887]; RA: p value = 0.4724, 95 % CI: [-0.2287, 0.5221]). Due to these contradictory results with published data, I also examined the effect of IL-1α or RA on *ADAM15* expression at the protein level. HTB-94 cells were serum starved for 24 hours and stimulated with IL-1α or RA for 48 hours to allow proteins to accumulate. Cell lysates were collected and immunoblotting was

performed to detect ADAM15 using methods described in Section 2.2.6.3. As shown in Figure 4.7 (D&F), IL-1α and RA stimulation increased ADAM15 as well as actin expression in HTB-94, which was expected as both stimuli are known to increase cell proliferation in some cell types (Luheshi et al., 2009; Noy, 2010). To account for the effect of cell growth, I normalised ADAM15 expression to actin and, as shown in Figure 4.7 (E&G), neither IL-1α nor RA affected ADAM15 expression at the protein level (IL-1α: p value = 0.8159, 95 % CI: [-0.7796, 0.9329]; RA: p value = 0.8852, 95 % CI: [-0.6821, 0.7621]).

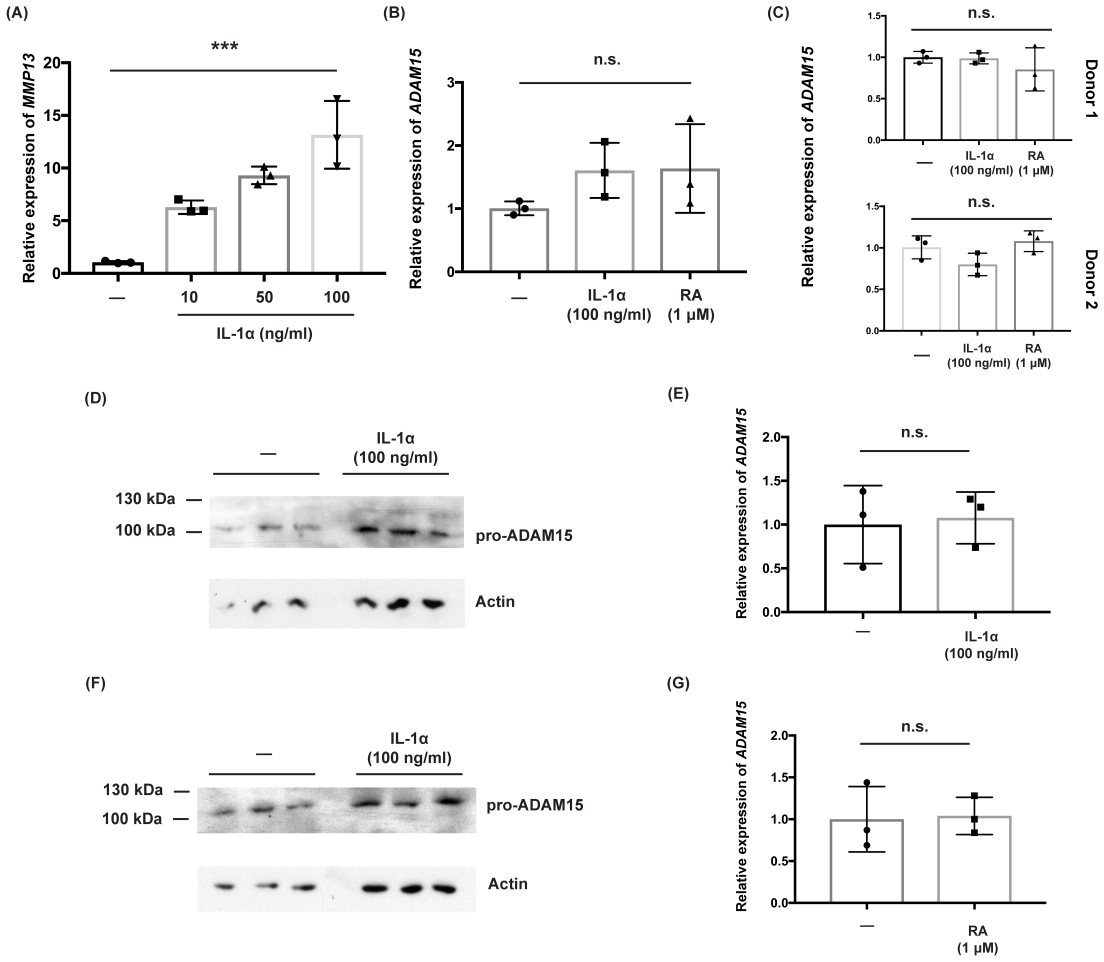

Figure 4.7 IL-1α and RA did not increase ADAM15 expression at mRNA and protein levels in HTB-94 and primary human OA chondrocytes.
To analyse the effect of IL-1α and RA on ADAM15 expression at the mRNA level in HTB-94, cells were serum starved for 24 hours, then stimulated with the indicated concentration of IL-1 or RA for 24 hours.

RNA was extracted from controls and stimulated cells, reverse transcribed and quantified using qPCR. *ADAM15* expression was normalised using the housekeeping gene *RPLP0* and calculated using the ΔΔCt method detailed in Section 2.2.5.4. In each case, relative expression of *MMP13* or *ADAM15* was normalised to the average expression of the unstimulated control (—). To analyse the effect of IL-1α and RA on ADAM15 expression at the protein level, cells were serum starved for 24 hours, then stimulated with indicated concentration of IL-1 or RA for 48 hours. Cells were lysed in 80 µl 2X SDS sample buffer and expression of ADAM15 was analysed using immunoblotting, with β-actin expression used as an internal control.
(A) *MMP13* expression increased with IL-1α stimulation (24 hours) in a dose-dependent manner (p value = 0.0001) between 10 ng/ml and 100 ng/ml (n = 3 for each concentration), indicating the activation signalling pathways downstream of IL-1.
(B) IL-1α (100 ng/ml) and RA (1 µM) treatment for 24 hours did not affect *ADAM15* expression in HTB-94 (n = 3 for each condition, IL-1α: p value = 0.2891, 95 % CI: [-1.727, 0.5267]; RA: p value = 0.2624, 95 % CI: [-1.757, 0.4967]).
(C) In primary human chondrocytes isolated from two OA patients who underwent TKA (donor 1: 59 years of age, donor 2: 67 years of age), IL-1α (100 ng/ml) and RA (1 µM) treatment for 24 hours did not affect *ADAM15* expression in human OA primary chondrocytes (IL-1α: p value = 0.9924, 95 % CI: [-0.3621, 0.3887]; RA: p value = 0.4724, 95 % CI: [-0.2287, 0.5221]).
(D) IL-1α (100 ng/ml) stimulation for 48 hours increased both ADAM15 and actin expression in HTB-94 at the protein level.
(E) Band intensities in **(D)** were quantified using Phoretix 1D software. ADAM15 expression was normalised to actin, and the relative expression of ADAM15 was normalised to the average intensity of the unstimulated control (—). As shown in the graph, IL-1α stimulation did not increase ADAM15 expression after normalisation (IL-1α: p value = 0.8159, 95 % CI: [-0.7796, 0.9329]).
(F) RA (1 µM) stimulation for 48 hours increased both ADAM15 and actin expression in HTB-94 at the protein level.
(G) Band intensities in **(F)** were quantified using Phoretix 1D software. ADAM15 expression was normalised to actin, and the relative expression of ADAM15 was normalised to the average intensity of the unstimulated control (—). RA stimulation did not increase ADAM15 expression after normalisation (RA: p value = 0.8852, 95 % CI: [-0.6821, 0.7621]).
Data are shown as mean ± SD, n.s., not significant, ***, $p \leq 0.001$. The statistical significance of comparison between treatment groups in **(A-C)** were analysed with one-way ANOVA, with post hoc multiple comparisons corrected using Tukey's test, whilst **(E&G)** were analysed with Student's t test (two-tailed).

4.6. DHT and E2 treatments did not regulate *ADAM15* expression in HTB-94

Another published stimulus of ADAM15 is the male sex hormone DHT. Garritano et al. (2015) found that DHT, but not E2, up-regulated *ADAM15* expression in the androgen receptor (AR) over-expressing breast cancer cell line MCF-7. To test whether these hormones have any effect on *ADAM15* expression without AR over-expression, I serum starved HTB-94 cells for 24 hours in phenol red-free Opti-MEM, then stimulated the cells with 0.1 µM DHT or E2 for another 24 hours. Phenol red-free Opti-MEM was used in these experiments because phenol red is known to be a weak agonist of oestrogen (Berthois et al., 1986). As shown in Figure 4.8 (A&B), neither

hormone had any effect on *ADAM15* expression in HTB-94 cells 24 hours after stimulation (MeOH vs. DHT: p value = 0.1178, 95 % CI: [-0.2568, 1.55]; EtOH vs. E2: p value = 0.1271, 95 % CI: [-0.1617, 0.8883]). Notably, since E2 and DHT responsive genes were not included as positive controls in these preliminary screening experiments, the effects of sex hormone-related pathways on *ADAM15* expression cannot be fully excluded.

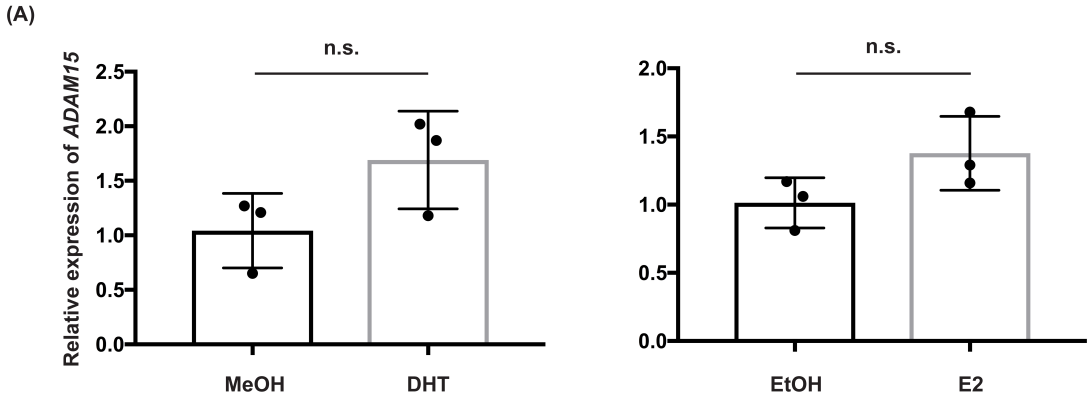

Figure 4.8 DHT and E2 treatments did not increase *ADAM15* expression in HTB-94 cells.
HTB-94 cells were serum starved for 24 hours in phenol red-free Opti-MEM, then stimulated with 0.1 μM DHT or E2 for another 24 hours. DHT was dissolved in methanol, whilst E2 was dissolved in ethanol, so each alcohol was added to the cells as the respective control for DHT and E2. RNA was extracted from controls and stimulated cells, reverse transcribed and quantified using qPCR. *ADAM15* expression was normalised using the housekeeping gene *RPLP0* and calculated using the ΔΔCt method detailed in Section 2.2.5.4. In each case, relative expression of *ADAM15* was normalised to the average *ADAM15* expression of the unstimulated control.
(A) DHT did not increase *ADAM15* expression in HTB-94 (p value = 0.1178, 95 % CI: [-0.2568, 1.55]).
(B) E2 did not increase *ADAM15* expression in HTB-94 (p value = 0.1271, 95 % CI: [-0.1617, 0.8883]).
Data are shown as mean ± SD, n.s., not significant. The statistical significance of comparisons were analysed with Student's t test (two-tailed).

4.7. Identification of potential regulator(s) of *ADAM15* expression

My data suggest that treatment of HTB-94 with modulators of several ageing-related cellular processes, including autophagy and senescence, had no effect on ADAM15 expression, and that these processes are thus unlikely to be responsible for the age-

related reduction of ADAM15 expression in cartilage. Furthermore, previously published regulators of ADAM15 also had no effect on *ADAM15* expression in HTB-94 cells. In order to identify potential regulators which may be at least partially responsible for the age-related change in *ADAM15* expression, I screened the effect of various pro- and anti-inflammatory cytokines, growth factors, chemokines, etc. on *ADAM15* expression in HTB-94 cells using the method described in Section 2.2.4.3. Cells were serum starved for 24 hours before stimulation, and were stimulated as indicated in Table 2.8. Since reagents were dissolved in different solvents (i.e. serum-free DMEM, DMSO and ultrapure water), stimuli were grouped into three categories according to which solvent was used to solubilised them. Figure 4.9 (A) depicts those dissolved in serum-free DMEM (IL-6, IL-10 and TNF), and shows that neither the pro-inflammatory cytokines IL-6 and TNF, nor the anti-inflammatory cytokine IL-10 affected *ADAM15* expression in HTB-94 cells 24 hours after stimulation ($n = 6$, p value = 0.2050). Figure 4.9 (B) depicts those solubilised in DMSO (PMA and dexamethasone). As expected, the Protein Kinase C activator PMA, which is known to activate ADAM17 activity without affecting its expression (Pruessmeyer et al., 2010), did not change *ADAM15* expression, nor did the anti-inflammatory corticosteroid dexamethasone ($n = 3$, p value = 0.2303). Figure 4.9 (C) shows all the stimuli which were reconstituted in aqueous buffer (all other stimuli). TGF-β was used at different concentrations since studies indicated that cellular responses to TGF-β is highly concentration-dependent and opposite effects can be observed at low and high concentrations (Gordon et al., 2008). However, all the concentrations tested (10 pg to 10 ng) did not affect *ADAM15* expression.

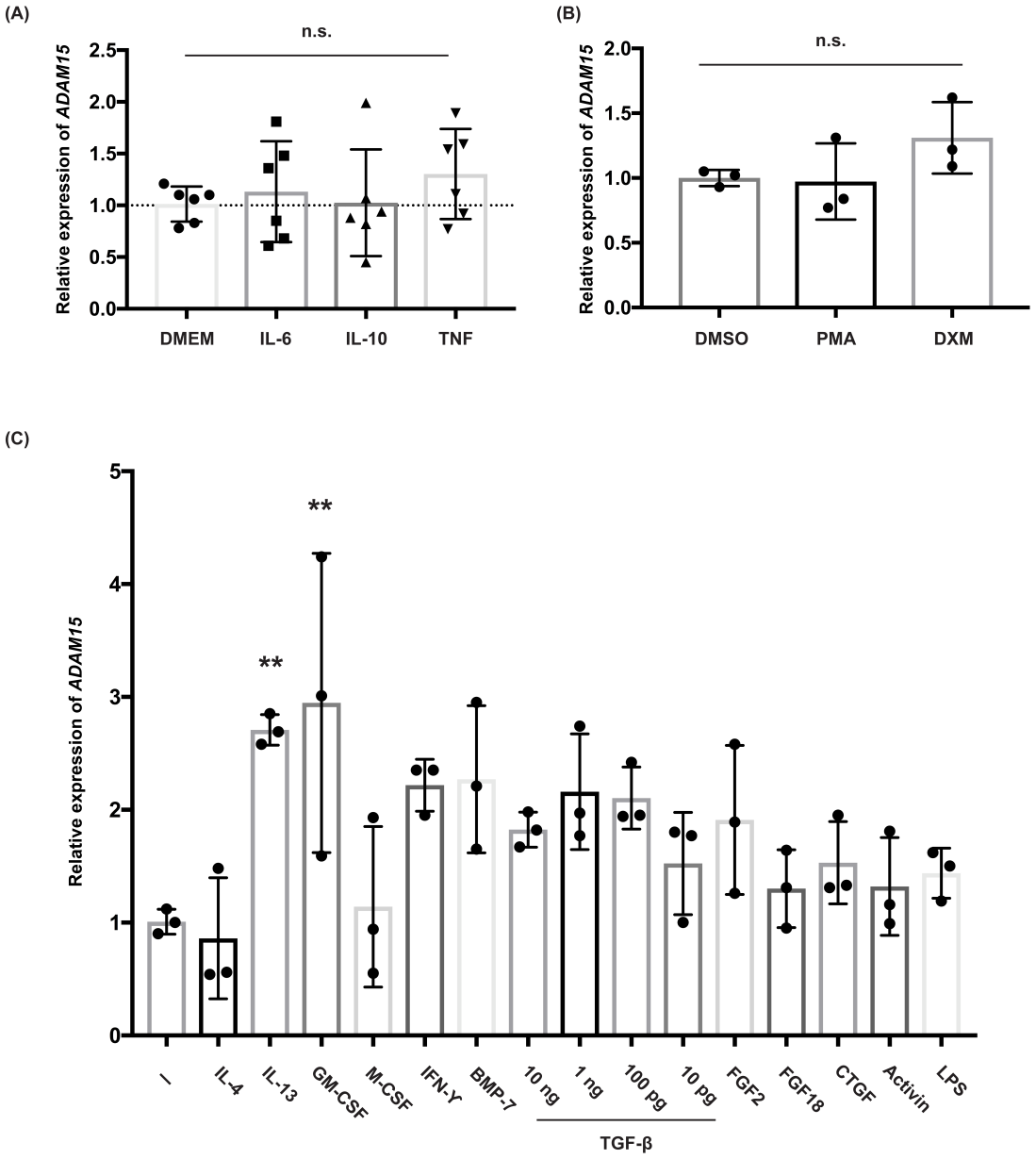

Figure 4.9 Stimuli screening identified that IL-13 and GM-CSF increased *ADAM15* expression in HTB-94 cells 24 hours after stimulation.

To identify potential regulators of *ADAM15* expression at the mRNA level in HTB-94, cells were serum starved for 24 hours, then treated with stimuli at the indicated concentrations (Table 2.8) for another 24 hours. RNA was extracted, reverse transcribed and quantified using qPCR. *ADAM15* expression was normalised using the housekeeping gene *RPLP0* and calculated using the ΔΔCt method detailed in Section 2.2.5.4. IL-6, IL-10 and TNF were dissolved in serum-free DMEM and are depicted in panel **(A)**, PMA and DXM were solubilised in DMSO and are depicted in panel **(B)**, whilst all other stimuli which were reconstituted in ultrapure water are depicted in panel **(C)**. Serum-free DMEM, DMSO and ultrapure water were thus added to unstimulated cells as the respective unstimulated controls. In each panel, relative expression of *ADAM15* was normalised to the average expression of the respective unstimulated control group.

(A) IL-6, IL-10 and TNF did not change *ADAM15* expression in HTB-94 cells 24 hours after stimulation (n = 6, p value = 0.2050).

(B) PMA and dexamethasone did not change *ADAM15* expression in HTB-94 cells 24 hours after stimulation (n = 3, p value = 0.2303).

(C) Amongst all the stimuli tested, only IL-13 and GM-CSF significantly increased *ADAM15* expression in HTB-94 cells 24 hours after stimulation (n = 3, IL-13: adjusted P Value = 0.0059; GM-CSF: adjusted P Value = 0.0013). None of the stimuli tested decreased *ADAM15* expression in our screening panel.

Data are shown as mean ± SD, n.s., not significant; **, p ≥ 0.01. The statistical significance of comparison

between treatment groups were analysed with one-way ANOVA, with post hoc multiple comparisons corrected using Dunnett test.

Amongst all the stimuli tested, none reduced *ADAM15* expression significantly, and only IL-13 and GM-CSF increased *ADAM15* expression after correcting for multiple comparisons using Dunnett test (n = 3, IL-13: adjusted p value = 0.0059; GM-CSF: adjusted p value = 0.0013). Between these two cytokines, IL-13 is particularly relevant because a study published by Cleaver et al. (2001) indicates that IL-13 blocked IL-1α and oncostatin M induced collagen breakdown in bovine nasal cartilage. This study suggests that IL-13 is a chondroprotective anti-inflammatory cytokine, and I considered whether it may exert its chondroprotective functions at least partially through up-regulating *ADAM15* expression. I tested this hypothesis first by validating the screening result using qPCR. HTB-94 cells were serum starved for 24 hours and stimulated with IL-13 (100 ng/ml) for another 24 hours. For this validation experiment, I increased the sample size of the qPCR experiment (n = 18) in order to increase the power of the statistical significance test. As shown in Figure 4.10 (A), IL-13 (100 ng/ml) treatment for 24 hours increased *ADAM15* expression in HTB-94 by approximately one fold (p value $\leq$ 0.0001, 95 % CI: [0.8426, 2.691]) with noticeable variation. I additionally tested whether IL-13 modulated ADAM15 expression in primary human OA chondrocytes (monolayer culture) from 2 patients under the age of 70. However, the results were too variable to be reliably interpreted and so were not included in this thesis.

Next, I examined whether IL-13 also increased ADAM15 expression at the protein level. Cells were serum starved for 24 hours, then stimulated with 100 ng/ml IL-13 for

48 hours to allow proteins to accumulate. As shown in Figure 4.10 (B), multiple bands were detected, with the upmost band corresponding to the molecular weight of the pro-form ADAM15 (~93 kDa) and the second upmost band corresponding to the molecular weight of the active form ADAM15 (~85 kDa). The lower two bands may be autocatalytic breakdown products of ADAM15, as ADAM15 is predicted to be an proteolytically active metalloproteinase based on its conserved catalytic domain (the HEXXHXLGXXHD zinc-binding motif) (Kratzschmar et al., 1996). Band intensity of the strongest three bands was quantified and normalised to β-actin. Figure 4.10 (C-E) show the quantification results of pro-ADAM15, ADAM15 and the most abundant breakdown product. Additionally, the sum of all four band intensities was also quantified and normalised to β-actin , as shown in Figure 4.10 (F). In all cases, IL-13 treated HTB-94 had higher ADAM15 expression at the protein level (pro-ADAM15: p value = 0.0091, 95 % CI: [1.757, 9.61]; ADAM15: p value = 0.0015, 95 % CI: [1.066, 3.324]; the breakdown product: p value = 0.0053, 95 % CI: [0.7819, 3.435]; Sum: p value = 0.0017, 95 % CI: [0.8426, 2.691]). I did not follow up effect of GM-CSF on *ADAM15* expression due to the high variability of the data and time.

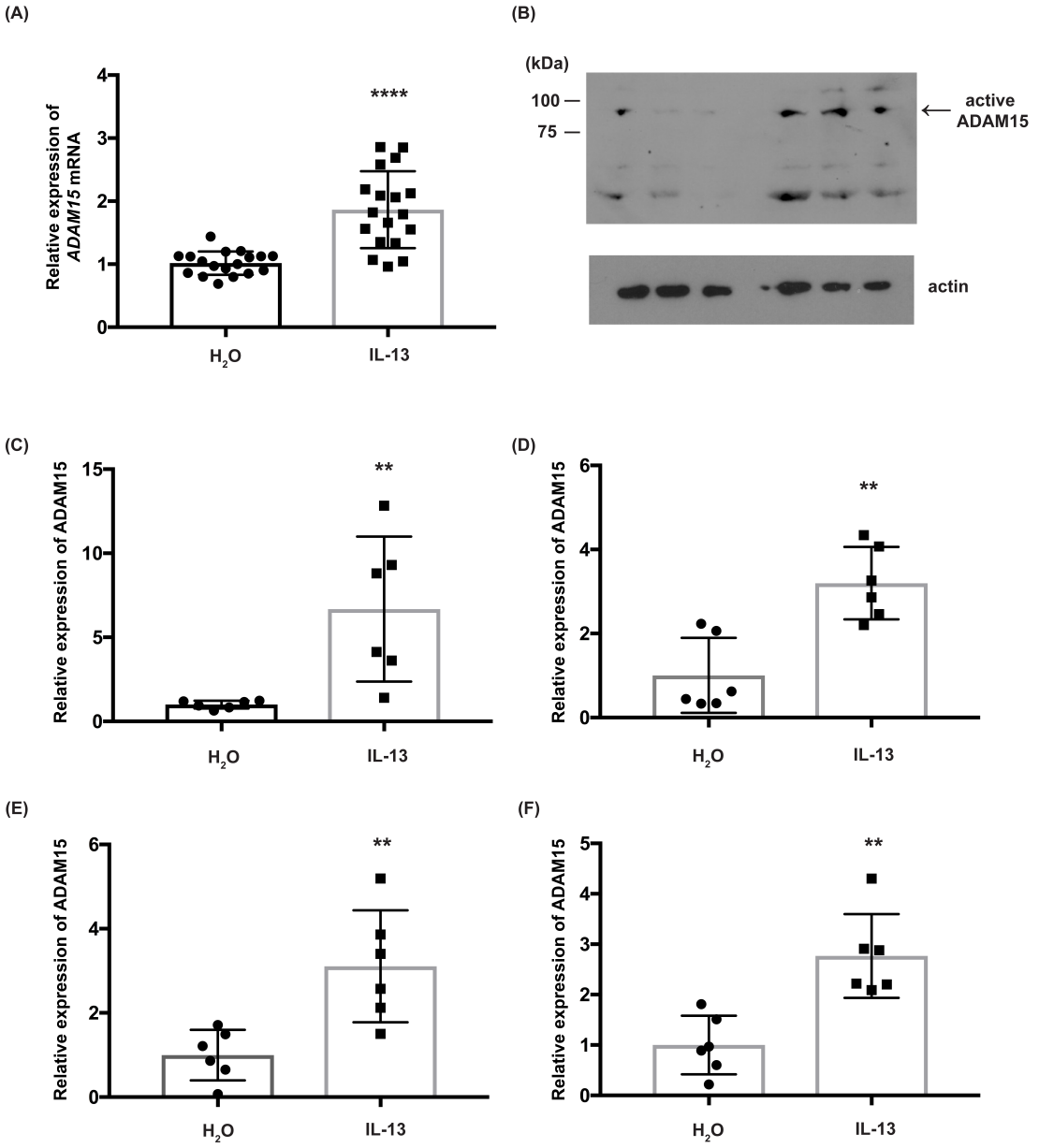

Figure 4.10 qPCR and immunoblotting validated that IL-13 increased ADAM15 expression at both the mRNA and protein levels.

To analyse the effect of IL-13 on ADAM15 expression at the mRNA level in HTB-94, cells were serum starved for 24 hours, then stimulated with IL-13 (100 ng/ml) for another 24 hours. RNA was extracted from controls and stimulated cells, reverse transcribed and quantified using qPCR. *ADAM15* expression was normalised using the housekeeping gene *RPLP0* and calculated using the ΔΔCt method detailed in Section 2.2.5.4. In each case, relative expression of *ADAM15* was normalised to the average expression of the unstimulated control (H_2O). To analyse the effect of IL-13 on ADAM15 expression at the protein level, cells were serum starved for 24 hours, then stimulated with IL-13 (100 ng/ml) for 48 hours. Cells were lysed in 80 µl 2X SDS sample buffer and expression of ADAM15 was analysed using immunoblotting, with β-actin expression used as an internal control. Band intensities of the immunoblot were quantified using Phoretix 1D software. ADAM15 expression was normalised to actin, and the relative expression of ADAM15 was normalised to the average intensity of the unstimulated control (H_2O). Two immunoblotting experiments were performed in triplicate. When quantified, data from both experiments were included (n = 6).

(A) IL-13 (100 ng/ml) treatment for 24 hours increased *ADAM15* mRNA expression in HTB-94 by about one fold (n = 18 for each condition, p value ≤ 0.0001, 95 % CI: [0.8426, 2.691]).

(B) IL-1α (100 ng/ml) stimulation for 48 hours increased ADAM15 expression in HTB-94 (100,000 cells per well in a 6-well plate) at the protein level. Four bands at different molecular weight were observed. The band which corresponds to the size of the active form of ADAM15 is indicated. Figure shows

representative data of two independent experiments.
(C) Quantification of the upmost band in **(B)**. IL-13 stimulation increased ADAM15 expression after normalisation (p value = 0.0091, 95 % CI: [1.757, 9.61]).
(D) Quantification of the upper band which corresponds to the size of the active ADAM15 in **(B)**. IL-13 stimulation increased ADAM15 expression after normalisation (p value = 0.0015, 95 % CI: [1.066, 3.324]).
(E) Quantification of the lowest band in **(B)**. IL-13 stimulation increased ADAM15 expression after normalisation (p value = 0.0053, 95 % CI: [0.7819, 3.435]).
(F) Quantification of the sum of all bands in **(B)**. IL-13 stimulation increased ADAM15 expression after normalisation (p value = 0.0017, 95 % CI: [0.8426, 2.691]).
Data are shown as mean ± SD, ****, $p \leq 0.0001$' **, $p \leq 0.01$. The statistical significance of comparisons were analysed with Student's t test (two-tailed).

Take together, these experiments suggest that IL-13 increased ADAM15 expression at both the mRNA and the protein levels. I thus considered that IL-13 may regulate the age-dependent change of *ADAM15* expression I observed in the human cartilage and murine joints.

To test this hypothesis, I examined the expression of *Il13* in the murine joints I used to investigate *Adam15* expression. As shown in Figure 4.11, *Il13* expression was significantly decreased in the 18-month old joints compared to the 3.5- and 4.5-month old joints (3.5-month: adjusted p = 0.0075, mean difference: 3.645, 95 % CI: [0.7799, 6.511]; adjusted p = 0.0062, mean difference: 3.928, 95 % CI: [0.903, 6.953]), though the reduction was less pronounced than the reduction of *Adam15* in the 18-month old joint (< 72% reduction in *Il13* expression vs. < 95% reduction in *Adam15* expression, Figure 3.5). Also noticeable is that *Il13* expression was not significantly different (p value = 0.3400) between the 5.5- and 18-month old joints, which indicates that reduction of *Il13* expression preceded the reduction of *Adam15* expression in the murine joints.

Collectively, our data suggested that IL-13 may be partially responsible for the age-related reduction in ADAM15 expression in the human cartilage and murine joints. However, it is worth noting that, in the present study, the effect of decreasing IL-13

(e.g. via siRNA) on ADAM15 expression was not investigated. This effect needs to be explored to ascertain that reduction of IL-13 can indeed decrease ADAM15 expression.

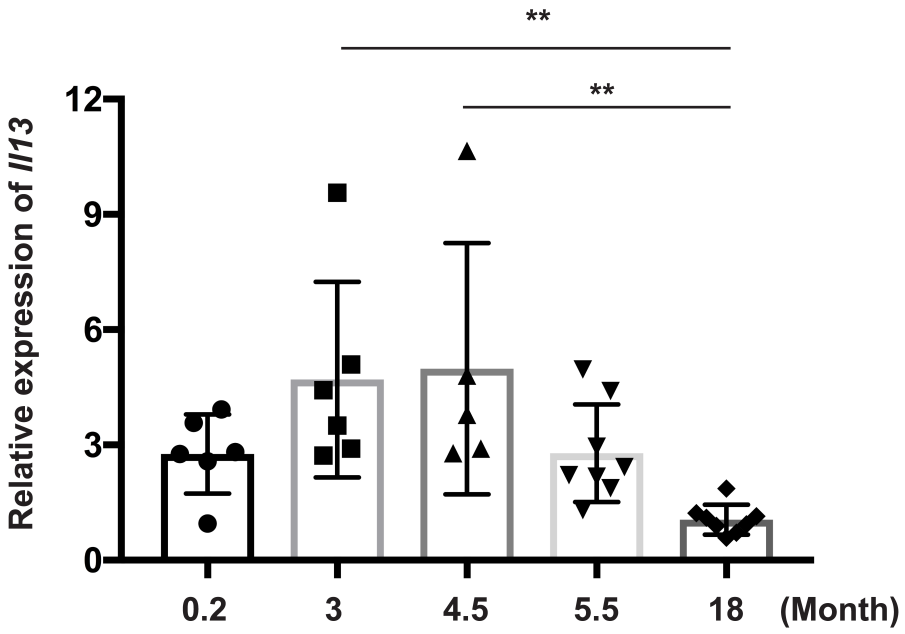

Figure 4.11 *Il13* expression decreased with age in murine joints.
RNA extracted from joints of 0.2-month (n = 6), 3-month (n = 6), 4.5-month (n = 5), 5.5-month (n = 6) and 18-month (n = 8) old male mice was reverse transcribed and quantified using qPCR. Expression of *Il13* was normalised to the housekeeping gene *Rplp0* and relative expression calculated using the ΔΔCt method detailed in Section 2.2.5.4. Relative expression of *Il13* in each age group was normalised to the average *Il13* expression of the 18-month old group. *Il13* expression in the joints from the 18-month old mice was significantly decreased compared to the 3-month old group (adjusted p = 0.0075, mean difference: 3.645, 95 % CI: [0.7799, 6.511]) and the 4.5-month old group (adjusted p = 0.0062, mean difference: 3.928, 95 % CI: [0.903, 6.953]). No significant differences were found between all other possible comparisons. Data are shown as mean ± SD, **, $p \leq 0.01$. The statistical significance of comparison between age groups was analysed with one-way ANOVA, with post hoc multiple comparisons corrected using Tukey's test.

4.8. Discussion

Studies have shown that tight regulation of ADAM15 expression is critical for homeostasis, as ADAM15 over-expression and down-regulation have been linked to several diseases (Bohm et al., 2005; Burdelski et al., 2017; Horiuchi et al., 2003; Kuefer et al., 2006; Najy et al., 2008a, b; Ricci et al., 2015). However, regulation of ADAM15 under various physiological and pathological conditions remains as a relatively unexplored field.

In murine cartilage, *Adam15*-deficiency has been shown to lead to accelerated, spontaneous development of knee OA. Since OA generally affects older mice, it is plausible that *Adam15* expression is decreased, or even completely lost in aged murine joints. In Chapter 3, I demonstrated that there was indeed a dramatic reduction in *Adam15* expression in the aged murine joints. More importantly, a similar reduction was also found in old human cartilage at both the mRNA and the protein levels. This indicates that my findings in mice may be translated to human ageing. In this chapter, I aimed to explore how ADAM15 expression decreases in human cartilage by identifying potential regulators of ADAM15 expression.

I screened several modulators of age-related processes (e.g. cellular senescence, autophagy, and age-related changes in gene expression induced by *SIRT1*) and explored their effects on *ADAM15* expression in HTB-94. Suppression of the main drivers of cellular senescence *CDKN2A* and *CDKN1A* did not affect *ADAM15* expression, which suggests that these two senescence regulators do not contribute to the reduction of *ADAM15* found in aged human cartilage. This is consistent with the finding that aged human cartilage and murine joints did not show higher *CDKN2A*

and *CDKN1A* expression (Figure 3.7 and Figure 3.10). Whether this means that cartilage is less senescent than other tissues of the same chronological age, or that senescence in cartilage is driven by other, unidentified pathways is unclear. To further investigate the effect of cellular senescence on *ADAM15* expression, in this chapter, I treated HTB-94 cells with mirin with an attempt to induce senescence. Surprisingly, I found that mirin treatment for 24 hours slightly but significantly decreased *ADAM15* expression, although this effect was not maintained at 48 hours. These findings were reproducible as an independent experiment found a similar trend. This suggests that mirin-induced *ADAM15* reduction was time-sensitive, and a potential negative feedback loop may exist to maintain an adequate level of *ADAM15* expression. Further experiments and analyses confirmed that mirin did not induce cellular senescence in HTB-94 at both time points, thus the observed reduction was unrelated to cellular senescence and the mechanism underlying this transient reduction is unclear. Given that the magnitude of reduction was relatively small (less than 40%), and this reduction was only observed at the 24-hour time point, the biological significance of this reduction is questionable. The mirin experiment thus did not help us to completely exclude the possibility that cellular senescence contributes to the age-related reduction of ADAM15 expression in human cartilage, though collectively my data do not support that senescence has a prominent role in regulating ADAM15 expression.

Next, I investigated the effect of SIRT1 modulators on *ADAM15* expression. *SIRT1* expression is known to decrease with age, leading to reduced SIRT1 activity (Yuan et al., 2016). SIRT1 induces expression of multiple genes and extends mouse life span, thus it is possible that reduced SIRT1 expression contributes to the development of

age-related diseases. Role of SIRT1 has been extensively investigated, Li et al. (2016b) found that SIRT1 expression is negatively correlated with OA severity in human, and Matsuzaki et al. (2014) reported that cartilage-specific knock out of *Sirt1* in mice causes accelerated development of surgically-induced and spontaneous OA, suggesting that SIRT1 is protective against OA in cartilage. I thus hypothesised that SIRT1 modulators, resveratrol and Ex-527, may regulate ADAM15 expression in human cartilage. Nevertheless, I found that *Sirt1* expression did not decrease in aged murine joints (Figure 3.6) and SIRT1 modulators did not change *ADAM15* expression in HTB-94. To my best knowledge, this is the first study directly investigated change in *SIRT1* expression in cartilage, and my data suggests that decreased *SIRT1* expression in human OA cartilage is unlikely to be induced by ageing and the protective effect of SIRT1 on cartilage is independent of ADAM15.

Autophagy is another cellular process that is reduced with ageing. It is thus plausible that autophagy reduction was responsible for the age-related decrease of ADAM15 expression in cartilage. To investigate this, HTB-94 cells were treated with a small molecule autophagy inhibitor 3-MA. Unexpectedly, *ADAM15* expression was slightly increased when cells were treated with 3-MA. This contradicts with my hypothesis that decreased autophagy in old age is responsible for the reduction of ADAM15. Moreover, the magnitude of increase in *ADAM15* expression was less than 27%, suggesting that even if autophagy indeed has a role in regulating *ADAM15* expression, its influence on the age-related reduction of *ADAM15* expression is likely to be negligible. Additionally, since 3-MA also influences other signalling pathways (Lin et al., 2012), the effect I observed may be due to macroautophagy-independent functions.

Since I was not able to identify a prominent regulator of ADAM15 which may be responsible for the age-related reduction of *ADAM15* expression, I decided to take a different approach to investigate the previously published potential regulators of ADAM15. I began with IL-1, as Flannery et al. (1999) found that IL-1β up-regulated *ADAM15* expression in OA chondrocytes cultured as a monolayer. IL-1 is a pro-inflammatory cytokine which is often found up-regulated in aged cells and has been used as a senescent SASP marker (Coppe et al., 2010), and has been suggested to be a mediator of inflammageing (Xia et al., 2016). Therefore, it is reasonable to assume that IL-1 may be a negative regulator of ADAM15 which decreases its expression. However, this prediction is contradictory to the finding published by Flannery et al (1999). In the present experiments, I found that IL-1α had no effects on ADAM15 expression at the mRNA and protein levels in both HTB-94 cells and human primary OA chondrocytes. Notably, IL-1α was used in the experiments, as IL-1β was not available in our laboratory. Although IL-1α and IL-1β are considered to be functionally equivalent (Weber et al., 2010), it is possible that differences between these two cytokines may explain why my results were different from the results published by Flannery et al. (1999).

RA is another molecule found to up-regulate *ADAM15* expression in OA chondrocytes cultured as a monolayer by Flannery et al. (1999), and the abundance of RA has been shown to decrease in aged rat brain (Enderlin et al., 1997) and human peripheral blood mononuclear cells (Feart et al., 2005). Thus the finding that RA increased ADAM15 expression in human OA chondrocytes implies that RA may contribute to the age-dependent decrease of ADAM15 found in human cartilage. However, I was unable to replicate the effect of RA on ADAM15 in HTB-94 and human OA chondrocytes at both

the mRNA and protein level. It remains unclear why I could not replicate the results published by Flannery et al. (1999), but it is possible that IL-1 and RA-induced *ADAM15* expression is cell-type dependent, or that there is considerable biological variation in human OA chondrocytes. In my experiments, chondrocytes from two different OA patients were isolated and three technical replicates were used when performing IL-1 and RA stimulation, whilst in the study conducted by Flannery et al. (1999), they stated that the stimulation was performed in triplicate, with no information regarding whether this refers to technical or biological replicates. Given that the sample size in both studies was relatively small, and the known heterogeneity of OA (Driban et al., 2010), biological variations may be a plausible explanation of the contradictory results found between these two studies. Therefore, more studies with a larger sample size will be necessary to determine whether IL-1 and RA have any effect on *ADAM15* expression.

In addition to Flannery et al. (1999), Garritano et al. (2015) reported that DHT up-regulated *ADAM15* expression by more than 50% in the AR over-expressing breast cancer cell line MCF-7, but not in the mock-transfected MCF-7. Since MCF-7 is a AR-positive cell line (Subik et al., 2010), the finding by Garritano et al. (2015) suggests that only highly amplified AR signalling is able to enhance *ADAM15* expression, which is unlikely to happen under physiological conditions or in ageing. HTB-94, like MCF-7, is a AR-positive female cell line (Meijer et al., 2011). Therefore, I expected that DHT-treated HTB-94 without AR over-expression would not display higher *ADAM15* expression. Indeed, I found that neither DHT nor E2 showed any effect on *ADAM15* expression. However, it remains unclear whether baseline AR signalling is required to maintain basal levels of *ADAM15* expression and whether reduced AR signalling

caused by reduced AR expression, male hormone levels, or both, contribute to the age-related reduction of ADAM15 expression in cartilage. Transient suppression of AR or generation of AR knock-out HTB-94 cell line will be necessary to address these questions.

As mentioned in Section 4.1, studies investigating ADAM15 regulation at the transcription level are limited, and the published ADAM15 regulators tested in this project suggest that they are not responsible for the age-related reduction of ADAM15 expression in human cartilage. I therefore set up an experiment to screen for reagents which affect *ADAM15* expression at the mRNA level in HTB-94. None of the stimuli tested were able to decrease *ADAM15* expression, whilst IL-13 and GM-CSF were able to enhance *ADAM15* expression. Between these two, I decided to further explore the effect of IL-13 on *ADAM15* expression because a previous study suggests that IL-13 is a chondroprotective cytokine in a bovine nasal cartilage model (Cleaver et al., 2001). Surprisingly, I found that the effect of IL-13 stimulation on *ADAM15* expression was highly variable, and increased sample size was needed to establish the relationship between IL-13 stimulation and *ADAM15* expression. One plausible explanation of this variability is that HTB-94 cells may be at different cell cycle stages when performing stimulation. Dr. Chanalaris and I have found that serum starvation for as long as 72 hours was unable to induce cell cycle arrest in HTB-94 efficiently, with a certain percentage of cells remaining in the proliferative state. Preliminary data produced by Dr. Chanalaris indicates that cells at different cell cycle stages responded differently to stimulation, for example the expression of various HS genes changed with the cell cycle (unpublished data). Therefore, it is possible that IL-13 stimulation was similarly affected by cell cycle and can at least partially explain the observed variability.

Unexpectedly, this variability was not observed when I examined the effect of IL-13 on ADAM15 expression at the protein level, as two independent experiments (each in triplicate) both show that IL-13 stimulation increased ADAM15 protein expression. Therefore, more detailed investigation will be required to dissect the discrepancy in the variability of ADAM15 responsiveness to IL-13 at the mRNA and the protein levels. Furthermore, since our data in Chapter 3 suggests that ADAM15 expression at both the protein and mRNA levels are decreased in aged cartilage, it would be critical to establish whether reduced IL-13 expression will lower ADAM15 expression via knocking down *IL13* expression in HTB-94 cells or healthy chondrocytes. Another important future study which can further validate the effect of IL-13 on ADAM15 expression is switching the cell system to human primary chondrocytes. Chondrocytes from donors without OA would be preferable since OA chondrocytes from different donors may be at different disease stages, hence more heterogeneous. Although primary chondrocytes cultured as a monolayer will gradually lose their chondrocytic phenotypes, this limitation can be partially circumvented by performing experiments exclusively on cells within the first two passages, when chondrocytic phenotypes are still largely retained. Moreover, cell cycle arrest is easier to be achieved by serum starvation, which may reduce the variability I observed in HTB-94. Unfortunately, due to the unavailability of cartilage from donors without OA, I was unable to conduct validation using primary human normal chondrocytes. An alternative approach would be to conduct these experiments using healthy porcine or bovine chondrocytes, however, the availability of porcine or bovine IL-13, and whether the IL-13 signalling pathways are conserved in these species would need to be explored before carrying out such experiments.

Mechanistically, how IL-13 amplifies ADAM15 expression is unclear. A review published by Rawlings et al. (2004) suggests that both IL-13 and GM-CSF signal through the JAK/STAT pathway, specifically JAK2. I thus tested the effect of JAK2 inhibition using a small molecule inhibitor, AZD1480, on *ADAM15* expression in HTB-94 cells. siRNA specifically targeting *JAK2* was also used to repress *JAK2* expression in an independent experiment to explore its effect on *ADAM15* expression. However, the data from both approaches were too variable to be conclusive (data not shown), maybe due to the same unsynchronised cell cycle issue observed when conducting IL-13 stimulation. Therefore, primary chondrocytes or other chondrocyte-like cell lines in which cell cycle arrest can be more easily induced by serum starvation may be used in future experiments to dissect the underlying mechanism of IL-13-induced increase of ADAM15 expression.

The results in Figure 4.11 indicate that IL-13 increases ADAM15 expression at both the mRNA and protein level in HTB-94, I thus hypothesised that IL-13 is a regulator of ADAM15 which is responsible for the reduction of ADAM15 expression in aged human cartilage. To test this hypothesis, I examined *Il13* expression in murine joints. The result indicates that *Il13* expression was indeed decreased by more than 70% in the aged murine joints (18-month old) compared to 3.5- and 4.5-month old murine joints. However, no statistically significant difference was found between 5.5-month old and 18-month old joints, though a trend of reduction in *Il13* expression was found. This may suggest that *Il13* reduction preceded *Adam15* reduction in the murine joints, though increased sample size will be needed to confirm this observation. If decrease in *IL13* expression indeed precedes ADAM15 reduction, this indicates that other players may exist to sustain ADAM15 expression when IL-13 expression has begun to decline.

To ascertain the effect of IL-13 reduction on decreasing ADAM15 expression, direct manipulation of IL-13 expression will be necessary. As mentioned earlier, several other reagents (e.g. autophagy, mirin) were found to affect ADAM15 expression in HTB-94, thus the reduction of ADAM15 in aged cartilage is likely to be a cumulative consequence results from a complicated interplay between multiple factors, which gradually decrease the expression of ADAM15 in cartilage.

Notably, in Figure 4.11, the magnitude of IL-13-induced increase in ADAM15 expression was about 2-fold at the mRNA level, and less than 4-fold at the protein level. This level of increase is compatible to the reduction found in the female murine joints and bones in Figure 3.8, and also similar to the magnitude of decrease of *ADAM15* found in aged human cartilage (Figure 3.4). Surprisingly, in male murine joints, the reduction in the old age was more prominent (> 95% reduction), which also suggests that other unknown players may also be involved in regulating *Adam15* expression.

In summary, findings in this chapter add to the current knowledge in the field of ADAM15 regulation, which is still in its infancy. The data presented in Chapter 4 supports the hypothesis that decreased IL-13 expression contributes to the age-related reduction of ADAM15 expression, although it cannot be excluded that other players may also contribute to ADAM15 reduction in cartilage. More systemic approaches will be necessary to identify more regulators of ADAM15 in cartilage and validate my preliminary results. For example, siRNA array or small molecule inhibitor library will be advantageous to screen for the regulators of ADAM15 *in vitro*. Since aberrant ADAM15 expression is associated with various disease pathogenesis, more knowledge

towards how ADAM15 is regulated at various levels will be essential to identify druggable targets or pathways to treat different diseases.

Chapter 5. Identification of proteins regulated by ADAM15

5.1. Introduction

Unlike ADAM10 and ADAM17, research regarding functional aspects of ADAM15 is still in its infancy. The first insight into ADAM15's biological functions *in vivo* came from a study performed by Horiuchi et al. (Horiuchi et al., 2003), who found that ADAM15 expression was high at E9.5 in the vasculature, endocardium of the developing heart, and hypertrophic chondrocytes. In adult mice, *Adam15* expression was intense in the pyramidal layer of the hippocampus, the granular layer of the dentate gyrus and the Purkinje cell layer of the cerebellum. No data regarding ADAM15 expression in endothelial cells was presented. Horiuchi and colleagues generated *Adam15*-deficient mice and examined them for defects in various tissues. No apparent abnormalities were identified in embryos (E13.5) and young mice (4-week-old), suggesting that ADAM15 may not be required developmentally. Gross examination of the weight, behaviour, appearance, mortality and morbidity of the *Adam15*-deficient mice showed that they were not significantly different from age- and gender-matched wild-type littermates, indicating that *Adam15*-deficiency did not drastically affect critical house-keeping biological processes. However, when *Adam15*-deficiency was coupled with a mouse model of proliferative retinopathy, 7-day old *Adam15*-null mice showed a dramatic reduction (64%) in neovascularisation when moved from high oxygen conditions (75%) to normal oxygen levels, which is known to induce strong pathological neovascularisation in wild-type mice. This led them to conduct a tumour-implantation experiment using B16F0 mouse melanoma cells. *Adam15*-deficient mice implanted with B16F0 had significantly smaller tumours than their wild-type littermates 2 to 3 weeks after injection of tumour cells. Further examination of the tumour vasculature showed no difference in gross tumour morphology and vascular density. Therefore, although *Adam15*-deficiency reduce

pathological neovascularisation in a mouse model of proliferative retinopathy, it remains to be determined whether the enzyme has a role in limiting tumour-induced pathological neovascularisation.

Another early study on ADAM15's role *in vivo* was conducted by Bohm et al. (2005). In their previous study, Bohm and colleagues (1999) reported that *ADAM15* expression was increased in human osteoarthritic chondrocytes. Although contradictory findings have subsequently been reported, as discussed in Chapter 3 and in my recent review (Yang et al., 2017), their finding led them to investigate the role of ADAM15 in murine cartilage and they found that *Adam15*-deficiency resulted in a significantly higher OA score in 12-14 month old male mice, indicating that lack of *Adam15* led to accelerated spontaneous OA. In the same study, they showed that stable expression of ADAM15 enhanced adhesion of T/C28a4 cells, an chondrocyte cell line, to type II and VI collagen. This enhanced adhesion resulted in increased resistance to serum starvation-induced cell death.

Subsequently, several studies have attempted to dissect the functions of ADAM15 *in vitro* using various cell culture systems. Bohm and colleagues (2010) showed in a separate study that the enhanced resistance to apoptosis-induced by various stimuli in ADAM15-over-expressing T/C-28a4 cells was associated with reduced caspase 3/7 activation in a X-linked inhibitor of apoptosis (XIAP)-dependent way, as inhibition of *XIAP* expression using siRNA in ADAM15-overexpressing T/C-28a4 cells rescued the activation of caspase 3/7. In parallel, Fried et al. (2012) showed that the anti-apoptotic property of ADAM15 was associated with its cytoplasmic domain, since T/C28a4 cells over-expressing a cytoplasmic domain-truncated ADAM15 were not protected against

apoptosis induced by genotoxicity. They further reported that interaction between the cytoplasmic domain of ADAM15 and the C-terminus of Focal Adhesion Kinase (FAK) enhanced FAK phosphorylation, which in turn, led to binding of Src to the phosphorylated FAK and the activation of FAK/Src downstream anti-apoptotic signalling.

Similar to the findings in the chondrocyte cell line, Bohm et al. (2013) showed that ADAM15 exerted an anti-apoptotic function in primary RA synovial fibroblasts (RASFs) under genotoxic stress, since *ADAM15* suppression using siRNA resulted in activation of caspase 3/7. They also found that FasL-induced FAK/Src pro-survival signalling was ADAM15-dependent, as *ADAM15* suppression resulted in significantly weaker phosphorylation of Src at the Y416 phosphorylation site. Since Bohm et al. (2001) have previously reported that *ADAM15* expression is up-regulated in both human RA macrophage-like and fibroblast-like synoviocytes, as well as in the plasma cells that infiltrate the RA synovium, this may indicate a pathogenic role of ADAM15 in sustaining the survival of auto-reactive immune cells in RA patients.

Using a domain deletion strategy, Bohm et al. (2009) showed that binding of ADAM15 to type II collagen in T/C28a4 cells was mediated by its pro-domain. Binding of ADAM15 to type II collagen was found to decrease FAK autophosphorylation at Y397, a known Src binding site, suggesting that the interaction between type II collagen and the ADAM15 pro-domain decreased FAK/Src activation, which was inconsistent with their previous finding that ADAM15-mediated type II collagen adhesion enhanced cell survival.

Investigation of ADAM15's biological functions have not significantly progressed

beyond these studies of its role in regulating cell survival. Moreover, while ADAM15 is predicted to be proteolytically active, with several substrates proposed in different cell types, ADAM15's role as a sheddase and/or a ECM-cleaving protease has not been investigated in a systematic way. Since ADAM15 is predicted to be transported to the cell surface after furin cleavage of its pro-domain, I consider the plasma membrane to be the main location where ADAM15 is likely to exert its functions, either by shedding its substrates or by interacting with other membrane proteins.

An important step towards understanding the role of ADAM15 is to systematically identify its substrates. One way to do this is quantitative proteomic analysis. In the past, quantitative proteomic analysis was performed using differential labelling to enable quantitation of the relative protein abundance under different treatment conditions. One of the earliest techniques was fluorescence two-dimensional difference gel electrophoresis, where proteins extracted from the whole cell or a particular cellular compartment (e.g. nucleus or the plasma membrane) were labelled with Cy3 or Cy5, and were separated according to their molecular weight and charge using two-dimensional (2D) gel electrophoresis. The relative abundance of a particular protein was proportional to its fluorescence intensity, so the ratio of Cy3/Cy5 fluorescence could be used as an indicator of which proteins were differentially regulated under the different treatment conditions. These proteins could then be identified using shotgun mass spectrometry analysis, thus defining the differentially affected proteome for a particular treatment compared to its control (McNamara et al., 2010). The main challenge of this method is the technical difficulty and variability of 2D gel electrophoresis, making the reproducibility of the method less than ideal.

Other gel-free, labelled, quantitative proteomic methods have been developed to circumvent the limitations introduced by gel electrophoresis. For example, stable isotopic labelling of amino acids in cell culture (SILAC) (Amanchy et al., 2005; Ong et al., 2002), isotope-coded affinity tag (ICAT) technology (Colangelo et al., 2006; Haqqani et al., 2008) and the isobaric tags for relative and absolute quantification (iTRAQ) (Wiese et al., 2007) approaches were developed as alternatives to fluorescence labelling of proteins. These techniques involve either isotopes or isobaric chemical groups. In addition to being gel-free, these methods generally allow absolute quantification of proteins when used with appropriate controls. Variation in labelling efficiency is the major problem that increases variability and special training and safety procedures are required for radioisotope-labelling, reducing accessiblity of these methods.

To circumvent the problems of gel-free, label-based quantitative proteomics, label-free quantitative (LfQ) proteomics was developed (Bantscheff et al., 2012; Schulze et al., 2010; Wong et al., 2010). Label-free quantitation is based on the assumption that the m/z (mass-to-charge ratio) spectral peak intensity of a particular peptide identified by mass spectrometry is proportional to the peptide's concentration. Since peptides are generated by fragmentation of proteins in the sample, protein concentration is thus also proportional to the peptide's spectral peak intensity (Bondarenko et al., 2002; Chelius et al., 2002). Therefore, by directly comparing the intensities of mass spectral peaks between samples, relative quantification can be reliably achieved. Importantly, LfQ proteomics has been successfully used to investigate proteins differentially regulated between two different treatment conditions in CM (secretome analysis), with a particular emphasis on identifying substrates of sheddases (Kuhn et al., 2016; Kuhn et al., 2012; Muller et al., 2016), and to conduct differential analysis of membrane

proteins (Le Bihan et al., 2006). Therefore, in this chapter, I selected LfQ shotgun proteomic analysis to identify membrane proteins regulated by ADAM15.

5.2 Identification of proteins regulated by ADAM15 in the secretome of ADAM15-over-expressing HTB-94 cells

As mentioned in Chapter 5.1, ADAM15 is predicted to be an active protease and several potential substrates have been proposed, such as FGFR2iiib (Maretzky et al., 2009b), E-cadherin (Najy et al., 2008b), N-cadherin (Najy et al., 2008a), CD23 (Fourie et al., 2003), collagen IV (Martin et al., 2002), and gelatin (Moss et al., 2016). However, ADAM15 substrate identification has not been done in a systematic manner, nor has it been done in a chondrocyte-related cell type. Therefore, I aimed to use LfQ proteomics to identify substrates of ADAM15 in the HTB-94 chondrosarcoma cell line. Since ADAM15 is predicted to be an active sheddase, I hypothesised that its main substrates would be proteins residing on the plasma membrane. To identify these membrane substrates in a systematic way, I used a quantitative proteomic method to compare the abundance of individual proteins in the conditional media (CM) of ADAM15-over-expressing HTB-94 cells relative to their abundance in mock-transfected CM controls. I predicted that there would be more active ADAM15 on the plasma membrane of ADAM15-over-expressing HTB-94 cells, leading to increased shedding of membrane substrates of ADAM15, and an increase in their abundance in the CM of ADAM15-over-expressing cells compared to mock-transfected CM (Figure 2.1).

I started by validating the anti-ADAM15 antibodies used for immunoblotting (all immunoblotting experiments in this chapter were performed under reducing

conditions with β-mercaptoethanol). Figure 5.1 (A) shows that both anti-ADAM15_EPR and anti-ADAM15_HTA were able to detect a commercially available full length form of ADAM15 (Abcam, Cat. ab131862, with an unspecified tag, predicted molecular weight 110 kDa) and in-house immunoprecipitated full-length recombinant ADAM15 (FLAG-tagged) at approximately the same concentration (0.05 μg). Notably, the commercial full length ADAM15 lane contains several bands of lower molecular weight, likely to be breakdown products, which were not observed in the lane loaded with immunoprecipitated ADAM15. The predicted molecular weight of pro-ADAM15 is 93 kDa, while the molecular weight of the mature form is predicted to be 85 kDa. For many metalloproteases, two bands (i. e. the pro- and active forms) can be observed using immunoblotting, but only one major band was observed for ADAM15, irrespective of its source. Based on the size of these bands [~125 kDa and ~100 kDa for Abcam and immunoprecipitated ADAM15, respectively, Figure 5.1 (A)], they are likely to represent pro-ADAM15 rather than the mature form of the enzyme. The molecular weights may be slightly higher than predicted for the pro-form due to glycosylation, which has been previously reported for ADAM15 (Kratzschmar et al., 1996).

More intense bands were seen using the anti-ADAM15_HTA antibody, suggesting that it has a higher sensitivity or titre. Furthermore, only anti-ADAM15_HTA was able to detect 0.02 μg of commercially available truncated ADAM15 (Sino Biological, Cat. 10517-H08H, His tag, predicted molecular weight: 54 kDa), further supporting that this antibody was more sensitive than anti-ADAM15_EPR. Therefore, in subsequent experiments, anti-ADAM15_HTA was used to detect endogenous ADAM15, and anti-ADAM15_EPR was used to detect over-expressed ADAM15.

The specificity of anti-ADAM15_HTA was validated using cell lysates from si*ADAM15*-treated HTB-94. Figure 5.1 (B) shows that the intensity of a band at ~95 kDa was substantially reduced in si*ADAM15*-treated HTB-94 cell lysates compared to non-targeting siRNA-treated controls, indicating that anti-ADAM15_HTA was indeed able to recognise endogenous ADAM15. An additional intense non-specific band was observed at ~120 kDa, which did not show any decrease in intensity in the si*ADAM15*-treated HTB-94 lysates. Some breakdown products were also observed at similar molecular wights reported by a previous study (Kratzschmar et al., 1996). Since anti-ADAM15_EPR was not able to reliably detect endogenous ADAM15 in HTB-94 due to relatively low signal and higher background (data not shown), such validation was not performed for this antibody. As an alternative, the specificity of anti-ADAM15_EPR was partially supported by the experiment shown in Figure 5.2 (A), where anti-ADAM15_EPR was shown to detect over-expressed FLAG-tagged ADAM15 but not purified ADAMTS-5. Additionally, bands at the predicted size of ADAM15 were detected in the lysate of ADAM15-over-expressing HTB-94 using an anti-FLAG M2 antibody (Sigma-Aldrich). This same antibody was able to detect purified FLAG-tagged TIMP-3 but not purified full-length recombinant ADAM15 without a FLAG tag (Abcam) [Figure 5.2 (B)]. In most cases, pro- and active ADAM15 could not be observed for either over-expressed and endogenous ADAM15.

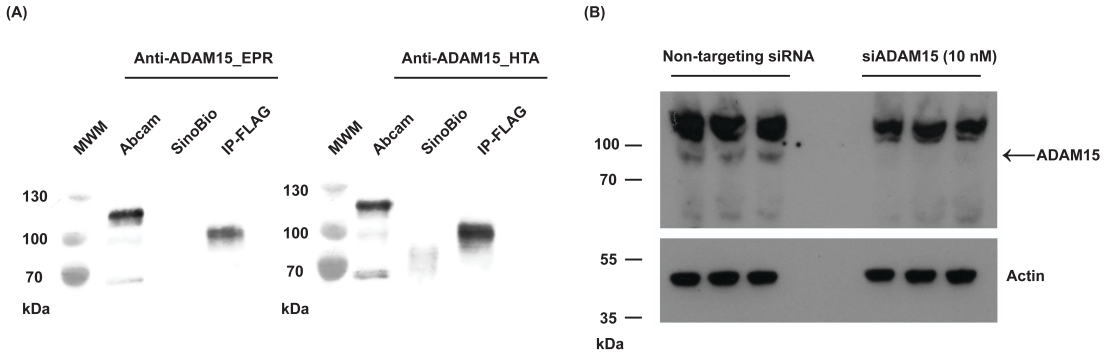

Figure 5.1 Anti-ADAM15 antibodies used for this study were validated using recombinant ADAM15 proteins and immunoprecipitated ADAM15-FLAG.
To validate the two anti-ADAM15 antibodies used in this project, a pre-determined amount of a full-length recombinant ADAM15 (Abcam, Cat. Ab131862, predicted molecular weight: 110 kDa including an unspecified tag), recombinant ADAM15 ectodomain (Sino Biological, Cat. 10517-H08S, predicted molecular weight: 65-70 kDa including a His tag) and ADAM15-FLAG immunoprecipitated from ADAM15-over-expressing HTB-94 cells with anti-FLAG M2 agarose affinity gel (Sigma-Aldrich, Cat: A2220). The anti-ADAM15_EPR antibody (Abcam, Cat. ab124698) and the anti-ADAM15_HTA antibody (Cambridge Bioscience, Cat. HPA011633) were used at experimentally determined optimal concentrations (1:1000 for anti-ADAM15_EPR and 1:500 for anti-ADAM15_HTA). Additionally, anti-ADAM15_HTA was further validated using cell lysates from HTB-94 cells transfected with si*ADAM15* and non-targeting siRNA.
(A) The anti-ADAM15_EPR antibody was able to detect recombinant full-length (0.05 μg) and immunoprecipitated FLAG-tagged ADAM15 (~0.05 μg), but it did not detect 0.02 μg of the ADAM15 ectodomain when AP was used as the detection method. On the contrary, anti-ADAM15_HTA was able to detect all three recombinant proteins tested at these concentrations using the same detection method.
(B) The anti-ADAM15_HTA was able to detect endogenous ADAM15 (~95 kDa) in HTB-94 cells treated with non-targeting siRNA using HRP-based detection. An intense non-specific band at ~120 kDa was also observed, along with some breakdown products. However, ADAM15 was almost un-detectable in HTB-94 cells treated with si*ADAM15* (10 nM).
MWM, molecular weight marker; Abcam, full-length recombinant ADAM15; SinoBio, truncated, ectodomain-only recombinant ADAM15; IP-FLAG, immunoprecipitated ADAM15-FLAG.

To optimise transient over-expression of ADAM15 for secretome analysis, different amounts of M-pCMV2-human ADAM15-FLAG vector (0.5, 1, 2.5 and 5 μg) were transfected into $5x10^5$ cells (Section 2.2.4.1) for 48 hours before lysates were collected. Figure 5.2 (A) shows that transfection using 1 μg of vector gave strongest ADAM15 over-expression. Therefore, ADAM15 over-expression in all subsequent experiments was performed using 1 μg plasmid DNA per $5x10^5$ cells. To transfect large numbers of cells, the amount of DNA was scaled up according to the manufacturer's guide. Over-expression of ADAM15 had no impact on cell growth or viability, with no significant

difference in cell survival found between non-transfected, mock-transfected and ADAM15-vector transfected HTB-94 cells [Figure 5.2 (C)]. Notably, when ADAM15 was over-expressed, two bands were observed in some experiments, which may represent pro- and active form of ADAM15 [Figure 5.2 (A)].

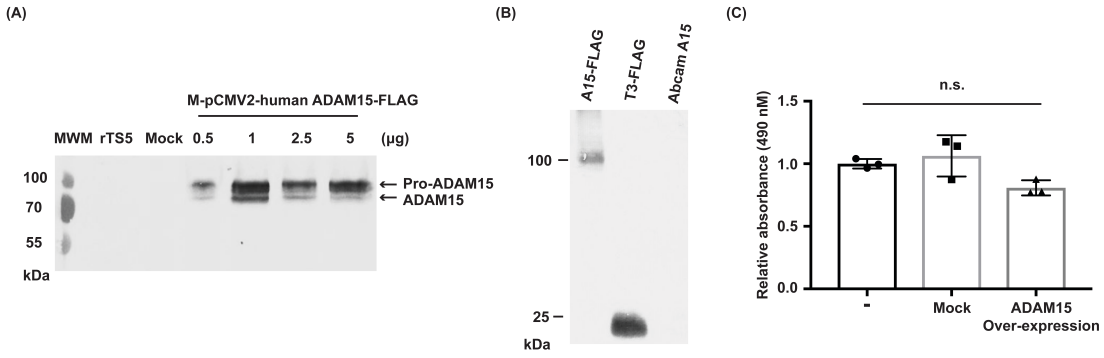

Figure 5.2 Over-expression of ADAM15 in HTB-94 was optimised and did not cause increased cell death.

ADAM15 over-expression was conducted according to Section 2.2.4.1.

(A) Different amounts of M-pCMV2-human ADAM15-FLAG plasmid (0.5, 1, 2.5 and 5 µg) were transfected into HTB-94 cells ($5x10^5$) using *Trans*IT 2020 (Mirus Bio) according to Section 2.2.4.1. Cells were lysed in 2X SDS sample buffer, electrophoresed, and probed with anti-ADAM15_EPR antibody. To investigate the specificity of the antibody, recombinant ADAMTS-5 (rTS5) was run on the same gel. The anti-ADAM15_EPR antibody did not cross-reacted with ADAMTS-5. Blots were developed using the AP detection system.

(B) HTB-94 cells were transfected with 1 µg of ADAM15-FLAG expression vector and the resultant cell lysates were immunoblotted using an anti-FLAG M2 antibody (Sigma-Aldrich, Cat. F1804). Recombinant TIMP-3-FLAG (T3-FLAG) and full-length recombinant ADAM15 (Abcam A15) without a FLAG-tag were added as controls. The anti-FLAG M2 antibody detected ADAM15-FLAG over-expressed in HTB-94 cells and TIMP-3-FLAG, but not the full-length recombinant ADAM15 (Abcam) without a FLAG-tag. Blots were developed using the AP detection system.

(C) To examine the effect of ADAM15 over-expression on cell metabolic rate, the MTS assay was performed on untransfected HTB-94, HTB-94 transfected with 1 µg of ADAM15-FLAG expression vector or with the control vector (mock) as described in Section 2.2.4.5. Colometric readouts were normalised to the average readout of untransfected HTB-94. The statistical significance of comparison between treatment groups was analysed with one-way ANOVA, with no statistically significant difference found between the 3 treatment groups ($p = 0.0537$).

Data are shown as mean ± SD, n.s., non-significant.

After showing that ADAM15 over-expression was detectable at the protein level 48 hours after transfection, I further optimised this over-expression protocol to fit the purposes of secretome analysis. CM was changed to fresh Opti-MEM 48 hours after

transfection, and cells were cultured for another 24 hours to generate CM reflecting changes induced by ADAM15 over-expression. Successfully over-expression of ADAM15 in the scaled up procedure was confirmed using immunoblotting 48 and 72 hours after transient transfection [Figure 5.3 (B)].

For optimal mass spectrometry analysis of the secretome, cells were washed to remove BSA present in culture media. Since mass spectrometry can only detect proteins within 4 orders of magnitude range in abundance (Anderson et al., 2002), BSA in the 10% FBS added to DMEM for culturing cells would mask the signals of less abundant secreted and shed proteins in the CM. A washing protocol was modified from Chevallet et al. (2007). Cells were washed twice with 10 ml ice-cold PBS and once with 15 ml of ice-cold PBS with agitation immediately before transfection. The efficiency of BSA removal was examined using Coomassie Brilliant Blue staining. As shown in Figure 5.3 (C&D), 99% of BSA in the full DMEM used to culture cells was effectively removed using this method. For each sample prepared for LfQ mass spectrometry analysis, protein quantity and BSA removal efficiency were checked before shipping to our collaborators, Dr. Simone Dario Scilabra and Dr. Stephan Müller, at the DZNE, Munich, to ensure the quality of CM used for LfQ mass spectrometry analysis was satisfactory.

At least 25 μg of protein per sample is required for LfQ mass spectrometry sample preparation. To err on the side of caution, I aimed to provide enough sample to perform LfQ mass spectrometry analysis at least twice (> 50 μg), and so over-expression was scaled up to a 10 cm^2 dish and CM concentrated 75-fold using a spin filter as described in Section 2.2.9.1. The total amount of protein in the concentrated

CM was determined using the DC protein assay kit (Bio-Rad). As shown in Figure 5.3 (A), a standard curve was prepared to estimate the amount of protein in concentrated CM. The amount of protein in each sample sent for LfQ mass spectrometry analysis is listed in Figure 5.3 (A). Total protein amounts in the CM ranged from 88.5 µg to 169 µg.

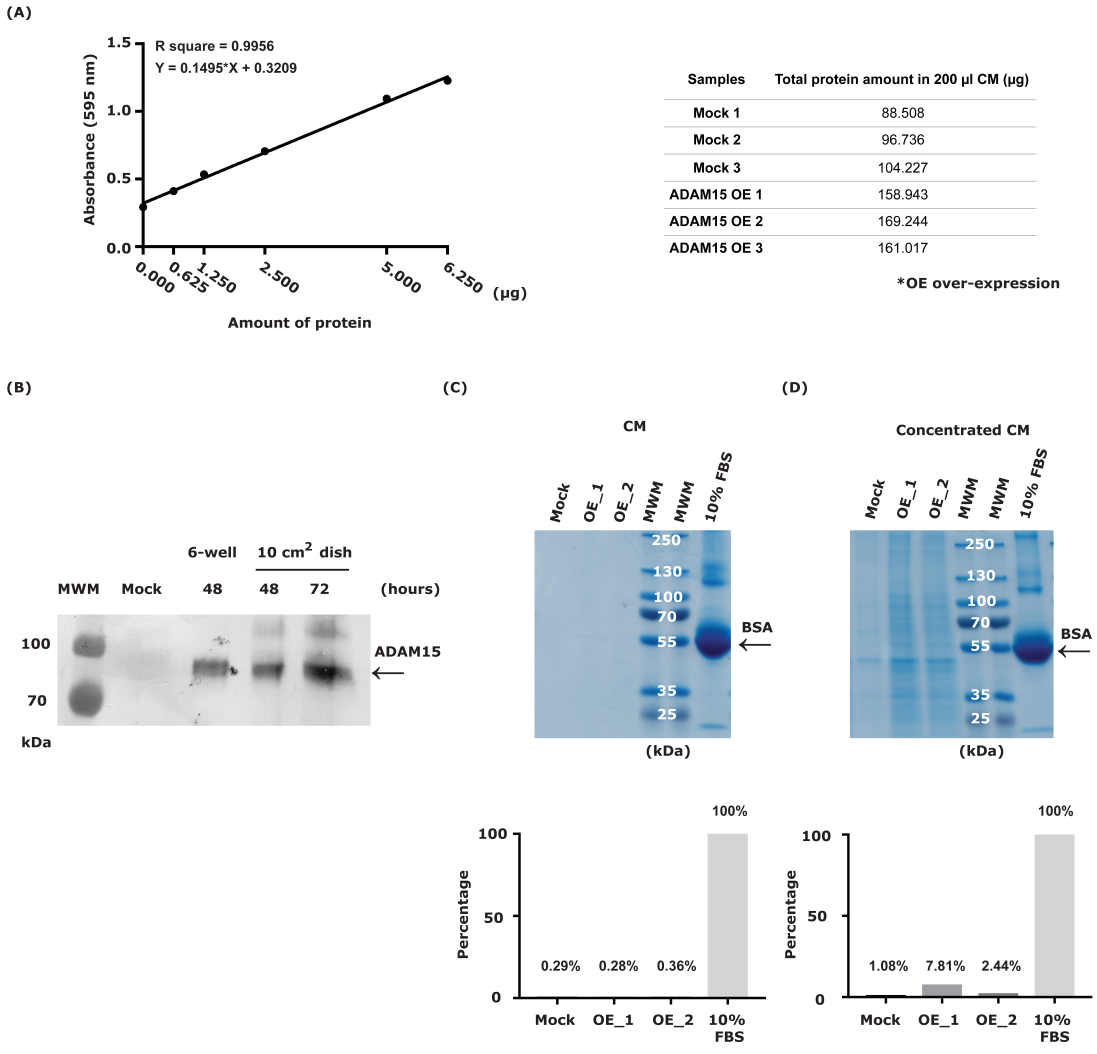

Figure 5.3 Optimisation of ADAM15 over-expression protocol for LfQ mass spectrometry analysis of the secretome.
ADAM15 over-expression was conducted as described in Section 2.2.9.1. Protein quantity, ADAM15 over-expression and BSA removal were examined before samples were sent for LfQ mass spectrometry analysis.
(A) The amount of protein in CM was determined using a DC protein assay kit according to the manufacturer's guide. In brief, CM was concentrated 75-fold (15 ml to 200 µl) using 10 kDa MWCO Microcon centrifugal filters (Millipore), followed by a smaller capacity 5 kDa MWCO Vivaspin 500 (GE

Healthcare) spin filter 72 hours after transfection (48 hours transfection plus 24 hours culture). A standard curve was created with BSA to establish the relationship between absorbance at 595 nm and protein amount. Linear regression was used to calculate the amount of protein in samples. 10 µl of the BSA solution and concentrated CM were mixed with 200 µl DC protein dye (in duplicate), left for 5 minutes at room temperature and absorbance at 595 nm measured. Only standard curves with an R square ≥ 0.95 were considered acceptable to measure protein quantity. The amount of protein in the 200 µl CM sent for LfQ mass spectrometry analysis is listed.
(B) To confirm ADAM15 over-expression in the scaled up 10 cm^2 dish 48 and 72 hours after transfection, cell lysates were analysed by immunoblotting. Cell lysates from ADAM15-over-expression in HTB-94 in a 6-well plate were included as a control. Endogenous ADAM15 was undetectable using anti-ADAM15_EPR 72 hours after empty vector was transfected. ADAM15 over-expression was detected in cells transfected with ADAM15-expressing vector 48 and 72 hours after transfection in 10 cm^2 dishes. Notably, observed bands correspond to the predicted molecular weight of mature ADAM15 (~ 85 kDa).
(C) To remove BSA, cells were washed twice with 10 ml ice-cold PBS and once with 15 ml of ice-cold PBS immediately before transfection. 15 µl of CM was subjected to SDS-PAGE separation on a 7.5% acrylamide gel followed by Coomassie Brilliant Blue staining. The same volume of CM with 10% FBS was included on the gel for comparison. A band corresponding to the predicted molecular weight of BSA (68 kDa) was essentially undetectable in the CM after washing compared to the strong BSA band detected in the CM containing 10% FBS. Quantification of band intensities showed that more than 99% of BSA was removed by this wash protocol.
(D) In addition, residual BSA in 75-fold concentrated CM was also measured using the same method. Even after concentration, the intensity of bands corresponding to BSA was more than 90% reduced after washing.
MWM, molecular weight marker; OE, ADAM15 over-expression; 10% FBS, 10% fetal bovine serum in DMEM.

Additionally, ADAM15 over-expression was examined in cell lysates after CM were collected. As shown in Figure 5.4 (A), HTB-94 cells transfected with the ADAM15 expression vector showed high levels of ADAM15 expression in cell lysates, while endogenous ADAM15 in the mock-transfected cells was below the detection limit of anti-ADAM15_EPR, demonstrating that cells transfected with the ADAM15 expression vector indeed expressed higher levels of ADAM15.

For LfQ mass spectrometry analysis of the secretomes, CM samples were processed (Section 2.2.9.1) and LfQ mass spectrometry analysis conducted (Section 2.2.9.7) at DZNE, and the resultant proteomic data analysed as described in Section 2.2.9.8.

Figure 5.4 shows the results obtained from LfQ mass spectrometry analysis of the secretome of ADAM15-over-expressing and mock-transfected HTB-94 cells (n = 3 for

each condition). Among the 1237 proteins identified and quantified in the CM, 273 were membrane proteins and 142 were secreted proteins, based on annotations in the reviewed canonical FASTA database of *Homo sapiens* from UniProt [Figure 5.4 (B)]. Only 33.5% of proteins identified in the secretome were secreted proteins, suggesting considerable noise from cytosolic and nuclear proteins in this experiment. Figure 5.4 (C) shows that 51 of the 273 membrane proteins were type 1 transmembrane proteins, 23 of them were type 2 and 10 of them were GPI-anchored proteins based on annotations in the same FASTA database. Proteins identified in the secretome are depicted as a volcano plot [Figure 5.4 (D)], with the X-axis showing the $\log_2$-based ratio of protein abundance in the secretome of ADAM15-over-expressing cells relative to mock transfected cells (ADAM15/Mock), and the Y-axis showing $\log_{10}$ of the p-value. There were significant changes in abundance of 412 proteins in the secretome, depicted above the two black curved lines and highlighted in blue. In this analysis, proteins with increased abundance in CM from ADAM15-over-expressing cells compared to mock-transfected cells are shown on the right, whilst those with decreased abundance are shown on the left. As shown in Figure 2.1, potential substrates of ADAM15 should appear on the right hand side of this plot, since ADAM15-over-expression would increase their shedding from the plasma membrane. However, Figure 5.4 (D) shows that proteins with most significant and highest changes in this region (e.g. RPL30, XRCC6, PAICS and UGDH) were intracellular proteins, suggesting that this secretome analysis of ADAM15-over-expressing cells was unlikely to identify novel ADAM15 substrates.

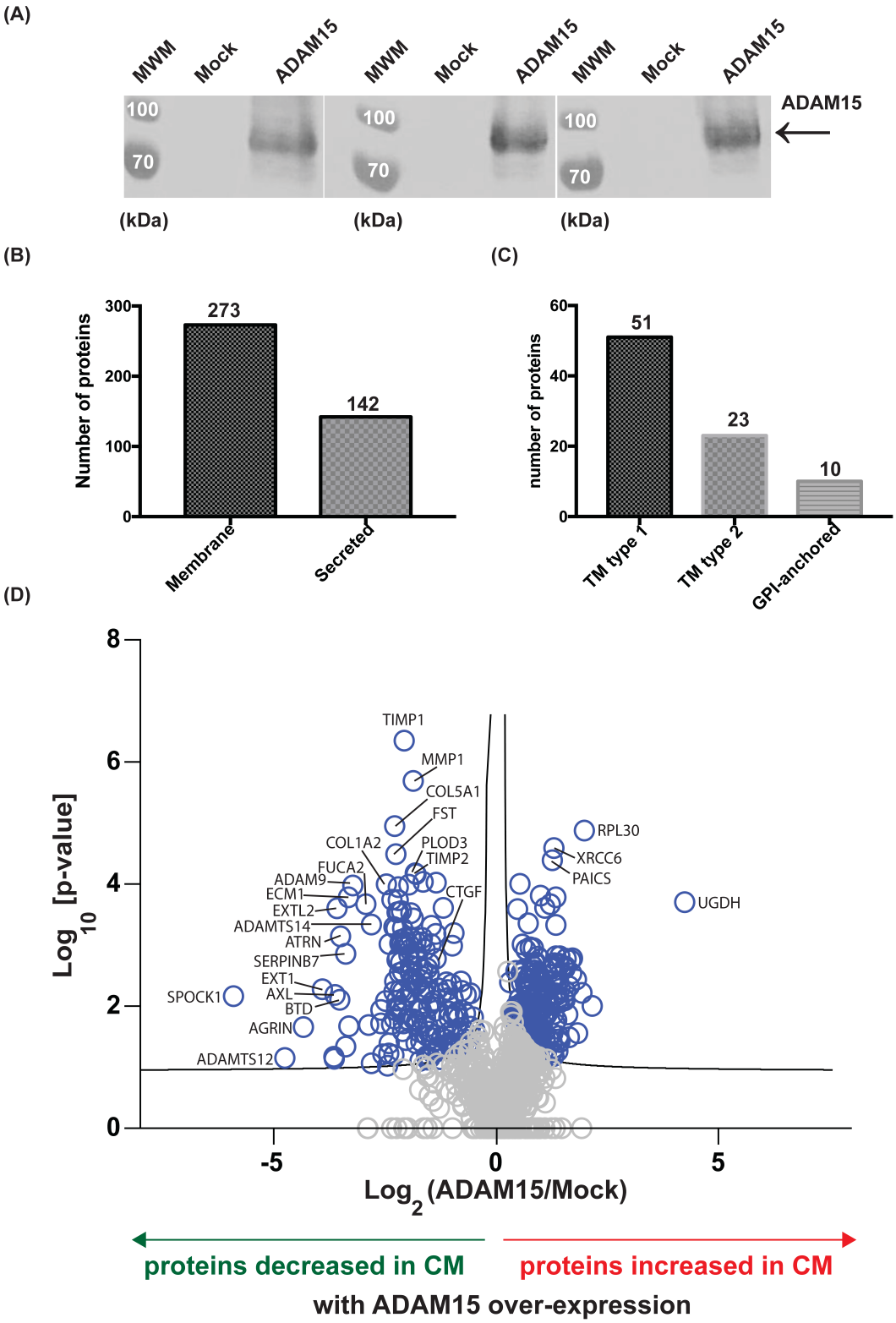

Figure 5.4 Identification of proteins regulated by ADAM15 in the secretome of ADAM15-over-expressing cells.

(A) ADAM15 over-expression was confirmed before mass spectrometry analysis. Cells were lysed in 2X SDS sample buffer (500 µl) after CM were collected and expression of ADAM15 detected by immunoblotting with the anti-ADAM15_EPR antibody. Anti-ADAM15_EPR was not able to detect endogenous ADAM15 in HTB-94 cells transfected with an empty expression vector. However, in cells transfected with ADAM15 expression vector, ADAM15 was detected using the same antibody.

(B) 1237 proteins were identified and quantified by LfQ mass spectrometry of CM (n = 3 for each condition). Amongst these, 273 were membrane proteins and 142 were secreted proteins based on annotations in the reviewed canonical FASTA database of *Homo sapiens* from UniProt.
(C) Amongst the 273 membrane proteins, 51 are type 1 transmembrane proteins, 23 are type 2 and 10 are glycosylphosphatidylinositol (GPI)-anchored proteins based on annotations in the reviewed canonical FASTA database of *Homo sapiens* from UniProt.
(D) Data obtained from LfQ secretome analysis are depicted as a volcano plot, in which the X-axis shows $\log_2$ of the ratio of protein abundance in secretomes of ADAM15-over-expressing and mock transfected cells (ADAM15/Mock), whilst the Y-axis shows $\log_{10}$ of the p-value. 412 proteins had statistically significant changes in abundance in the secretome of ADAM15-over-expressing cells compared to that from mock-transfected cells, and are shown in blue above the two black curved lines. Statistical analysis and multiple comparison correction methods used for the LfQ secretome analysis are described in Section 2.2.9.8.
MWM, molecular weight marker.

Although I was not able to identify substrates of ADAM15, many proteins had decreased abundance in the secretome of ADAM15-over-expressing cells. Since the majority of these proteins were intracellular proteins (> 66%), suggesting considerable noise in the analysis, I only selected 4 proteins (TIMP-1, -2, -3 and CTGF) with potential association with OA for validation by immunoblotting.

I transfected HTB-94 cells with ADAM15 expression vector for these validation experiments. Figure 5.5 (A) shows that endogenous ADAM15 was undetectable in mock-transfected HTB-94 lysates using anti-ADAM15_EPR, but that the enzyme was detectable in lysates from cells transfected with the ADAM15 expression vector, indicating successful ADAM15 over-expression. Figure 5.5 (B&C) show that CTGF expression decreased significantly in CM of ADAM15 over-expressing HTB-94 cells compared to controls ($p = 0.0003$, 95% CI: [-0.8804, -0.5396], difference between means = -0.71 ± 0.06137), and importantly, the level of reduction was comparable to the level identified by secretome analysis (~70% reduction). These data suggest that ADAM15 over-expression decreased release of CTFG to the cell surroundings.

Secretome analysis also indicated that TIMP-1 and TIMP-2 were less abundant in CM

of ADAM15-over-expressing cells, and due to their relevance in regulating activities of various metalloproteinases, they were also selected for validation. Importantly, TIMP-3 was only present in CM of ADAM15 over-expressing cells, so it was also included for validation (since TIMP-3 was not present in the CM of mock-transfected cells, its abundance ratio and its p-value could not be calculated). As shown in Figure 5.5 (D), immunoblotting indicated that TIMP-1 and -2 were not significantly less abundant in CM of ADAM15 over-expressing cells, and TIMP-3 did not show any detectable difference in abundance in CM of control and ADAM15 over-expressing cells. While the secretome analysis showed that TIMP-1 and -2 exhibited a similar level of reduction as CTFG (77% and 70% reduction for TIMP-1 and TIMP-2, respectively), immunoblotting experiments suggested that they are likely to be false positive "hits".

Given that our secretome analysis of ADAM15 over-expressing cells did not identify any potential substrates of ADAM15 and contained considerable noise from intracellular proteins, I consider this proteomic analysis to be less than reliable. Therefore, instead of validating more proteins identified by the secretome analysis of ADAM15-over-expressing cells, I set up a second secretome analysis using an ADAM15 knockdown approach. I predicted that the proteins identified in both secretomes (secretomes of ADAM15-over-expressing and ADAM15-suppressed cells), but changed in the opposite direction were more likely to be real "hits". Moreover, since the over-expression approach created a supra-physiological condition where ADAM15 expression is abnormally high, I considered that the knockdown approach was likely to provide more insight into what happens when ADAM15 expression changes physiologically.

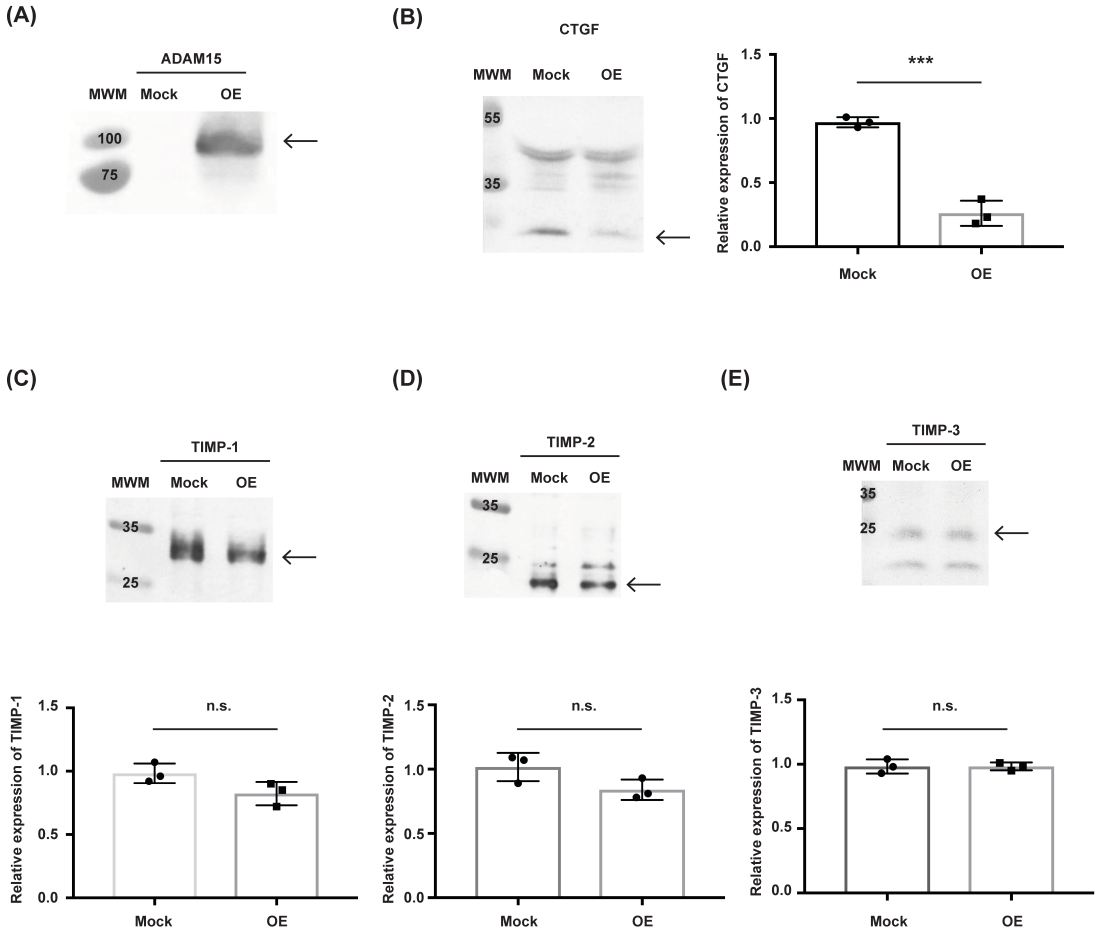

Figure 5.5 Immunoblotting validation showed that CTGF abundance decreased in CM of ADAM15-over-expressing HTB-94.

(A) Representative data from mock-transfected and ADAM15-over-expressing HTB-94 cells. Endogenous ADAM15 was undetectable using anti-ADAM15_EPR, but was detected in ADAM15-over-expressing cells (n = 3).

(B) Representative immunoblot for CTGF in the CM from mock-transfected and ADAM15-over-expressing HTB-94 cells. CTGF was decreased in CM of ADAM15-over-expressing HTB-94 cells (n = 3, p = 0.0003, 95% CI: [-0.8804, -0.5396]), which was consistent with the secretome analysis. Expression of CTGF in CM was normalised to the average expression of CTGF in CM of mock-transfected cells. Quantification was performed using Phoretix 1D software.

(C) Representative immunoblot for TIMP-1 in CM from mock-transfected and ADAM15-over-expressing HTB-94 cells. TIMP-1 abundance did not change in CM of ADAM15-over-expressing HTB-94 cells (n = 3, p = 0.0840, 95% CI: [-0.3541, 0.03413]), which was inconsistent with the secretome analysis. Expression of TIMP-1 in CM was normalised to the average expression of TIMP-1 in CM of mock-transfected cells. Quantification was performed using Phoretix 1D software.

(D) Representative immunoblot for TIMP-2 in the CM from mock-transfected and ADAM15-over-expressing HTB-94 cells. TIMP-2 abundance did not change in CM of ADAM15-over-expressing HTB-94 cells (n = 3, p = 0.0873, 95% CI: [-0.3943, 0.04097]), which was inconsistent with the secretome analysis. Expression of TIMP-2 in CM was normalised to the average expression of TIMP-2 in CM of mock-transfected cells. Quantification was performed using Phoretix 1D software.

(E) Representative immunoblot for TIMP-3 in the CM from mock-transfected and ADAM15-over-expressing HTB-94 cells. TIMP-3 abundance did not change in CM of ADAM15-over-expressing HTB-94 cells (n = 3, p > 0.9999, 95% CI: [-0.101, 0.101]), which was inconsistent with the secretome analysis. Expression of TIMP-3 in CM was normalised to the average expression of TIMP-3 in CM of mock-transfected cells. Quantification was performed using Phoretix 1D software.

Data are shown as mean ± SD, MWM, molecular weight marker, Mock, mock-transfected control, OE, ADAM15 over-expression, ***, p ≤ 0.001, n.s. not significant. The statistical significance of comparison between mock and OE was analysed with Student's t test (two-tailed).

5.3. Identification of proteins regulated by ADAM15 in the secretome of *ADAM15*-knockdown HTB-94 cells

To suppress ADAM15 expression, I used siRNA which was designed to specifically target *ADAM15* by RNA interference. In order to compare the secretome of ADAM15-suppressed cells to the secretome of ADAM15-over-expressing cells, the timelines of these two experiments were kept the same. Additionally, previous experience from our colleagues suggested that since some proteins have slow turnover rates, manipulation at the mRNA level may only be reflected at the protein level 48 hours after transfection, (Dr. Yoshi Itoh, personal communication). Therefore, transient transfection with si*ADAM15* using JetPRIME transfection reagent (Polyplus, Cat. 114-15) in 1×10^5 cells for 72 hours was performed to ensure that ADAM15 knockdown also occurred at the protein level, and to allow time for abundance of potential substrates to be altered. All 6 wells of a 6-well plate (total 6×10^5 cells) were pooled together and treated as one sample in order to obtain enough protein for mass spectrometry analysis, and 6 samples of si*ADAM15* and 6 of non-targeting control were analysed by mass spectrometry and subsequent statistical analysis.

The timeline of the experimental design is shown in Figure 5.2 (A). In brief, transfection with si*ADAM15* (40 nM) or the same concentration of non-targeting control was performed as described in Section 2.2.9.2. and CM replaced with fresh serum-free DMEM 24 hours after transfection. Transfected cells were then cultured for another 48 hours and CM collected, processed and stored according to Section 2.2.9.2. In parallel, the remaining cell lysates were collected, and the effect of *ADAM15* suppression at the 72-hour time point confirmed using qPCR. As shown in Figure 5.2

(B), significant reduction of ADAM15 was observed in si*ADAM15*-treated HTB-94 cells (> 95% reduction, $p < 0.0001$, 95% CI: [-1.058, -0.9048]). Since anti-ADAM15_HTA was not yet available when this experiment was conducted, and ADAM15 suppression at the protein level could not be reliably detected using anti-ADAM15_EPR, ADAM15 repression at the protein level is not shown here.

To examine the effect of si*ADAM15* on cell survival, an MTS assay was performed according as described in Section 2.2.4.5 in an independent experiment. 72 hours after transfection [Figure 5.2 (C)], no difference in absorbance was detected between the non-targeting siRNA- and si*ADAM15*-transfected cells ($p = 0.5645$, 95% CI: [-0.2315, 0.1462]), indicating that ADAM15 knockdown using 40 nM si*ADAM15* did not have significant effects on cell survival.

Secretome analysis of non-targeting and si*ADAM15*-transfected HTB-94 was performed according to Section 2.2.9.2. and analysed as described in Section 2.2.9.8. 3 CM from ADAM15-knockdown cells and 3 CM from non-targeting siRNA-treated cells were first analysed in an exploratory study, and the results indicated that increased statistical power was required to detect differences between the two secretomes (data not shown). Therefore, another set of 3 CM from ADAM15-knockdown cells and 3 CM from non-targeting siRNA-treated cells were processed and analysed using LC-MS/MS, and the results of all 12 samples (6 per condition) are shown in Figure 5.6 (D&E). Figure 5.6 (D) shows that, among the 2697 proteins identified and quantified by LfQ mass spectrometry of the CM, 642 were membrane proteins and 227 were secreted proteins based on annotations in the reviewed canonical FASTA database of *Homo sapiens* from UniProt. Therefore, ~68% of the total identified proteins were intracellular

proteins, which indicates that a similar level of noise was found in this secretome analysis as in the previous over-expression approach. Within the membrane category, 115 proteins were type 1 transmembrane proteins, 61 were type 2+3 transmembrane proteins, and 18 were GPI-anchored proteins.

Although more than 2,500 proteins were identified and quantified successfully, only one protein, AXL, was found to reach the threshold of statistical significance and was decreased in the secretome of si*ADAM15*-transfected cells. Since the si*ADAM15*-transfected cells were expected to have less ADAM15 on the plasma membrane to exert shedding, substrates of ADAM15 were expected to be released in lower amounts to the CM of si*ADAM15*-transfected cells. Therefore, AXL, which was decreased in the secretome of si*ADAM15*-transfected cells, was initially considered to be a potential substrate of ADAM15. However, after comparison of the secretome of ADAM15-over-expression and ADAM15-knockdown cells, I found that AXL was also significantly decreased in the secretome of ADAM15-over-expressing cells compared to the mock-transfected cells. This argues against AXL being an ADAM15 substrate, and suggests an indirect or artificial result.

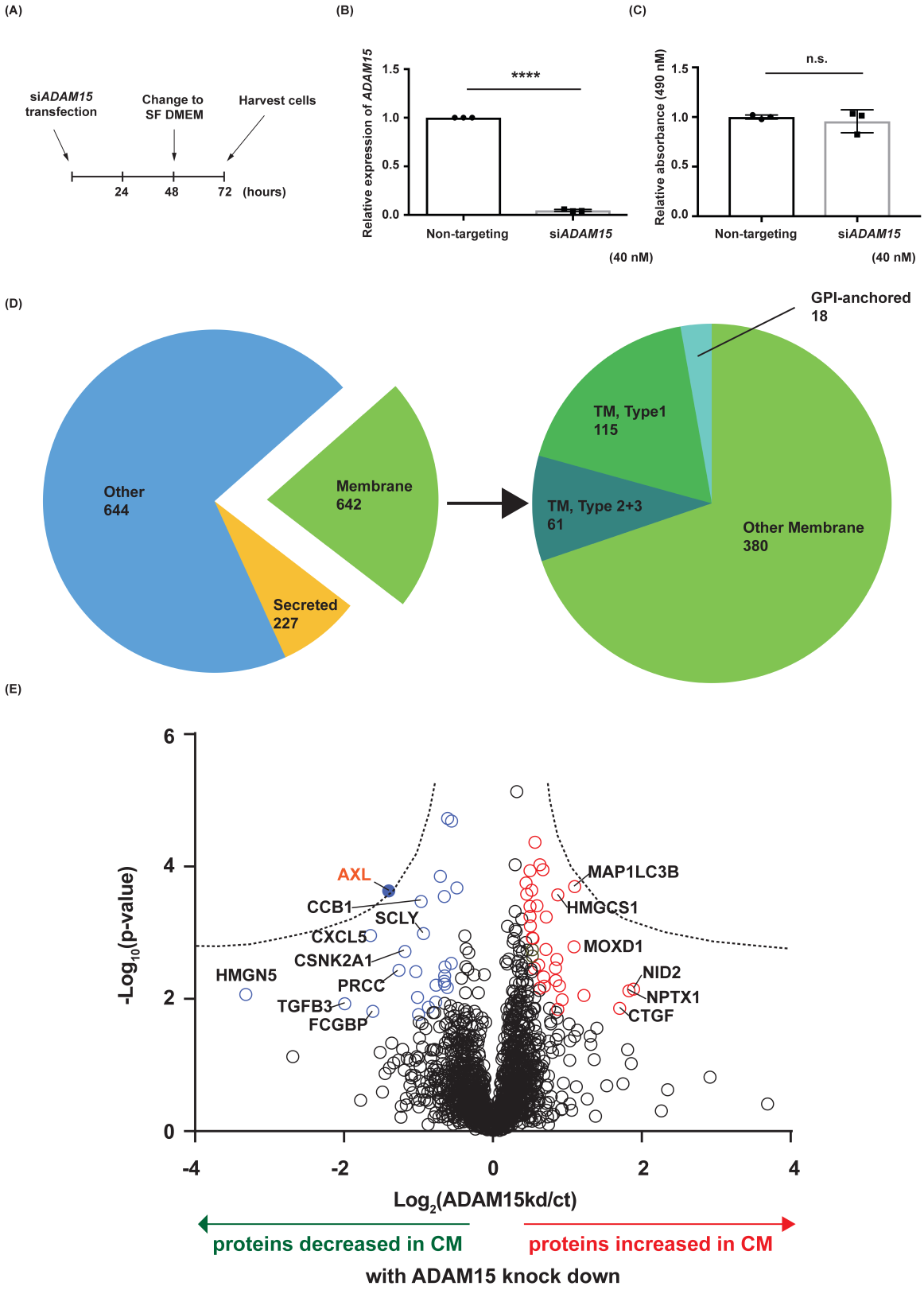

Figure 5.6 Identification of proteins regulated by ADAM15 in the secretome of ADAM15-knockdown cells

(A) Experimental design for conducting ADAM15 knockdown. Cells were changed to fresh serum-free DMEM 24 hours after transfection to remove proteins already in the CM before si*ADAM15* had taken effect. Transfected cells were left for another 48 hours for proteins to accumulate, and CM and cell lysates collected for further processing.

(B) *ADAM15* expression was significantly decreased at the mRNA level in HTB-94 cells 72 hours after transfection ($p < 0.0001$, 95% CI: [-1.058, -0.9048], Difference between means: -0.9814 ± 0.0276). To quantify the relative expression of *ADAM15* in non-targeting and si*ADAM15* transfected cells, total mRNA was extracted from cell lysates and quantified using qPCR. Expression of *ADAM15* was normalised to the housekeeping gene *RPLP0* and relative expression calculated using the ΔΔCt method detailed in Section 2.2.5.4. and normalised to the average expression of *ADAM15* in non-targeting siRNA treated cells.
(C) An independent ADAM15 knockdown experiment was performed in a 96-well plate as described in Section 2.2.4.5. Cell viability was assessed by MTS assay (Section 2.2.4.5.), and relative absorbance was normalised to the average absorbance of non-targeting transfected cells. No difference in viability was found between cells transfected with non-targeting siRNA and si*ADAM15* ($p = 0.5645$, 95% CI: [-0.2315, 0.1462]).
(D) 2697 proteins were identified and quantified by LfQ mass spectrometry of the CM ($n = 6$ for each condition). Amongst these, 642 were membrane proteins (115 type 1 transmembrane proteins, 61 type 2+3 transmembrane proteins and 18 GPI-anchored proteins); and 227 were secreted proteins based on annotations in the reviewed canonical FASTA database of *Homo sapiens* from UniProt.
(E) Data obtained from LfQ secretome analysis are depicted as a volcano plot, in which the X-axis shows $\log_2$ of the ratio between protein abundance in the secretome of cells transfected with si*ADAM15* and with non-targeting siRNA (ADAM15kd/ct), whilst the Y-axis shows $\log_{10}$ of the p-value. Proteins above the two black curved lines are considered to reach the threshold of statistical significance and are highlighted in blue. Only 1 protein (AXL) was identified to have significantly altered abundance in the secretome of ADAM15 knockdown cells compared to the secretome of non-targeting siRNA-transfected cells. Statistical analysis and multiple correction methods used for the LfQ secretome analysis are described in Section 2.2.9.8.
Data in **(B&C)** are shown as mean ± SD, n.s., not significant, ****, $p \leq 0.0001$. The statistical significance of comparison between mock and OE was analysed with Student's t test (two-tailed).

Given these contradictory results, I investigated AXL abundance using immunoblotting. Since anti-ADAM15_HTA was not available when these experiments were performed, I examined the efficiency of *ADAM15* knockdown at the mRNA level using qPCR. Figure 5.7 (A) shows that *ADAM15* expression was indeed decreased in HTB-94 cells treated with si*ADAM15* 72 hours after transfection ($p = 0.0014$, 95% CI: [-1.311, -0.6261). Next, I investigated the effect of *ADAM15* knockdown on the abundance of AXL in the cell lysates and CM. As shown in Figure 5.7 (B&C), abundance of AXL decreased in CM of ADAM15 knockdown cells compared to the non-targeting siRNA-treated cells ($p = 0.0016$, 95% CI: [-0.9112, -0.4222]). However, AXL levels in the cell lysates also decreased in cells treated with si*ADAM15*, indicating that the decreased AXL level in the CM of *ADAM15* knockdown cells was unlikely to be the result of ADAM15 shedding (reduction of AXL in the cell lysates was not quantified since AXL was below the detection limit in the *ADAM15* knockdown cells

when immunoblotting was developed using AP). Due to this overall reduction of AXL expression at the protein level, I examined whether *AXL* expression also decreased at the mRNA level in ADAM15 knockdown cells. As shown in Figure 5.7 (D), *AXL* expression was decreased at the mRNA level in ADAM15 knockdown cells ($p < 0.0001$, 95% CI: [-0.727, -0.6252]), and the magnitude of reduction was comparable to what was found at the protein level (~67% reduction).

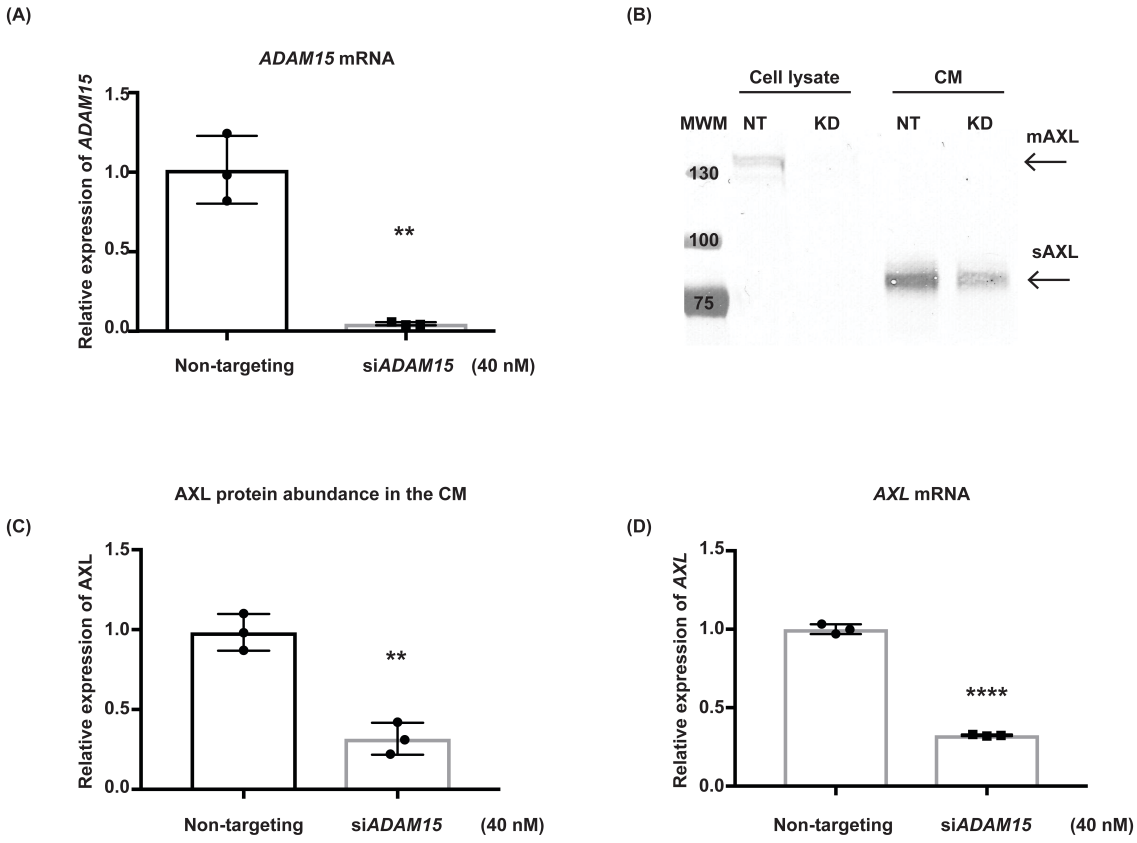

Figure 5.7 AXL expression decreased at the mRNA and protein levels upon *ADAM15* knockdown.
(A) *ADAM15* expression was significantly decreased at the mRNA level in HTB-94 cells 72 hours after transfection with si*ADAM15* ($p = 0.0014$, 95% CI: [-1.311, -0.6261], Difference between means: -0.9684 ± 0.1233). To quantify the relative expression of *ADAM15* in non-targeting and si*ADAM15* transfected cells, total mRNA was extracted from cell lysates and quantified using qPCR. Expression of *ADAM15* was normalised to the housekeeping gene *RPLP0* and relative expression calculated using the ΔΔCt method detailed in Section 2.2.5.4. and normalised to the average expression of *ADAM15* in non-targeting siRNA treated cells.
(B) Representative data (n = 3) demonstrating that AXL expression was decreased at the protein level both in the cell lysates and CM of *ADAM15*-knockdown cells compared to cells treated with non-targeting siRNA 72 hours after transfection.
(C) Quantification of results in **(B)**. Expression of AXL at the protein level in CM was normalised to the average expression of AXL in the CM of non-targeting siRNA treated cells ($p = 0.0016$, 95% CI: [-0.9112, -0.4222], Difference between means: -0.6667 ± 0.08807). Quantification was performed using Phoretix 1D software.

(D) *AXL* expression was also significantly decreased at the mRNA level in HTB-94 cells 72 hours after transfection ($p < 0.0001$, 95% CI: [-0.727, -0.6252], Difference between means: -0.6761 ± 0.01832). To quantify the relative expression of *AXL* in non-targeting and si*ADAM15* transfected cells, total mRNA was extracted from cell lysates and quantified using qPCR. Expression of *AXL* was normalised to the housekeeping gene *RPLP0* and relative expression calculated using the ΔΔCt method detailed in Section 2.2.5.4. and normalised to the average expression of *AXL* in non-targeting siRNA treated cells.
Data in **(A, C and D)** are shown as mean ± SD, MWM, molecular weight marker, mAXL, full length transmembrane AXL, sAXL, shed, solubilised AXL, **, $p \leq 0.01$, ****, $p \leq 0.0001$. The statistical significance of comparison between cells treated with si*ADAM15* and non-targeting siRNA was analysed with Student's t test (two-tailed).

In parallel, I found that the si*ADAM15* I used for knocking down *ADAM15* showed unexpected effects on expression of various other genes. Figure 5.8 (A) shows that si*ADAM15* showed a dose-dependent effect on *ADAM15* suppression, as 40 nM si*ADAM15* showed a greater reduction of *ADAM15* expression than 10 nM si*ADAM15* (> 95% vs. > 85% reduction in cells treated with 40 nM and 10 nM si*ADAM15*, respectively). As shown in Figure 5.8 (B), a similar dose-dependent effect on some randomly selected genes (*GPNMB*, *CHI3L1*, *MMP9* and *CTGF*), as well as *AXL*, was also observed. Since the si*ADAM15* I used was a mixture of two siRNA that target *ADAM15* (20 nM each), I examined the effect of each si*ADAM15* individually. Moreover, since the data shown above indicate that 10 nM siRNA treatment had reduced effects on expression of non-target genes, for subsequent experiments, 10 nM of the individual si*ADAM15* was used instead. As shown in Figure 5.8 (C), si*ADAM15*_2 (10 nM) had a stronger influence than si*ADAM15*_1 on the expression of the genes tested, suggesting that the effects of si*ADAM15* (10 nM) on off-target gene expression were mainly due to si*ADAM15*_2. Therefore, for the following ADAM15 knockdown experiments, I only used si*ADAM15*_1 to suppress *ADAM15* expression.

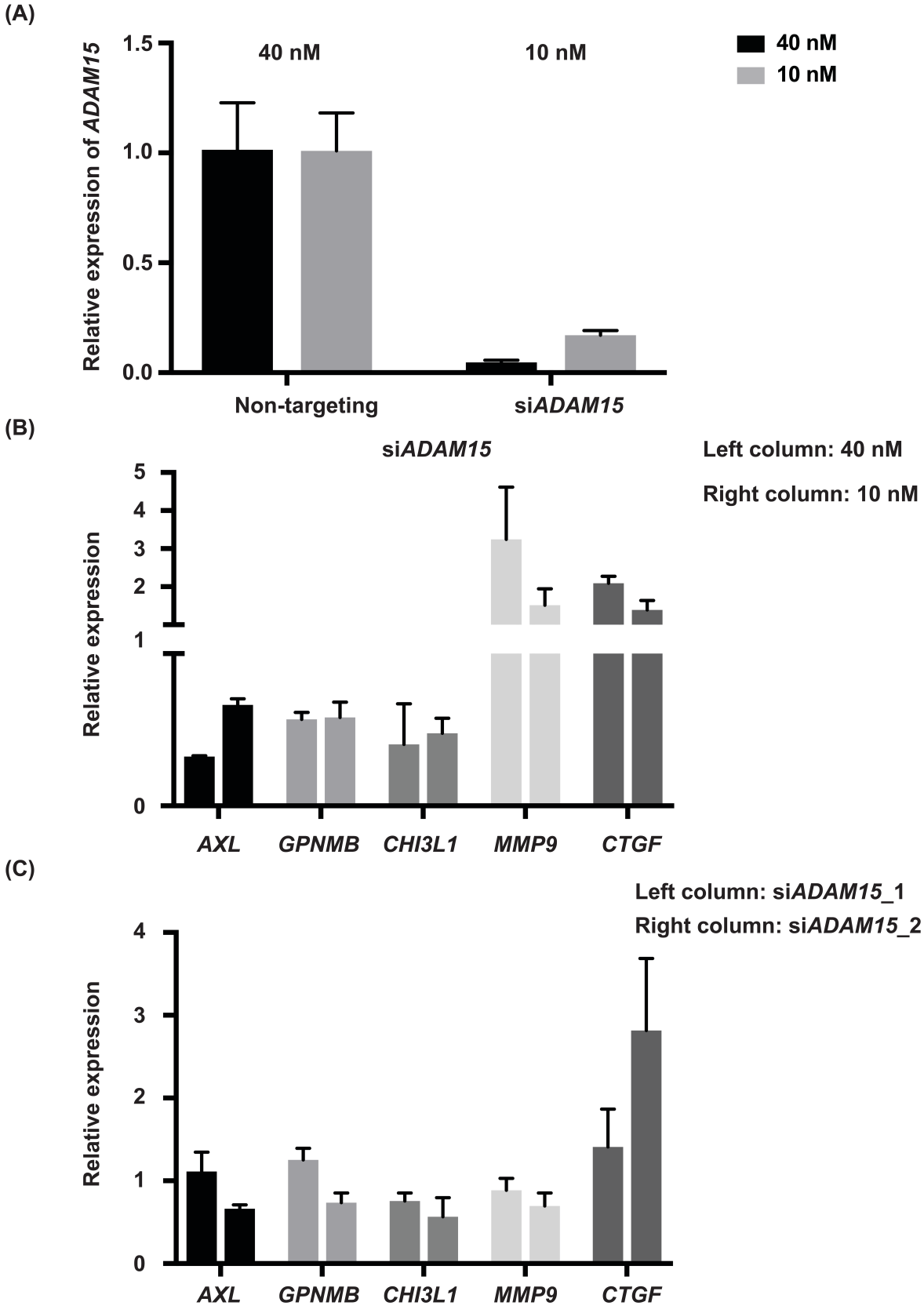

Figure 5.8 The off-target effects of si*ADAM15* on gene expression were mainly due to si*ADAM15*_2
(A) The effect of si*ADAM15* on *ADAM15* expression was dose-dependent, as HTB-94 cells treated with 40 nM si*ADAM15* (n = 3, p = 0.0062, 95% CI: [-1.675, -0.5198], Difference between means: -1.097 ± 0.2081) showed a greater reduction in *ADAM15* expression than cells treated with 10 nM si*ADAM15* (n = 3, p = 0.0011, 95% CI: [-1.117, -0.5619], Difference between means: -0.8395 ± 0.1). Two-way ANOVA was not

performed to compare means between groups due to insufficient sample size. To quantify the relative expression of *ADAM15* in non-targeting and si*ADAM15* transfected cells, total mRNA was extracted from cell lysates and quantified using qPCR. Expression of *ADAM15* was normalised to the housekeeping gene *RPLP0* and relative expression calculated using the ΔΔCt method detailed in Section 2.2.5.4. and normalised to the average expression of *ADAM15* in non-targeting siRNA-treated cells.
(B) A similar dose-dependent effect of si*ADAM15* on gene expression was observed for *GPNMB*, *CHI3L1*, *MMP9*, *CTGF* and *AXL*, with cells treated with 40 nM si*ADAM15* showing a larger effect on gene expression than those treated with 10 nM si*ADAM15*. To quantify the relative expression of each gene in non-targeting and si*ADAM15* transfected cells, total mRNA was extracted from cell lysates and quantified using qPCR. Expression of each gene was normalised to the housekeeping gene *RPLP0* and relative expression calculated using the ΔΔCt method detailed in Section 2.2.5.4. and normalised to the average expression of their respective control in non-targeting siRNA treated cells. Two-way ANOVA was not performed to compare means between groups due to insufficient sample size.
(C) 10 nM si*ADAM15*_1 treatment showed a reduced effect on the expression of *GPNMB*, *CHI3L1*, *MMP9*, *CTGF*, and *AXL* compared to the same concentration of si*ADAM15*_2. To quantify the relative expression of each gene in non-targeting and si*ADAM15*_1 or si*ADAM15*_2 transfected cells, total mRNA was extracted from cell lysates and quantified using qPCR. Expression of each gene was normalised to the housekeeping gene *RPLP0* and relative expression calculated using the ΔΔCt method detailed in Section 2.2.5.4. and normalised to the average expression of their respective control in non-targeting siRNA treated cells. Two-way ANOVA was not performed to compare means between groups due to insufficient sample size.
Data are shown as mean ± SD, NT, non-targeting siRNA, KD, ADAM15 knockdown.

To optimise suppression of ADAM15 expression with *siADAM15*_1, transient transfection was performed according to the method described in Section 2.2.4.2. I knockdown *ADAM15* using 10 nM si*ADAM15*_1 and, since anti-ADAM15_HTA had become available by the time when I performed these experiments, I examined the effect of si*ADAM15*_1 on ADAM15 expression at both the mRNA and protein levels 36, 48 and 72 hours after transfection. As shown in Figure 5.9 (A), decrease in *ADAM15* expression at the mRNA level was observed at all three time points tested ($n = 3$ for each time point, 24-hour: $p < 0.0001$, Mean difference = 0.9307, 48-hour: $p < 0.0001$, Mean difference = 0.9318, 72-hour: $p < 0.0001$, Mean difference = 0.8925). I then tested the effects of si*ADAM15*_1 on *ADAM15* expression at even earlier time points (4-, 12-, 24-, 36-hour) to better understand the dynamics of *ADAM15* knockdown using si*ADAM15*_1. As shown in Figure 5.9 (B), significant reduction in *ADAM15* expression was observed as early as 4 hours after transfection, and the magnitude of reduction increased with time until 36 hours after transfection, where more than 95% of

ADAM15 was removed using si*ADAM15*_1 (n = 3 for each time point, 4-hour: p = 0.0030, Mean difference = 0.1986, 12-hour: p < 0.0001, Mean difference = 0.5383, 24-hour: p < 0.0001, Mean difference = 0.8665, 36-hour: p < 0.0001, Mean difference = 0.9685). This indicates *ADAM15* mRNA is likely to be rapidly turned over.

Similarly, ADAM15 expression was also significantly decreased at the protein level 36, 48 and 72 hours after transfection, as shown in Figure 5.9 (C-E), with highest mean difference between cells treated with si*ADAM15*_1 and non-targeting siRNA observed at 36 hours. Taken together, these data suggest that ADAM15 has relatively quick turnover rate even at the protein level and may imply that expression of ADAM15 is tightly controlled at the post-translational level.

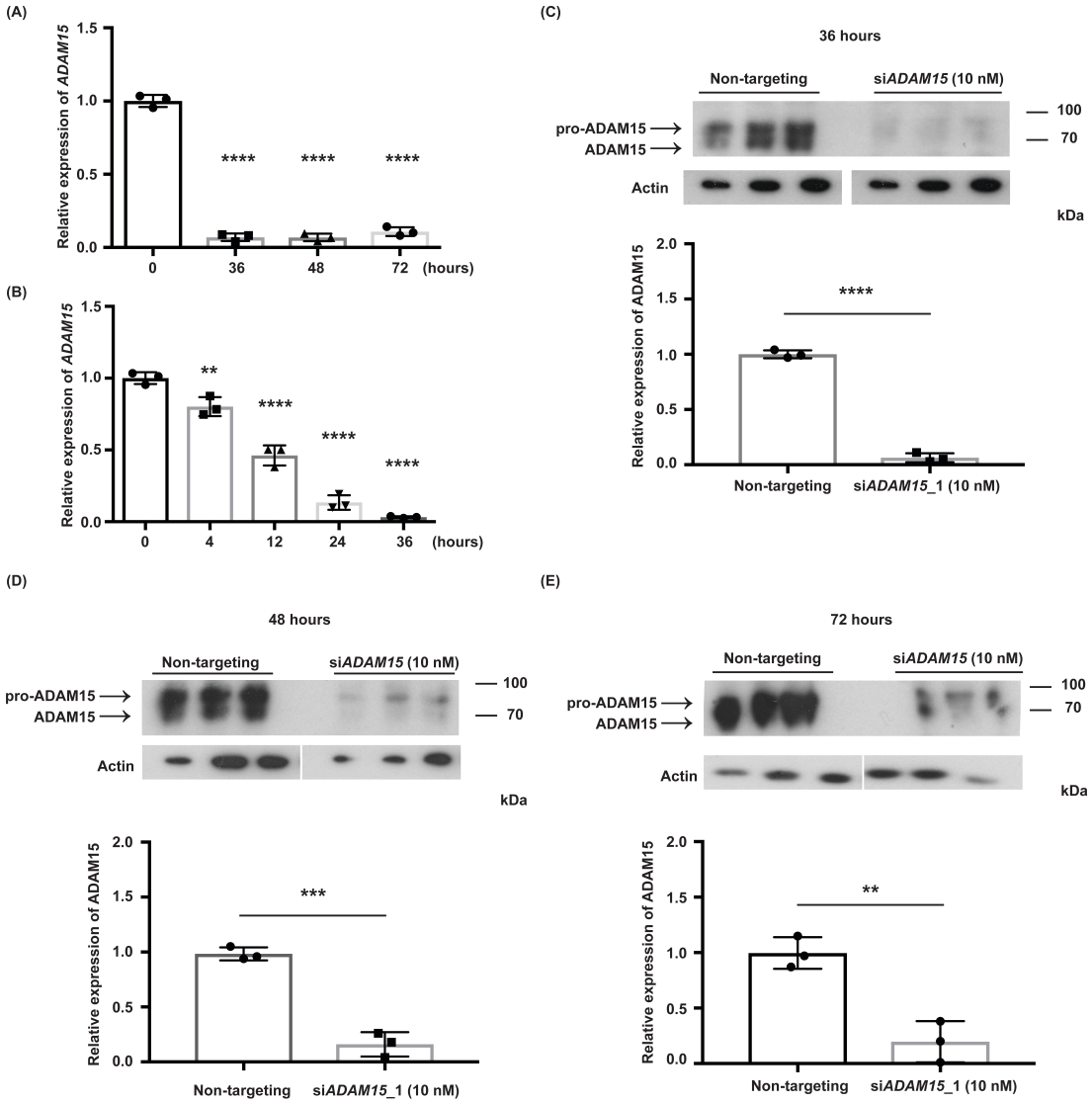

Figure 5.9 ADAM15 expression was significantly decreased at both mRNA and protein levels in HTB-94 cells treated with si*ADAM15*_1 36, 48 and 72 hours after transfection.

(A) HTB-94 cells treated with si*ADAM15*_1 (10 nM) showed decreased *ADAM15* expression at the mRNA level 36, 48 and 72 hours after transfection compared to 0 hour (n = 3 for each time point, 24-hour: $p < 0.0001$, Mean difference = 0.9307, 48-hour: $p < 0.0001$, Mean difference = 0.9318, 72-hour: $p < 0.0001$, Mean difference = 0.8925). To quantify the relative expression of *ADAM15*, total mRNA was extracted from cell lysates and quantified using qPCR. Expression of *ADAM15* was normalised to the housekeeping gene *RPLP0* and relative expression calculated using the ΔΔCt method detailed in Section 2.2.5.4. and normalised to the average expression of *ADAM15* at the 0-hour time point.

(B) *ADAM15* expression was also significantly reduced at 4, 12, and 24 hours after transfection with si*ADAM15*_1 (n = 3 for each time point, 4-hour: $p = 0.0030$, Mean difference = 0.1986, 12-hour: $p < 0.0001$, Mean difference = 0.5383, 24-hour: $p < 0.0001$, Mean difference = 0.8665, 36-hour: $p < 0.0001$, Mean difference = 0.9685). However, > 90% reduction was only observed at the 36-hour time point.

(C-E) HTB-94 cells treated with si*ADAM15*_1 (10 nM) exhibited decreased ADAM15 expression at the protein level 36 **(C)**, 48 **(D)** and 72 **(E)** hours after transfection compared to cells treated with non-targeting control (n = 3 for each time point, 24-hour: $p < 0.0001$, 95% CI: [-1.025, -0.8484], Difference between means: -0.9367 ± 0.0318, 48-hour: $p = 0.0003$, 95% CI: [-1.025, -0.6216], Difference between means: -0.8233 ± 0.07265, 72-hour: $p = 0.0040$, 95% CI: [-1.174, -0.4262], Difference between means: -0.8 ± 0.1346). Quantification was performed using Phoretix 1D software. ADAM15 expression was normalised to the expression of actin, which was used as the internal control. Relative expression of ADAM15 was normalised to the average expression of ADAM15 in the cells treated with non-targeting siRNA.

Data are shown as mean ± SD, **, $p \leq 0.01$, ***, $p \leq 0.001$, ****, $p \leq 0.0001$. The statistical significance of comparison of *ADAM15* expression at the mRNA level between time points **(A&B)** was analysed with ordinary one-way ANOVA, with multiple comparison corrected using Dunnett's test, whilst the statistical

significance of comparison of ADAM15 expression at the protein level between cells treated with si*ADAM15*_1 and non-targeting siRNA **(C-E)** was analysed with Student's t test (two-tailed).

Based on the observation described above, I examined AXL expression at the protein level in the same cell lysates and in CM from cells treated with si*ADAM15*_1 or non-targeting siRNA (10 nM). Figure 5.10 shows that AXL abundance in CM of si*ADAM15*_1-treated cells was elevated at the 36-hour time point in [Figure 5.10 (B)], whilst reduced AXL (full length) abundance in the cell lysates of si*ADAM15*_1-treated cells was found at the 48-hour time point [Figure 5.10 (D)]. This decreased abundance of full length AXL in cell lysates may be a negative feedback response to the increased AXL abundance in the CM of si*ADAM15*_1 treated HTB-94 cells at the 36-hour time point. If true, this indicates the existence of a regulatory system which maintains the level of shed AXL in the cell surroundings.

Importantly, AXL abundance in the CM was not changed at the 72-hour time point when knockdown was performed using 10 nM si*ADAM15*_1, suggesting the result shown in Figure 5.6 (C) was likely to be an artefact. Since AXL is the only "hit" identified in that secretome experiment, I concluded that this experiment was unable to identify substrates of ADAM15. Given that my data suggest that ADAM15 has a relatively quick turnover rate, the 72-hour time point for the ADAM15 over-expression secretome experiment may not be ideal. Moreover, since the transfected cells were kept in serum-free DMEM for the whole 72 hours to prevent BSA from masking the signals of other proteins when conducting mass spectrometry-based proteomic analysis, these cells may not be in the most physiological conditions. Therefore, alternative proteomic methods which can circumvent these limitations were explored to identify proteins

regulated by ADAM15.

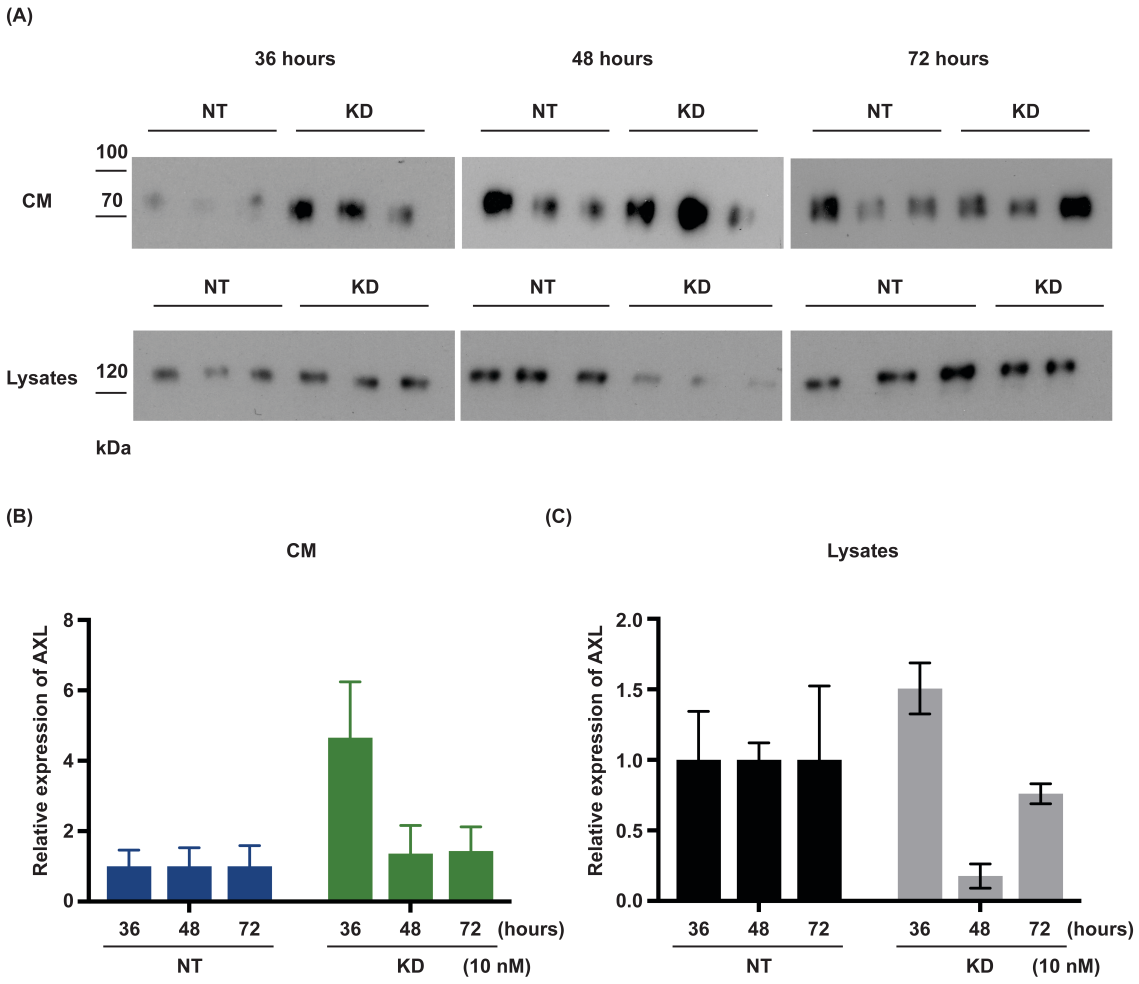

Figure 5.10 Effects of ADAM15 knockdown on solubilised and transmembrane AXL expression were time dependent.

(A) Immunoblotting indicates that ADAM15 knockdown with si*ADAM15*_1 did not decrease AXL abundance in the CM of ADAM15-knockdown cells.

(B) The abundance of solubilised AXL in the CM of si*ADAM15*_1 treated cells was elevated at the 36-hour time point, but remained unchanged at 48 hours and 72 hours compared to CM acquired from non-targeting siRNA-treated cells (n =3).

(C) The abundance of transmembrane AXL was decreased in cell lysates of si*ADAM15*_1 treated cells only at the 48-hour time point compared to the lysates acquired from non-targeting siRNA-treated cells (n = 3, except for lysates from si*ADAM15*_1 treated cells at the 72-hour time point, which only has only two data points due to technical issue).

Quantification was performed using Phoretix 1D software. Relative expression of AXL was normalised to the average expression of AXL in cells treated with non-targeting siRNA at each time point. Abundance of transmembrane AXL only decreased at the 48-hour time point ($p = 0.0006$, 95% CI: [-1.059, -0.5876], Difference between means: -0.8233 ± 0.08492), but remained unchanged at the 36- and 72-hour time point (36-hour: $p = 0.0870$, 95% CI: [-0.1167, 1.13]; 72-hour: $p = 0.5838$, 95% CI: [-1.488, 1.008]).

Data in **(B&C)** are shown as mean ± SD. The statistical significance of comparison (two-way ANOVA) was not performed to compare means between groups due to insufficient sample size.

5.4. Identification of glycoproteins regulated by ADAM15 in the SPECS secretome of *ADAM15*-knockdown HTB-94 cells

The previous conventional secretome analyses were not able to identify membrane or secreted proteins regulated by ADAM15, nor did they identify potential substrates of ADAM15. These results may suggest that the effects induced by manipulating ADAM15 expression were relatively small, hence the conventional, gross proteomic methods were not sensitive enough to detect these changes. Therefore, I decided to further enrich proteins before conducting proteomic analysis. To this end, I used the SPECS method to enrich glycoproteins in the secretome. Principles and the protocol used for preparing the SPECS samples are detailed in Section 2.2.9. and 2.2.9.3., and illustrated in Figure 2.2. Based on the ADAM15 knockdown optimisation done in Section 5.3., knockdown was performed for 36 hours with 10 nM si*ADAM15*_1. Additionally, since the optimisation was done in 6-well plates, ADAM15 knockdown for the SPECS secretome LfQ mass spectrometry analysis was also performed using 6-well plates, and all 6 wells in a 6-well plate were pooled together and treated as one sample in order to obtain enough protein for analysis. For the SPECS secretome LfQ mass spectrometry analysis, 3 replicates of si*ADAM15*_1 and 3 replicates of non-targeting control were used for mass spectrometry and subsequent statistical analysis.

To perform ADAM15 knockdown, cells were kept in full DMEM throughout this experiment. 10 nM si*ADAM15*_1 or non-targeting siRNA was transfected into HTB-94 cells after media were changed to fresh full DMEM immediately before transfection. Media were replaced again 12 hours after transfection and 50 μM ManNAz sugar added. Cells were cultured for another 24 hours, CM collected, processed and analysed using LfQ mass spectrometry.

ManNAz sugar will be metabolically converted to N-azidoacetyl-sialic acid and incorporated into N- and O-linked glycans at the terminal positions (Sletten et al., 2011), therefore, ManNAz added to the cells will label newly synthesised glycoproteins. Since 66% of secreted proteins and 87% of type I and type II transmembrane proteins are glycoproteins, most of these proteins will be labelled by ManNAz, making it a suitable method for enriching secreted and membrane proteins. Importantly, ManNAz labelled, N-azidoacetyl-sialic acid-containing glycoproteins can be covalently linked to sulfo-DBCO-biotin via copper-free click chemistry, allowing these biotinylated proteins to be pulled down from the CM using streptavidin-coated beads. Since BSA in the full DMEM is not newly synthesised, it will not be labelled by ManNAz, and most of the BSA will be effectively removed by the pull-down procedure. The remaining BSA is removed when performing in-gel digestion, where the BSA band will be cut out from the gel before sample processing. Therefore, the advantages of the SPECS secretome method are 3-fold: 1) it enriches the glycoproteins, thereby making LfQ mass spectrometry of the secretome more sensitive to changes in the abundance of glycoproteins, enabling detection of smaller changes; 2) it only labels newly synthesised glycoproteins, thus more precisely reflecting the changes induced by manipulating ADAM15 expression, effectively reducing the noise in the proteomic analysis; 3) it allows cells to be cultured in full DMEM, reducing cell stress and cell cycle arrest, and keeping cells under more physiological conditions.

As will be discussed later in Section 5.6., cell lysates of this experiment were also collected to performed SurfSPECS analysis, therefore, after CM were collected, cell

lysates were not available to check the efficiency of ADAM15 knockdown. As an alternative, a parallel ADAM15 knockdown experiment (in triplicate) was performed simultaneously. As shown in Figure 5.12 (A), endogenous ADAM15 was detected in HTB-94 cells transfected with non-targeting siRNA, but was beyond the detection limit in cells treated with si*ADAM15*_1, even when the more sensitive HRP development method was used for developing the immunoblot, suggesting that ADAM15 was indeed successfully suppressed in cells treated with si*ADAM15*_1.

As shown in Figure 5.12 (B), the SPECS secretome LfQ mass spectrometry analysis identified 265 proteins in the CM of ADAM15 knockdown or control cells, with 99 and 125 of these annotated as membrane and secreted proteins respectively, based on annotations in the reviewed canonical FASTA database of *Homo sapiens* from UniProt. Therefore, using the SPECS method, > 84% of the protein identified in the secretome were either membrane or secreted proteins (> 37% were membrane proteins, whilst > 47% were secreted proteins). Compared to the conventional secretome LfQ mass spectrometry analysis in which <35% of identified proteins were membrane or secreted proteins, this result indicates a huge improvement in terms of noise reduction. Amongst the 99 membrane proteins identified, 50 were type 1 transmembrane proteins, 16 were type 2+3 transmembrane proteins and 15 were GPI-anchored proteins. Figure 5.12 (C) show the comparisons by protein groups between the secretomes analysed using conventional and SPECS methods. As evident in the figure, conventional secretome analysis identified many more proteins than the SPECS secretome analysis. These may include proteins which were not newly synthesised and had slow turnover rates, and non-glycosylated proteins. Since the SPECS secretome contains much less noise from intracellular proteins, I considered SPECS to be a better

way of analysing the ADAM15-knockdown secretome.

Unexpectedly, as shown in Figure 5.12 (D), the SPECS secretome did not identify major changes in protein abundance induced by ADAM15 suppression, with only one secreted protein (Dermcidin, or DCD) found to increase in the secretome of ADAM15 knockdown cells. Dermcidin was close to the statistical threshold of significance after correcting for multiple comparison using the FDR method, but no proteins reached the statistical threshold of significance. Since dermcidin is mainly expressed by epithelial cells, it is unlikely that this protein is expressed by chondrocytes. This together with the fact that it did not meet statistical significance, let me to conclude that dermcidin is likely to be a false positive "hit".

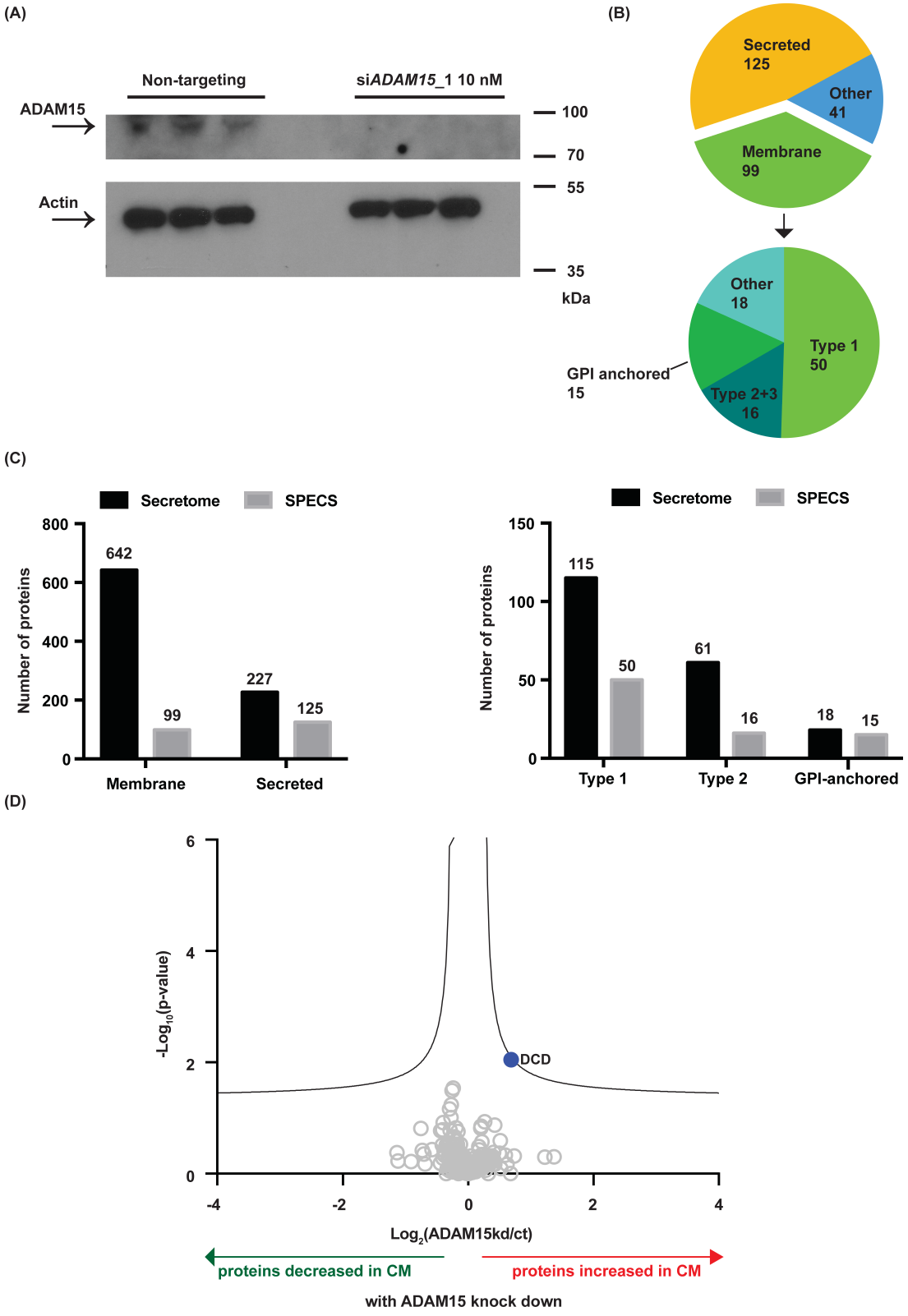

Figure 5.11 Identification of proteins regulated by ADAM15 in the SPECS secretome of ADAM15-knockdown cells.

(A) ADAM15 knockdown was examined in a parallel experiment performed simultaneously before CM were shipped to DZNE. Cells were lysed in 2X SDS sample buffer (80 µl) after CM were collected and expression of ADAM15 detected using immunoblotting with the anti-ADAM15_HTA antibody. Anti-ADAM15_HTA was not able to detect endogenous ADAM15 in HTB-94 cells 36 hours after transfection with 10 nM si*ADAM15*_1, but ADAM15 was detectable in cells transfected with non-targeting control

siRNA (n = 3).
(B) 265 proteins were identified and quantified by LfQ mass spectrometry in the secretomes (n = 3 for each condition). Amongst these, 99 were membrane proteins, (consisting of 50 type 1 transmembrane proteins, 16 type 2+3 transmembrane proteins and 15 GPI-anchored proteins), and 125 were secreted proteins based on annotations in the reviewed canonical FASTA database of *Homo sapiens* from UniProt. Less than 14% of the proteins identified using the SPECS method were not membrane or secreted proteins, indicating lower noise from intracellular proteins.
(C) Membrane and secreted proteins identified in the secretomes using the conventional and SPECS methods. 642 membrane proteins were identified in the secretome using the conventional method, while 99 were identified using the SPECS method. Likewise, 227 secreted proteins were identified in the secretome using the conventional method, whilst 125 were identified using the SPECS method. Overall, the conventional method was able to identify more membrane and secreted proteins. However, as shown in **(B)**, SPECS enrichment resulted in much lower noise from intracellular proteins.
(D) Data obtained from LfQ SPECS secretome analysis are depicted as a volcano plot, in which the X-axis shows $\log_2$ of the ratio between protein abundance in the secretome of cells transfected with si*ADAM15* and cells transfected with non-targeting siRNA (ADAM15kd/ct). The Y-axis shows $\log_{10}$ of the p-value. Proteins above the two black curved lines were considered to reach the threshold of statistical significance. As shown in the volcano plot, no proteins were identified to have significantly altered abundance in the secretome of ADAM15 knockdown cells compared to the secretome of non-targeting siRNA-transfected cells. The protein closest to the statistical threshold of significance after correcting for multiple comparison using the FDR method (Dermcidin, or DCD) is labeled as a blue dot.
Statistical analysis and multiple correction methods used for the LfQ secretome analysis are described in Section 2.2.9.8.

5.5. Identification of proteins regulated by ADAM15 in the secretome of *Adam15*-null immature murine chondrocytes

Since both conventional and SPECS secretome LfQ mass spectrometry analyses were not able to identify membrane and secreted glycoproteins regulated by ADAM15, I decided to use murine *Adam15*-null chondrocytes to confirm the results. Since murine knee articular cartilage contains few chondrocytes, it is not feasible to acquire enough chondrocytes from a small number of animals to perform LfQ mass spectrometry analysis. Therefore, immature murine costal chondrocytes from 6-day old C57Bl/6 mice were used instead. The advantage of using *Adam15*-null murine chondrocytes are 2-fold compared to the ADAM15 knockdown method performed in HTB-94 cells: 1) it eliminates the possibility that residual ADAM15 remaining after knockdown would be sufficient to exert biological activity; 2) it allowed me to investigate ADAM15 substrate in cartilage directly, rather than in the HTB-94 chondrosarcoma model. However, our

data in chapter 3 suggests that immature chondrocytes from young age may have low ADAM15 expression, and immature costal chondrocytes may have different level of ADAM15 at the protein level compared to articular chondrocytes. ADAM15 was detectable in the secretome of wild-type but not *Adam15*-deficient isolated immature costal chondrocytes. Among the 1574 proteins identified in this experiment, ADAM15 was ranked number 578, and was expressed at a similar level to TGFβ3 and Complement factor B. This indicates that despite the young age of donor mice, the immature costal chondrocytes express sufficient ADAM15 for these cells to be a useful model for these proteomic studies.

To isolate immature murine costal chondrocytes, I optimised the isolation protocol published by Gosset et al [Section 2.2.9.2 (Gosset et al., 2008)]. The optimised protocol was shared with Dr. Guadalupe Hiles and Prof. Mark Day (Department of Urology, University of Michigan, USA) who maintain a colony of *Adam15*-null C57Bl/6 mice, and isolation of the *Adam15*-null and wild-type immature murine costal chondrocytes was performed by Dr. Guadalupe Hiles with technical support from Dr. Anastasios Chanalaris and myself. Chondrocytes were rested for 6 days in full DMEM, and washed using the optimised protocol described previously (Section 5.2.) before changing to Opti-MEM for an additional 48 hours. The resultant CM from *Adam15*-null and wild-type chondrocytes were harvested, frozen and shipped on dry ice to the DZNE and further processed and analysed by our collaborators, Dr. Simone Dario Scilabra and Dr. Stephan Müller, using methods described in Sections 2.2.9.2., 2.2.9.7. and 2.2.9.8. Due to temporal and technical difficulties, conventional secretome analysis was performed instead of SPECS secretome analysis.

As shown in Figure 5.13, *Adam15* knockout did not induce major changes in the secretome of *Adam15*-null chondrocytes compared wild-type chondrocytes, as no proteins reached the threshold of statistical significance after correcting for multiple comparison. The protein closest to statistical significance was a secreted protein (arylsulfatase K, or ARSK) that increased in the medium of *Adam15*-null chondrocytes. Arylsulfatase K has recently been suggested to be involved in glycosaminoglycan degradation (Dhamale et al., 2017), implying a potential link to cartilage homeostasis and OA development. Since arylsulfatase K was increased in the secretome of *Adam15*-null chondrocytes, it is possible that ADAM15 could mediate joint protection by suppressing arylsulfatase K. However, the present data do not support arylsulfatase K as a statistically significant "hit", and do not warrant further validation of this enzyme. Additionally, dermcidin was not found in the secretomes of *Adam15*-null and wild-type chondrocytes, supporting my decision not to pursue dermcidin as a candidate ADAM15 substrate.

The result of LfQ mass spectrometry analysis of the secretome from *Adam15*-null chondrocytes is consistent with the results of LfQ mass spectrometry of conventional and SPECS secretomes from ADAM15-knockdown HTB-94, with that no major changes in protein abundance induced by ADAM15 identified using any of these methods.

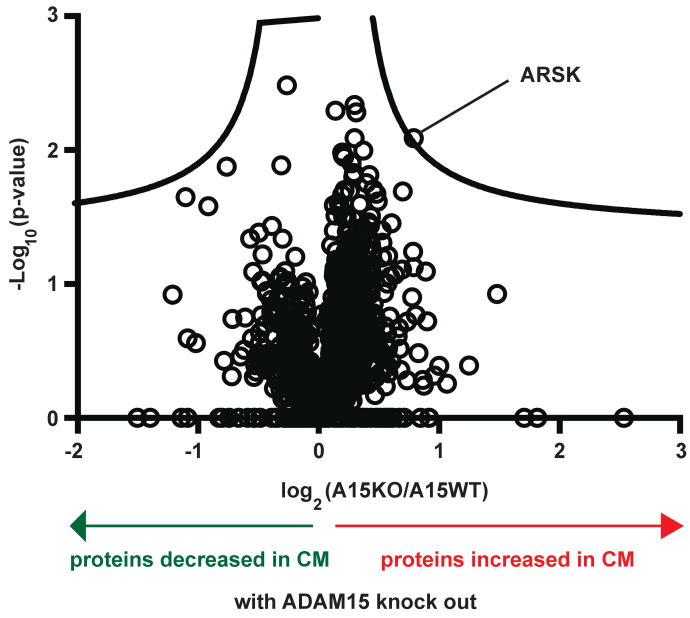

Figure 5.12 Identification of proteins regulated by ADAM15 in the secretome of *Adam15*-null immature murine costal chondrocytes

Adam15-null and wild-type immature murine costal chondrocytes were isolated from 6-day old C57Bl/6 mice by Dr. Guadalupe Hiles (Department of Urology, University of Michigan, USA). Isolated chondrocytes were rested in a tissue culture flask for 6 days in full DMEM, washed twice using 10 ml PBS and once with 15 ml PBS before changing to 15 ml Opti-MEM for an additional 48 hours to allow proteins to accumulate in the CM. CM were then frozen and shipped on dry ice to the German Center for Neurodegenerative Diseases (DZNE), Technical University Munich (TUM), Munich and further processed by our collaborators, Dr. Simone Dario Scilabra and Dr. Stephan Müller. Conventional LfQ mass spectrometry of the secretome was performed.
Data obtained from LfQ secretome analysis are depicted as a volcano plot, in which the X-axis shows $\log_2$ of the ratio between protein abundance in the secretome of *Adam15*-null and wild-type immature murine costal chondrocytes (A15KO/A15WT). The Y-axis shows $\log_{10}$ of the p-value. Proteins above the two black curved lines were considered to reach the threshold of statistical significance. No proteins were found to have significantly altered abundance in the secretome of ADAM15 knockdown cells compared to the secretome of non-targeting siRNA-transfected cells. Arylsulfatase K (ARSK), the protein closest to the statistical threshold of significance after correcting for multiple comparison using the FDR method, is labeled. Statistical analysis and multiple correction methods used for the LfQ secretome analysis are described in Section 2.2.9.8.

5.6. Identification of glycoproteins regulated by ADAM15 in the SurfSPECS of *ADAM15*-knockdown HTB-94 cells

Finally, the cell lysates of si*ADAM15*_1 and non-targeting siRNA-treated cells were used for SurfSPECS analysis using LfQ mass spectrometry analysis (n = 3). This method analyses cell surface glycoproteins, enriched by ManNAz labelling and biotinylation. To prepare samples for SurfSPECS analysis, cells were washed twice with ice cold PBS after CM were collected, and incubated in 2 ml PBS. Click reaction

was performed by adding 1 µl sulfo-DBCO-biotin conjugate (from 50 mM stock) to the PBS, and cells incubated for 2 hours at 4 °C in the dark. Since sulfo-DBCO-biotin is membrane impermeable, it only labels glycoproteins on the cell surface or in the extracellular space. Excess sulfo-DBCO-biotin was washed off and cells lysed in MS lysis buffer (50 mM Tris, pH 7.5, 150 mM NaCl, 2 mM EDTA, 1% Triton-X-100). Cells were then processed as described in Sections 2.2.9.4. to 2.2.9.7., and analysed as described in Section 2.2.9.8. Preliminary analyses indicated that changes in abundance of membrane glycoproteins induced by ADAM15 knockdown were small, so another set of 3 samples per group (3 ADAM15 knockdown and 3 non-targeting control) were processed and analysed.

Figure 5.14 (A) shows that 816 proteins were identified and quantified by LfQ mass spectrometry of the surfaceome. Amongst these, 498 were membrane proteins, which constitute more than 61% of the total proteins identified by this method. Hence, the efficiency of membrane protein enrichment was lower than for the SPCES secretome, where >84% of identified proteins were either membrane or secreted proteins. The non-membrane proteins identified by SurfSPECS were mainly secreted and intracellular proteins. The former may be remnants after washing, or were secreted while the click reaction was performed, whilst the latter may come from cells which died during the click reaction. However, SurfSPECS still displayed a better enrichment compared to the conventional secretome methods described in Section 5.2 and 5.3.

Figure 5.14 (B) shows the volcano plot of the SurfSPECS analysis, with the X-axis showing $\log_2$ of the ratio of protein abundance between ADAM15-knockdown and non-targeting transfected cells (ADAM15kd/ct), and the Y-axis showing $\log_{10}$ of the p-

value. In this analysis, proteins which showed increased abundance in the surfaceome from ADAM15-knockdown cells compared to non-targeting transfected cells are shown on the right, whilst those with decreased abundance are shown on the left. 13 proteins showed significant changes in abundance in the surfaceome from ADAM15-knockdown cells and are depicted above the two black curved lines as solid blue circles, whilst proteins close to significant changes are labelled as open blue circles. Notably, ADAM15 was identified as the most significantly altered protein with the highest magnitude of reduction in the surfaceome, indicating successful ADAM15 knockdown by si*ADAM15*_1. Since the first triplicate of these samples were also used for the SPECS secretome analysis in Section 5.4., this provides further evidence that ADAM15 was indeed decreased in the SPECS secretome, and that the lack of major changes in the SPECS secretome was not due to a failure in ADAM15 knockdown.

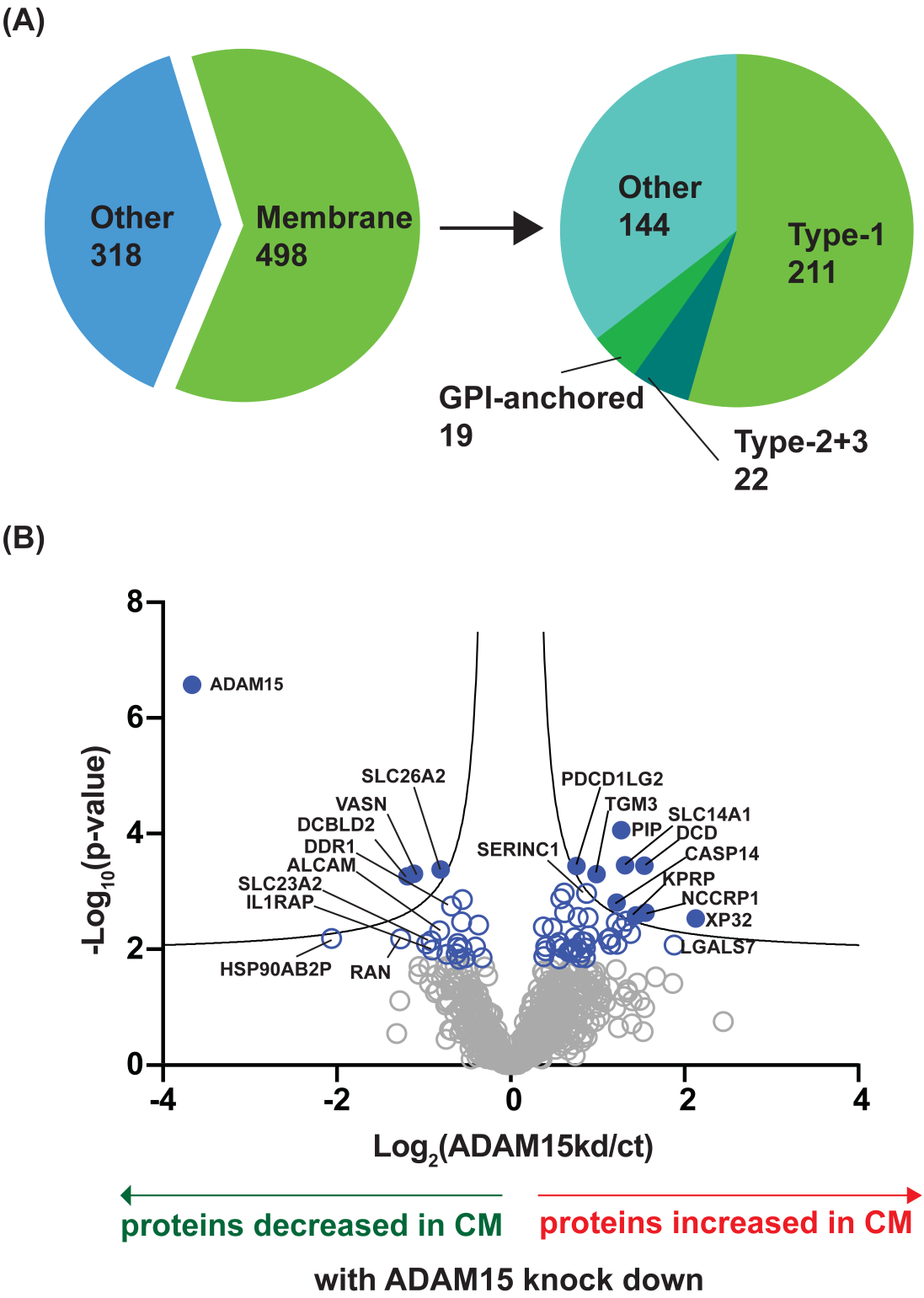

Figure 5.13 Identification of glycoproteins regulated by ADAM15 in the SurfSPECS of ADAM15-repressing HTB-94 cells

(A) 816 proteins were identified and quantified by LfQ mass spectrometry in the surfaceome (n = 6 for each condition). Amongst these, 498 were membrane proteins, with 211 type 1 transmembrane proteins, 22 type 2+3 transmembrane proteins, 19 GPI-anchored proteins, and 144 other transmembrane proteins including multi-passing transmembrane proteins based on annotations in the reviewed canonical FASTA database of *Homo sapiens* from UniProt. More than 61% of the proteins identified using the SurfSPECS method were membrane proteins.

(B) Data obtained from SurfSPECS analysis are depicted as a volcano plot, in which the X-axis shows Log_2 of the ratio between protein abundance in the surfaceome of cells transfected with

si*ADAM15* and that cells transfected with non-targeting siRNA (ADAM15kd/ct). The Y-axis shows $\log_{10}$ of the p-value. Proteins above the two black curved lines were considered to reach the threshold of statistical significance. 13 proteins showed significant changes in their abundance in the surfaceome acquired from ADAM15-knockdown cells and are depicted above the two black curved lines and and highlighted as solid blue circles, whilst proteins with close to significant changes are labelled and highlighted as open blue circles.
Statistical analysis and multiple correction methods used for the LfQ surfaceome analysis are described in Section 2.2.9.8.

Less than 3% (13/498) of the identified proteins showed significant changes upon ADAM15 suppression, suggesting that, as in the secretome, decrease in ADAM15 did not induce major changes in membrane protein abundance in HTB-94 cells. Among those proteins which showed significant changes (excluding ADAM15), only 3 were decreased in the surfaceome of ADAM15-knockdown cells. All 3 are transmembrane proteins, with SLC26A2 being a multi-pass membrane protein, whilst VASORIN (VASN) and DCBLD2 are type-1 transmembrane proteins. Some of the significantly increased proteins in the surfaceome of ADAM15-knockdown cells were intracellular proteins (e.g. XP32, NCCRP1, TGM3 and CASP14), and were thus excluded from further validation. Additionally, expression of PIP (prolactin induced protein), which was identified as up-regulated on the surface of ADAM15-knockdown cells, could not be detected by qPCR using two different Taqman qPCR primers (data not shown). This suggests that the dataset of proteins up-regulated by ADAM15 knockdown (right hand side) contains higher noise. Therefore, when performing validation, more effort was focused on proteins which were decreased upon ADAM15 suppression (left hand side), with SLC26A2 and VASORIN, both of which have known influence on cartilage homeostasis, selected from this group for validation. SLC26A2 is a sulfate transporter and its mutation causes chondrodysplasia (Forlino et al., 2005), whilst VASORIN is a TGF-β-binding protein which inhibits TGF-β signalling (Ikeda et al., 2004) and TGF-β signalling is known to have crucial roles in OA development (Shen et al., 2014).

DCBLD2 from this group was not chosen for validation due to its unclear function and limited available literature.

As for proteins from the right hand side, only PDCD1LG2 (Programmed cell death 1 ligand 2, PD-L2, or CD273) was chosen for further validation. PDCD1LG2 showed increased expression on the surface of ADAM15-knockdown cells. Like its homolog PD-L1, PDCD1LG2 binds to its receptor PD-1 and inhibits inflammation, particularly through inhibiting T cell activation (Latchman et al., 2001). Given its role in regulating inflammation and that ADAM15 has also been suggested to play a critical role in regulating inflammation (Charrier-Hisamuddin et al., 2008), I explored the possibility that ADAM15 may regulate PDCD1LG2.

I first examined the effect of *ADAM15* knockdown on the expression of candidates at the mRNA level. *ADAM15* knockdown was performed using the same method as for LfQ mass spectrometry analysis of SurfSPECS. As shown in Figure 5.15 (A), *ADAM15* expression was significantly decreased in si*ADAM15*_1 transfected cells compared to non-targeting siRNA treated cells ($p < 0.0001$, 95% CI: [-0.9258, -0.7842], Difference between means: -0.855 ± 0.03413) 36 hours after transfection. Figure (B-D) show that the expression of all three candidates was not affected at the mRNA level by *ADAM15* suppression (*PDCD1LG2*: $p = 0.4748$, 95% CI: [-0.0463, 0.0963], Difference between means: 0.025 ± 0.03438; *SLC26A2*: $p = 0.7459$, 95% CI: [-0.09148, 0.06648], Difference between means: -0.0125 ± 0.03808; *VASORIN*: $p = 0.7956$, 95% CI: [-0.1262, 0.09786], Difference between means: -0.01417 ± 0.05402).

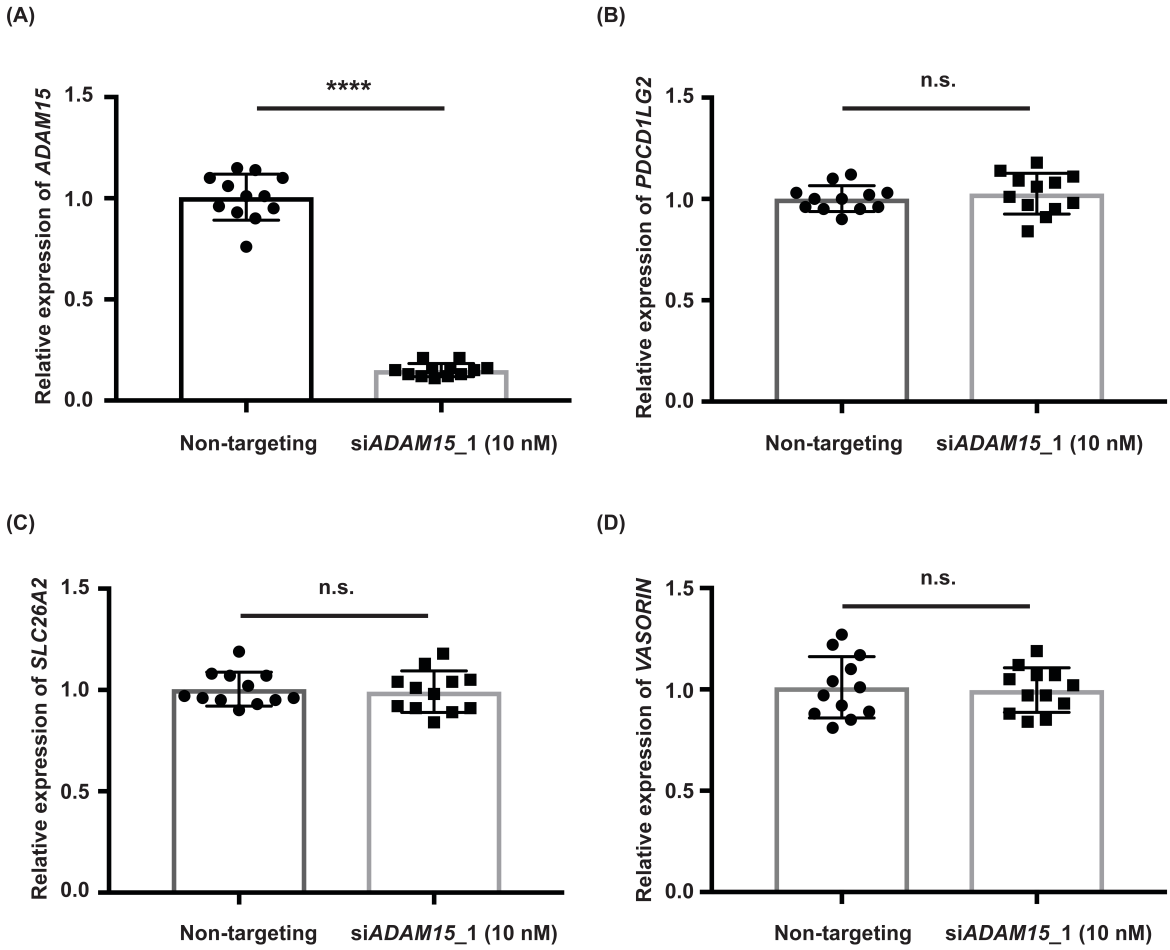

Figure 5.14 *ADAM15* knockdown did not affect mRNA expression of *PDCD1LG2*, *SLC26A2* and *VASORIN*.

To investigate the effect of *ADAM15* knockdown on the expression of selected candidate genes, 10 nM si*ADAM15*_1 or the same concentration of non-targeting siRNA was transfected into HTB-94 cells for 36 hours (Section 2.2.9.4.). To quantify the relative expression of *ADAM15*, *PDCD1LG2*, *SLC26A2* and *VASORIN*, total mRNA was extracted from cell lysates and quantified using qPCR. Expression of these genes was normalised to the housekeeping gene *RPLP0* and their relative expression calculated using the ΔΔCt method (Section 2.2.5.4.) and normalised to the average expression of the respective gene in non-targeting siRNA treated cells.

(A) *ADAM15* expression was significantly decreased in si*ADAM15*_1 transfected cells compared to non-targeting siRNA treated cells ($p < 0.0001$, 95% CI: [-0.9258, -0.7842], Difference between means: -0.855 ± 0.03413).

(B) *ADAM15* suppression did not affect mRNA expression of *PDCD1LG2* ($p = 0.4748$, 95% CI: [-0.0463, 0.0963], Difference between means: 0.025 ± 0.03438).

(C) *ADAM15* suppression did not affect mRNA expression of *SLC26A2* ($p = 0.7459$, 95% CI: [-0.09148, 0.06648], Difference between means: -0.0125 ± 0.03808).

(D) *ADAM15* suppression did not affect mRNA expression of *VASORIN* ($p = 0.7956$, 95% CI: [-0.1262, 0.09786], Difference between means: -0.01417 ± 0.05402).

Data are shown as mean ± SD, NT, non-targeting control, KD, ADAM15 knockdown, n.s., not significant, ****, $p \leq 0.0001$. The statistical significance of comparison between NT and KD was analysed with Student's t test (two-tailed).

Next, I investigated whether ADAM15 knockdown affected abundance of these candidates at the protein level. ADAM15 knockdown was performed using the method described in Section 2.2.9.4. To detect candidate protein expression in whole cell lysates, cells were lysed in 80 µl 2X SDS sample buffer and analysed by immunoblotting. To evaluate expression of candidate proteins on the cell surface, cells were processed using the same method which was used to generate samples for LfQ mass spectrometry analysis of SurfSPECS (detailed in Section 2.2.9.4.), with the 'clicked' membrane proteins eluted from streptavidin-agarose (Pierce/Thermo Fisher Scientific, Cat. 21134) using 50 µl 2X SDS sample buffer and analysed using immunoblotting. To quantify the expression of proteins in the cell lysate, band intensity was normalised to the average expression of actin, which was used as an internal control. Since actin was not detectable after streptavidin pull-down, expression of proteins on the cell surface was not normalised.

Figure 5.16 (A) shows that HTB-94 cells treated with si*ADAM15*_1 showed significant decrease in ADAM15 abundance in the whole cell lysate and on the cell surface, indicating successfully ADAM15 knockdown (cell lysates: $p = 0.0008$, 95% CI: [-1.17, -0.6305], Difference between means: -0.9 ± 0.09707; surface: $p < 0.0082$, 95% CI: [-1.229, -0.3372], Difference between means: -0.7833 ± 0.1607). Notably, two bands were detected on the surface of non-targeting siRNA treated cells, and their molecular weights correspond to active and pro-ADAM15 respectively, and both disappeared in the si*ADAM15*_1 treated cells. This may indicate that pro-ADAM15 was also present on the cell surface. On the contrary, in the cell lysates, high levels of pro-ADAM15 were detected, which obscured any active ADAM15 that may have been present, thus most ADAM15 appears to be expressed as pro-form, even on the cell surface.

Figure 5.16 (B) shows that three bands between 70 and 100 kDa were detected in cell lysates and on the cell surface with the anti-SLC26A2 antibody. Since all three bands were reasonably close to the predicted molecular weight of SLC26A2 (81 kDa), these bands may correspond to SLC26A2 with different degrees of glycosylation. Therefore, when performing quantification, all three bands were quantified and the sum of their intensities analysed. As shown in Figure 5.16 (B), si*ADAM15*_1 treatment did not affect SLC26A2 expression in the cell lysates ($p = 0.1361$, 95% CI: [-0.4899, 0.09658], Difference between means: -0.1967 ± 0.1056). However, SLC26A2 expression on the cell surface showed a trend towards decrease that did not reach statistical significance ($p = 0.0629$, 95% CI: [-0.7024, 0.0291], Difference between means: -0.3367 ± 0.1317). The result of SurfSPECS analysis showed a ~ 43% reduction in SLC26A2 expression on the cell surface, which was comparable to the reduction I observed using immunoblotting (~34%). Notably, there was substantial variation between independent experiments. Therefore, more experiments with larger sample sizes may be needed to determine whether ADAM15 suppression indeed reduces the level of SLC26A2 on the cell surface.

Figure 5.16 (C) shows that two bands between 100 and 130 kDa were detected in cell lysates and on the cell surface using the anti-VASORIN antibody. Since both bands were reasonably close to the predicted molecular weight of VASORIN (110 kDa), both bands may correspond to VASORIN with different degrees of glycosylation. Therefore, when performing quantification, both bands were quantified and the sum of their intensities analysed. As shown in Figure 5.16 (c), si*ADAM15*_1 treatment did not affect VASORIN expression in the cell lysates or on the cell surface (cell lysates: $p = 0.5726$, 95% CI: [-0.976, 0.6227], Difference between means: -0.1767 ± 0.2879; surface: $p =$

0.3214, 95% CI: [-0.07278, 0.1728], Difference between means: 0.05 ± 0.04422).

Figure 5.16 (D) shows that two bands between 25 and 45 kDa were detected in cell lysates probed with the anti-PDCD1LG2 antibody. Since both bands were reasonably close to the predicted molecular weight of PDCD1LG2 (31 kDa), both bands may correspond to PDCD1LG2 with different degrees of glycosylation. Therefore, when performing quantification, both bands were quantified and the sum of their intensities analysed. As shown in Figure 5.16 (D), si*ADAM15*_1 treatment did not affect PDCD1LG2 expression in the cell lysates ($p = 0.6770$, 95% CI: [-0.3355, 0.2422], Difference between means: -0.04667 ± 0.104). PDCD1LG2 was not detected on the cell surface. Finally, Figure 5.16 (E) shows the actin blot used to normalised loading of the cell lysates.

These validation experiments suggest that there is a high chance that the "hits" identified by SurfSPECS were false positives, or that effect sizes were too variable to be reliably detected by immunoblotting. SLC26A2 was the only selected hit which showed a trend towards decrease upon ADAM15 suppression. Given its critical role in cartilage homeostasis (Forlino et al., 2005), it may be worthwhile to perform a more detailed study with larger sample sizes to explore a potential causal relationship between ADAM15 and SLC26A2.

Overall, my results in this chapter suggest that ADAM15 did not induce major changes in the secretome or surfaceome of the HTB-94 cells, or that the changes it induced could not be detected using the present methods.

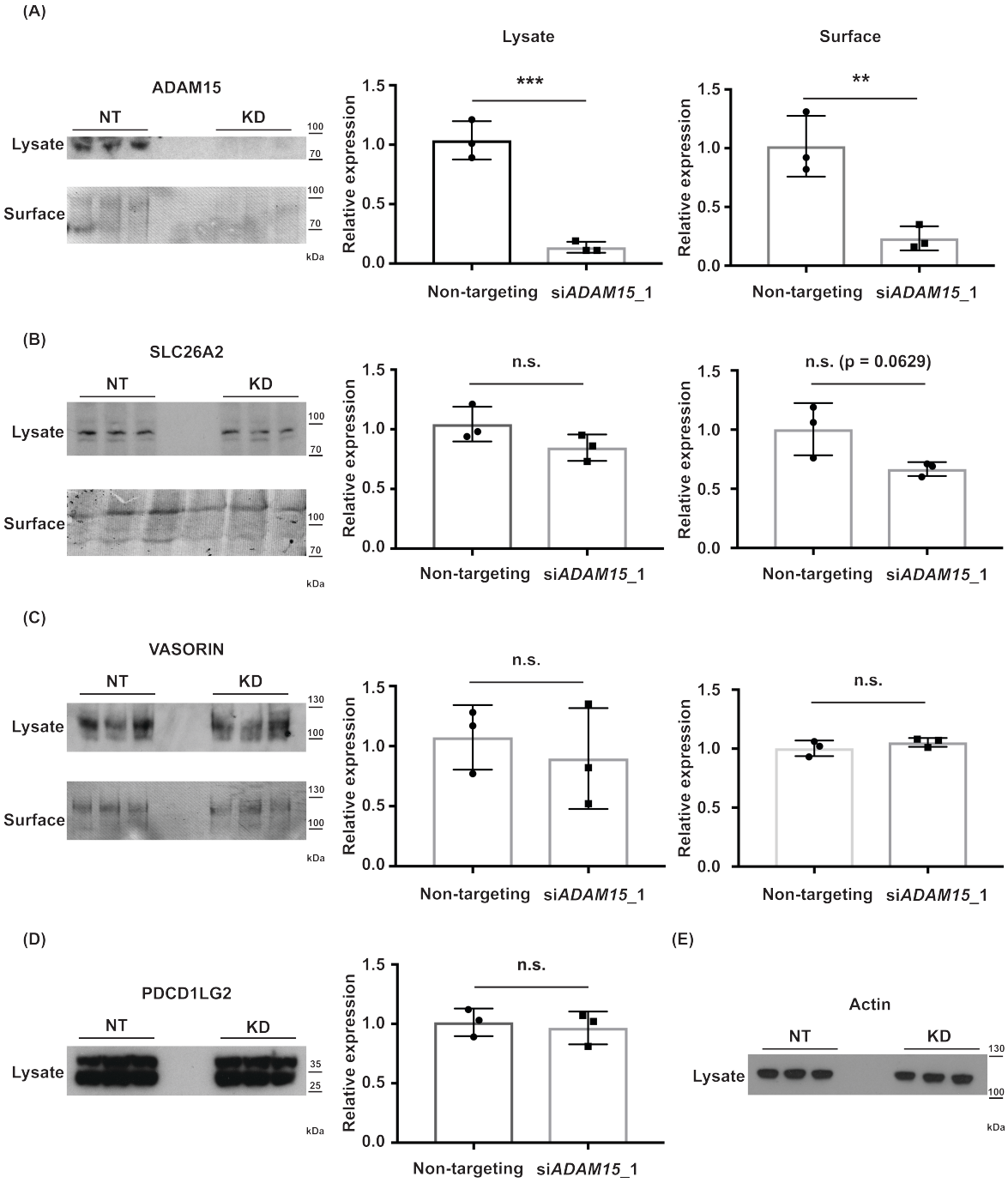

Figure 5.15 ADAM15 knockdown may decrease surface levels of SLC26A2.
To investigate the effect of ADAM15 suppression on surface levels of candidate proteins, 10 nM si*ADAM15*_1 or the same concentration of non-targeting siRNA was transfected into HTB-94 cells for 36 hours. Cells were lysed using 80 µl 2X SDS sample buffer to perform immunoblotting of the cell lysates. For immunoblotting for surface proteins, cells were processed using the same method used for LfQ mass spectrometry analysis of SurfSPECS (Section 2.2.9.4.) and the 'clicked' membrane proteins were eluted from Streptavidin-agarose using 50 µl 2X SDS sample buffer for immunoblotting. Quantification was performed using Phoretix 1D software, expression of each protein in the cell lysate was normalised to the average expression of actin, which was used as an internal control. Expression of the surface proteins was not normalised. Relative expression of each protein in cell lysates and cell surface was normalised to the average expression of the respective protein in the non-targeting siRNA treated cells.
(A) ADAM15 expression was significantly decreased in si*ADAM15*_1 transfected cells compared to non-targeting siRNA treated cells in the cell lysates and on the surface (cell lysates: $p = 0.0008$, 95% CI: [-1.17, -0.6305], Difference between means: -0.9 ± 0.09707; surface: $p < 0.0082$, 95% CI: [-1.229, -0.3372], Difference between means: -0.7833 ± 0.1607). Both bands detected on the cell surface were quantified together.

(B) ADAM15 suppression did not affect expression of SLC26A2 in the cells ($p = 0.1361$, 95% CI: [-0.4899, 0.09658], Difference between means: -0.1967 ± 0.1056), but may affect surface levels of SLC26A2 ($p = 0.0629$, 95% CI: [-0.7024, 0.0291], Difference between means: -0.3367 ± 0.1317). Three bands were detected both in the cell lysates and on the cell surface, bar graphs indicate the sum of the intensity of all three bands.
(C) ADAM15 suppression did not affect expression of VASORIN in the cells and on the cell surface (cell lysates: $p = 0.5726$, 95% CI: [-0.976, 0.6227], Difference between means: -0.1767 ± 0.2879; surface: $p = 0.3214$, 95% CI: [-0.07278, 0.1728], Difference between means: 0.05 ± 0.04422). Two bands were detected in the cell lysates and on the cell surface, bar graphs indicate the sum of the intensity of both bands.
(D) shows that ADAM15 suppression did not affect expression of PDCD1LG2 in the cells ($p = 0.6770$, 95% CI: [-0.3355, 0.2422], Difference between means: -0.04667 ± 0.104), while PDCD1LG2 was not detected on the cell surface (data not shown). Two bands were detected both in the cell lysates, bar graph indicates the sum of the intensity of both bands.
(E) Immunoblotting for actin as internal control for whole cell lysates.
Bar graphs are shown as mean ± SD, NT, non-targeting control, KD, ADAM15 knockdown, n.s., not significant, ***, $p \leq 0.001$, **, $p \leq 0.01$. The statistical significance of comparison between NT and KD was analysed with Student's t test (two-tailed).

5.7 Discussion

In this chapter, I used various cutting-edge proteomic methods with specialised protein enrichment techniques to identify proteins regulated by ADAM15. Since other ADAMs, such as ADAM10, 12 and 17, have been found to principally shed proteins from the plasma membrane into the CM, and ADAM15 is known to be transported to the plasma membrane after maturation (Lum et al., 1998), I chose label-free, quantitative proteomic methods optimised to detect changes in abundance of membrane and secreted proteins.

I started by over-expressing ADAM15 in HTB-94 cells and performed an analysis of the secretome of ADAM15 over-expressing and mock-transfected cells. Over-expression was performed in serum free Opti-MEM for 72 hours to allow proteins to accumulate in the CM, and I optimised a protocol for removing BSA from the CM before conducting LfQ mass spectrometry analysis. As shown in Figure 5.4 and Section 5.2., only ~33.5% of the proteins identified in the secretome were secreted or

membrane proteins, with considerable noise from cytosolic and nuclear proteins. This noise may be inherent to the over-expression approach, which is known to induce cellular stress and may induce apoptosis. Although the result from the MTS assay shown in Figure 5.2 (C) suggests no apparent difference in cell metabolism, the MTS assay was performed on cells transfected with *ADAM15*-over-expressing vector but without all other procedures optimised for preparing secretome samples, such as the wash protocol aimed at removing BSA. Therefore, it is possible that ADAM15 over-expression under serum free conditions increases cellular stress and predisposes them to apoptosis or necrosis upon subsequent manipulation. Additionally, I performed the MTS assay in a 96-well format while the ADAM15 over-expression for LfQ mass spectrometry analysis was conducted in 10 cm^2 dishes. The scaled-up protocol suggested by the manufacturer involved use of higher amounts of the plasmid DNA and transfection reagents per cell than was used in smaller scale experiments, and this may have induced more cell death.

Several membrane and secreted proteins were found to have significantly altered abundance in the secretome of ADAM15-over-expressing cells. At the time of performing this experiment, my aim was mainly to identify substrates of ADAM15. I hypothesised that ADAM15 over-expression would result in more active ADAM15 on the plasma membrane, and hence elevated shedding activity, with membrane proteins significantly increased in CM considered to be potential substrates of ADAM15. However, the proteins which showed the most significant increase (i.e., RPL30, XRCC6, PAICS and UGDH) were all intracellular proteins. Moreover, TIMP-3, a protein which was completely absent from the secretome of mock-transfected cells, was found in the CM of both ADAM15-over-expressing and mock-transfected cells

when validation was conducted using immunoblotting, suggesting that TIMP-3 was a false positive "hit" from mass spectrometry. Given that proteins with the highest and most significant changes were either intracellular or could not be validated, I concluded that the ADAM15 over-expression approach was not ideal to identify ADAM15 substrates.

Next, I explored whether proteins found to have decreased abundance in the secretome of ADAM15-over-expressing cells compared to mock-transfected cells may contain OA-related real "hits". Due to the high noise in the secretome dataset, only those proteins with known OA relevance were considered for validation. Expression of CTGF is elevated in OA at both the mRNA and protein levels (Komatsu et al., 2015; Omoto et al., 2004), and CTGF was thus selected for validation. By immunoblotting, I validated that CTGF was indeed decreased in the secretome of ADAM15-over-expressing cells [Figure 5.5 (B&C)]. Since ADAM15 is reported to protect against OA (Bohm et al., 2005), ADAM15-induced reduction of CTGF would suggest that reduced CTGF levels are beneficial to joint homeostasis. This hypothesis is inconsistent with research reported by Nishida et al. (2004) who reported that CTGF induced cartilage regeneration in a monoiodoacetic acid-induced rat model of osteoarthritis. However, another study reported by Blaney Davidson et al. (2006) found that CTGF over-expression in mouse synovium induced proteoglycan depletion in cartilage , suggesting a pathogenic role in CTGF. Importantly, a recent study using chondrocyte-specific *CTGF*-null mice showed that the protective effects of CTGF were temporary, with protection only observed 4 weeks after surgical induction of OA, but was not evident 8 weeks after surgery. Moreover, in a non-surgical, loading-induced mouse model of OA, CTGF showed protective effects on OA development (Keenan et al.,

2018). Taken together, these studies suggest that the effect of CTGF on cartilage may be tissue-dependent, and its effects on cartilage may be small. The study which identified a protective role for ADAM15 in the joint utilised mice with constitutive deletion of *Adam15* throughout the body (Bohm et al., 2005), it is possible that ADAM15 may induce different or even opposite effects on different cell types, and that the observed OA protection represents a cumulative consequence of these effects. Tissue-specific, inducible deletion of *Adam15* may be required to ascertain the effects on CTGF and whether this contributes to OA protection.

Another potential explanation is that ADAM15's effect on joint health is dose-sensitive. Moderate amounts of ADAM15 may protect the joint from developing OA, but high expression levels may be detrimental for joint health. Moreover, ADAM15 over-expression has been shown to result in increased abundance of the pro-form ADAM15 on the cell surface, both by others (Lum et al., 1998) and in the current study [Figure 5.4 (A)]. Pro-ADAM15 may compete with active ADAM15 for interactions with substrates or other binding partners (e. g. integrins), thus inhibiting the activity of endogenous ADAM15. Over-expression may also promote interactions which do not normally happen under physiological conditions. However, to the best of my knowledge, over-expression of ADAM15 has not been documented in any joint tissues in OA, so ADAM15's effect on CTGF may not be relevant in this biological context.

To better understand the effects of ADAM15 on joint health under more physiological contexts, I investigated the effect of knocking down ADAM15 expression on abundance of secreted and membrane proteins using LfQ mass spectrometry secretome analysis. To compare these results with those from ADAM15 over-

expression, the timeline was kept the same (72 hours). The secretome dataset of ADAM15-knockdown cells still contained relatively high levels of noise, and only identified one significant hit, AXL, which was decreased in the secretome of ADAM15-knockdown cells and was thus considered as a potential substrate of ADAM15. AXL is a tyrosine kinase receptor belonging to the TAM family, and its interactions with its ligand, growth arrest-specific protein 6 (GAS6), is critical in controlling cell proliferation (Gay et al., 2017). AXL over-expression has been found in various cancers (Gay et al., 2017) and reduced AXL shedding by ADAM10 and -17 is thought to be responsible for cancer cell resistance to tyrosine kinase inhibitor treatments (Miller et al., 2016).

Further analysis indicated that ADAM15 knockdown decreased mRNA and protein expression of AXL. Given the long time (72 hours) between siRNA transfection and CM collection, it is possible that the ADAM15-mediated reduction of AXL was a secondary effect. Importantly, the si*ADAM15* I used to perform ADAM15 knockdown consisted of two siRNA sequences that target *ADAM15*, called si*ADAM15*_1 and si*ADAM15*_2, and si*ADAM15*_2, but not si*ADAM15*_1, was found to exhibit off-target effects on 4 randomly selected genes [Figure 5.8 (C)].

I re-optimised ADAM15 knockdown using si*ADAM15*_1 (10 nM) alone, and found that *ADAM15* mRNA expression decreased by ~50% as early as 12 hours after transfection, and by >90% after 36 hours. ADAM15 expression at the protein level was also significantly decreased (>90%) 36 hours after transfection, indicating that ADAM15 as a rapid turnover in HTB-94 cells. ADAM15 on the cell surface may be

constitutively endocytosed and degraded, as has been suggested for other ADAMs (Mygind et al., 2018; Stautz et al., 2012).

Using an optimised ADAM15 knockdown procedure (10 nM, si*ADAM15*_1, 36 hours), no its effects on AXL expression were observed at the 72-hour time point (Figure 5.10). Interestingly, effects on AXL protein expression in cells lysates (mAXL) and CM (sAXL) were observed at earlier time points. sAXL in the CM of ADAM15-knockdown cells increased at 36 hours, and then returned to a level comparable to non-targeting siRNA-treated cells [Figure 5.10 (A)]. Since mRNA levels of AXL were not changed at this time point [Figure 5.8 (C)], this may indicate increased AXL shedding, potentially by ADAM10 and 17 (Miller et al. 2016), in the absence of ADAM15. mAXL levels were decreased in ADAM15-knockdown cells at 48 hours, but were comparable to control cells at 36 and 72 hours. This indicates dynamic regulation of AXL expression, in line with its important roles in cell growth, proliferation and oncogenic transformation (Axelrod et al., 2014). The mechanism by which ADAM15 modulates AXL was not further investigated, but appears to be complex, since sAXL also increased in the secretome of ADAM15-over-expressing cells.

Since conventional secretome methods did not identify novel substrates of ADAM15, I performed a third proteomic analysis using SPECS, which enriches for glycoproteins. Since 66% of secreted proteins and 87% of type I and type II transmembrane proteins are glycoproteins, SPECS provides a more sensitive analysis of changes in abundance of these proteins. SPECS was used to analyse both the secretome and surfaceome of ADAM15-knockdown cells compared to non-targeting siRNA-treated cells. SPECS dramatically reduced noise from intracellular proteins (>61% and >84% of identified in

the SPECS secretome and surfaceome were membrane and secreted proteins, respectively), demonstrating successful enrichment. However, SPECS was unable to identify any novel "hits" regulated by ADAM15. This was supported by conventional LfQ mass spectrometry analysis of the *Adam15*-null chondrocyte secretome.

Several possibilities may explain why I was not able to identify ADAM15 substrate using these hypothesis-free approaches. Firstly, quantitative secretome analysis relies on detecting proteins that are shed and released into the CM. Increased ADAM15 expression was expected to increase shedding of substrates into the CM, and decreased ADAM15 expression to reduce shedding. However, this method cannot detect cleavage by a protease that only cleaves membrane proteins which have already been cleaved by other sheddases (sequential processing). One such example is the β-amyloid precursor protein (APP), which undergoes either non-amyloidogenic processing by α-secretases (e. g. ADAM10) and then γ-secretases, or amyloidogenic processing by β-secretases (e. g. Beta-site APP cleaving enzyme 1, or BACE1) and then γ-secretases in a sequentially manner. Since γ-secretases only cleave processed APP, and the LfQ mass spectrometry analysis can only differentiate quantitative differences in abundance caused by shedding, and not qualitative changes in the shed peptides (i. e. the sequence of the cleavage site), the secretome method used here cannot detect γ-secretases processing. If ADAM15 plays a similar role to γ-secretases in that it further processes proteins which have already been cleaved by another protease, its substrates will not be identified using this method. Similarly, if ADAM15 processes ECM components or secreted proteins, this activity will also not be identified since these proteins will be present in the CM regardless of ADAM15 activity. A more targeted

proteomic approach that can differentiate different cleavage sites (and often involves isotope labelling) will be necessary to overcome this issue.

Another possibility is that ADAM15 sheds substrates which are also shed by other highly active sheddases, such as ADAM10 and/or -17, but is less active. In this scenario, the effect of ADAM15 will be masked by the activity of the more active sheddases. For example, if 99% of the shedding of a particular protein is mediated by ADAM17, it will be hard to detect this protein as a substrate of ADAM15 without simultaneously suppressing ADAM17. In this case, double knockdown will be required to identify ADAM15 substrates.

A third possibility is that ADAM15 has very low shedding activity, or has low constitutive activity and required activation to exert substantial shedding activity. Notably, *Adam15*-null mice have relatively normal gross phenotypes, even in embryonic and adult tissues where *Adam15* expression is relatively high [e. g. hypertrophic chondrocytes, Purkinje cells and endothelial cells (Horiuchi et al., 2003)], abnormalities were only observed when animals were challenged [e. g. by reducing oxygen tension to induce neovascularisation (Horiuchi et al., 2003)], or after prolonged periods of time [e. g. increased spontaneous OA after 12 months (Bohm et al., 2005)]. These studies support the idea that effects of ADAM15 may be cumulative or evident only under conditions of physiological challenge, and may be too subtle to detect by proteomic methods.

Finally, although ADAM15 has a conserved metalloproteinase domain with a predicted active catalytic site, it is also possible that it is not a physiologically active

protease and that its primary functions are not related to shedding or protein cleavage. Horiuchi et al. (2003) reported that murine ADAM15 is required for pathological neovascularisation but Maretzky et al. (2014) found that knock-in mice carrying a catalytically inactivate point mutation (E305A) showed comparable pathological neovascularisation to mice-over-expressing wild-type ADAM15. This indicates that the catalytic function of ADAM15 is not required for its role in neovascularisation. Moreover, they were unable to identify any substrates relevant to angiogenesis, further supporting the possibility that ADAM15's physiological and pathological roles may be independent of its shedding or proteolytic activity. Interestingly, other than ADAM10 and -17, surprisingly little is known about ADAM *in vivo* substrates or the biological relevance of their shedding activity, despite tremendous efforts in this field. Therefore, though ADAM15 has a conserved catalytic domain, it would be beneficial to consider the possibility that ADAM15 may have important, non-catalytic functions.

In this regard, I performed surfaceome analysis to investigate effects of ADAM15 on plasma membrane glycoproteins. Very few proteins were significantly regulated by ADAM15 repression [Figure 5.14 (B)], and 2 out of 3 selected candidates (SLC26A2, VASORIN, and PDCD1LG2) could not be validated using immunoblotting (Figure 5.16). The only candidate showing a detectable difference, SLC26A2, failed to reach the threshold of statistical significance ($p = 0.0629$). Since the trend towards reduction in SLC26A2 abundance on the surface of HTB-94 cells was relatively small (Difference between means: -0.3367 ± 0.1317), increased sample sizes will be required to confirm this finding. SLC26A2 is a sulfate transporter expressed in various tissues, but the only tissue affected by loss-of-function mutations of SLC26A2 are cartilage and bone (Forlino et al., 2005; Haila et al., 2001). Its down-regulation or mutation results in

glycosaminoglycan undersulfation in humans and mice (Forlino et al., 2005; Haila et al., 2001; Rossi et al., 1996) and, depending on the severity of the mutation, leads to a spectrum of cartilage and skeletal abnormalities, ranging from a non-lethal recessive form of multiple epiphyseal dysplasia (Superti-Furga et al., 1999), to diastrophic dysplasia (Hastbacka et al., 1994), postnatally lethal atelosteogenesis type 2 (Hastbacka et al., 1996), and embryonically lethal achondrogenesis 1B (Superti-Furga et al., 1996). The fact that SLC26A2 mutation displays dose-dependent effects on cartilage is particularly relevant because data in this chapter suggest that ADAM15's effect, if any, on SLC26A2 is mild. Reductions in the sulfate transporter function of SLC26A2 by ADAM15 are likely to reduce glycosaminoglycan sulfation. Since glycosaminoglycan sulfation is known to be critical in determining growth factor bioavailability, modulating outside-in signals through cell–cell and cell–ECM interactions, and in creating important microenvironment critical for development and homeostasis (Soares da Costa et al., 2017), slight but chronic undersulfation may have profound impacts on joint health later in life. For example, Cortes et al. (2009) showed that undersulfation of chondroitin sulfate (CS) chains resulted in diminished Indian hedgehog (Ihh) signalling, potentially by changing Ihh distribution in the cartilage ECM. They further showed that reduced Ihh caused decreased chondrocyte proliferation in the growth plate, suggesting that GAG undersulfation can indeed affect cartilage homeostasis. Likewise, the effects of heparan sulfate (HS) undersulfation on growth factor signalling have been studied extensively, and sulfation patterns can affect BMP, FGF and Wnt signalling via changing their binding affinities for HS, as summarised by Stephane et al. (2011). Therefore, considering the importance of SLC26A2 in cartilage and bone development, and the seemingly small effect of ADAM15, it may be worthwhile to further dissect the relationship between

ADAM15 and SLC26A2 in future studies. Importantly, studies [as reviewed by Stephane et al. (2011)] have suggested that, in addition to the overall sulfation status, the sulfation pattern of HS also plays a critical role in regulating growth factor binding to HS, hence dissecting whether impaired SLC26A2 function predominantly affects a particular GAG (e.g. HS or CS), or preferentially affects a particular sulfation site will help us to better understand how ADAM15 influences cartilage homeostasis.

The secretomes of ADAM15 knockdown cells (Figure 5.6) and *Adam15*-null cells (Figure 5.13) display a similar trend in that, though mostly insignificant, more proteins were increased in the secretome of cells with decreased ADAM15 expression level. This is opposite to what is generally found for more active sheddases such as ADAM10 and -17 (Kawahara et al., 2014; Kuhn et al., 2016), where many proteins were decreased in the secretome of cells with decreased ADAM10 or 17 expression. This suggests that ADAM15 may function as a weak anti-sheddase, and interfere with interactions between active sheddases and their substrates. Thus when ADAM15 expression is suppressed, these sheddases would be able to interact with their substrates more freely. One way to test this hypothesis is to conduct a shotgun proteomic analysis on immunoprecipitated complexes of ADAM15 and the proteins it interacts with. This may help to identify proteins that bind to ADAM15 and, combined with bioinformatics, may help to narrow down candidate sheddases which may be inhibited by ADAM15. Additionally, ADAM15 may bind to these sheddases directly, and in this scenario, these sheddases will be revealed by the proteomic analysis.

Chapter 6 Discussion

6.1. ADAM15 plays a minor role during development

In the present study, I showed that ADAM15 expression is not differentially regulated between normal and OA cartilage, which is consistent with all but one publication I reviewed on this topic (Yang et al., 2017). However, I identified that ADAM15 expression varied with age at the mRNA level, with lower *Adam15* expression in the joints of musculoskeletally immature (0.2-month old) mice than in adult joints.

This finding suggests that ADAM15 does not play a critical role during musculoskeletal development. Indeed, *Adam15*-deficient mice did not display any observable developmental defects (Horiuchi et al., 2003), indicating either redundancy in ADAM15 activity or that ADAM15 plays only a minor role in development. In those developing tissues where *Adam15* expression is relatively high (such as developing bone and cartilage, vasculature and brain), abnormalities were observed after birth when the mice were challenged with strong stimuli [e. g. a sudden decrease in oxygen concentration resulted in impaired neovascularisation in *Adam15*-null animals (Horiuchi et al., 2003)] or after prolonged periods of time [e. g. *Adam15*-deficient mice developed accelerated osteoarthritis which was only apparent at 12- to 14-months of age (Bohm et al., 2005)]. These findings suggest that ADAM15 serves a protective or homeostatic role during development, rather than actively participating in the developmental process. In this model, tissues would develop normally in the absence of ADAM15 without any insults, but would not respond optimally to abnormal stimuli or insults, causing a slow accumulation of tissue damage during adulthood. The effects of ADAM15 deficiency may thus not be evident early in life or without challenge, but would become evident in conditions of physiological stress or ageing. *Adam15*-null mice may consequently develop chronic conditions when intrinsic repair

pathways are overcome by the cumulative effects of tissue damage.

Since *Adam15* expression is also high in the cerebellum during development, it will be interesting to investigate under what conditions ADAM15 may affect cerebellum homeostasis if the proposed hypothesis is correct. Moreover, uncovering how ADAM15 exerts it functions will help to explain why ADAM15 is more important in certain tissues than in others, and define the molecular mechanism of ADAM15's safeguarding effects in these tissues.

6.2. Decreased ADAM15 expression with age may hamper joint protection

I also identified that *Adam15* expression was lower in joints of aged (18-months) mice than adult (3- to 5.5-months) mice. A similar trend was observed in human cartilage at both the mRNA and protein levels. ADAM15 is thought to protect the joint against OA (Bohm et al., 2005), and ageing is the most prominent risk factor for OA (Loeser et al., 2016), so this loss of ADAM15 expression in cartilage with age may potentially be a mechanism by which ageing increases OA risk. The molecular pathways of this protection remain to be defined. Importantly, the study (Bohm et al., 2005) demonstrating that ADAM15 protects mice against OA was performed using constitutive *Adam15* knock out mice, so the contribution of other tissues in the joint cannot be excluded, and tissue-specific *Adam15* knock out mice will be needed to dissect the effects of *Adam15* in different tissues, especially those tissues which have known involvement in OA pathogenesis, such as bone and synovium. Additionally, my data shows that *Adam15* expression was not reduced with age in all tissues, with no change observed in aged brain, spleen, and heart. The reduced *Adam15* expression in aged joints and bones was not accompanied by elevated *Cdkn2a* and *Cdkn1a*

expression, indicating that *Adam15* expression in these tissues may be regulated by unidentified, age-related pathways. Since the synovium also plays a critical role in maintaining joint homeostasis, it will be interesting to examine whether a similar trend of age-dependent decrease in ADAM15 expression without elevated *Cdkn2a* and *Cdkn1a* expression also occurs in the synovium. Micro-dissection of murine synovium or synovium from OA patients undergoing TKA will be necessary to examine this question. Importantly, since the age-dependent reduction of ADAM15 expression was only found in bone and cartilage, but not heart and brain, this will allow us to investigate tissue-specific mechanisms regulating ADAM15 expression using different tissues from the same mouse (e.g. test the effect of IL-13 on ADAM15 in heart muscle cells or different neurons in the brain, or screening for regulators of ADAM15 using neurons, then test the effect of identified regulator of ADAM15 in chondrocytes). Since these tissues will be acquired from the same mouse, they will be age-matched and have the same genetic background, making it easier to dissect the tissue-specific mechanisms of ADAM15 regulation.

6.3. IL-13 may contribute to the age-related reduction in ADAM15 expression

Using HTB-94 cells, I demonstrated that IL-13 can up-regulate ADAM15 expression at both the mRNA and protein levels. IL-13 is reportedly protective in cartilage, reducing cartilage degradation in both an *ex vivo* IL-1-induced bovine nasal cartilage model (Cleaver et al., 2001) and an immune complex-induced murine inflammatory arthritis model (Nabbe et al., 2005). The observed protective effects of IL-13 may be partially due to its ability to up-regulate ADAM15 expression. Importantly, both ADAM15 (Bohm et al., 2010; Bohm et al., 2005) and IL-13 (Nabbe et al., 2005) are thought to protect cartilage, at least in part, by reducing chondrocyte apoptosis, further

strengthening my hypothesis that IL-13 may protect joints against OA in an ADAM15-dependent manner. Moreover, I found that *Il13* expression is also reduced with age, which may contribute to the observed reduction in ADAM15 expression in aged joints. The effect of IL-13 on ADAM15 expression in normal human chondrocytes should be investigated to confirm that my observations in HTB-94 cells apply in a more physiologically relevant cell type. This could be done in a 3D alginate culture to mimic the physiological chondrocyte environment. To further test my hypothesis that IL-13 regulates ADAM15 expression, I would inject *IL13*-encoding adenoviruses (developed by Nabbe et al, 2005) intra-articularly in wild-type and *Adam15*-deficient mice undergoing DMM. *IL13* over-expression should protect wild-type but not *Adam15*-deficient mice from developing DMM-induced OA if the chondroprotective effects of IL-13 are indeed ADAM15-dependent. Additionally, it is also possible that ADAM15 can affect IL-13 expression, potentially through a feedback mechanism. Further studies will be necessary to uncover the regulatory circuit between these two molecules.

IL-13 has been shown to signal through both IL-4 receptor-dependent and IL-4-receptor-independent pathways (Minty et al., 1993; Rael et al., 2011; Zurawski et al., 1994). Since my data show that IL-4 had no effect on *ADAM15* expression, it is likely that IL-13 induced up-regulation of ADAM15 is mediated through a receptor other than the IL-4 receptor. The identity of this receptor was not uncovered in my study, and requires further investigation.

6.4. Secretome analyses did not identify ADAM15 substrates

Since ADAM15 has a conserved zinc-binding motif, it is considered to be an active sheddase. To identify its substrates, I used 4 different secretome approaches

(*ADAM15*-over-expression in HTB-94 cells coupled with conventional secretome analysis, *ADAM15*-knock down in HTB-94 cells coupled with conventional secretome analysis, *ADAM15*-knock down in HTB-94 cells coupled with SPECS analysis, and *Adam15*-knock out in immature chondrocytes coupled with conventional secretome analysis). The secretome approaches used here have previously enabled identification of novel ADAM10 and 17 substrates with great success, but in the present study, none of the 4 approaches identified ADAM15 substrates.

Important technical limitations may explain the current result, even if ADAM15 is indeed a sheddase. Firstly, the shedding activity of ADAM15 may be too weak to be reliably detected with a limited number of samples using these proteomic approaches. Although increased sample size may help to resolve this hurdle, the variability between technical replicates and the noise from intracellular proteins may still be too large to be overcome. Secondly, ADAM15 may shed the same substrates as other highly active sheddases (e. g. ADAM10 and 17), so the influence of losing ADAM15 may not be detectable while these other sheddases remain active. Double knock down or knock out will be necessary to overcome this redundancy. Thirdly, these approaches will not detect ADAM15 activity if the enzyme only cleaves membrane proteins which have already been cleaved by other sheddases. Labelled secretome approaches rather than LfQ will be essential to identify ADAM15 substrates if this is the case. Another possibility is that the shedding activity of ADAM15 may be cell-type dependent. For example, ADAM15 has been shown to cleave E- and N-cadherins (Najy et al., 2008a, b) in breast and prostate cancer cells, respectively. However, to the best of my knowledge, similar shedding activities have not been observed in other cell types which also express E- and N-cadherins, and my secretome data also did not identify N-cadherin

as a substrate of ADAM15 even using *Adam15*-null murine chondrocytes. Therefore, HTB-94 cells may be a cell type in which ADAM15 does not principally function as a sheddase. Finally, it is also possible that ADAM15 needs to be activated to become proteolytically active. However, without known substrates, it will be difficult to screen for such ADAM15 activators.

Another possibility is that ADAM15 does not function as a sheddase. The secretome analyses I used are designed to identify membrane proteins which are cleaved by ADAM15 and shed into the CM, with the assumption that the plasma membrane is the main location where ADAM15 exerts its proteolytic activity. However, if ADAM15 cleaves proteins in the CM, such as secreted proteins or ECM components, or if ADAM15 only further processes membrane proteins released by other sheddases, the approaches used here will be unlikely to detect ADAM15 activity. Importantly, other ADAMs (e.g. ADAM9 and 12) have been reported to cleave non-membrane proteins (Loechel et al., 1998; Mazzocca et al., 2005), suggesting that proteolytically active ADAMs can indeed have proteolytic functions other than shedding. Moreover, it is also possible that ADAM15 does not exert its functions principally on the plasma membrane. Several ADAMs have been shown to exist in secreted forms, including ADAM10 (Yavari et al., 1998) and ADAM12 (Shi et al., 2000), with extracellular activities reported for ADAM12 (Roy et al., 2004; Shi et al., 2000). ADAM15 has been detected in exosomes, implying potential extracellular activities (Lee et al., 2012). Additionally, some ADAMs [e.g. ADAM9 (Mygind et al., 2018) and ADAM12 (Stautz et al., 2012)] can be internalised and stored inside cells, and an unpublished study has shown that ADAM15 expression at the protein level is increased in intracellular compartments of TIMP-3-over-expressing HEK-293 cells (Simone D. Scilabra, personal

communication). Together, these studies suggest that ADAM15 may exert its function intracellularly or extracellularly (e. g. in exosomes), and that alternative proteomics approaches may be necessary to identify ADAM15 activity.

Finally, it is also possible that, although ADAM15 contains a conserved catalytic domain, it does not function as an active enzyme. The concept that ADAMs are sheddases is mainly rooted from investigation of ADAM10 and 17, both of which are highly active with numerous reported substrates. However, substrates of most other ADAMs are less clearly defined (Edwards et al., 2008). Using a Uniprot phylogenetic alignment tool, I aligned the catalytic domains of ADAM10 and 17 with other ADAMs, and observed that ADAM10 and 17 are closely related to each other and more distant from all other ADAMs. They also have larger catalytic domains, which may explain their lower substrate selectivity. Taken together, it is likely that ADAM10 and 17 are outliers in terms of proteolytic activity. Therefore, it is possible that ADAMs other than ADAM10 and 17 have more restricted proteolytic activity, or are more selective due to their smaller catalytic pockets. It is theoretically possible that comparatively recent mutations in ADAM15 which further restrict the accessibility of its catalytic pocket could have occurred. If the proteolytic activity of ADAM15 is not indispensable (potentially because of redundancy with other active ADAMs), then ADAM15 could have lost its proteolytic function completely, without losing its conserved zinc-binding motif. ADAM15 has been reported to cleave proteins such as FGFR2iiiB, type IV collagen and small peptide fragments *in vitro* under non-physiological conditions (Maretzky et al., 2014; Maretzky et al., 2009b; Martin et al., 2002; Moss et al., 2016), demonstrating that it is capable of exerting proteolytic activity against small substrates or at high enzyme concentrations, but cleavage of these substrates under physiological

conditions has not been reported, suggesting that *in vitro* activity may not reflect physiological behaviour of the enzyme.

6.5. ADAM15 may protect cartilage from OA through maintaining SLC26A2 level on the cell surface

Finally, I explored ADAM15's effects on the abundance of surface proteins, under the same assumption that the plasma membrane is the principal location where ADAM15 exerts its functions. The SurfSPECS results suggest that ADAM15 did not greatly affect the abundance of most membrane proteins, as >98% reduction in ADAM15 expression on the cell surface resulted in less than 3% of the proteins identified by SurfSPECS being significantly regulated, and the magnitude of change for most of these proteins was less than 50%. Moreover, validation of the proteins identified by SurfSPECS using immunoblotting suggests that many of the "hits" were either false positives or that changes were too small to be reliably detected using immunoblotting. This finding is consistent with the finding that *Adam15*-deficient mice did not exhibit dramatic phenotypes, suggesting that ADAM15 may more likely act to fine-tune the abundance of other proteins. This may also fit with the proposed safeguarding role of ADAM15, as loss of ADAM15 itself may not directly result in deviation from homeostasis, but will greatly reduce cells' ability to resolve other insults. Therefore, appropriate stimulations will be required to visualise those proteins affected by ADAM15 on the cell surface.

Notably, I identified that SLC26A2, a sulfate transporter, was decreased on the cell surface when *ADAM15* was knocked down. Validation of this SurfSPECS finding

using immunoblotting showed a trend towards decreased surface abundance of SLC26A2 when *ADAM15* was knocked down. Although this did not reach statistical significance, I consider the potential relationship between ADAM15 and SLC26A2 worthwhile of further investigation, as mutations of SLC26A2 affect sulfation of GAGs [e.g. undersulfated chondroitin as shown by sulfate disaccharide analysis (Rossi et al., 1998)] and aggrecan [as shown by toluidine blue and alcian blue staining (Rossi et al., 1996; Rossi et al., 1997)] and such mutations have been linked to cartilage and bone abnormalities. Most importantly, depending on how severely the mutations affect SLC26A2 function, a whole spectrum of cartilage phenotypes is observed, ranging from diastrophic dysplasia (a non-lethal recessive form of multiple epiphyseal dysplasia), to atelosteogenesis type 2 (a postnatally lethal disease) and achondrogenesis 1B (embryonically lethal) (Haila et al., 2001; Hastbacka et al., 1994; Hastbacka et al., 1996; Rossi et al., 1996; Superti-Furga et al., 1996). This suggests that even slight changes in SLC26A2's surface abundance may have substantial effects on cartilage health. This is consistent with the finding that *Adam15*-null mice only developed spontaneous OA 12 to 14 months after birth. Undersulfation of chondroitin sulfate may affect the ability of aggrecan in the cartilage ECM to provide compressive resistance, thereby altering the mechanical loading of cartilage, and chronically impairing cartilage health. In addition to its effects on chondroitin sulfate, SLC26A2 mutation may reduce sulfation of heparan sulfate and so hamper the retention and biological activity of growth factors. This may not result in an evident phenotype in young mice, but may impair the repair capacity of cartilage, and so predispose joints to development of OA after injury.

To further investigate the relationship between ADAM15 and SLC26A2, the effect of

ADAM15 knock down or over-expression on GAG sulfation could be characterised using an *in vitro* system, and the surface abundance of SLC26A2 in chondrocytes of *Adam15*-null mice will need to be examined. Furthermore, mice over-expressing *Adam15* could be crossed with mice harbouring mild mutation of *Slc26a2* to investigate whether *Adam15* over-expression is sufficient to counteract the effect of GAG undersulfation resulting from dysfunctional SLC26A2. Finally, unravelling the underpinning mechanism linking ADAM15 to SLC26A2 surface abundance will provide necessary evidence to establish the relationship between these two proteins.

6.6. Concluding remarks and further direction

In my DPhil project, I discovered a possible novel mechanism regulating abundance of ADAM15 (the IL-13-ADAM15 axis) that may contribute to age-dependent reduction in ADAM15 expression, and hence loss of joint protection in old age. However, since I did not investigate whether decrease in *IL13* expression (e.g. via siRNA) regulates ADAM15, the causal relationship between decreased *Il13* expression and reduced *Adam15* expression in mouse joints remains to be established. Interestingly, my data suggests that, in mouse joints, *Il13* and *Adam15* display a similar expression pattern across the age ranges I examined, indicating that *Il13* may also be responsible for the up-regulation of *Adam15* in young adult mouse joint. Only a few studies have examined IL-13's roles in cartilage, so how it is up-regulated in the young joint, and whether the same mechanism regulates the potential causal relationship between *Il13* and *Adam15* expression in both young and old joints remains to be determined.

Importantly, even with my best efforts, it remains unclear how ADAM15 exerts its protective effects, as I was not able to identify substrates of ADAM15, and potential regulation of SLC26A2 by ADAM15 needs to be further validated using other methods. Importantly, most of my experiments which aimed to uncover the function of ADAM15 were designed with the assumption that ADAM15 exerts its functions on the plasma membrane. Since these studies did not identify any major effects, it may be helpful to explore whether ADAM15 actually functions in other cellular compartments, such as intracellularly or extracellularly (e. g. in exosomes). In addition, investigation of ADAM15's functions should not be limited to its shedding or proteolytic activities, as my studies suggest that ADAM15 may not be a highly active sheddase, or may even have limited activity under physiological conditions. Finally,

most studies on ADAM15 indicate that ADAM15 is important in preventing damage from accumulating in tissues and so guarding against chronic conditions. Therefore, the function of ADAM15 may be more evident with appropriate stimulation, challenge or ageing of murine models. It will be necessary to take these observations into account when designing future experiments to understand the physiological functions of ADAM15.

7. References

1. Abbaszade, I., Liu, R.Q., Yang, F., Rosenfeld, S.A., Ross, O.H., Link, J.R., Ellis, D.M., Tortorella, M.D., Pratta, M.A., Hollis, J.M., *et al.* (1999). Cloning and characterization of ADAMTS11, an aggrecanase from the ADAMTS family. J Biol Chem *274*, 23443-23450.
2. Akeson, G., and Malemud, C.J. (2017). A Role for Soluble IL-6 Receptor in Osteoarthritis. J Funct Morphol Kinesiol *2*.
3. Al-Fakhri, N., Wilhelm, J., Hahn, M., Heidt, M., Hehrlein, F.W., Endisch, A.M., Hupp, T., Cherian, S.M., Bobryshev, Y.V., Lord, R.S., *et al.* (2003). Increased expression of disintegrin-metalloproteinases ADAM-15 and ADAM-9 following upregulation of integrins alpha5beta1 and alphavbeta3 in atherosclerosis. J Cell Biochem *89*, 808-823.
4. Alvarez, J., Balbin, M., Santos, F., Fernandez, M., Ferrando, S., and Lopez, J.M. (2000). Different bone growth rates are associated with changes in the expression pattern of types II and X collagens and collagenase 3 in proximal growth plates of the rat tibia. J Bone Miner Res *15*, 82-94.
5. Amanchy, R., Kalume, D.E., and Pandey, A. (2005). Stable isotope labeling with amino acids in cell culture (SILAC) for studying dynamics of protein abundance and posttranslational modifications. Sci STKE *2005*, pl2.
6. Amour, A., Knight, C.G., Webster, A., Slocombe, P.M., Stephens, P.E., Knauper, V., Docherty, A.J., and Murphy, G. (2000). The in vitro activity of ADAM-10 is inhibited by TIMP-1 and TIMP-3. FEBS Lett *473*, 275-279.
7. Anders, A., Gilbert, S., Garten, W., Postina, R., and Fahrenholz, F. (2001). Regulation of the alpha-secretase ADAM10 by its prodomain and proprotein convertases. FASEB J *15*, 1837-1839.
8. Anderson, N.L., and Anderson, N.G. (2002). The human plasma proteome: history, character, and diagnostic prospects. Mol Cell Proteomics *1*, 845-867.
9. Andrianakos, A.A., Kontelis, L.K., Karamitsos, D.G., Aslanidis, S.I., Georgountzos, A.I., Kaziolas, G.O., Pantelidou, K.V., Vafiadou, E.V., Dantis, P.C., and Group, E.S. (2006). Prevalence of symptomatic knee, hand, and hip osteoarthritis in Greece. The ESORDIG study. J Rheumatol *33*, 2507-2513.
10. Artavanis-Tsakonas, S., Rand, M.D., and Lake, R.J. (1999). Notch signaling: cell fate control and signal integration in development. Science *284*, 770-776.
11. Axelrod, H., and Pienta, K.J. (2014). Axl as a mediator of cellular growth and survival. Oncotarget *5*, 8818-8852.
12. Bantscheff, M., Lemeer, S., Savitski, M.M., and Kuster, B. (2012). Quantitative mass spectrometry in proteomics: critical review update from 2007 to the present. Anal Bioanal Chem *404*, 939-965.
13. Baren, J.P., Stewart, G.D., Stokes, A., Gray, K., Pennington, C.J., O'Neill, R., Deans, D.A., Paterson-Brown, S., Riddick, A.C., Edwards, D.R., *et al.* (2012). mRNA profiling of the cancer degradome in oesophago-gastric adenocarcinoma. Br J Cancer *107*, 143-149.
14. Bayliss, M.T., Osborne, D., Woodhouse, S., and Davidson, C. (1999). Sulfation of chondroitin

sulfate in human articular cartilage. The effect of age, topographical position, and zone of cartilage on tissue composition. J Biol Chem *274*, 15892-15900.

15. Beck, V., Herold, H., Benge, A., Luber, B., Hutzler, P., Tschesche, H., Kessler, H., Schmitt, M., Geppert, H.G., and Reuning, U. (2005). ADAM15 decreases integrin alphavbeta3/vitronectin-mediated ovarian cancer cell adhesion and motility in an RGD-dependent fashion. Int J Biochem Cell Biol *37*, 590-603.
16. Bell, D.M., Leung, K.K., Wheatley, S.C., Ng, L.J., Zhou, S., Ling, K.W., Sham, M.H., Koopman, P., Tam, P.P., and Cheah, K.S. (1997). SOX9 directly regulates the type-II collagen gene. Nat Genet *16*, 174-178.
17. Berenbaum, F. (2013). Osteoarthritis as an inflammatory disease (osteoarthritis is not osteoarthrosis!). Osteoarthritis Cartilage *21*, 16-21.
18. Berthois, Y., Katzenellenbogen, J.A., and Katzenellenbogen, B.S. (1986). Phenol red in tissue culture media is a weak estrogen: implications concerning the study of estrogen-responsive cells in culture. Proc Natl Acad Sci U S A *83*, 2496-2500.
19. Bhosale, A.M., and Richardson, J.B. (2008). Articular cartilage: structure, injuries and review of management. Br Med Bull *87*, 77-95.
20. Bi, W., Deng, J.M., Zhang, Z., Behringer, R.R., and de Crombrugghe, B. (1999). Sox9 is required for cartilage formation. Nat Genet *22*, 85-89.
21. Bjedov, I., Toivonen, J.M., Kerr, F., Slack, C., Jacobson, J., Foley, A., and Partridge, L. (2010). Mechanisms of life span extension by rapamycin in the fruit fly Drosophila melanogaster. Cell Metab *11*, 35-46.
22. Black, R.A., Rauch, C.T., Kozlosky, C.J., Peschon, J.J., Slack, J.L., Wolfson, M.F., Castner, B.J., Stocking, K.L., Reddy, P., Srinivasan, S., *et al.* (1997). A metalloproteinase disintegrin that releases tumour-necrosis factor-alpha from cells. Nature *385*, 729-733.
23. Bland, J.H. (1983). The reversibility of osteoarthritis: a review. Am J Med *74*, 16-26.
24. Blaney Davidson, E.N., Vitters, E.L., Mooren, F.M., Oliver, N., Berg, W.B., and van der Kraan, P.M. (2006). Connective tissue growth factor/CCN2 overexpression in mouse synovial lining results in transient fibrosis and cartilage damage. Arthritis Rheum *54*, 1653-1661.
25. Bohm, B., Hess, S., Krause, K., Schirner, A., Ewald, W., Aigner, T., and Burkhardt, H. (2010). ADAM15 exerts an antiapoptotic effect on osteoarthritic chondrocytes via up-regulation of the X-linked inhibitor of apoptosis. Arthritis Rheum *62*, 1372-1382.
26. Bohm, B.B., Aigner, T., Blobel, C.P., Kalden, J.R., and Burkhardt, H. (2001). Highly enhanced expression of the disintegrin metalloproteinase MDC15 (metargidin) in rheumatoid synovial tissue. Arthritis Rheum *44*, 2046-2054.
27. Bohm, B.B., Aigner, T., Gehrsitz, A., Blobel, C.P., Kalden, J.R., and Burkhardt, H. (1999). Up-regulation of MDC15 (metargidin) messenger RNA in human osteoarthritic cartilage. Arthritis

Rheum *42*, 1946-1950.

28. Bohm, B.B., Aigner, T., Roy, B., Brodie, T.A., Blobel, C.P., and Burkhardt, H. (2005). Homeostatic effects of the metalloproteinase disintegrin ADAM15 in degenerative cartilage remodeling. Arthritis Rheum *52*, 1100-1109.
29. Bohm, B.B., Freund, I., Krause, K., Kinne, R.W., and Burkhardt, H. (2013). ADAM15 adds to apoptosis resistance of synovial fibroblasts by modulating focal adhesion kinase signaling. Arthritis Rheum *65*, 2826-2834.
30. Bohm, B.B., Schirner, A., and Burkhardt, H. (2009). ADAM15 modulates outside-in signalling in chondrocyte-matrix interactions. J Cell Mol Med *13*, 2634-2644.
31. Bondarenko, P.V., Chelius, D., and Shaler, T.A. (2002). Identification and relative quantitation of protein mixtures by enzymatic digestion followed by capillary reversed-phase liquid chromatography-tandem mass spectrometry. Anal Chem *74*, 4741-4749.
32. Bondeson, J., Wainwright, S., Hughes, C., and Caterson, B. (2008). The regulation of the ADAMTS4 and ADAMTS5 aggrecanases in osteoarthritis: a review. Clin Exp Rheumatol *26*, 139-145.
33. Boschetti, F., and Peretti, G.M. (2008). Tensile and compressive properties of healthy and osteoarthritic human articular cartilage. Biorheology *45*, 337-344.
34. Bouaziz, W., Sigaux, J., Modrowski, D., Devignes, C.S., Funck-Brentano, T., Richette, P., Ea, H.K., Provot, S., Cohen-Solal, M., and Hay, E. (2016). Interaction of HIF1alpha and beta-catenin inhibits matrix metalloproteinase 13 expression and prevents cartilage damage in mice. Proc Natl Acad Sci U S A *113*, 5453-5458.
35. Boyce, B.F., Xiu, Y., Li, J., Xing, L., and Yao, Z. (2015). NF-kappaB-Mediated Regulation of Osteoclastogenesis. Endocrinol Metab (Seoul) *30*, 35-44.
36. Brew, K., and Nagase, H. (2010). The tissue inhibitors of metalloproteinases (TIMPs): an ancient family with structural and functional diversity. Biochim Biophys Acta *1803*, 55-71.
37. Bultmann, A., Li, Z., Wagner, S., Gawaz, M., Ungerer, M., Langer, H., May, A.E., and Munch, G. (2011). Loss of protease activity of ADAM15 abolishes protective effects on plaque progression in atherosclerosis. Int J Cardiol *152*, 382-385.
38. Burdelski, C., Fitzner, M., Hube-Magg, C., Kluth, M., Heumann, A., Simon, R., Krech, T., Clauditz, T., Buscheck, F., Steurer, S., *et al.* (2017). Overexpression of the A Disintegrin and Metalloproteinase ADAM15 is linked to a Small but Highly Aggressive Subset of Prostate Cancers. Neoplasia *19*, 279-287.
39. Burr, D.B., and Gallant, M.A. (2012). Bone remodelling in osteoarthritis. Nat Rev Rheumatol *8*, 665-673.
40. Bury, A. (1981). Analysis of protein and peptide mixtures. Evaluation of three sodium dodecyl sulfate-polyacrylamide gel electrophoresis buffer systems. J Chromatography *213*, 491-500.
41. Calvete, J.J., Marcinkiewicz, C., Monleon, D., Esteve, V., Celda, B., Juarez, P., and Sanz, L. (2005).

Snake venom disintegrins: evolution of structure and function. Toxicon *45*, 1063-1074.

42. Campisi, J. (2013). Aging, cellular senescence, and cancer. Annu Rev Physiol *75*, 685-705.
43. Campisi, J., and d'Adda di Fagagna, F. (2007). Cellular senescence: when bad things happen to good cells. Nat Rev Mol Cell Biol *8*, 729-740.
44. Cerretti, D.P., DuBose, R.F., Black, R.A., and Nelson, N. (1999). Isolation of two novel metalloproteinase-disintegrin (ADAM) cDNAs that show testis-specific gene expression. Biochem Biophys Res Commun *263*, 810-815.
45. Chalaris, A., Rabe, B., Paliga, K., Lange, H., Laskay, T., Fielding, C.A., Jones, S.A., Rose-John, S., and Scheller, J. (2007). Apoptosis is a natural stimulus of IL6R shedding and contributes to the proinflammatory trans-signaling function of neutrophils. Blood *110*, 1748-1755.
46. Chan, T.F., Couchourel, D., Abed, E., Delalandre, A., Duval, N., and Lajeunesse, D. (2011). Elevated Dickkopf-2 levels contribute to the abnormal phenotype of human osteoarthritic osteoblasts. J Bone Miner Res *26*, 1399-1410.
47. Chanalaris, A., Doherty, C., Marsden, B.D., Bambridge, G., Wren, S.P., Nagase, H., and Troeberg, L. (2017). Suramin Inhibits Osteoarthritic Cartilage Degradation by Increasing Extracellular Levels of Chondroprotective Tissue Inhibitor of Metalloproteinases 3. Mol Pharmacol *92*, 459-468.
48. Charrier, L., Yan, Y., Driss, A., Laboisse, C.L., Sitaraman, S.V., and Merlin, D. (2005). ADAM-15 inhibits wound healing in human intestinal epithelial cell monolayers. Am J Physiol Gastrointest Liver Physiol *288*, G346-353.
49. Charrier-Hisamuddin, L., Laboisse, C.L., and Merlin, D. (2008). ADAM-15: a metalloprotease that mediates inflammation. FASEB J *22*, 641-653.
50. Chatterjee, V., Beard, R.S., Jr., Reynolds, J.J., Haines, R., Guo, M., Rubin, M., Guido, J., Wu, M.H., and Yuan, S.Y. (2014). MicroRNA-147b regulates vascular endothelial barrier function by targeting ADAM15 expression. PLoS One *9*, e110286.
51. Chelius, D., and Bondarenko, P.V. (2002). Quantitative profiling of proteins in complex mixtures using liquid chromatography and mass spectrometry. J Proteome Res *1*, 317-323.
52. Chen, C.G., Thuillier, D., Chin, E.N., and Alliston, T. (2012). Chondrocyte-intrinsic Smad3 represses Runx2-inducible matrix metalloproteinase 13 expression to maintain articular cartilage and prevent osteoarthritis. Arthritis Rheum *64*, 3278-3289.
53. Chen, D., Shen, J., Zhao, W., Wang, T., Han, L., Hamilton, J.L., and Im, H.J. (2017). Osteoarthritis: toward a comprehensive understanding of pathological mechanism. Bone Res *5*, 16044.
54. Chevallet, M., Diemer, H., Van Dorssealer, A., Villiers, C., and Rabilloud, T. (2007). Toward a better analysis of secreted proteins: the example of the myeloid cells secretome. Proteomics *7*, 1757-1770.
55. Cho, C., Bunch, D.O., Faure, J.E., Goulding, E.H., Eddy, E.M., Primakoff, P., and Myles, D.G. (1998). Fertilization defects in sperm from mice lacking fertilin beta. Science *281*, 1857-1859.
56. Chowdhury, T.T., Bader, D.L., and Lee, D.A. (2006). Anti-inflammatory effects of IL-4 and dynamic

compression in IL-1beta stimulated chondrocytes. Biochem Biophys Res Commun *339*, 241-247.

57. Cleaver, C.S., Rowan, A.D., and Cawston, T.E. (2001). Interleukin 13 blocks the release of collagen from bovine nasal cartilage treated with proinflammatory cytokines. Ann Rheum Dis *60*, 150-157.
58. Clemmons, D.R., Busby, W.H., Jr., Garmong, A., Schultz, D.R., Howell, D.S., Altman, R.D., and Karr, R. (2002). Inhibition of insulin-like growth factor binding protein 5 proteolysis in articular cartilage and joint fluid results in enhanced concentrations of insulin-like growth factor 1 and is associated with improved osteoarthritis. Arthritis Rheum *46*, 694-703.
59. Colangelo, C.M., and Williams, K.R. (2006). Isotope-coded affinity tags for protein quantification. Methods Mol Biol *328*, 151-158.
60. Collins-Racie, L.A., Flannery, C.R., Zeng, W., Corcoran, C., Annis-Freeman, B., Agostino, M.J., Arai, M., DiBlasio-Smith, E., Dorner, A.J., Georgiadis, K.E., *et al.* (2004). ADAMTS-8 exhibits aggrecanase activity and is expressed in human articular cartilage. Matrix Biol *23*, 219-230.
61. Conde, J., Scotece, M., Gomez, R., Lopez, V., Gomez-Reino, J.J., and Gualillo, O. (2011). Adipokines and osteoarthritis: novel molecules involved in the pathogenesis and progression of disease. Arthritis *2011*, 203901.
62. Coppe, J.P., Desprez, P.Y., Krtolica, A., and Campisi, J. (2010). The senescence-associated secretory phenotype: the dark side of tumor suppression. Annu Rev Pathol *5*, 99-118.
63. Cortes, M., Baria, A.T., and Schwartz, N.B. (2009). Sulfation of chondroitin sulfate proteoglycans is necessary for proper Indian hedgehog signaling in the developing growth plate. Development *136*, 1697-1706.
64. D'Souza, S.E., Ginsberg, M.H., and Plow, E.F. (1991). Arginyl-glycyl-aspartic acid (RGD): a cell adhesion motif. Trends Biochem Sci *16*, 246-250.
65. Dai, S.M., Shan, Z.Z., Nakamura, H., Masuko-Hongo, K., Kato, T., Nishioka, K., and Yudoh, K. (2006). Catabolic stress induces features of chondrocyte senescence through overexpression of caveolin 1: possible involvement of caveolin 1-induced down-regulation of articular chondrocytes in the pathogenesis of osteoarthritis. Arthritis Rheum *54*, 818-831.
66. Das, U.N. (2001). Is obesity an inflammatory condition? Nutrition *17*, 953-966.
67. de Hooge, A.S., van de Loo, F.A., Bennink, M.B., Arntz, O.J., de Hooge, P., and van den Berg, W.B. (2005). Male IL-6 gene knock out mice developed more advanced osteoarthritis upon aging. Osteoarthritis Cartilage *13*, 66-73.
68. Dhamale, O.P., Lawrence, R., Wiegmann, E.M., Shah, B.A., Al-Mafraji, K., Lamanna, W.C., Lubke, T., Dierks, T., Boons, G.J., and Esko, J.D. (2017). Arylsulfatase K is the Lysosomal 2-Sulfoglucuronate Sulfatase. ACS Chem Biol *12*, 367-373.
69. Diaz-Rodriguez, E., Montero, J.C., Esparis-Ogando, A., Yuste, L., and Pandiella, A. (2002). Extracellular signal-regulated kinase phosphorylates tumor necrosis factor alpha-converting enzyme at threonine 735: a potential role in regulated shedding. Mol Biol Cell *13*, 2031-2044.

70. Dillon, C.F., Rasch, E.K., Gu, Q., and Hirsch, R. (2006). Prevalence of knee osteoarthritis in the United States: arthritis data from the Third National Health and Nutrition Examination Survey 1991-94. J Rheumatol *33*, 2271-2279.

71. Dong, D.D., Zhou, H., and Li, G. (2015). ADAM15 targets MMP9 activity to promote lung cancer cell invasion. Oncol Rep *34*, 2451-2460.

72. Dreymueller, D., Uhlig, S., and Ludwig, A. (2015). ADAM-family metalloproteinases in lung inflammation: potential therapeutic targets. Am J Physiol Lung Cell Mol Physiol *308*, L325-343.

73. Driban, J.B., Sitler, M.R., Barbe, M.F., and Balasubramanian, E. (2010). Is osteoarthritis a heterogeneous disease that can be stratified into subsets? Clin Rheumatol *29*, 123-131.

74. Du, W.W., Fang, L., Li, M., Yang, X., Liang, Y., Peng, C., Qian, W., O'Malley, Y.Q., Askeland, R.W., Sugg, S.L., *et al.* (2013). MicroRNA miR-24 enhances tumor invasion and metastasis by targeting PTPN9 and PTPRF to promote EGF signaling. J Cell Sci *126*, 1440-1453.

75. Duffy, M.J., Mullooly, M., O'Donovan, N., Sukor, S., Crown, J., Pierce, A., and McGowan, P.M. (2011). The ADAMs family of proteases: new biomarkers and therapeutic targets for cancer? Clin Proteomics *8*, 9.

76. Dupre, A., Boyer-Chatenet, L., Sattler, R.M., Modi, A.P., Lee, J.H., Nicolette, M.L., Kopelovich, L., Jasin, M., Baer, R., Paull, T.T., *et al.* (2008). A forward chemical genetic screen reveals an inhibitor of the Mre11-Rad50-Nbs1 complex. Nat Chem Biol *4*, 119-125.

77. Edwards, D.R., Handsley, M.M., and Pennington, C.J. (2008). The ADAM metalloproteinases. Mol Aspects Med *29*, 258-289.

78. Enderlin, V., Alfos, S., Pallet, V., Garcin, H., Azais-Braesco, V., Jaffard, R., and Higueret, P. (1997). Aging decreases the abundance of retinoic acid (RAR) and triiodothyronine (TR) nuclear receptor mRNA in rat brain: effect of the administration of retinoids. FEBS Lett *412*, 629-632.

79. Escrevente, C., Morais, V.A., Keller, S., Soares, C.M., Altevogt, P., and Costa, J. (2008). Functional role of N-glycosylation from ADAM10 in processing, localization and activity of the enzyme. Biochim Biophys Acta *1780*, 905-913.

80. Eto, K., Puzon-McLaughlin, W., Sheppard, D., Sehara-Fujisawa, A., Zhang, X.P., and Takada, Y. (2000). RGD-independent binding of integrin alpha9beta1 to the ADAM-12 and -15 disintegrin domains mediates cell-cell interaction. J Biol Chem *275*, 34922-34930.

81. Fain, J.N. (2010). Release of inflammatory mediators by human adipose tissue is enhanced in obesity and primarily by the nonfat cells: a review. Mediators Inflamm *2010*, 513948.

82. Fan, H., Turck, C.W., and Derynck, R. (2003). Characterization of growth factor-induced serine phosphorylation of tumor necrosis factor-alpha converting enzyme and of an alternatively translated polypeptide. J Biol Chem *278*, 18617-18627.

83. Feart, C., Pallet, V., Boucheron, C., Higueret, D., Alfos, S., Letenneur, L., Dartigues, J.F., and Higueret, P. (2005). Aging affects the retinoic acid and the triiodothyronine nuclear receptor mRNA

expression in human peripheral blood mononuclear cells. Eur J Endocrinol *152*, 449-458.

84. Felson, D.T., Naimark, A., Anderson, J., Kazis, L., Castelli, W., and Meenan, R.F. (1987). The prevalence of knee osteoarthritis in the elderly. The Framingham Osteoarthritis Study. Arthritis Rheum *30*, 914-918.
85. Fernandes, J.C., Martel-Pelletier, J., and Pelletier, J.P. (2002). The role of cytokines in osteoarthritis pathophysiology. Biorheology *39*, 237-246.
86. Ferretti, M., Gassner, R., Wang, Z., Perera, P., Deschner, J., Sowa, G., Salter, R.B., and Agarwal, S. (2006). Biomechanical signals suppress proinflammatory responses in cartilage: early events in experimental antigen-induced arthritis. J Immunol *177*, 8757-8766.
87. Flannery, C.R., Little, C.B., Caterson, B., and Hughes, C.E. (1999). Effects of culture conditions and exposure to catabolic stimulators (IL-1 and retinoic acid) on the expression of matrix metalloproteinases (MMPs) and disintegrin metalloproteinases (ADAMs) by articular cartilage chondrocytes. Matrix Biol *18*, 225-237.
88. Forlino, A., Piazza, R., Tiveron, C., Della Torre, S., Tatangelo, L., Bonafe, L., Gualeni, B., Romano, A., Pecora, F., Superti-Furga, A., *et al.* (2005). A diastrophic dysplasia sulfate transporter (SLC26A2) mutant mouse: morphological and biochemical characterization of the resulting chondrodysplasia phenotype. Hum Mol Genet *14*, 859-871.
89. Fourie, A.M., Coles, F., Moreno, V., and Karlsson, L. (2003). Catalytic activity of ADAM8, ADAM15, and MDC-L (ADAM28) on synthetic peptide substrates and in ectodomain cleavage of CD23. J Biol Chem *278*, 30469-30477.
90. Fried, D., Bohm, B.B., Krause, K., and Burkhardt, H. (2012). ADAM15 protein amplifies focal adhesion kinase phosphorylation under genotoxic stress conditions. J Biol Chem *287*, 21214-21223.
91. Galvez-Rosas, A., Gonzalez-Huerta, C., Borgonio-Cuadra, V.M., Duarte-Salazar, C., Lara-Alvarado, L., de los Angeles Soria-Bastida, M., Cortes-Gonzalez, S., Ramon-Gallegos, E., and Miranda-Duarte, A. (2010). A COL2A1 gene polymorphism is related with advanced stages of osteoarthritis of the knee in Mexican Mestizo population. Rheumatol Int *30*, 1035-1039.
92. Gao, J., Zheng, W., Wang, L., and Song, B. (2015). A disintegrin and metallproteinase 15 knockout decreases migration of fibroblast-like synoviocytes and inflammation in rheumatoid arthritis. Mol Med Rep *11*, 4389-4396.
93. Garritano, S., Romanel, A., Ciribilli, Y., Bisio, A., Gavoci, A., Inga, A., and Demichelis, F. (2015). In-silico identification and functional validation of allele-dependent AR enhancers. Oncotarget *6*, 4816-4828.
94. Garton, K.J., Gough, P.J., Philalay, J., Wille, P.T., Blobel, C.P., Whitehead, R.H., Dempsey, P.J., and Raines, E.W. (2003). Stimulated shedding of vascular cell adhesion molecule 1 (VCAM-1) is mediated by tumor necrosis factor-alpha-converting enzyme (ADAM 17). J Biol Chem *278*, 37459-37464.

95. Gaultier, A., Cousin, H., Darribere, T., and Alfandari, D. (2002). ADAM13 disintegrin and cysteine-rich domains bind to the second heparin-binding domain of fibronectin. J Biol Chem *277*, 23336-23344.

96. Gay, C.M., Balaji, K., and Byers, L.A. (2017). Giving AXL the axe: targeting AXL in human malignancy. Br J Cancer *116*, 415-423.

97. Gebauer, M., Saas, J., Sohler, F., Haag, J., Soder, S., Pieper, M., Bartnik, E., Beninga, J., Zimmer, R., and Aigner, T. (2005). Comparison of the chondrosarcoma cell line SW1353 with primary human adult articular chondrocytes with regard to their gene expression profile and reactivity to IL-1beta. Osteoarthritis Cartilage *13*, 697-708.

98. Gendron, C., Kashiwagi, M., Lim, N.H., Enghild, J.J., Thogersen, I.B., Hughes, C., Caterson, B., and Nagase, H. (2007). Proteolytic activities of human ADAMTS-5: comparative studies with ADAMTS-4. J Biol Chem *282*, 18294-18306.

99. Giacinti, C., and Giordano, A. (2006). RB and cell cycle progression. Oncogene *25*, 5220-5227.

100. Giebeler, N., and Zigrino, P. (2016). A Disintegrin and Metalloprotease (ADAM): Historical Overview of Their Functions. Toxins (Basel) *8*, 122.

101. Gilpin, B.J., Loechel, F., Mattei, M.G., Engvall, E., Albrechtsen, R., and Wewer, U.M. (1998). A novel, secreted form of human ADAM 12 (meltrin alpha) provokes myogenesis in vivo. J Biol Chem *273*, 157-166.

102. Gladden, A.B., and Diehl, J.A. (2003). Cell cycle progression without cyclin E/CDK2: breaking down the walls of dogma. Cancer Cell *4*, 160-162.

103. Glasson, S.S., Askew, R., Sheppard, B., Carito, B., Blanchet, T., Ma, H.L., Flannery, C.R., Peluso, D., Kanki, K., Yang, Z., *et al.* (2005). Deletion of active ADAMTS5 prevents cartilage degradation in a murine model of osteoarthritis. Nature *434*, 644-648.

104. Glasson, S.S., Askew, R., Sheppard, B., Carito, B.A., Blanchet, T., Ma, H.L., Flannery, C.R., Kanki, K., Wang, E., Peluso, D., *et al.* (2004). Characterization of and osteoarthritis susceptibility in ADAMTS-4-knockout mice. Arthritis Rheum *50*, 2547-2558.

105. Goldring, M.B., and Marcu, K.B. (2009). Cartilage homeostasis in health and rheumatic diseases. Arthritis Res Ther *11*, 224.

106. Goldring, M.B., and Otero, M. (2011). Inflammation in osteoarthritis. Curr Opin Rheumatol *23*, 471-478.

107. Goldring, S.R. (2009). Role of bone in osteoarthritis pathogenesis. Med Clin North Am *93*, 25-35, xv.

108. Gonzales, P.E., Solomon, A., Miller, A.B., Leesnitzer, M.A., Sagi, I., and Milla, M.E. (2004). Inhibition of the tumor necrosis factor-alpha-converting enzyme by its pro domain. J Biol Chem *279*, 31638-31645.

109. Goodman, S.B., Gomez Barrena, E., Takagi, M., and Konttinen, Y.T. (2009). Biocompatibility of

total joint replacements: A review. J Biomed Mater Res A *90*, 603-618.

110.Gooz, M. (2010). ADAM-17: the enzyme that does it all. Crit Rev Biochem Mol Biol *45*, 146-169.

111.Gordon, K.J., and Blobe, G.C. (2008). Role of transforming growth factor-beta superfamily signaling pathways in human disease. Biochim Biophys Acta *1782*, 197-228.

112.Gosset, M., Berenbaum, F., Thirion, S., and Jacques, C. (2008). Primary culture and phenotyping of murine chondrocytes. Nat Protoc *3*, 1253-1260.

113.Greene, M.A., and Loeser, R.F. (2015). Aging-related inflammation in osteoarthritis. Osteoarthritis Cartilage *23*, 1966-1971.

114.Grynpas, M.D., Alpert, B., Katz, I., Lieberman, I., and Pritzker, K.P. (1991). Subchondral bone in osteoarthritis. Calcif Tissue Int *49*, 20-26.

115.Gschwind, A., Hart, S., Fischer, O.M., and Ullrich, A. (2003). TACE cleavage of proamphiregulin regulates GPCR-induced proliferation and motility of cancer cells. EMBO J *22*, 2411-2421.

116.Guilak, F., Nims, R.J., Dicks, A., Wu, C.L., and Meulenbelt, I. (2018). Osteoarthritis as a disease of the cartilage pericellular matrix. Matrix Biol.

117.Haila, S., Hastbacka, J., Bohling, T., Karjalainen-Lindsberg, M.L., Kere, J., and Saarialho-Kere, U. (2001). SLC26A2 (diastrophic dysplasia sulfate transporter) is expressed in developing and mature cartilage but also in other tissues and cell types. J Histochem Cytochem *49*, 973-982.

118.Haqqani, A.S., Kelly, J.F., and Stanimirovic, D.B. (2008). Quantitative protein profiling by mass spectrometry using isotope-coded affinity tags. Methods Mol Biol *439*, 225-240.

119.Hart, S., Fischer, O.M., Prenzel, N., Zwick-Wallasch, E., Schneider, M., Hennighausen, L., and Ullrich, A. (2005). GPCR-induced migration of breast carcinoma cells depends on both EGFR signal transactivation and EGFR-independent pathways. Biological Chemistry *386*, 845-855.

120.Hartmann, D., de Strooper, B., Serneels, L., Craessaerts, K., Herreman, A., Annaert, W., Umans, L., Lubke, T., Lena Illert, A., von Figura, K., *et al.* (2002). The disintegrin/metalloprotease ADAM 10 is essential for Notch signalling but not for alpha-secretase activity in fibroblasts. Hum Mol Genet *11*, 2615-2624.

121.Hartmann, M., Herrlich, A., and Herrlich, P. (2013). Who decides when to cleave an ectodomain? Trends Biochem Sci *38*, 111-120.

122.Hasegawa, A., Otsuki, S., Pauli, C., Miyaki, S., Patil, S., Steklov, N., Kinoshita, M., Koziol, J., D'Lima, D.D., and Lotz, M.K. (2012). Anterior cruciate ligament changes in the human knee joint in aging and osteoarthritis. Arthritis Rheum *64*, 696-704.

123.Hastbacka, J., de la Chapelle, A., Mahtani, M.M., Clines, G., Reeve-Daly, M.P., Daly, M., Hamilton, B.A., Kusumi, K., Trivedi, B., Weaver, A., *et al.* (1994). The diastrophic dysplasia gene encodes a novel sulfate transporter: positional cloning by fine-structure linkage disequilibrium mapping. Cell *78*, 1073-1087.

124.Hastbacka, J., Superti-Furga, A., Wilcox, W.R., Rimoin, D.L., Cohn, D.H., and Lander, E.S. (1996).

Atelosteogenesis type II is caused by mutations in the diastrophic dysplasia sulfate-transporter gene (DTDST): evidence for a phenotypic series involving three chondrodysplasias. Am J Hum Genet *58*, 255-262.

125. Havelka, S., Horn, V., Spohrova, D., and Valouch, P. (1984). The calcified-noncalcified cartilage interface: the tidemark. Acta Biol Hung *35*, 271-279.

126. Heinlein, U.A.O., Wallat, S., Senftleben, A., and Lemaire, L. (1994). Male Germ Cell-Expressed Mouse Gene Taz83 Encodes a Putative, Cysteine-Rich Transmembrane Protein (Cyritestin) Sharing Homologies with Snake Toxins and Sperm-Egg Fusion Proteins. Dev Growth Differ *36*, 49-58.

127. Helmick, C.G., Felson, D.T., Lawrence, R.C., Gabriel, S., Hirsch, R., Kwoh, C.K., Liang, M.H., Kremers, H.M., Mayes, M.D., Merkel, P.A., *et al.* (2008). Estimates of the prevalence of arthritis and other rheumatic conditions in the United States. Part I. Arthritis Rheum *58*, 15-25.

128. Henn, V., Slupsky, J.R., Grafe, M., Anagnostopoulos, I., Forster, R., Muller-Berghaus, G., and Kroczek, R.A. (1998). CD40 ligand on activated platelets triggers an inflammatory reaction of endothelial cells. Nature *391*, 591-594.

129. Hernandez-Segura, A., Nehme, J., and Demaria, M. (2018). Hallmarks of Cellular Senescence. Trends Cell Biol.

130. Herren, B., Garton, K.J., Coats, S., Bowen-Pope, D.F., Ross, R., and Raines, E.W. (2001). ADAM15 overexpression in NIH3T3 cells enhances cell-cell interactions. Exp Cell Res *271*, 152-160.

131. Hiles, G.L., Bucheit, A., Rubin, J.R., Hayward, A., Cates, A.L., Day, K.C., El-Sawy, L., Kunju, L.P., Daignault, S., Lee, C.T., *et al.* (2016). ADAM15 Is Functionally Associated with the Metastatic Progression of Human Bladder Cancer. Plos One *11*.

132. Hino, K., Saito, A., Kido, M., Kanemoto, S., Asada, R., Takai, T., Cui, M., Cui, X., and Imaizumi, K. (2014). Master regulator for chondrogenesis, Sox9, regulates transcriptional activation of the endoplasmic reticulum stress transducer BBF2H7/CREB3L2 in chondrocytes. J Biol Chem *289*, 13810-13820.

133. Horiuchi, K., Weskamp, G., Lum, L., Hammes, H.P., Cai, H., Brodie, T.A., Ludwig, T., Chiusaroli, R., Baron, R., Preissner, K.T., *et al.* (2003). Potential role for ADAM15 in pathological neovascularization in mice. Mol Cell Biol *23*, 5614-5624.

134. Hotoda, N., Koike, H., Sasagawa, N., and Ishiura, S. (2002). A secreted form of human ADAM9 has an alpha-secretase activity for APP. Biochem Biophys Res Commun *293*, 800-805.

135. Houard, X., Goldring, M.B., and Berenbaum, F. (2013). Homeostatic mechanisms in articular cartilage and role of inflammation in osteoarthritis. Curr Rheumatol Rep *15*, 375.

136. Howard, L., Nelson, K.K., Maciewicz, R.A., and Blobel, C.P. (1999). Interaction of the metalloprotease disintegrins MDC9 and MDC15 with two SH3 domain-containing proteins, endophilin I and SH3PX1. J Biol Chem *274*, 31693-31699.

137. Hoyland, J.A., Thomas, J.T., Donn, R., Marriott, A., Ayad, S., Boot-Handford, R.P., Grant, M.E.,

and Freemont, A.J. (1991). Distribution of type X collagen mRNA in normal and osteoarthritic human cartilage. Bone Miner *15*, 151-163.

138. Hunter, D.J., and Felson, D.T. (2006). Osteoarthritis. BMJ *332*, 639-642.

139. Ikeda, Y., Imai, Y., Kumagai, H., Nosaka, T., Morikawa, Y., Hisaoka, T., Manabe, I., Maemura, K., Nakaoka, T., Imamura, T., *et al.* (2004). Vasorin, a transforming growth factor beta-binding protein expressed in vascular smooth muscle cells, modulates the arterial response to injury in vivo. Proc Natl Acad Sci U S A *101*, 10732-10737.

140. Isozaki, T., Rabquer, B.J., Ruth, J.H., Haines, G.K., 3rd, and Koch, A.E. (2013). ADAM-10 is overexpressed in rheumatoid arthritis synovial tissue and mediates angiogenesis. Arthritis Rheum *65*, 98-108.

141. Jacobsen, J., Visse, R., Sorensen, H.P., Enghild, J.J., Brew, K., Wewer, U.M., and Nagase, H. (2008). Catalytic properties of ADAM12 and its domain deletion mutants. Biochemistry *47*, 537-547.

142. Janes, P.W., Saha, N., Barton, W.A., Kolev, M.V., Wimmer-Kleikamp, S.H., Nievergall, E., Blobel, C.P., Himanen, J.P., Lackmann, M., and Nikolov, D.B. (2005). Adam meets Eph: an ADAM substrate recognition module acts as a molecular switch for ephrin cleavage in trans. Cell *123*, 291-304.

143. Jay, G.D., and Waller, K.A. (2014). The biology of lubricin: near frictionless joint motion. Matrix Biol *39*, 17-24.

144. Jeon, O.H., Kim, C., Laberge, R.M., Demaria, M., Rathod, S., Vasserot, A.P., Chung, J.W., Kim, D.H., Poon, Y., David, N., *et al.* (2017). Local clearance of senescent cells attenuates the development of post-traumatic osteoarthritis and creates a pro-regenerative environment. Nat Med *23*, 775-781.

145. Jeon, O.H., Kim, D., Choi, Y.J., Kim, S.H., Choi, W.S., and Kim, D.S. (2007). Novel function of human ADAM15 disintegrin-like domain and its derivatives in platelet aggregation. Thromb Res *119*, 609-619.

146. Jewett, J.C., and Bertozzi, C.R. (2010). Cu-free click cycloaddition reactions in chemical biology. Chem Soc Rev *39*, 1272-1279.

147. Johnson, V.L., and Hunter, D.J. (2014). The epidemiology of osteoarthritis. Best Pract Res Clin Rheumatol *28*, 5-15.

148. Jordan, J.M., Helmick, C.G., Renner, J.B., Luta, G., Dragomir, A.D., Woodard, J., Fang, F., Schwartz, T.A., Abbate, L.M., Callahan, L.F., *et al.* (2007). Prevalence of knee symptoms and radiographic and symptomatic knee osteoarthritis in African Americans and Caucasians: the Johnston County Osteoarthritis Project. J Rheumatol *34*, 172-180.

149. Kang, T., Zhao, Y.G., Pei, D., Sucic, J.F., and Sang, Q.X. (2002). Intracellular activation of human adamalysin 19/disintegrin and metalloproteinase 19 by furin occurs via one of the two consecutive recognition sites. J Biol Chem *277*, 25583-25591.

150. Kapoor, M., Martel-Pelletier, J., Lajeunesse, D., Pelletier, J.P., and Fahmi, H. (2011). Role of proinflammatory cytokines in the pathophysiology of osteoarthritis. Nat Rev Rheumatol *7*, 33-42.
151. Kappelhoff, R., Puente, X.S., Wilson, C.H., Seth, A., Lopez-Otin, C., and Overall, C.M. (2017). Overview of transcriptomic analysis of all human proteases, non-proteolytic homologs and inhibitors: Organ, tissue and ovarian cancer cell line expression profiling of the human protease degradome by the CLIP-CHIP DNA microarray. Biochim Biophys Acta *1864*, 2210-2219.
152. Karsdal, M.A., Leeming, D.J., Dam, E.B., Henriksen, K., Alexandersen, P., Pastoureau, P., Altman, R.D., and Christiansen, C. (2008). Should subchondral bone turnover be targeted when treating osteoarthritis? Osteoarthritis Cartilage *16*, 638-646.
153. Kashiwagi, M., Tortorella, M., Nagase, H., and Brew, K. (2001). TIMP-3 is a potent inhibitor of aggrecanase 1 (ADAM-TS4) and aggrecanase 2 (ADAM-TS5). J Biol Chem *276*, 12501-12504.
154. Kawahara, R., Lima, R.N., Domingues, R.R., Pauletti, B.A., Meirelles, G.V., Assis, M., Figueira, A.C., and Paes Leme, A.F. (2014). Deciphering the role of the ADAM17-dependent secretome in cell signaling. J Proteome Res *13*, 2080-2093.
155. Keenan, C., Milner, P., Kanakis, I., Carter, A., Abraham, D., Leask, A., Van 't Hof, R., Bou-Gharios, G., and Poulet, B. (2018). Ccn2 Deficiency in Chondrocytes Does Not Exacerbate Osteoarthritis in Trauma-Induced Mouse Models. Osteoarthr Cartilage *26*, S79-S79.
156. Kiani, C., Chen, L., Wu, Y.J., Yee, A.J., and Yang, B.B. (2002). Structure and function of aggrecan. Cell Res *12*, 19-32.
157. Kim, Y.J., Sah, R.L., Grodzinsky, A.J., Plaas, A.H., and Sandy, J.D. (1994). Mechanical regulation of cartilage biosynthetic behavior: physical stimuli. Arch Biochem Biophys *311*, 1-12.
158. Kirsch, T., and von der Mark, K. (1992). Remodelling of collagen types I, II and X and calcification of human fetal cartilage. Bone Miner *18*, 107-117.
159. Kleino, I., Ortiz, R.M., and Huovila, A.P. (2007). ADAM15 gene structure and differential alternative exon use in human tissues. BMC Mol Biol *8*, 90.
160. Kleino, I., Ortiz, R.M., Yritys, M., Huovila, A.P., and Saksela, K. (2009). Alternative splicing of ADAM15 regulates its interactions with cellular SH3 proteins. J Cell Biochem *108*, 877-885.
161. Komatsu, M., Nakamura, Y., Maruyama, M., Abe, K., Watanapokasin, R., and Kato, H. (2015). Expression profiles of human CCN genes in patients with osteoarthritis or rheumatoid arthritis. J Orthop Sci *20*, 708-716.
162. Komori, T., Yagi, H., Nomura, S., Yamaguchi, A., Sasaki, K., Deguchi, K., Shimizu, Y., Bronson, R.T., Gao, Y.H., Inada, M., *et al.* (1997). Targeted disruption of Cbfa1 results in a complete lack of bone formation owing to maturational arrest of osteoblasts. Cell *89*, 755-764.
163. Koonce, R.C., and Bravman, J.T. (2013). Obesity and osteoarthritis: more than just wear and tear. J Am Acad Orthop Surg *21*, 161-169.
164. Kratzschmar, J., Lum, L., and Blobel, C.P. (1996). Metargidin, a membrane-anchored

metalloprotease-disintegrin protein with an RGD integrin binding sequence. J Biol Chem *271*, 4593-4596.

165. Kuefer, R., Day, K.C., Kleer, C.G., Sabel, M.S., Hofer, M.D., Varambally, S., Zorn, C.S., Chinnaiyan, A.M., Rubin, M.A., and Day, M.L. (2006). ADAM15 disintegrin is associated with aggressive prostate and breast cancer disease. Neoplasia *8*, 319-329.

166. Kuhn, P.H., Colombo, A.V., Schusser, B., Dreymueller, D., Wetzel, S., Schepers, U., Herber, J., Ludwig, A., Kremmer, E., Montag, D., *et al.* (2016). Systematic substrate identification indicates a central role for the metalloprotease ADAM10 in axon targeting and synapse function. Elife *5*.

167. Kuhn, P.H., Koroniak, K., Hogl, S., Colombo, A., Zeitschel, U., Willem, M., Volbracht, C., Schepers, U., Imhof, A., Hoffmeister, A., *et al.* (2012). Secretome protein enrichment identifies physiological BACE1 protease substrates in neurons. EMBO J *31*, 3157-3168.

168. Kuno, K., Okada, Y., Kawashima, H., Nakamura, H., Miyasaka, M., Ohno, H., and Matsushima, K. (2000). ADAMTS-1 cleaves a cartilage proteoglycan, aggrecan. FEBS Lett *478*, 241-245.

169. Lamas, J.R., Rodriguez-Rodriguez, L., Vigo, A.G., Alvarez-Lafuente, R., Lopez-Romero, P., Marco, F., Camafeita, E., Dopazo, A., Callejas, S., Villafuertes, E., *et al.* (2010). Large-scale gene expression in bone marrow mesenchymal stem cells: a putative role for COL10A1 in osteoarthritis. Ann Rheum Dis *69*, 1880-1885.

170. Langer, H., May, A.E., Bultmann, A., and Gawaz, M. (2005). ADAM 15 is an adhesion receptor for platelet GPIIb-IIIa and induces platelet activation. Thromb Haemost *94*, 555-561.

171. Latchman, Y., Wood, C.R., Chernova, T., Chaudhary, D., Borde, M., Chernova, I., Iwai, Y., Long, A.J., Brown, J.A., Nunes, R., *et al.* (2001). PD-L2 is a second ligand for PD-1 and inhibits T cell activation. Nat Immunol *2*, 261-268.

172. Le Bihan, T., Goh, T., Stewart, II, Salter, A.M., Bukhman, Y.V., Dharsee, M., Ewing, R., and Wisniewski, J.R. (2006). Differential analysis of membrane proteins in mouse fore- and hindbrain using a label-free approach. J Proteome Res *5*, 2701-2710.

173. Le Gall, S.M., Maretzky, T., Issuree, P.D., Niu, X.D., Reiss, K., Saftig, P., Khokha, R., Lundell, D., and Blobel, C.P. (2010). ADAM17 is regulated by a rapid and reversible mechanism that controls access to its catalytic site. J Cell Sci *123*, 3913-3922.

174. Lee, H.D., Koo, B.H., Kim, Y.H., Jeon, O.H., and Kim, D.S. (2012). Exosome release of ADAM15 and the functional implications of human macrophage-derived ADAM15 exosomes. FASEB J *26*, 3084-3095.

175. Lee, M.H., Rapti, M., and Murphy, G. (2005). Total conversion of tissue inhibitor of metalloproteinase (TIMP) for specific metalloproteinase targeting: fine-tuning TIMP-4 for optimal inhibition of tumor necrosis factor-{alpha}-converting enzyme. J Biol Chem *280*, 15967-15975.

176. Lefebvre, V., Peeters-Joris, C., and Vaes, G. (1990). Production of collagens, collagenase and collagenase inhibitor during the dedifferentiation of articular chondrocytes by serial subcultures.

Biochim Biophys Acta *1051*, 266-275.

177. Leong, D.J., Li, Y.H., Gu, X.I., Sun, L., Zhou, Z., Nasser, P., Laudier, D.M., Iqbal, J., Majeska, R.J., Schaffler, M.B., *et al.* (2011). Physiological loading of joints prevents cartilage degradation through CITED2. FASEB J *25*, 182-191.

178. Leong, D.J., and Sun, H.B. (2014). Mechanical loading: potential preventive and therapeutic strategy for osteoarthritis. J Am Acad Orthop Surg *22*, 465-466.

179. Lewis, J. (1998). Notch signalling and the control of cell fate choices in vertebrates. Semin Cell Dev Biol *9*, 583-589.

180. Li, Y., Shen, Y., Hohensinner, P., Ju, J., Wen, Z., Goodman, S.B., Zhang, H., Goronzy, J.J., and Weyand, C.M. (2016a). Deficient Activity of the Nuclease MRE11A Induces T Cell Aging and Promotes Arthritogenic Effector Functions in Patients with Rheumatoid Arthritis. Immunity *45*, 903-916.

181. Li, Y., Xiao, W., Wu, P., Deng, Z., Zeng, C., Li, H., Yang, T., and Lei, G. (2016b). The expression of SIRT1 in articular cartilage of patients with knee osteoarthritis and its correlation with disease severity. J Orthop Surg Res *11*, 144.

182. Lin, Y.C., Kuo, H.C., Wang, J.S., and Lin, W.W. (2012). Regulation of inflammatory response by 3-methyladenine involves the coordinative actions on Akt and glycogen synthase kinase 3beta rather than autophagy. J Immunol *189*, 4154-4164.

183. Lin, Z., Willers, C., Xu, J., and Zheng, M.H. (2006). The chondrocyte: biology and clinical application. Tissue Eng *12*, 1971-1984.

184. Little, C.B., Barai, A., Burkhardt, D., Smith, S.M., Fosang, A.J., Werb, Z., Shah, M., and Thompson, E.W. (2009). Matrix metalloproteinase 13-deficient mice are resistant to osteoarthritic cartilage erosion but not chondrocyte hypertrophy or osteophyte development. Arthritis Rheum *60*, 3723-3733.

185. Little, C.B., Hughes, C.E., Curtis, C.L., Janusz, M.J., Bohne, R., Wang-Weigand, S., Taiwo, Y.O., Mitchell, P.G., Otterness, I.G., Flannery, C.R., *et al.* (2002). Matrix metalloproteinases are involved in C-terminal and interglobular domain processing of cartilage aggrecan in late stage cartilage degradation. Matrix Biol *21*, 271-288.

186. Liu, Q., Hu, X., Zhang, X., Duan, X., Yang, P., Zhao, F., and Ao, Y. (2016). Effects of mechanical stress on chondrocyte phenotype and chondrocyte extracellular matrix expression. Sci Rep *6*, 37268.

187. Liu-Bryan, R., and Terkeltaub, R. (2015). Emerging regulators of the inflammatory process in osteoarthritis. Nat Rev Rheumatol *11*, 35-44.

188. Livshits, G., Zhai, G., Hart, D.J., Kato, B.S., Wang, H., Williams, F.M., and Spector, T.D. (2009). Interleukin-6 is a significant predictor of radiographic knee osteoarthritis: The Chingford Study. Arthritis Rheum *60*, 2037-2045.

189. Loechel, F., Gilpin, B.J., Engvall, E., Albrechtsen, R., and Wewer, U.M. (1998). Human ADAM 12 (meltrin alpha) is an active metalloprotease. J Biol Chem *273*, 16993-16997.

190. Loeser, R.F., Collins, J.A., and Diekman, B.O. (2016). Ageing and the pathogenesis of osteoarthritis. Nat Rev Rheumatol *12*, 412-420.

191. Loeser, R.F., Goldring, S.R., Scanzello, C.R., and Goldring, M.B. (2012). Osteoarthritis: a disease of the joint as an organ. Arthritis Rheum *64*, 1697-1707.

192. Lopez-Otin, C., Blasco, M.A., Partridge, L., Serrano, M., and Kroemer, G. (2013). The hallmarks of aging. Cell *153*, 1194-1217.

193. Lorenzen, I., Lokau, J., Korpys, Y., Oldefest, M., Flynn, C.M., Kunzel, U., Garbers, C., Freeman, M., Grotzinger, J., and Dusterhoft, S. (2016). Control of ADAM17 activity by regulation of its cellular localisation. Sci Rep *6*, 35067.

194. Losina, E., Weinstein, A.M., Reichmann, W.M., Burbine, S.A., Solomon, D.H., Daigle, M.E., Rome, B.N., Chen, S.P., Hunter, D.J., Suter, L.G., *et al.* (2013). Lifetime risk and age at diagnosis of symptomatic knee osteoarthritis in the US. Arthritis Care Res (Hoboken) *65*, 703-711.

195. Lotz, M., and Loeser, R.F. (2012). Effects of aging on articular cartilage homeostasis. Bone *51*, 241-248.

196. Loughlin, J., Dowling, B., Chapman, K., Marcelline, L., Mustafa, Z., Southam, L., Ferreira, A., Ciesielski, C., Carson, D.A., and Corr, M. (2004). Functional variants within the secreted frizzled-related protein 3 gene are associated with hip osteoarthritis in females. Proc Natl Acad Sci U S A *101*, 9757-9762.

197. Loughlin, J., Mustafa, Z., Smith, A., Irven, C., Carr, A.J., Clipsham, K., Chitnavis, J., Bloomfield, V.A., McCartney, M., Cox, O., *et al.* (2000). Linkage analysis of chromosome 2q in osteoarthritis. Rheumatology (Oxford) *39*, 377-381.

198. Lu, D., Scully, M., Kakkar, V., and Lu, X. (2010). ADAM-15 disintegrin-like domain structure and function. Toxins (Basel) *2*, 2411-2427.

199. Luheshi, N.M., Rothwell, N.J., and Brough, D. (2009). Dual functionality of interleukin-1 family cytokines: implications for anti-interleukin-1 therapy. Br J Pharmacol *157*, 1318-1329.

200. Lum, L., Reid, M.S., and Blobel, C.P. (1998). Intracellular maturation of the mouse metalloprotease disintegrin MDC15. J Biol Chem *273*, 26236-26247.

201. Mansell, J.P., Collins, C., and Bailey, A.J. (2007). Bone, not cartilage, should be the major focus in osteoarthritis. Nat Clin Pract Rheumatol *3*, 306-307.

202. March, L.M., and Bachmeier, C.J. (1997). Economics of osteoarthritis: a global perspective. Baillieres Clin Rheumatol *11*, 817-834.

203. Maretzky, T., Blobel, C.P., and Guaiquil, V. (2014). Characterization of oxygen-induced retinopathy in mice carrying an inactivating point mutation in the catalytic site of ADAM15. Invest Ophthalmol Vis Sci *55*, 6774-6782.

204. Maretzky, T., Evers, A., Le Gall, S., Alabi, R.O., Speck, N., Reiss, K., and Blobel, C.P. (2015). The cytoplasmic domain of a disintegrin and metalloproteinase 10 (ADAM10) regulates its constitutive activity but is dispensable for stimulated ADAM10-dependent shedding. J Biol Chem *290*, 7416-7425.

205. Maretzky, T., Le Gall, S.M., Worpenberg-Pietruk, S., Eder, J., Overall, C.M., Huang, X.Y., Poghosyan, Z., Edwards, D.R., and Blobel, C.P. (2009a). Src stimulates fibroblast growth factor receptor-2 shedding by an ADAM15 splice variant linked to breast cancer. Cancer Res *69*, 4573-4576.

206. Maretzky, T., Reiss, K., Ludwig, A., Buchholz, J., Scholz, F., Proksch, E., de Strooper, B., Hartmann, D., and Saftig, P. (2005). ADAM10 mediates E-cadherin shedding and regulates epithelial cell-cell adhesion, migration, and beta-catenin translocation. Proc Natl Acad Sci U S A *102*, 9182-9187.

207. Maretzky, T., Yang, G., Ouerfelli, O., Overall, C.M., Worpenberg, S., Hassiepen, U., Eder, J., and Blobel, C.P. (2009b). Characterization of the catalytic activity of the membrane-anchored metalloproteinase ADAM15 in cell-based assays. Biochem J *420*, 105-113.

208. Martel-Pelletier, J., Alaaeddine, N., and Pelletier, J.P. (1999). Cytokines and their role in the pathophysiology of osteoarthritis. Front Biosci *4*, D694-703.

209. Martel-Pelletier, J., Barr, A.J., Cicuttini, F.M., Conaghan, P.G., Cooper, C., Goldring, M.B., Goldring, S.R., Jones, G., Teichtahl, A.J., and Pelletier, J.P. (2016). Osteoarthritis. Nat Rev Dis Primers *2*, 16072.

210. Martin, J., Eynstone, L.V., Davies, M., Williams, J.D., and Steadman, R. (2002). The role of ADAM 15 in glomerular mesangial cell migration. J Biol Chem *277*, 33683-33689.

211. Martinez-Lopez, N., Athonvarangkul, D., and Singh, R. (2015). Autophagy and aging. Adv Exp Med Biol *847*, 73-87.

212. Marzia, M., Guaiquil, V., Horne, W.C., Blobel, C.P., Baron, R., and Chiusaroli, R. (2011a). Lack of ADAM15 in mice is associated with increased osteoblast function and bone mass. Biol Chem *392*, 877-885.

213. Marzia, M., Guaiquil, V., Horne, W.C., Blobel, C.P., Baron, R., and Chiusaroli, R. (2011b). Lack of ADAM15 in mice is associated with increased osteoblast function and bone mass. Biological Chemistry *392*, 877-885.

214. Massberg, S., Brand, K., Gruner, S., Page, S., Muller, E., Muller, I., Bergmeier, W., Richter, T., Lorenz, M., Konrad, I., *et al.* (2002). A critical role of platelet adhesion in the initiation of atherosclerotic lesion formation. J Exp Med *196*, 887-896.

215. Massicotte, F., Lajeunesse, D., Benderdour, M., Pelletier, J.P., Hilal, G., Duval, N., and Martel-Pelletier, J. (2002). Can altered production of interleukin-1beta, interleukin-6, transforming growth factor-beta and prostaglandin E(2) by isolated human subchondral osteoblasts identify two subgroups of osteoarthritic patients. Osteoarthritis Cartilage *10*, 491-500.

216. Matsuzaki, T., Matsushita, T., Takayama, K., Matsumoto, T., Nishida, K., Kuroda, R., and Kurosaka, M. (2014). Disruption of Sirt1 in chondrocytes causes accelerated progression of osteoarthritis under mechanical stress and during ageing in mice. Ann Rheum Dis *73*, 1397-1404.

217. Matthews, A.L., Noy, P.J., Reyat, J.S., and Tomlinson, M.G. (2017). Regulation of A disintegrin and metalloproteinase (ADAM) family sheddases ADAM10 and ADAM17: The emerging role of tetraspanins and rhomboids. Platelets *28*, 333-341.

218. May, A.E., Kalsch, T., Massberg, S., Herouy, Y., Schmidt, R., and Gawaz, M. (2002). Engagement of glycoprotein IIb/IIIa (alpha(IIb)beta3) on platelets upregulates CD40L and triggers CD40L-dependent matrix degradation by endothelial cells. Circulation *106*, 2111-2117.

219. Mazzocca, A., Coppari, R., De Franco, R., Cho, J.Y., Libermann, T.A., Pinzani, M., and Toker, A. (2005). A secreted form of ADAM9 promotes carcinoma invasion through tumor-stromal interactions. Cancer Res *65*, 4728-4738.

220. McGlashan, S.R., Jensen, C.G., and Poole, C.A. (2006). Localization of extracellular matrix receptors on the chondrocyte primary cilium. J Histochem Cytochem *54*, 1005-1014.

221. McKie, N., Edwards, T., Dallas, D.J., Houghton, A., Stringer, B., Graham, R., Russell, G., and Croucher, P.I. (1997). Expression of members of a novel membrane linked metalloproteinase family (ADAM) in human articular chondrocytes. Biochem Biophys Res Commun *230*, 335-339.

222. McNamara, L.E., Dalby, M.J., Riehle, M.O., and Burchmore, R. (2010). Fluorescence two-dimensional difference gel electrophoresis for biomaterial applications. J R Soc Interface *7 Suppl 1*, S107-118.

223. Meijer, D., Gelderblom, H., Karperien, M., Cleton-Jansen, A.M., Hogendoorn, P.C., and Bovee, J.V. (2011). Expression of aromatase and estrogen receptor alpha in chondrosarcoma, but no beneficial effect of inhibiting estrogen signaling both in vitro and in vivo. Clin Sarcoma Res *1*, 5.

224. Meulenbelt, I., Bos, S.D., Chapman, K., van der Breggen, R., Houwing-Duistermaat, J.J., Kremer, D., Kloppenburg, M., Carr, A., Tsezou, A., Gonzalez, A., *et al.* (2011). Meta-analyses of genes modulating intracellular T3 bio-availability reveal a possible role for the DIO3 gene in osteoarthritis susceptibility. Ann Rheum Dis *70*, 164-167.

225. Meulenbelt, I., Min, J.L., Bos, S., Riyazi, N., Houwing-Duistermaat, J.J., van der Wijk, H.J., Kroon, H.M., Nakajima, M., Ikegawa, S., Uitterlinden, A.G., *et al.* (2008). Identification of DIO2 as a new susceptibility locus for symptomatic osteoarthritis. Hum Mol Genet *17*, 1867-1875.

226. Milla, M.E., Leesnitzer, M.A., Moss, M.L., Clay, W.C., Carter, H.L., Miller, A.B., Su, J.L., Lambert, M.H., Willard, D.H., Sheeley, D.M., *et al.* (1999). Specific sequence elements are required for the expression of functional tumor necrosis factor-alpha-converting enzyme (TACE). J Biol Chem *274*, 30563-30570.

227. Miller, M.A., Oudin, M.J., Sullivan, R.J., Wang, S.J., Meyer, A.S., Im, H., Frederick, D.T., Tadros, J., Griffith, L.G., Lee, H., *et al.* (2016). Reduced Proteolytic Shedding of Receptor Tyrosine Kinases Is a

Post-Translational Mechanism of Kinase Inhibitor Resistance. Cancer Discov *6*, 382-399.

228. Minty, A., Chalon, P., Derocq, J.M., Dumont, X., Guillemot, J.C., Kaghad, M., Labit, C., Leplatois, P., Liauzun, P., Miloux, B., *et al.* (1993). Interleukin-13 is a new human lymphokine regulating inflammatory and immune responses. Nature *362*, 248-250.

229. Mochizuki, S., Shimoda, M., Shiomi, T., Fujii, Y., and Okada, Y. (2004). ADAM28 is activated by MMP-7 (matrilysin-1) and cleaves insulin-like growth factor binding protein-3. Biochem Biophys Res Commun *315*, 79-84.

230. Mollenhauer, J.A. (2008). Perspectives on articular cartilage biology and osteoarthritis. Injury *39 Suppl 1*, S5-12.

231. Monteagudo, S., and Lories, R.J. (2017). Cushioning the cartilage: a canonical Wnt restricting matter. Nat Rev Rheumatol *13*, 670-681.

232. Mosnier, J.F., Jarry, A., Bou-Hanna, C., Denis, M.G., Merlin, D., and Laboisse, C.L. (2006). ADAM15 upregulation and interaction with multiple binding partners in inflammatory bowel disease. Lab Invest *86*, 1064-1073.

233. Moss, M.L., Miller, M.A., Vujanovic, N., Yoneyama, T., and Rasmussen, F.H. (2016). Fluorescent substrates for ADAM15 useful for assaying and high throughput screening. Anal Biochem *514*, 42-47.

234. Muller, S.A., Scilabra, S.D., and Lichtenthaler, S.F. (2016). Proteomic Substrate Identification for Membrane Proteases in the Brain. Front Mol Neurosci *9*, 96.

235. Munoz-Espin, D., and Serrano, M. (2014). Cellular senescence: from physiology to pathology. Nat Rev Mol Cell Biol *15*, 482-496.

236. Murphy, G. (2011). Tissue inhibitors of metalloproteinases. Genome Biol *12*, 233.

237. Mygind, K.J., Storiko, T., Freiberg, M.L., Samsoe-Petersen, J., Schwarz, J., Andersen, O.M., and Kveiborg, M. (2018). Sorting nexin 9 (SNX9) regulates levels of the transmembrane ADAM9 at the cell surface. J Biol Chem *293*, 8077-8088.

238. Nabbe, K.C., van Lent, P.L., Holthuysen, A.E., Sloetjes, A.W., Koch, A.E., Radstake, T.R., and van den Berg, W.B. (2005). Local IL-13 gene transfer prior to immune-complex arthritis inhibits chondrocyte death and matrix-metalloproteinase-mediated cartilage matrix degradation despite enhanced joint inflammation. Arthritis Res Ther *7*, R392-401.

239. Najy, A.J., Day, K.C., and Day, M.L. (2008a). ADAM15 supports prostate cancer metastasis by modulating tumor cell-endothelial cell interaction. Cancer Res *68*, 1092-1099.

240. Najy, A.J., Day, K.C., and Day, M.L. (2008b). The ectodomain shedding of E-cadherin by ADAM15 supports ErbB receptor activation. J Biol Chem *283*, 18393-18401.

241. Nakajima, M., Takahashi, A., Kou, I., Rodriguez-Fontenla, C., Gomez-Reino, J.J., Furuichi, T., Dai, J., Sudo, A., Uchida, A., Fukui, N., *et al.* (2010). New sequence variants in HLA class II/III region associated with susceptibility to knee osteoarthritis identified by genome-wide association study.

PLoS One *5*, e9723.

242. Neuhold, L.A., Killar, L., Zhao, W., Sung, M.L., Warner, L., Kulik, J., Turner, J., Wu, W., Billinghurst, C., Meijers, T., *et al.* (2001). Postnatal expression in hyaline cartilage of constitutively active human collagenase-3 (MMP-13) induces osteoarthritis in mice. J Clin Invest *107*, 35-44.

243. Ng, L.J., Wheatley, S., Muscat, G.E., Conway-Campbell, J., Bowles, J., Wright, E., Bell, D.M., Tam, P.P., Cheah, K.S., and Koopman, P. (1997). SOX9 binds DNA, activates transcription, and coexpresses with type II collagen during chondrogenesis in the mouse. Dev Biol *183*, 108-121.

244. Nikolaev, A., McLaughlin, T., O'Leary, D.D., and Tessier-Lavigne, M. (2009). APP binds DR6 to trigger axon pruning and neuron death via distinct caspases. Nature *457*, 981-989.

245. Nishida, T., Kubota, S., Kojima, S., Kuboki, T., Nakao, K., Kushibiki, T., Tabata, Y., and Takigawa, M. (2004). Regeneration of defects in articular cartilage in rat knee joints by CCN2 (connective tissue growth factor). J Bone Miner Res *19*, 1308-1319.

246. Noy, N. (2010). Between death and survival: retinoic acid in regulation of apoptosis. Annu Rev Nutr *30*, 201-217.

247. Nurminskaya, M., and Linsenmayer, T.F. (1996). Identification and characterization of up-regulated genes during chondrocyte hypertrophy. Dev Dyn *206*, 260-271.

248. Oksala, N., Levula, M., Airla, N., Pelto-Huikko, M., Ortiz, R.M., Jarvinen, O., Salenius, J.P., Ozsait, B., Komurcu-Bayrak, E., Erginel-Unaltuna, N., *et al.* (2009). ADAM-9, ADAM-15, and ADAM-17 are upregulated in macrophages in advanced human atherosclerotic plaques in aorta and carotid and femoral arteries--Tampere vascular study. Ann Med *41*, 279-290.

249. Omoto, S., Nishida, K., Yamaai, Y., Shibahara, M., Nishida, T., Doi, T., Asahara, H., Nakanishi, T., Inoue, H., and Takigawa, M. (2004). Expression and localization of connective tissue growth factor (CTGF/Hcs24/CCN2) in osteoarthritic cartilage. Osteoarthritis Cartilage *12*, 771-778.

250. Ong, S.E., Blagoev, B., Kratchmarova, I., Kristensen, D.B., Steen, H., Pandey, A., and Mann, M. (2002). Stable isotope labeling by amino acids in cell culture, SILAC, as a simple and accurate approach to expression proteomics. Mol Cell Proteomics *1*, 376-386.

251. Ortiz, R.M., Karkkainen, I., and Huovila, A.P. (2004). Aberrant alternative exon use and increased copy number of human metalloprotease-disintegrin ADAM15 gene in breast cancer cells. Genes Chromosomes Cancer *41*, 366-378.

252. Otto, F., Thornell, A.P., Crompton, T., Denzel, A., Gilmour, K.C., Rosewell, I.R., Stamp, G.W., Beddington, R.S., Mundlos, S., Olsen, B.R., *et al.* (1997). Cbfa1, a candidate gene for cleidocranial dysplasia syndrome, is essential for osteoblast differentiation and bone development. Cell *89*, 765-771.

253. Otto, T., and Sicinski, P. (2017). Cell cycle proteins as promising targets in cancer therapy. Nat Rev Cancer *17*, 93-115.

254. Pan, D., and Rubin, G.M. (1997). Kuzbanian controls proteolytic processing of Notch and

mediates lateral inhibition during Drosophila and vertebrate neurogenesis. Cell *90*, 271-280.

255. Parrish, W.R., Byers, B.A., Su, D., Geesin, J., Herzberg, U., Wadsworth, S., Bendele, A., and Story, B. (2017). Intra-articular therapy with recombinant human GDF5 arrests disease progression and stimulates cartilage repair in the rat medial meniscus transection (MMT) model of osteoarthritis. Osteoarthritis Cartilage *25*, 554-560.

256. Pauli, C., Grogan, S.P., Patil, S., Otsuki, S., Hasegawa, A., Koziol, J., Lotz, M.K., and D'Lima, D.D. (2011). Macroscopic and histopathologic analysis of human knee menisci in aging and osteoarthritis. Osteoarthritis Cartilage *19*, 1132-1141.

257. Peiretti, F., Canault, M., Deprez-Beauclair, P., Berthet, V., Bonardo, B., Juhan-Vague, I., and Nalbone, G. (2003). Intracellular maturation and transport of tumor necrosis factor alpha converting enzyme. Exp Cell Res *285*, 278-285.

258. Peschon, J.J., Slack, J.L., Reddy, P., Stocking, K.L., Sunnarborg, S.W., Lee, D.C., Russell, W.E., Castner, B.J., Johnson, R.S., Fitzner, J.N., *et al.* (1998). An essential role for ectodomain shedding in mammalian development. Science *282*, 1281-1284.

259. Phan, M.N., Leddy, H.A., Votta, B.J., Kumar, S., Levy, D.S., Lipshutz, D.B., Lee, S.H., Liedtke, W., and Guilak, F. (2009). Functional characterization of TRPV4 as an osmotically sensitive ion channel in porcine articular chondrocytes. Arthritis Rheum *60*, 3028-3037.

260. Philipot, D., Guerit, D., Platano, D., Chuchana, P., Olivotto, E., Espinoza, F., Dorandeu, A., Pers, Y.M., Piette, J., Borzi, R.M., *et al.* (2014). p16INK4a and its regulator miR-24 link senescence and chondrocyte terminal differentiation-associated matrix remodeling in osteoarthritis. Arthritis Res Ther *16*, R58.

261. Pitsillides, A.A., and Beier, F. (2011). Cartilage biology in osteoarthritis--lessons from developmental biology. Nat Rev Rheumatol *7*, 654-663.

262. Poghosyan, Z., Robbins, S.M., Houslay, M.D., Webster, A., Murphy, G., and Edwards, D.R. (2002). Phosphorylation-dependent interactions between ADAM15 cytoplasmic domain and Src family protein-tyrosine kinases. J Biol Chem *277*, 4999-5007.

263. Pratta, M.A., Yao, W., Decicco, C., Tortorella, M.D., Liu, R.Q., Copeland, R.A., Magolda, R., Newton, R.C., Trzaskos, J.M., and Arner, E.C. (2003). Aggrecan protects cartilage collagen from proteolytic cleavage. J Biol Chem *278*, 45539-45545.

264. Pregizer, S.K., Kiapour, A.M., Young, M., Chen, H., Schoor, M., Liu, Z., Cao, J., Rosen, V., and Capellini, T.D. (2018). Impact of broad regulatory regions on Gdf5 expression and function in knee development and susceptibility to osteoarthritis. Ann Rheum Dis *77*, 450.

265. Price, M.D., and Herndon, J.H. (2009). Gender differences in osteoarthritis. Menopause *16*, 624-625.

266. Prieto-Alhambra, D., Judge, A., Javaid, M.K., Cooper, C., Diez-Perez, A., and Arden, N.K. (2014). Incidence and risk factors for clinically diagnosed knee, hip and hand osteoarthritis: influences of

age, gender and osteoarthritis affecting other joints. Ann Rheum Dis *73*, 1659-1664.

267. Pruessmeyer, J., Martin, C., Hess, F.M., Schwarz, N., Schmidt, S., Kogel, T., Hoettecke, N., Schmidt, B., Sechi, A., Uhlig, S., *et al.* (2010). A disintegrin and metalloproteinase 17 (ADAM17) mediates inflammation-induced shedding of syndecan-1 and -4 by lung epithelial cells. J Biol Chem *285*, 555-564.

268. Rael, E.L., and Lockey, R.F. (2011). Interleukin-13 signaling and its role in asthma. World Allergy Organ J *4*, 54-64.

269. Ramachandran, M., Achan, P., Salter, D.M., Bader, D.L., and Chowdhury, T.T. (2011). Biomechanical signals and the C-type natriuretic peptide counteract catabolic activities induced by IL-1beta in chondrocyte/agarose constructs. Arthritis Res Ther *13*, R145.

270. Rappsilber, J., Ishihama, Y., and Mann, M. (2003). Stop and go extraction tips for matrix-assisted laser desorption/ionization, nanoelectrospray, and LC/MS sample pretreatment in proteomics. Anal Chem *75*, 663-670.

271. Rass, E., Grabarz, A., Plo, I., Gautier, J., Bertrand, P., and Lopez, B.S. (2009). Role of Mre11 in chromosomal nonhomologous end joining in mammalian cells. Nat Struct Mol Biol *16*, 819-824.

272. Ratnayake, M., Ploger, F., Santibanez-Koref, M., and Loughlin, J. (2014). Human chondrocytes respond discordantly to the protein encoded by the osteoarthritis susceptibility gene GDF5. PLoS One *9*, e86590.

273. Rawlings, J.S., Rosler, K.M., and Harrison, D.A. (2004). The JAK/STAT signaling pathway. J Cell Sci *117*, 1281-1283.

274. Reddy, P., Slack, J.L., Davis, R., Cerretti, D.P., Kozlosky, C.J., Blanton, R.A., Shows, D., Peschon, J.J., and Black, R.A. (2000). Functional analysis of the domain structure of tumor necrosis factor-alpha converting enzyme. J Biol Chem *275*, 14608-14614.

275. Rego, I., Fernandez-Moreno, M., Fernandez-Lopez, C., Gomez-Reino, J.J., Gonzalez, A., Arenas, J., and Blanco, F.J. (2010). Role of European mitochondrial DNA haplogroups in the prevalence of hip osteoarthritis in Galicia, Northern Spain. Ann Rheum Dis *69*, 210-213.

276. Rego-Perez, I., Fernandez-Moreno, M., Fernandez-Lopez, C., Arenas, J., and Blanco, F.J. (2008). Mitochondrial DNA haplogroups: role in the prevalence and severity of knee osteoarthritis. Arthritis Rheum *58*, 2387-2396.

277. Reiss, K., Maretzky, T., Ludwig, A., Tousseyn, T., de Strooper, B., Hartmann, D., and Saftig, P. (2005). ADAM10 cleavage of N-cadherin and regulation of cell-cell adhesion and beta-catenin nuclear signalling. EMBO J *24*, 742-752.

278. Ricci, C., and Ferri, N. (2015). Naturally occurring PDGF receptor inhibitors with potential anti-atherosclerotic properties. Vascul Pharmacol *70*, 1-7.

279. Rigoglou, S., and Papavassiliou, A.G. (2013). The NF-kappaB signalling pathway in osteoarthritis. Int J Biochem Cell Biol *45*, 2580-2584.

280. Roberts, C.M., Tani, P.H., Bridges, L.C., Laszik, Z., and Bowditch, R.D. (1999). MDC-L, a novel metalloprotease disintegrin cysteine-rich protein family member expressed by human lymphocytes. J Biol Chem *274*, 29251-29259.

281. Robson, H., Siebler, T., Stevens, D.A., Shalet, S.M., and Williams, G.R. (2000). Thyroid hormone acts directly on growth plate chondrocytes to promote hypertrophic differentiation and inhibit clonal expansion and cell proliferation. Endocrinology *141*, 3887-3897.

282. Rodriguez-Manzaneque, J.C., Westling, J., Thai, S.N., Luque, A., Knauper, V., Murphy, G., Sandy, J.D., and Iruela-Arispe, M.L. (2002). ADAMTS1 cleaves aggrecan at multiple sites and is differentially inhibited by metalloproteinase inhibitors. Biochem Biophys Res Commun *293*, 501-508.

283. Roghani, M., Becherer, J.D., Moss, M.L., Atherton, R.E., Erdjument-Bromage, H., Arribas, J., Blackburn, R.K., Weskamp, G., Tempst, P., and Blobel, C.P. (1999). Metalloprotease-disintegrin MDC9: intracellular maturation and catalytic activity. J Biol Chem *274*, 3531-3540.

284. Roos, E.M. (2005). Joint injury causes knee osteoarthritis in young adults. Curr Opin Rheumatol *17*, 195-200.

285. Rossi, A., Bonaventure, J., Delezoide, A.L., Cetta, G., and Superti-Furga, A. (1996). Undersulfation of proteoglycans synthesized by chondrocytes from a patient with achondrogenesis type 1B homozygous for an L483P substitution in the diastrophic dysplasia sulfate transporter. J Biol Chem *271*, 18456-18464.

286. Rossi, A., Bonaventure, J., Delezoide, A.L., Superti-Furga, A., and Cetta, G. (1997). Undersulfation of cartilage proteoglycans ex vivo and increased contribution of amino acid sulfur to sulfation in vitro in McAlister dysplasia/atelosteogenesis type 2. Eur J Biochem *248*, 741-747.

287. Rossi, A., Kaitila, I., Wilcox, W.R., Rimoin, D.L., Steinmann, B., Cetta, G., and Superti-Furga, A. (1998). Proteoglycan sulfation in cartilage and cell cultures from patients with sulfate transporter chondrodysplasias: relationship to clinical severity and indications on the role of intracellular sulfate production. Matrix Biol *17*, 361-369.

288. Roughley, P.J., and White, R.J. (1980). Age-related changes in the structure of the proteoglycan subunits from human articular cartilage. J Biol Chem *255*, 217-224.

289. Roy, R., Wewer, U.M., Zurakowski, D., Pories, S.E., and Moses, M.A. (2004). ADAM 12 cleaves extracellular matrix proteins and correlates with cancer status and stage. J Biol Chem *279*, 51323-51330.

290. Rubinsztein, D.C., Marino, G., and Kroemer, G. (2011). Autophagy and aging. Cell *146*, 682-695.

291. Ruhlen, R., and Marberry, K. (2014). The chondrocyte primary cilium. Osteoarthritis Cartilage *22*, 1071-1076.

292. Ruoslahti, E. (1996). RGD and other recognition sequences for integrins. Annu Rev Cell Dev Biol *12*, 697-715.

293.Ryu, J.H., Kim, S.J., Kim, S.H., Oh, C.D., Hwang, S.G., Chun, C.H., Oh, S.H., Seong, J.K., Huh, T.L., and Chun, J.S. (2002). Regulation of the chondrocyte phenotype by beta-catenin. Development *129*, 5541-5550.

294.Sagane, K., Hayakawa, K., Kai, J., Hirohashi, T., Takahashi, E., Miyamoto, N., Ino, M., Oki, T., Yamazaki, K., and Nagasu, T. (2005). Ataxia and peripheral nerve hypomyelination in ADAM22-deficient mice. BMC Neurosci *6*, 33.

295.Sagane, K., Ohya, Y., Hasegawa, Y., and Tanaka, I. (1998). Metalloproteinase-like, disintegrin-like, cysteine-rich proteins MDC2 and MDC3: novel human cellular disintegrins highly expressed in the brain. Biochem J *334 (Pt 1)*, 93-98.

296.Sahin, U., Weskamp, G., Kelly, K., Zhou, H.M., Higashiyama, S., Peschon, J., Hartmann, D., Saftig, P., and Blobel, C.P. (2004). Distinct roles for ADAM10 and ADAM17 in ectodomain shedding of six EGFR ligands. J Cell Biol *164*, 769-779.

297.Sandy, J.D. (2006). A contentious issue finds some clarity: on the independent and complementary roles of aggrecanase activity and MMP activity in human joint aggrecanolysis. Osteoarthritis Cartilage *14*, 95-100.

298.Sandy, J.D., Barrach, H.J., Flannery, C.R., and Plaas, A.H. (1987). The biosynthetic response of the mature chondrocyte in early osteoarthritis. J Rheumatol *14 Spec No*, 16-19.

299.Sandy, J.D., and Verscharen, C. (2001). Analysis of aggrecan in human knee cartilage and synovial fluid indicates that aggrecanase (ADAMTS) activity is responsible for the catabolic turnover and loss of whole aggrecan whereas other protease activity is required for C-terminal processing in vivo. Biochem J *358*, 615-626.

300.Sarrazin, S., Lamanna, W.C., and Esko, J.D. (2011). Heparan sulfate proteoglycans. Cold Spring Harb Perspect Biol *3*.

301.Satoh, A., Brace, C.S., Rensing, N., Cliften, P., Wozniak, D.F., Herzog, E.D., Yamada, K.A., and Imai, S. (2013). Sirt1 extends life span and delays aging in mice through the regulation of Nk2 homeobox 1 in the DMH and LH. Cell Metab *18*, 416-430.

302.Scanzello, C.R., and Goldring, S.R. (2012). The role of synovitis in osteoarthritis pathogenesis. Bone *51*, 249-257.

303.Scarisbrick, I.A. (2008). The multiple sclerosis degradome: enzymatic cascades in development and progression of central nervous system inflammatory disease. Curr Top Microbiol Immunol *318*, 133-175.

304.Schafer, B., Gschwind, A., and Ullrich, A. (2004). Multiple G-protein-coupled receptor signals converge on the epidermal growth factor receptor to promote migration and invasion. Oncogene *23*, 991-999.

305.Schmidt, M.B., Chen, E.H., and Lynch, S.E. (2006). A review of the effects of insulin-like growth factor and platelet derived growth factor on in vivo cartilage healing and repair. Osteoarthritis

Cartilage *14*, 403-412.

306.Schulz, B., Pruessmeyer, J., Maretzky, T., Ludwig, A., Blobel, C.P., Saftig, P., and Reiss, K. (2008). ADAM10 regulates endothelial permeability and T-Cell transmigration by proteolysis of vascular endothelial cadherin. Circ Res *102*, 1192-1201.

307.Schulze, W.X., and Usadel, B. (2010). Quantitation in mass-spectrometry-based proteomics. Annu Rev Plant Biol *61*, 491-516.

308.Schumacher, B.L., Block, J.A., Schmid, T.M., Aydelotte, M.B., and Kuettner, K.E. (1994). A novel proteoglycan synthesized and secreted by chondrocytes of the superficial zone of articular cartilage. Arch Biochem Biophys *311*, 144-152.

309.Schweisguth, F. (2004). Regulation of notch signaling activity. Curr Biol *14*, R129-138.

310.Seals, D.F., and Courtneidge, S.A. (2003). The ADAMs family of metalloproteases: multidomain proteins with multiple functions. Genes Dev *17*, 7-30.

311.Shen, J., Li, S., and Chen, D. (2014). TGF-beta signaling and the development of osteoarthritis. Bone Res *2*.

312.Shevchenko, A., Tomas, H., Havlis, J., Olsen, J.V., and Mann, M. (2006). In-gel digestion for mass spectrometric characterization of proteins and proteomes. Nat Protoc *1*, 2856-2860.

313.Shi, Z., Xu, W., Loechel, F., Wewer, U.M., and Murphy, L.J. (2000). ADAM 12, a disintegrin metalloprotease, interacts with insulin-like growth factor-binding protein-3. J Biol Chem *275*, 18574-18580.

314.Shimizu, E., Yasui, A., Matsuura, K., Hijiya, N., Higuchi, Y., and Yamamoto, S. (2003). Structure and expression of the murine ADAM 15 gene and its splice variants, and difference of interaction between their cytoplasmic domains and Src family proteins. Biochem Biophys Res Commun *309*, 779-785.

315.Shukla, M., Htoo, H.H., Wintachai, P., Hernandez, J.F., Dubois, C., Postina, R., Xu, H., Checler, F., Smith, D.R., Govitrapong, P.*, et al.* (2015). Melatonin stimulates the nonamyloidogenic processing of betaAPP through the positive transcriptional regulation of ADAM10 and ADAM17. J Pineal Res *58*, 151-165.

316.Silberberg, M., and Silberberg, R. (1963a). Modifying action of estrogen on the evolution of osteoarthrosis in mice of different ages. Endocrinology *72*, 449-451.

317.Silberberg, M., and Silberberg, R. (1963b). Role of sex hormone in the pathogenesis of osteoarthrosis of mice. Lab Invest *12*, 285-289.

318.Slack, B.E., Ma, L.K., and Seah, C.C. (2001). Constitutive shedding of the amyloid precursor protein ectodomain is up-regulated by tumour necrosis factor-alpha converting enzyme. Biochem J *357*, 787-794.

319.Sletten, E.M., and Bertozzi, C.R. (2011). From mechanism to mouse: a tale of two bioorthogonal reactions. Acc Chem Res *44*, 666-676.

320.Smith, K.M., Gaultier, A., Cousin, H., Alfandari, D., White, J.M., and DeSimone, D.W. (2002). The cysteine-rich domain regulates ADAM protease function in vivo. J Cell Biol *159*, 893-902.

321.Soares da Costa, D., Reis, R.L., and Pashkuleva, I. (2017). Sulfation of Glycosaminoglycans and Its Implications in Human Health and Disorders. Annu Rev Biomed Eng *19*, 1-26.

322.Sokoloff, L. (1956). Natural history of degenerative joint disease in small laboratory animals. I. Pathological anatomy of degenerative joint disease in mice. AMA Arch Pathol *62*, 118-128.

323.Somerville, R.P., Longpre, J.M., Jungers, K.A., Engle, J.M., Ross, M., Evanko, S., Wight, T.N., Leduc, R., and Apte, S.S. (2003). Characterization of ADAMTS-9 and ADAMTS-20 as a distinct ADAMTS subfamily related to Caenorhabditis elegans GON-1. J Biol Chem *278*, 9503-9513.

324.Sophia Fox, A.J., Bedi, A., and Rodeo, S.A. (2009). The basic science of articular cartilage: structure, composition, and function. Sports Health *1*, 461-468.

325.Soto-Hermida, A., Fernandez-Moreno, M., Oreiro, N., Fernandez-Lopez, C., Pertega, S., Cortes-Pereira, E., Rego-Perez, I., and Blanco, F.J. (2014). Mitochondrial DNA (mtDNA) haplogroups influence the progression of knee osteoarthritis. Data from the Osteoarthritis Initiative (OAI). PLoS One *9*, e112735.

326.Spector, T.D., Cicuttini, F., Baker, J., Loughlin, J., and Hart, D. (1996). Genetic influences on osteoarthritis in women: a twin study. BMJ *312*, 940-943.

327.Srikanth, V.K., Fryer, J.L., Zhai, G., Winzenberg, T.M., Hosmer, D., and Jones, G. (2005). A meta-analysis of sex differences prevalence, incidence and severity of osteoarthritis. Osteoarthritis Cartilage *13*, 769-781.

328.Stanton, H., Rogerson, F.M., East, C.J., Golub, S.B., Lawlor, K.E., Meeker, C.T., Little, C.B., Last, K., Farmer, P.J., Campbell, I.K., *et al.* (2005). ADAMTS5 is the major aggrecanase in mouse cartilage in vivo and in vitro. Nature *434*, 648-652.

329.Stautz, D., Leyme, A., Grandal, M.V., Albrechtsen, R., van Deurs, B., Wewer, U., and Kveiborg, M. (2012). Cell-surface metalloprotease ADAM12 is internalized by a clathrin- and Grb2-dependent mechanism. Traffic *13*, 1532-1546.

330.Stupack, D.G. (2007). The biology of integrins. Oncology (Williston Park) *21*, 6-12.

331.Subik, K., Lee, J.F., Baxter, L., Strzepek, T., Costello, D., Crowley, P., Xing, L., Hung, M.C., Bonfiglio, T., Hicks, D.G., *et al.* (2010). The Expression Patterns of ER, PR, HER2, CK5/6, EGFR, Ki-67 and AR by Immunohistochemical Analysis in Breast Cancer Cell Lines. Breast Cancer (Auckl) *4*, 35-41.

332.Sun, C., Beard, R.S., Jr., McLean, D.L., Rigor, R.R., Konia, T., Wu, M.H., and Yuan, S.Y. (2013). ADAM15 deficiency attenuates pulmonary hyperpermeability and acute lung injury in lipopolysaccharide-treated mice. Am J Physiol Lung Cell Mol Physiol *304*, L135-142.

333.Sun, C., Wu, M.H., Guo, M., Day, M.L., Lee, E.S., and Yuan, S.Y. (2010). ADAM15 regulates endothelial permeability and neutrophil migration via Src/ERK1/2 signalling. Cardiovasc Res *87*,

348-355.

334. Sun, C., Wu, M.H., Lee, E.S., and Yuan, S.Y. (2012). A disintegrin and metalloproteinase 15 contributes to atherosclerosis by mediating endothelial barrier dysfunction via Src family kinase activity. Arterioscler Thromb Vasc Biol *32*, 2444-2451.

335. Sun, H.B. (2010). Mechanical loading, cartilage degradation, and arthritis. Ann N Y Acad Sci *1211*, 37-50.

336. Superti-Furga, A., Hastbacka, J., Wilcox, W.R., Cohn, D.H., van der Harten, H.J., Rossi, A., Blau, N., Rimoin, D.L., Steinmann, B., Lander, E.S., *et al.* (1996). Achondrogenesis type IB is caused by mutations in the diastrophic dysplasia sulphate transporter gene. Nat Genet *12*, 100-102.

337. Superti-Furga, A., Neumann, L., Riebel, T., Eich, G., Steinmann, B., Spranger, J., and Kunze, J. (1999). Recessively inherited multiple epiphyseal dysplasia with normal stature, club foot, and double layered patella caused by a DTDST mutation. J Med Genet *36*, 621-624.

338. Takahashi, E., Sagane, K., Nagasu, T., and Kuromitsu, J. (2006a). Altered nociceptive response in ADAM11-deficient mice. Brain Res *1097*, 39-42.

339. Takahashi, E., Sagane, K., Oki, T., Yamazaki, K., Nagasu, T., and Kuromitsu, J. (2006b). Deficits in spatial learning and motor coordination in ADAM11-deficient mice. BMC Neurosci *7*, 19.

340. Tellier, E., Canault, M., Poggi, M., Bonardo, B., Nicolay, A., Alessi, M.C., Nalbone, G., and Peiretti, F. (2008). HDLs activate ADAM17-dependent shedding. J Cell Physiol *214*, 687-693.

341. Tellier, E., Canault, M., Rebsomen, L., Bonardo, B., Juhan-Vague, I., Nalbone, G., and Peiretti, F. (2006). The shedding activity of ADAM17 is sequestered in lipid rafts. Exp Cell Res *312*, 3969-3980.

342. Theendakara, V., Patent, A., Peters Libeu, C.A., Philpot, B., Flores, S., Descamps, O., Poksay, K.S., Zhang, Q., Cailing, G., Hart, M., *et al.* (2013). Neuroprotective Sirtuin ratio reversed by ApoE4. Proc Natl Acad Sci U S A *110*, 18303-18308.

343. Thodeti, C.K., Albrechtsen, R., Grauslund, M., Asmar, M., Larsson, C., Takada, Y., Mercurio, A.M., Couchman, J.R., and Wewer, U.M. (2003). ADAM12/syndecan-4 signaling promotes beta 1 integrin-dependent cell spreading through protein kinase Calpha and RhoA. J Biol Chem *278*, 9576-9584.

344. Thoms, B.L., Dudek, K.A., Lafont, J.E., and Murphy, C.L. (2013). Hypoxia promotes the production and inhibits the destruction of human articular cartilage. Arthritis Rheum *65*, 1302-1312.

345. Tippmann, F., Hundt, J., Schneider, A., Endres, K., and Fahrenholz, F. (2009). Up-regulation of the alpha-secretase ADAM10 by retinoic acid receptors and acitretin. FASEB J *23*, 1643-1654.

346. Tortorella, M.D., Burn, T.C., Pratta, M.A., Abbaszade, I., Hollis, J.M., Liu, R., Rosenfeld, S.A., Copeland, R.A., Decicco, C.P., Wynn, R., *et al.* (1999). Purification and cloning of aggrecanase-1: a member of the ADAMTS family of proteins. Science *284*, 1664-1666.

347. Troeberg, L., and Nagase, H. (2012). Proteases involved in cartilage matrix degradation in

osteoarthritis. Biochim Biophys Acta *1824*, 133-145.

348. Tsezou, A. (2014). Osteoarthritis year in review 2014: genetics and genomics. Osteoarthritis Cartilage *22*, 2017-2024.

349. Ulrich-Vinther, M., Maloney, M.D., Schwarz, E.M., Rosier, R., and O'Keefe, R.J. (2003). Articular cartilage biology. J Am Acad Orthop Surg *11*, 421-430.

350. Ungerer, C., Doberstein, K., Burger, C., Hardt, K., Boehncke, W.H., Bohm, B., Pfeilschifter, J., Dummer, R., Mihic-Probst, D., and Gutwein, P. (2010). ADAM15 expression is downregulated in melanoma metastasis compared to primary melanoma. Biochem Biophys Res Commun *401*, 363-369.

351. Usami, Y., Gunawardena, A.T., Iwamoto, M., and Enomoto-Iwamoto, M. (2016). Wnt signaling in cartilage development and diseases: lessons from animal studies. Lab Invest *96*, 186-196.

352. Valdes, A.M., Lories, R.J., van Meurs, J.B., Kerkhof, H., Doherty, S., Hofman, A., Hart, D.J., Zhang, F., Luyten, F.P., Uitterlinden, A.G., *et al.* (2009). Variation at the ANP32A gene is associated with risk of hip osteoarthritis in women. Arthritis Rheum *60*, 2046-2054.

353. Valdes, A.M., and Spector, T.D. (2011). Genetic epidemiology of hip and knee osteoarthritis. Nat Rev Rheumatol *7*, 23-32.

354. van de Laar, I.M., Oldenburg, R.A., Pals, G., Roos-Hesselink, J.W., de Graaf, B.M., Verhagen, J.M., Hoedemaekers, Y.M., Willemsen, R., Severijnen, L.A., Venselaar, H., *et al.* (2011). Mutations in SMAD3 cause a syndromic form of aortic aneurysms and dissections with early-onset osteoarthritis. Nat Genet *43*, 121-126.

355. van der Kraan, P.M., and van den Berg, W.B. (2007). Osteophytes: relevance and biology. Osteoarthritis Cartilage *15*, 237-244.

356. van der Vorst, E.P., Keijbeck, A.A., de Winther, M.P., and Donners, M.M. (2012). A disintegrin and metalloproteases: molecular scissors in angiogenesis, inflammation and atherosclerosis. Atherosclerosis *224*, 302-308.

357. van Deursen, J.M. (2014). The role of senescent cells in ageing. Nature *509*, 439-446.

358. van Osch, G.J., van der Kraan, P.M., Vitters, E.L., Blankevoort, L., and van den Berg, W.B. (1993). Induction of osteoarthritis by intra-articular injection of collagenase in mice. Strain and sex related differences. Osteoarthritis Cartilage *1*, 171-177.

359. van Saase, J.L., van Romunde, L.K., Cats, A., Vandenbroucke, J.P., and Valkenburg, H.A. (1989). Epidemiology of osteoarthritis: Zoetermeer survey. Comparison of radiological osteoarthritis in a Dutch population with that in 10 other populations. Ann Rheum Dis *48*, 271-280.

360. Van Wart, H.E., and Birkedal-Hansen, H. (1990). The cysteine switch: a principle of regulation of metalloproteinase activity with potential applicability to the entire matrix metalloproteinase gene family. Proc Natl Acad Sci U S A *87*, 5578-5582.

361. Verma, P., and Dalal, K. (2011). ADAMTS-4 and ADAMTS-5: key enzymes in osteoarthritis. J Cell

Biochem *112*, 3507-3514.

362. von der Mark, K., Kirsch, T., Nerlich, A., Kuss, A., Weseloh, G., Gluckert, K., and Stoss, H. (1992). Type X collagen synthesis in human osteoarthritic cartilage. Indication of chondrocyte hypertrophy. Arthritis Rheum *35*, 806-811.

363. Wakatsuki, S., Kurisaki, T., and Sehara-Fujisawa, A. (2004). Lipid rafts identified as locations of ectodomain shedding mediated by Meltrin beta/ADAM19. J Neurochem *89*, 119-123.

364. Wang, H., and Dey, S.K. (2006a). Roadmap to embryo implantation: clues from mouse models. Nat Rev Genet *7*, 185-199.

365. Wang, M., Sampson, E.R., Jin, H., Li, J., Ke, Q.H., Im, H.J., and Chen, D. (2013). MMP13 is a critical target gene during the progression of osteoarthritis. Arthritis Res Ther *15*, R5.

366. Wang, Q., Rozelle, A.L., Lepus, C.M., Scanzello, C.R., Song, J.J., Larsen, D.M., Crish, J.F., Bebek, G., Ritter, S.Y., Lindstrom, T.M., *et al*. (2011). Identification of a central role for complement in osteoarthritis. Nat Med *17*, 1674-1679.

367. Wang, T.Y., and Chen, D. (2016). Differential roles of TGF-beta signalling in joint tissues during osteoarthritis development. Ann Rheum Dis *75*, e72.

368. Wang, W.M., Ge, G., Lim, N.H., Nagase, H., and Greenspan, D.S. (2006b). TIMP-3 inhibits the procollagen N-proteinase ADAMTS-2. Biochem J *398*, 515-519.

369. Weber, A., Wasiliew, P., and Kracht, M. (2010). Interleukin-1 (IL-1) pathway. Sci Signal *3*, cm1.

370. Wei, Z., and Li, H.H. (2015). IGFBP-3 may trigger osteoarthritis by inducing apoptosis of chondrocytes through Nur77 translocation. Int J Clin Exp Pathol *8*, 15599-15610.

371. Wiese, S., Reidegeld, K.A., Meyer, H.E., and Warscheid, B. (2007). Protein labeling by iTRAQ: a new tool for quantitative mass spectrometry in proteome research. Proteomics *7*, 340-350.

372. Williams, G.R. (2013). Thyroid hormone actions in cartilage and bone. Eur Thyroid J *2*, 3-13.

373. Wilusz, R.E., Sanchez-Adams, J., and Guilak, F. (2014). The structure and function of the pericellular matrix of articular cartilage. Matrix Biol *39*, 25-32.

374. Wisniewski, J.R., Zougman, A., Nagaraj, N., and Mann, M. (2009). Universal sample preparation method for proteome analysis. Nat Methods *6*, 359-362.

375. Wong, E., Maretzky, T., Peleg, Y., Blobel, C.P., and Sagi, I. (2015). The Functional Maturation of A Disintegrin and Metalloproteinase (ADAM) 9, 10, and 17 Requires Processing at a Newly Identified Proprotein Convertase (PC) Cleavage Site. J Biol Chem *290*, 12135-12146.

376. Wong, J.W., and Cagney, G. (2010). An overview of label-free quantitation methods in proteomics by mass spectrometry. Methods Mol Biol *604*, 273-283.

377. Xia, S., Zhang, X., Zheng, S., Khanabdali, R., Kalionis, B., Wu, J., Wan, W., and Tai, X. (2016). An Update on Inflamm-Aging: Mechanisms, Prevention, and Treatment. J Immunol Res *2016*, 8426874.

378. Yang, C.Y., Chanalaris, A., and Troeberg, L. (2017). ADAMTS and ADAM metalloproteinases in osteoarthritis - looking beyond the 'usual suspects'. Osteoarthritis Cartilage *25*, 1000-1009.

379. Yang, X., Chen, L., Xu, X., Li, C., Huang, C., and Deng, C.X. (2001). TGF-beta/Smad3 signals repress chondrocyte hypertrophic differentiation and are required for maintaining articular cartilage. J Cell Biol *153*, 35-46.

380. Yasuda, T. (2011). Activation of Akt leading to NF-kappaB up-regulation in chondrocytes stimulated with fibronectin fragment. Biomed Res *32*, 209-215.

381. Yasui, A., Matsuura, K., Shimizu, E., Hijiya, N., Higuchi, Y., and Yamamoto, S. (2004). Expression of splice variants of the human ADAM15 gene and strong interaction between the cytoplasmic domain of one variant and Src family proteins Lck and Hck. Pathobiology *71*, 185-192.

382. Yavari, R., Adida, C., Bray-Ward, P., Brines, M., and Xu, T. (1998). Human metalloprotease-disintegrin Kuzbanian regulates sympathoadrenal cell fate in development and neoplasia. Hum Mol Genet *7*, 1161-1167.

383. Yuan, Y., Cruzat, V.F., Newsholme, P., Cheng, J., Chen, Y., and Lu, Y. (2016). Regulation of SIRT1 in aging: Roles in mitochondrial function and biogenesis. Mech Ageing Dev *155*, 10-21.

384. Yusuf, E., Nelissen, R.G., Ioan-Facsinay, A., Stojanovic-Susulic, V., DeGroot, J., van Osch, G., Middeldorp, S., Huizinga, T.W., and Kloppenburg, M. (2010). Association between weight or body mass index and hand osteoarthritis: a systematic review. Ann Rheum Dis *69*, 761-765.

385. Zeng, W., Corcoran, C., Collins-Racie, L.A., Lavallie, E.R., Morris, E.A., and Flannery, C.R. (2006). Glycosaminoglycan-binding properties and aggrecanase activities of truncated ADAMTSs: comparative analyses with ADAMTS-5, -9, -16 and -18. Biochim Biophys Acta *1760*, 517-524.

386. Zhang, W., Ouyang, H., Dass, C.R., and Xu, J. (2016). Current research on pharmacologic and regenerative therapies for osteoarthritis. Bone Res *4*, 15040.

387. Zhang, Z., Li, L., Yang, W., Cao, Y., Shi, Y., Li, X., and Zhang, Q. (2017). The effects of different doses of IGF-1 on cartilage and subchondral bone during the repair of full-thickness articular cartilage defects in rabbits. Osteoarthritis Cartilage *25*, 309-320.

388. Zhen, G., Wen, C., Jia, X., Li, Y., Crane, J.L., Mears, S.C., Askin, F.B., Frassica, F.J., Chang, W., Yao, J., *et al.* (2013). Inhibition of TGF-beta signaling in mesenchymal stem cells of subchondral bone attenuates osteoarthritis. Nat Med *19*, 704-712.

389. Zhong, J.L., Poghosyan, Z., Pennington, C.J., Scott, X., Handsley, M.M., Warn, A., Gavrilovic, J., Honert, K., Kruger, A., Span, P.N., *et al.* (2008). Distinct functions of natural ADAM-15 cytoplasmic domain variants in human mammary carcinoma. Mol Cancer Res *6*, 383-394.

390. Zhou, H.W., Lou, S.Q., and Zhang, K. (2004). Recovery of function in osteoarthritic chondrocytes induced by p16INK4a-specific siRNA in vitro. Rheumatology (Oxford) *43*, 555-568.

391. Zurawski, G., and de Vries, J.E. (1994). Interleukin 13, an interleukin 4-like cytokine that acts on monocytes and B cells, but not on T cells. Immunol Today *15*, 19-26.